

**CHARACTERISING THE**  
**BIOLOGICAL RESPONSE TO UVA**  
**AND UVB RADIATION**

A thesis submitted for the degree of Doctor of Philosophy in the  
Faculty of Health and Medicine, Lancaster University

By

Harriet Louise Steel

Department of Biological Sciences, University of Lancaster

I declare that this thesis is my own work and has not been submitted  
in part, or as a whole, for the award of a higher degree or qualification  
at this university or elsewhere

# **CONTENTS**

<b><u>LIST OF FIGURES .....</u></b>	<b><u>VII</u></b>
-------------------------------------	-------------------

<b><u>LIST OF TABLES .....</u></b>	<b><u>X</u></b>
------------------------------------	-----------------

<b><u>ABBREVIATIONS .....</u></b>	<b><u>XI</u></b>
-----------------------------------	------------------

<b><u>ABSTRACT .....</u></b>	<b><u>XV</u></b>
------------------------------	------------------

<b><u>CHAPTER 1: INTRODUCTION .....</u></b>	<b><u>2</u></b>
---	-----------------

<b>1. UV Irradiation .....</b>	<b>2</b>
1.1 UV irradiation and human health.....	3
1.1.1 Skin Structure .....	4
<b>1.2 UVA and Carcinogenesis .....</b>	<b>7</b>
1.2.1 UVA and NMSC.....	7
1.2.2 UVA and Melanoma .....	8
<b>1.2.3 Animal models of UVA and melanoma .....</b>	<b>10</b>
<b>1.3 Sources of oxidative stress after UVA.....</b>	<b>13</b>
1.3.1 UVA and photosensitiser reactions .....	13
1.3.2 The UVA induction of reactive oxygen species .....	15
1.3.3 Singlet Oxygen .....	16
<b>1.4 Enzyme mediated processes .....</b>	<b>16</b>
1.4.1 NADPH oxidase.....	16
1.4.2 Haem oxygenase.....	18
<b>1.5 DNA damage by UV .....</b>	<b>20</b>
1.5.1 88-oxoGG.....	21
1.5.2 UV and cyclopyrimidine dimers .....	22
1.5.3 Dark CPDS .....	25
<b>1.6 The ability of UVA to form Double Strand Breaks .....</b>	<b>25</b>
1.6.1 H2AX phosphorylation and the DNA damage response .....	27
1.6.2 Mechanism of H2AX phosphorylation .....	28
1.6.3 H2AX in mitotic cells .....	31
<b>1.7 UVA and stress response pathways .....</b>	<b>31</b>
1.7.1 MAPK.....	32
1.7.2 UVA-dependent phosphorylation of ERK .....	33
1.7.3 UVA activation of p38 .....	34
1.7.4 UVA activation of JNK.....	35
1.7.5 UVA activation of AP1 and its role in carcinogenesis .....	37

<b>1.8 UV induction of apoptosis</b> .....	<b>38</b>
1.8.1 Mitochondrial Membrane Potential and Apoptosis.....	41
<b>1.9 Dose rate response</b> .....	<b>41</b>
<b>1.10 Long term consequences of UVA</b> .....	<b>42</b>
1.10.1 Persistent Genome Instability .....	43
<b>1.11 UV mutations in cancer</b> .....	<b>44</b>
1.11.1 UV mutations in Non-melanoma skin cancer.....	45
1.11.2 UV signatures in Melanoma.....	47
1.11.3 UV mutations in TERT .....	49
<b>1.12 UV, COX2 and tumorigenesis</b> .....	<b>51</b>
<b>1.13 General Aims</b> .....	<b>52</b>
1.13.1 The ability of UVA and UVB to induce the DNA damage response .....	52
1.13.2 Initiation of a DNA damage response in UVA bystander cells .....	52
1.13.3 Activation of MMPs in response to UVA .....	52
<b><u>2.0 METHODS</u></b> .....	<b><u>54</u></b>
<b>2.1.1 Materials</b> .....	<b>54</b>
<b>2.1.2 Buffers and Solutions</b> .....	<b>54</b>
<b>2.1.3 Antibodies</b> .....	<b>56</b>
Diphenyleneiodonium (DPI) .....	58
<b>2.2 Cell culture</b> .....	<b>59</b>
2.2.1 HaCaT cell culture .....	59
2.2.2 NHEK cell culture .....	59
2.2.3 Dermal Fibroblast Cell Culture.....	60
2.2.4 Bystander cell culture .....	61
<b>2.3 UV Irradiation</b> .....	<b>62</b>
2.3.1 UVA irradiation.....	62
2.3.2 UVB irradiations.....	63
<b>2.4 Clonogenic Assay Method</b> .....	<b>65</b>
<b>2.5 Western blotting</b> .....	<b>66</b>
2.5.1 Protein isolation .....	66
2.5.2 Protein concentration measured using Bradford assay. ....	66
2.5.3 SDS PAGE gel.....	67
2.5.4 Gel transfer system .....	67
2.5.5 Detection of proteins.....	67
<b>2.6 Immunofluorescence.</b> .....	<b>68</b>
2.6.1 Cell culture and irradiation for immunofluorescence .....	68
2.6.2 Processing of coverslips for detection of $\gamma$ H2AX .....	68

2.6.3 EdU labelling.....	68
<b>2.6.4 Confocal Microscopy .....</b>	<b>69</b>
<b>2.6.5 Image J analysis of fluorescence .....</b>	<b>69</b>
<b>2.6.6 ZEN analysis of fluorescence .....</b>	<b>70</b>
2.7 Flow cytometry.....	71
<b>2.8 Analysis of mitochondrial membrane potential .....</b>	<b>72</b>
2.8.1 Flow cytometry.....	72
2.8.2 Immunofluorescence .....	73
<b>2.9 Substrate Zymography .....</b>	<b>73</b>
2.9.1 Sample preparation.....	73
2.9.2 Casein Zymography .....	74
2.9.3 Collagen zymography.....	75
2.9.4 Casein digesting activity in confluent irradiated cells .....	75
2.9.8 Analysis of Zymograms with Image J.....	75
<b>2.10 Analysis of RT-PCR data.....</b>	<b>76</b>

## **CHAPTER 3- THE TIMEFRAMES AND KINETICS OF H2AX PHOSPHORYLATION FOLLOWING UVA AND UVB IRRADIATION .....**

<b>3.1 Introduction .....</b>	<b>79</b>
<b>3.2 Aims.....</b>	<b>80</b>
<b>3.3 Results.....</b>	<b>81</b>
3.3.1 Clonogenic survival of HaCaT cells following UVA and UVB .....	81
3.3.1.1 UVA clonogenic survival experiments .....	81
3.3.1.2 UVB Clonogenic survival experiments.....	84
3.3.2 Time course of H2AX phosphorylation following UVA or UVB irradiation .....	85
3.3.3 Dose response relationship between UVA, UVB and $\gamma$ H2AX foci formation.....	91
3.3.4 Investigating the effect of cell cycle progression on the ability of UVB to form $\gamma$ H2AX foci formation.....	96
3.3.5 Activation of ATM following UVA and UVB irradiation .....	100
3.3.6 Validation of PIK inhibitors .....	102
3.3.7 Mechanism of H2AX phosphorylation following UVA irradiation .....	106
3.3.8 Detection of 53BP1 in UVA-irradiated cells .....	112
3.3.9 Mechanism of H2AX phosphorylation following UVB .....	114
3.3.10 Induction of apoptosis in UVA/UVB irradiated cells as indicated by a loss of mitochondrial membrane potential.....	120
3.3.11 Mechanism of apoptosis induction following UVA or UVB irradiation .....	127
<b>3.4 Discussion.....</b>	<b>134</b>
3.4.1 Clonogenic survival of HaCaT cells following biological relevant doses of UVA or UVB ....	134
3.4.2 The ability of UVA and UVB to induce DNA damage detected by $\gamma$ H2AX.....	134

3.4.3 Dose response relationship between UVA/UVB and $\gamma$ H2AX foci formation .....	136
3.4.4 Mechanism of H2AX phosphorylation following UVA and UVB.....	137
3.4.5 Mitochondrial membrane potential following UVA and UVB irradiation. ....	138
3.4.6 Conclusions .....	139

## **CHAPTER 4 THE ABILITY OF UVA TO INDUCE A DNA DAMAGE RESPONSE IN BYSTANDER CELLS..... 145**

<b>4.1 Introduction .....</b>	<b>146</b>
4.1.1 Transmission of bystander signals .....	146
4.1.2 The mechanism of the bystander effect.....	148
4.1.2.1 Intercellular gap junction communication .....	149
4.1.2.2 A role for ROS in the bystander effect.....	151
4.1.2.3 A role for mitochondria in bystander effect.....	152
4.1.2.4 Contribution of the immune system in bystander effect induction.....	153
4.1.2.5 NF- $\kappa$ B.....	153
4.1.3 Activation of the DDR in bystander cells .....	154
4.1.4 UV and the bystander effect .....	155
<b>4.2 Aims.....</b>	<b>157</b>
<b>4.3 Results.....</b>	<b>158</b>
4.3.1 Formation of $\gamma$ H2AX in UVA bystander cells.....	158
4.3.2 The effect of cell cycle position on $\gamma$ H2AX foci formation in UVA bystander cells .....	163
4.3.3 Assessment of EdU uptake in bystander populations .....	167
4.3.4 Phosphorylation of Chk1 in UVA bystander cells .....	170
4.3.5 The effect of PIKK inhibitors on $\gamma$ H2AX foci formation in bystander cells .....	172
4.3.6 The role of ROS in $\gamma$ H2AX foci formation in bystander cells .....	176
4.3.6.2 The effect of DPI on H2AX phosphorylation in UVA bystander cells.....	179
4.3.7 Apoptosis induction in bystander cells.....	182
<b>4.4 Discussion.....</b>	<b>188</b>

## **CHAPTER 5 THE EFFECT OF UVA ON MMP RELEASE IN KERATINOCYTE AND FIBROBLAST CELL LINES..... 195**

<b>5.1 Introduction .....</b>	<b>196</b>
5.1.1 The structure of the dermis .....	196
5.1.2 ECM turnover.....	197
5.1.3 Matrix Metalloproteinases.....	198
5.1.4 Extrinsic skin ageing .....	202
5.1.5 UV and photoaging mechanisms .....	203
5.1.6 The role of Mitochondria .....	206
5.1.7 UV and matrix metalloproteases.....	208
<b>5.1.8 Aims .....</b>	<b>210</b>
5.2 Experimental Design .....	211

<b>5.3 Results.....</b>	<b>213</b>
5.3.1 Optimisation of casein zymography .....	213
5.3.2 Measurement of activity of MMPs in response to UVA.....	215
5.3.3 Effect of Confluence on MMP expression in HaCaT cells.....	217
5.3.4 The effect of confluence on MMP expression in HaCaT cells .....	222
5.3.6 The effect of UVA on MMP activity in dermal fibroblasts.....	226
5.3.7 The effect of confluence on MMP activity in dermal fibroblasts.....	229
<b>5.4 Discussion.....</b>	<b>231</b>
<b><u>CHAPTER 6 – GENERAL DISCUSSION .....</u></b>	<b><u>236</u></b>
6.1 The ability of UVA to form double strand breaks .....	238
6.2 The ability of UVA to induce H2AX phosphorylation in bystander cells .....	241
6.3 DNA damage response in directly irradiated and UVA bystander cells .....	243
6.4 The effect of UVA on MMP activity .....	244
<b><u>REFERENCES.....</u></b>	<b><u>247</u></b>
<b><u>APPENDIX.....</u></b>	<b><u>281</u></b>

## **List of Figures**

CHAPTER 1 GENERAL INTRODUCTION.....	1
FIGURE 1.1 THE POSITION OF UV IN THE ELECTROMAGNETIC SPECTRUM .....	3
FIGURE 1.2 UVA PENETRATES DEEPER INTO HUMAN SKIN COMPARED TO UVB. ....	5
FIGURE 1.3 CONSEQUENCES OF UVA EXPOSURE.....	7
FIGURE 1.4 WORLDWIDE PREVALENCE OF MALIGNANT MELANOMA.....	10
FIGURE 1.5 ABSORPTION SPECTRA OF DNA. ....	14
FIGURE 1.6 REACTION OF UVA WITH PHOTOSENSITISERS.....	15
FIGURE 1.7 UVA INDUCED EXPRESSION OF HO1 .....	19
FIGURE 1.8 THE FORMATION OF 8-OXOG FROM GUANINE .....	21
FIGURE 1.10 THE FORMATION OF CPDS.....	23
FIGURE 1.9 THE MECHANISM BEHIND THE PHOSPHORYLATION OF GAMMA H2AX. ....	30
FIGURE 1.12 UVA ACTIVATION OF MAPKINASES .....	37
FIGURE 1.11 UVA INDUCED PATHWAYS OF APOPTOSIS.....	40
FIGURE 2.1 UVA OUTPUT.....	63
FIGURE 2.2 UVB OUTPUT.....	64
FIGURE 3.1 CLONOGENIC CELL SURVIVAL ASSAYS OF HACAT CELLS FOLLOWING UVA EXPOSURE. .....	83
FIGURE 3.2 CLONOGENIC CELL SURVIVAL ASSAYS OF HACAT CELLS FOLLOWING EXPOSURE TO UVB.....	84
FIGURE 3.3 THE PHOSPHORYLATION OF H2AX IS AN EARLY EVENT FOLLOWING EXPOSURE TO UVA IRRADIATION IN HACAT CELLS .....	86
FIGURE 3.4 H2AX PHOSPHORYLATION IS AN EARLY EVENT IN NHEK CELLS EXPOSED TO A BIOLOGICALLY RELEVANT DOSE OF UVA.....	87
FIGURE 3.5 THE PHOSPHORYLATION OF H2AX IS A LATE EVENT FOLLOWING EXPOSURE TO UVB IRRADIATION .....	89
FIGURE 3.6 THE PHOSPHORYLATION OF H2AX IS A LATE OCCURRING EVENT IN NHEK CELLS EXPOSED TO UVB.....	90
FIGURE 3.7 PHOSPHORYLATION OF H2AX FOLLOWING UVA IRRADIATION SHOWS A PARTIAL DOSE RESPONSE .....	93
FIGURE 3.9 NHEK CELLS SHOW SIMILAR DOSE RESPONSE RELATIONSHIP OF H2AX PHOSPHORYLATION FOLLOWING UVA/UVB THAN THE IMMORTALISED HACAT .....	95
FIGURE 3.10 UVA INDUCED $\gamma$ H2AX IS INDEPENDENT OF REPLICATION.....	97
FIGURE 3.11 H2AX PHOSPHORYLATION FOLLOWING EXPOSURE TO UVB IRRADIATION IS DEPENDENT ON CELL CYCLE PROGRESSION .....	99
FIGURE 3.12 UVA BUT NOT UVB IS ABLE TO INDUCE PHOSPHORYLATION OF ATM .....	101
FIGURE 3.13 AN INHIBITOR TO ATM ABROGATES H2AX PHOSPHORYLATION FOLLOWING TREATMENT WITH ZEOCIN.....	104
FIGURE 3.14 AN INHIBITOR TO ATR ABROGATES H2AX PHOSPHORYLATION FOLLOWING APHIDICOLIN TREATMENT. ....	105
FIGURE 3.15 AN INHIBITOR TO ATM ABROGATES THE $\gamma$ H2AX RESPONSE OF UVA .....	107
FIGURE 3.16 THE RECRUITMENT OF ATM TO DOUBLE STRAND BREAKS IS DEPENDENT ON THE MRN COMPLEX.....	109
FIGURE 3.17 DNA -PK IS RECRUITED TO DNA ENDS OF DOUBLE STRAND BREAKS BY KU70/80 .....	110
FIGURE 3. 18 THE FORMATION OF $\gamma$ H2AX FOCI CAN BE ABROGATED BY PRE INCUBATION WITH A MRN INHIBITOR .....	111
FIGURE 3.19 UVA INDUCES AN INCREASE IN 53BP1 WITHIN THE SAME TIME FRAMES AS H2AX PHOSPHORYLATION.....	113
FIGURE 3.20 NEITHER AN INHIBITOR TO ATM OR ATR RESULT IN A DECREASE IN H2AX PHOSPHORYLATION FOLLOWING UVB IRRADIATION. ....	115

FIGURE 3.21 COMBINATION OF INHIBITORS TO ATM AND ATR RESULT IN ABROGATION OF $\gamma$ H2AX FOCI FORMATION FOLLOWING UVB IRRADIATION.....	117
FIGURE 3.22 UPREGULATION OF ATM PHOSPHORYLATION IS SEEN FOLLOWING UVB WHEN CELLS ARE PRE-TREATED WITH AN INHIBITOR TO ATR .....	118
FIGURE 3.23 A DECREASE IN MITOCHONDRIAL MEMBRANE POTENTIAL IS AN EVENT THAT CAN BE DETECTED EARLIER FOLLOWING UVA IRRADIATION COMPARED TO UVB IRRADIATION. ....	121
FIGURE 3.24 MITOCHONDRIAL MEMBRANE POTENTIAL IS DECREASED AT 3 HOURS FOLLOWING UVA IRRADIATION.....	123
FIGURE 3. 25 EXPOSURE TO UVB INITIATES A DECREASE IN MITOCHONDRIAL MEMBRANE POTENTIAL 24 HOURS POST EXPOSURE.....	125
FIGURE 3.26 APOPTOSIS INDUCTION FOLLOWING UVA IS INDEPENDENT OF ATM ACTIVATION .....	128
FIGURE 3.27 APOPTOSIS INDUCTION FOLLOWING UVB IS DEPENDENT ON ACTIVATION OF THE DDR .....	129
FIGURE 3.28 UVB BUT NOT UVA INDUCES ROBUST P53 ACCUMULATION .....	131
FIGURE 4.1 METHODS OF SIGNAL TRANSMISSIONS IN THE BYSTANDER EFFECT.....	147
FIGURE 4.2 MECHANISM OF THE BYSTANDER EFFECT .....	150
FIGURE 4.3 THE SETUP USED IN BYSTANDER EXPERIMENTS .....	159
FIGURE 4.4 UVA IRRADIATION IS ABLE TO INDUCE THE FORMATION OF $\gamma$ H2AX IN BYSTANDER CELLS WHEN THEY ARE INCUBATED WITH CELLS THAT HAVE BEEN EXPOSED TO UVA IRRADIATION .....	161
FIGURE 4.5 UVA BYSTANDER CELLS THAT ARE POSITIVE FOR $\gamma$ H2AX ARE THE ACTIVELY REPLICATING CELLS.....	164
FIGURE 4.6 REPLICATING FIBROBLASTS ARE ALSO SUSCEPTIBLE TO THE UVA BYSTANDER EFFECT.....	165
FIGURE 4.9 CHK1 IS PHOSPHORYLATED IN UVA BYSTANDER CELLS .....	171
FIGURE 4.10 INHIBITORS TO ATM AND ATR INCREASE H2AX PHOSPHORYLATION FOLLOWING PROLONGED INCUBATION .....	173
FIGURE 4.11 NEITHER AN INHIBITOR TO ATM OR ATR HAVE AN EFFECT ON THE FORMATION OF $\gamma$ H2AX IN BYSTANDER CELLS .....	175
177	
FIGURE 4.12 CATALASE CAUSES A DECREASE IN $\gamma$ H2AX IN BYSTANDER KERATINOCYTES .....	177
FIGURE 4.13 CATALASE CAUSES A DECREASE IN $\gamma$ H2AX IN BYSTANDER FIBROBLASTS.....	178
FIGURE 4.14 PREINCUBATION WITH NADPH OXIDASE INHIBITOR DPI CAUSES A DECREASE IN THE FORMATION OF $\gamma$ H2AX FOCI IN BYSTANDER KERATINOCYTES.....	180
FIGURE 4.16 A DECREASE IN MITOCHONDRIAL MEMBRANE POTENTIAL IS SEEN IN UVA BYSTANDER CELLS AT 48 BUT NOT 24 HOURS OF CO-CULTURE WITH IRRADIATED FEEDER CELLS .....	183
FIGURE 4.17 A DECREASE IN MITOCHONDRIAL MEMBRANE POTENTIAL CAN BE DETECTED IN UVA BYSTANDER CELLS.....	185
FIGURE 4.18 THERE IS NO DETECTABLE DIFFERENCE IN MITOCHONDRIAL MEMBRANE POTENTIAL OF UVA BYSTANDER DERMAL FIBROBLAST CELLS COMPARED TO THE CONTROL.....	187
FIGURE 5.1 COLLAGEN TURNOVER IN THE EXTRACELLULAR MATRIX.....	198
FIGURE 5.2 MMP ACTIVATION AND INACTIVATION .....	201
FIGURE 5.3 MECHANISM OF PHOTOAGING .....	207
FIGURE 5.4 MMP1 AND MMP3 EXPRESSION IS INCREASED FOLLOWING UVA RADIATION .....	210
FIGURE 5.5 LOADING OF 20MG OF PROTEIN IS OPTIMAL FOR CASEIN DETECTION OF CONDITIONED MEDIA .....	214
FIGURE 5.6 CASEIN DEGRADATION CONSTITUENTS OF SHAM IRRADIATED BUT NOT UVA IRRADIATED CONDITIONED MEDIA DECREASE OVER TIME.....	216

FIGURE 5.7 ANALYSIS OF CASEIN DEGRADATION FOLLOWING UVA IRRADIATION .....	218
FIGURE 5.8 THERE IS A STARK DIFFERENCE IN CONFLUENCE BETWEEN SHAM AND UVA IRRADIATED CELLS 48 HOURS POST IRRADIATION.....	220
FIGURE 5.9 NO CASEIN DEGRADATION IS SEEN IN CONDITIONED MEDIA COLLECTED FROM SHAM OR UVA IRRADIATED CONFLUENT POPULATIONS.....	221
FIGURE 5.10 MMP EXPRESSION IS AFFECTED BY CONFLUENCE .....	223
FIGURE 5.11 A BIOLOGICALLY RELEVANT DOSE OF SS HAS NO EFFECT ON RELEASE OF CASEIN DEGRADING MMPS .....	225
FIGURE 5.12 A ZYMOGRAM CONTAINING CONDITIONED MEDIA FROM UVA IRRADIATED AND SHAM IRRADIATED FIBROBLASTS .....	227
FIGURE 5.13 THE CONFLUENCE OF DERMAL FIBROBLASTS 48 HOURS AFTER SHAM AND UVA IRRADIATION. ....	228
FIGURE 5.14 NO CASEIN DEGRADATION IS SEEN IN CONDITIONED MEDIA COLLECTED FROM SHAM OR UVA IRRADIATED CONFLUENT DERMAL FIBROBLAST POPULATIONS .....	230

## **List of tables**

TABLE 1.1 THE MAIN DNA REPAIR PATHWAYS RESPONSIBLE FOR REPAIRING EACH TYPE OF DNA LESION.....	20
TABLE 1.2 MUTATIONS IDENTIFIED IN MELANOMA.....	50
TABLE 2.1 ANTIBODIES USED IN WESTERN BLOTTING.....	56
TABLE 2.2 ANTIBODIES USED IN IMMUNOFLUORESCENCE.....	57
TABLE 2.3 ANTIBODIES USED IN FLOW CYTOMETRY.....	58
TABLE 2.4 INHIBITORS USED.....	58
TABLE 2.5 CONCENTRATIONS OF SUPPLEMENTS IN NHEK MEDIA.....	59
TABLE 2.6 THE NHEK DETATCH KIT.....	60
TABLE 2.7 BYSTANDER SET UP.....	61
TABLE 2.8 EDU REACTION COCKTAIL.....	69
TABLE 2.9 RECIPE FOR CASEIN SDS-PAGE GEL.....	74
TABLE 5.1 MMPS AND THEIR SUBSTRATES.....	199

## **Abbreviations**

3D – 3 dimensional

4HNE – 4 Hydroxynonenal

6-4PP- 6,4 photoproducts

8-oxoG – 8 hydroxyguanine

AP – activator protein

ATM - Ataxia telangiectasia mutated

ATR - ataxia telangiectasia and Rad3-related protein

BCC – basal cell carcinoma

BSA – Bovine serum albumin

CC – cytosine cytosine

CHO-chinese hamster ovary

COX- cyclooxygenase

CPDs – cyclopyrimidine dimers

DDR- DNA Damage response

DMEM – Dulbecco's modified eagles medium

DMSC- dermal multipotent stem cell

DNA - deoxyribonucleic acid

DNA PK – DNA dependent protein kinase

DPI - diphenyliodine

DSB – double strand breaks

ECM – extracellular matrix

EDTA – ethylenediamine

EdU- 5' ethynyl -2'- deoxyuridine

EGF – epidermal growth factor

FBS- foetal bovine serum

GJIC – gap junction intercellular communication

GSH - Glutathione

H2AX – histone 2AX

HGF – hepatocyte growth factor

HO – haem oxygenase

IL-interleukin

KOSR – knockout serum replacement

L-Glut – L glutamine

LI – labile iron

LP- lipid peroxidation

MAPK- mitogen activated protein kinase

MDA – Malondialdehyde

MM – malignant melanoma

MMP – matrix metalloproteinase

MMPI – matrix metalloproteinase inhibitor

mRNA – messenger ribonucleic acid

mtDNA – mitochondrial deoxyribonucleic acid

NADPH – nictinamide adenine dinucleotide phosphate

NER – nucleotide excision repair

NHEK – normal human epidermal keratinocyte

NMSC – non- melanoma skin cancers

NO- nitric oxide

OGG – oxoguananine DNA glycosylase

PAPC – phospholipid – 1- palmitoyl – 2 arachidonoyl – sn – glycerol-3- phosphorylcholine

PBS – phosphate buffered saline

PCR – Polymerase chain reaction

PFA - Paraformaldehyde

PFUVA – protection factor ultra violet A

PGI – persistent genome instability

PI- propidium iodide

PIKK – phosphatidylinositol 3 kinase related kinase

RNA – ribonucleic acid

ROS – reactive oxygen species

RT-PCR – Reverse transcription polymerase chain reaction

SASP- senescence associated secretory phenotype

SCC – squamous cell carcinoma

SDS- sodium dodecyl sulphate

SDS-PAGE- sodium dodecyl sulphate polyacrylamide gel electrophoresis

SHG- second harmonic generation

SOD – superoxide dismutase

SPF – sun protection factor

SS- single strand breaks

TERT -telomerase reverse transcriptase

TGF – transforming growth factor

TIMP – tissue inhibitor matrix proteinases

TT – thymine thymine

UV- ultra violet

WES- whole exome sequencing

WGS – whole genome sequencing

WHO- World Health Organisation

ZN<sup>2+</sup> - zinc ion

## **Abstract**

Once considered fairly harmless due to its low energy UVA is now considered a class one carcinogen, the ability of UVA alone to induce Non-melanoma skin cancer is well accepted and although more controversial there is now significant evidence from epidemiological studies and animal models to suggest a role for UVA in the development of melanoma. Furthermore due to its high penetrance UVA is thought to play a larger role in photoaging than UVB.

Despite this current sun protection methods assess UVA protection only as a ratio of UVA: UVB that is blocked by the sun cream. Therefore it is desirable to have a more biologically relevant method to assess UVA protection offered by a sun cream. The work in this thesis focuses on the identification of a robust biomarker of UVA exposure, with the aim to identify biomarkers of UVA that could be used to assess the protection offered by different sun creams in order to develop a method in assessing protection similar to SPF that is currently used for UVB.

The primary focus was on looking at the DNA damage response following UVA irradiation, and the data presented here shows distinct differences in the mechanism underpinning the DNA damage response in directly irradiated cells and in the UVA bystander cells. The response following UVA has also been shown to be distinct to that following UVB irradiation, both in terms of the DDR and apoptosis induction.

## **Acknowledgements.**

Firstly, I would like thank Dr Sarah Allinson for all of her help, encouragement, patience and support throughout my PhD. I would also like to thank Professor Trevor McMillan for his help with proof reading and drafting this thesis as well as for valued input into experimental ideas in meetings. Additionally, I would like to a few other members of academic staff for their help along the way; Dr Nikki Copeland for all his help with setting up the EdU staining, helpful input in lab meetings and for 4 years of excellent lab banter. A huge thank you to Dr Jane Andre for all her help with confocal microscopy, especially in the earlier days. I would also like to thank Dr Mike Cogan for the opportunity to collaborate with him on his work on platinum complexes for applications in bio-imaging.

I would also like to thank my fellow post-graduate students for all of their help and support during my time in Lancaster, there are too many to name everyone but in particular to Amber Lynch and Louise Kerry who despite having now abandoned me in Lancaster alone remain great friends. Also to my office buddies Kurimun Ismail and Emily Smith, sharing an office with you has made writing significantly ( $P < 0.05$ ) less painful. Finally, to James Tollitt and Alex” the carrot” Jones for allowing me to bully you into running with me, it provided much needed stress relief in the writing months.

Outside of the Lancaster bubble I would like to thank my boyfriend Michael for being constantly supportive and loving and for providing me with wine at the end of both good and bad weeks. To my Mum and her partner her their support and encouragement allowing me to kidnap their dogs when I needed pet therapy – it works! And to my friends for their gentle mocking when I reply to no the question the ask every time I see them... “have you cured cancer yet”.

Thanks must also go to Boots and BBSRC for their funding.

# **Chapter 1 General Introduction**

## **Chapter 1: Introduction**

In this chapter I will be giving a basic introduction to ultraviolet (UV) radiation focusing mainly on the biologically relevant wavebands of UVA and UVB, before discussing the impact of UVA and UVB in human health such as roles in cancer and photoaging. I will then move on to discussing the effects of UVA and UVB at the cellular level, covering their ability to form multiple DNA lesions, initiation of the DNA damage response and consequent activation of stress signaling pathways and induction of apoptosis. In addition, this chapter will cover more long term effects such as persistent genome instability, the UV bystander effect and signature UV mutations frequently seen in cancer.

### **1. UV Irradiation**

Ultraviolet radiation makes up approximately 8% of the total energy emitted from the sun (Frederick et al., 1989). UV radiation is divided into 3 subtypes dependent on wavelength. UVC is of wavelengths below 280nm and is the most energetic and the most readily absorbed by DNA. However, UVC is of little biological relevance because it is completely blocked by the earth's atmosphere. The UV that reaches the earth's surface comprises of just 5 - 10% UVB (280-315nm) and UVA (315-400nm) makes up the remainder (Sutherland and Griffin, 1981). UVA can be further divided into UVAI (340 - 400nm) and UVAIL (315 - 340nm)(Diffey, 2002).

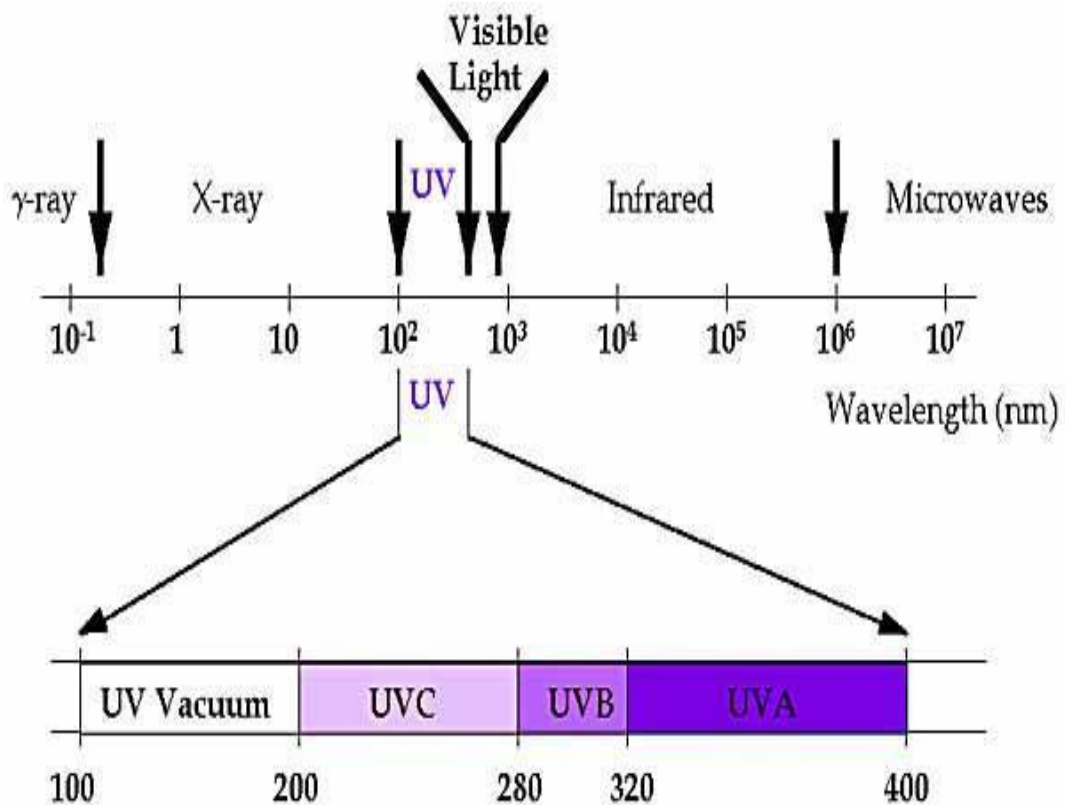


**Figure 1.1 The position of UV in the electromagnetic spectrum**

*Schematic representation of the position of Ultraviolet light in the electromagnetic spectrum. UV is made up of wavelengths from 100 -400 nm. UVC, is the shortest wavelength and most energetic at 100-280nm, UVB is 280-315nm and UVA is the longest wavelengths and least energetic at wavelengths 315-400nm.*

### **1.1 UV irradiation and human health**

The most recent figures from the World Health Organisation (WHO) state that one in every three cancers diagnosed is a skin cancer (WHO, WWW). Globally between two and three million non-melanoma skin cancers (NMSCs) are diagnosed every year and around 130,000 melanomas (WHO, WWW). Ultraviolet light is the etiological factor most strongly associated with the development of skin cancer.

The least energetic of the three subtypes, UVA was originally considered to be fairly harmless, however both UVA and UVB are now recognised as class one complete carcinogens. They are both able to act at each of the three stages of cancer development;

initiation, promotion and progression (IARC, WWW). UVA has been established to contribute 10-20% of the carcinogenic dose emitted from sunlight (de Laat et al., 1997). Increased research into the harmful effects of UVA coincides with the increased popularity of tanning beds, which emit primarily UVA and have now been listed as a carcinogen by IARC after meta-analysis indicated a link between incidence of cancer and use of sunbeds (Boniol et al., 2012). However, it is difficult to draw definitive links between sunbed use and skin cancer due to the relationship between the tendency of an individual to use tanning beds and their tendency to sunbathe (Sage et al., 2012)

Whilst UVA is much less energetic than UVB it is also far more abundant on the earth's surface and able to penetrate deeper into the skin; 50% of UVA rays reach the dermal layer and melanocytes whereas only 14% of UVB rays reach the lower epidermis (Bruls et al., 1984). The difference in the penetrative abilities of UVA and UVB are demonstrated in figure 1.2. UVA is also able to penetrate through glass windows, which block UVB (von Thaler et al., 2010). Earlier data suggested that UVA is not absorbed directly by DNA, instead that UVA was absorbed by photosensitisers in the skin, which become excited upon absorption of UVA and it is these excited photosensitisers which that cause DNA damage (Tyrrell, 2012). However, there is now some evidence to suggest that UVA can be directly absorbed by DNA and is able to cause damage in the absence of photosensitisers (Mouret et al., 2010; Jiang et al., 2009).

### **1.1.1 Skin Structure**

Human skin is made up of two distinct layers, the epidermis and the dermis. The epidermis is primarily made up of keratinocytes, which make up about 95% of the epidermal layer. The remainder is comprised of melanocytes, Langerhans cells, and Merkel cells. The dermis is comprised mainly of connective tissue; consisting of collagen, elastin and glycosaminoglycans, collectively termed the extracellular matrix (ECM). The main constituent of the dermis is the collagen family, which make up 75% of the dry

weight of the skin. To date 20 genetically distinct members of the collagen family have been identified, the most common of these is type I collagen which is about 80-90% of the total collagen content of the skin. Fibroblasts also form part of the dermal layer and play a role in maintenance of the ECM.

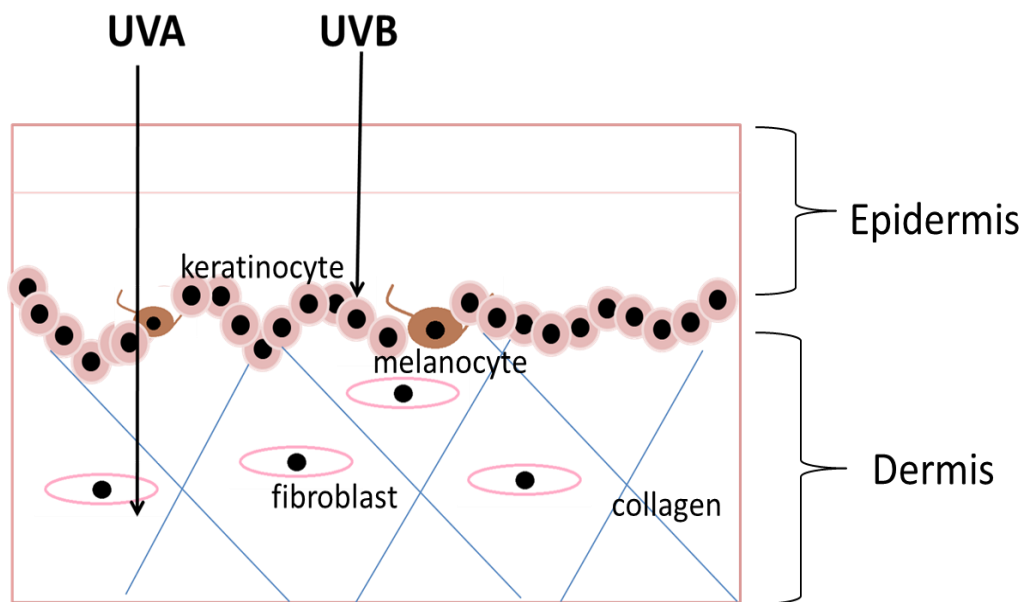


**Figure 1.2 UVA penetrates deeper into human skin compared to UVB.**

*This figure demonstrates the penetrative depths of UVA and UVB wavelengths in human skin. UVA can penetrate deep into the dermal layer of skin, which has led to the suggestion that it could play a greater role in photoaging than UVB. UVA also reaches melanocyte cells in far greater quantities than UVB, this, in part has highlighted the possibility of a larger role for UVA than UVB in the development of melanoma skin cancer.*

It has been suggested that UVA plays a more prominent role in photoaging than UVB; UVA is more penetrating than UVB and a higher proportion of UVA reaches the dermal layers of skin where the hallmarks of photoaging are seen. In addition, Reactive Oxygen species (ROS) have been found to be involved in the mechanism of photoaging and this ROS generation is characteristic of UVA exposure. Photoaging is a condition caused by chronic exposure to UV radiation which has characteristic clinical, histological, cellular and

immunological changes compared to both young skin and chronologically aged skin (Berneburg et al., 2000). The differences between photoaged and chronologically aged skin as well as the mechanisms behind photoaging will be discussed further in chapter 5.

The effects of UVA irradiation in skin cells are wide ranging and can be cell line dependent (Bachelor et al., 2002), wavelength dependent and dose dependent (Byrne et al., 2002).

UVA has been seen to activate a number of signaling pathways; deregulate the expression of a wide range of genes (Bender et al., 1997); cause changes to epigenetic patterns (Chen et al., 2012) as well as modulating the activity of a number of enzymes (Keyse and Tyrrell, 1989). In some cases, the dose needed to elicit these effects is far higher than that of UVB, but still biologically relevant (Bender et al., 1997).

The ability of UVA to cause a wide range of cellular effects is now well accepted. Attempts are being made to identify possible biomarkers for UVA damage. The identification of these biomarkers would serve to improve the testing of sun creams against UVA as the current methods of testing for UVA protection are persistent pigment darkening and immediate pigment darkening and it is not known how biologically relevant this is (Routaboul et al., 1999).

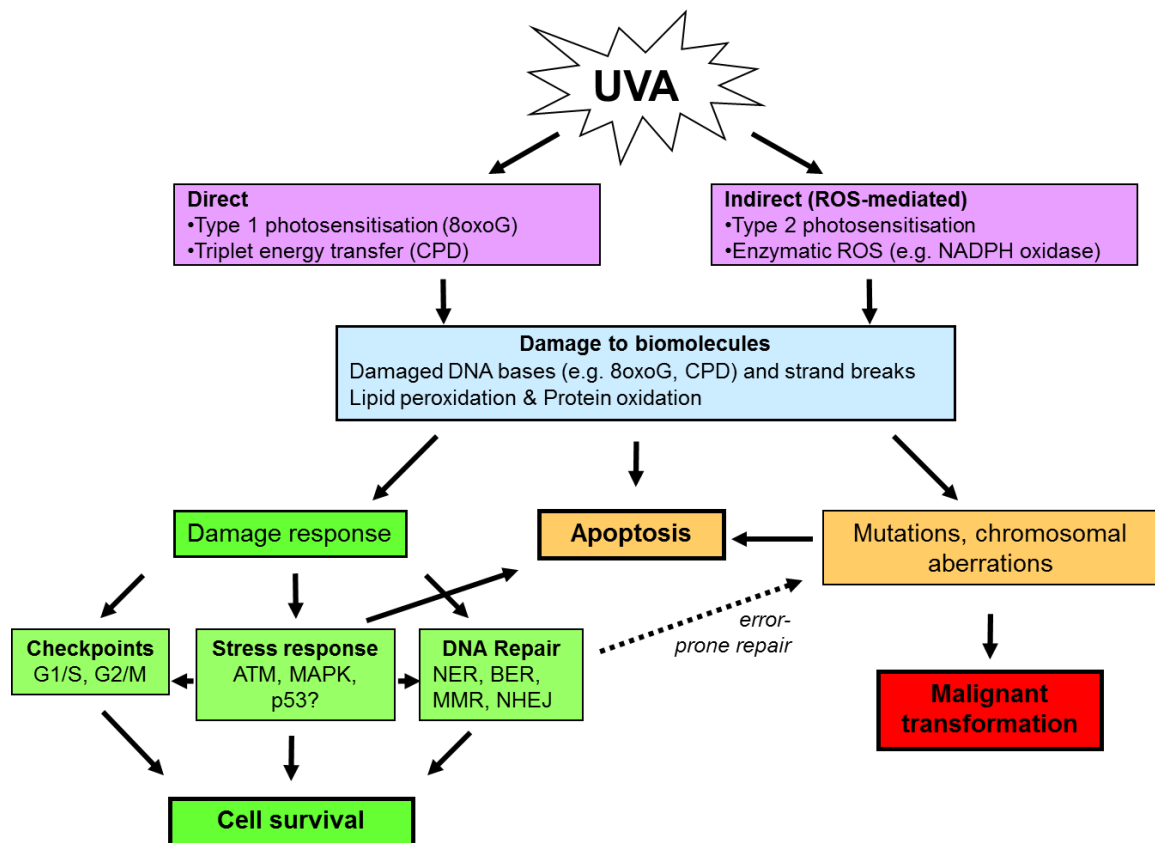


**Figure 1.3 Consequences of UVA exposure**

*Schematic to show the wide-ranging cellular effects that have been seen in UVA targeted cells through the photosensitiser reaction pathways and the consequences of these at a cellular level (Ridley et al., 2009).*

## **1.2 UVA and Carcinogenesis**

### **1.2.1 UVA and NMSC**

The role of UVA in skin cancers has been seen in NMSC (Kelfkens et al., 1990) but a role for UVA in the induction of melanoma remains controversial (Sage et al., 2012). NMSCs arise in keratinocytes and consist of basal cell carcinomas (BCC) and squamous cell carcinomas (SCC); together these make up 90% of all skin cancers diagnosed. However, this value may even be an underestimate due to the way in which these cancers are reported; for example people presenting with multiple BCCs or SCCs are often only counted as one case (Lomas et al., 2012).

Mouse models have shown that UVA alone is able to induce SCCs in mice but without the *TP53* mutations that are characteristic of UVB induced tumour (van Kranen et al., 1997). They additionally analysed the position of UVA and UVB associated adducts and signature mutations in basal and suprabasal keratinocytes from squamous cell tumours and premalignant solar keratosis, a pre-malignant growth which, if left untreated can form SCC. They found that UVA associated fingerprint mutations were found in the basal germinative layer whereas UVB signature mutations were localised mostly in suprabasal layers (Agar et al., 2004). 8-oxoguanine (8-oxoG) which is associated with UVA exposure was found predominantly in the basal epithelial layers. 8-oxoG is the oxidised form of guanine and will be discussed further in section 1.5.1. Whereas, cyclobutane thymine dimers (CPDs), which are more commonly associated with UVB exposure (and will be further discussed in section 1.5.2) were predominantly seen in the superficial layers.

### **1.2.2 UVA and Melanoma**

Melanoma is the rarest and deadliest form of skin cancer and its incidence has been rising annually at a rate faster than any other malignancies (Kohler 2011). Unlike NMSCs the mechanisms and causes behind the development of melanoma are currently unclear, although lifetime exposure to UVR is a well-accepted risk factor (Kanavy and Gerstenblith, 2011).

Molecular studies have shown that melanoma is a heterogeneous disease; the four subtypes of melanoma, acral, mucosal, skin with chronic sun-induced damage or the group on skin without chronic sun-induced damage were shown to have distinct sets of genetic alterations to one another (Curtin et al., 2005), confirming early work that indicated different mechanisms in melanomas on sun exposed and non-sun exposed areas (Whiteman et al., 2003). Common mutations in Melanoma include neuroblastoma ras (*N-ras*) and B- Rapidly Accelerated Fibrosarcoma (*BRAF*) (Davies et al., 2002) and the *BRAF* mutations are almost exclusively found in tumors in areas of the body which are

intermittently exposed to the sun (Maldonado et al., 2003). Conversely, melanomas deriving from frequently exposed areas have infrequent *BRAF* mutations but increased copies of the cyclin D1 (*CCND1*) gene (Curtin et al., 2005).

The role of UVA in the induction of melanoma has been suggested but not been proven (Mouret et al., 2010). UVA, being more penetrative than UVB, is believed to account for up to 99% of the UV that melanocytes are exposed to (Bennett, 2008). Whilst epidemiological evidence strongly suggests that UVA plays a role in the induction of melanoma, the animal models have been inconsistent see section 1.2.3.

The incidence of melanoma varies greatly depending on skin type occurring almost exclusively in Caucasians and with very low incidence in those with darker skin types (Garbe and Blum, 2001). Figure 1.3 demonstrates the worldwide prevalence of malignant melanoma and the increased prevalence of melanoma in countries with populations that are predominantly Caucasian is clear. Additionally, countries at different latitudes receive sunlight with different UVA: UVB ratios; Scandinavian countries receive sunlight with a much higher UVA: UVB ratio than countries closer to the equator such as Australia and have a much higher ratio of melanoma to NMSCs (Moan et al., 1999). Tanning beds emit rays that consist of mainly UVA radiation and recent data suggests that use of a tanning bed is associated with a 75% increased lifetime risk of melanoma (Zhang and Bowden, 2012) and the risk is thought to be furthered increased with repeated use and when initial use occurs at under 35 years old (Boniol et al., 2012).

In addition, a number of studies have found that both pilots and flight attendants have an increased lifetime risk of melanoma (Sanlorenzo et al., 2015). Increased exposure to UVB can be discounted because UVB is unable to pass through the windows but UVA can and so there is some argument to suggest that these individuals are exposed to increased levels of UVA irradiation that could play a role in the increased risk of melanoma seen in these individuals. However, it is unclear what role factors such as cosmic radiation,

lifestyle factors and the disruption of circadian rhythms could have on the increased melanoma risk (Rafnsson et al., 2000; Pukkala et al., 2003). Despite that there is increasing epidemiological evidence that suggest a prominent role for UVA radiation in the development of melanoma.

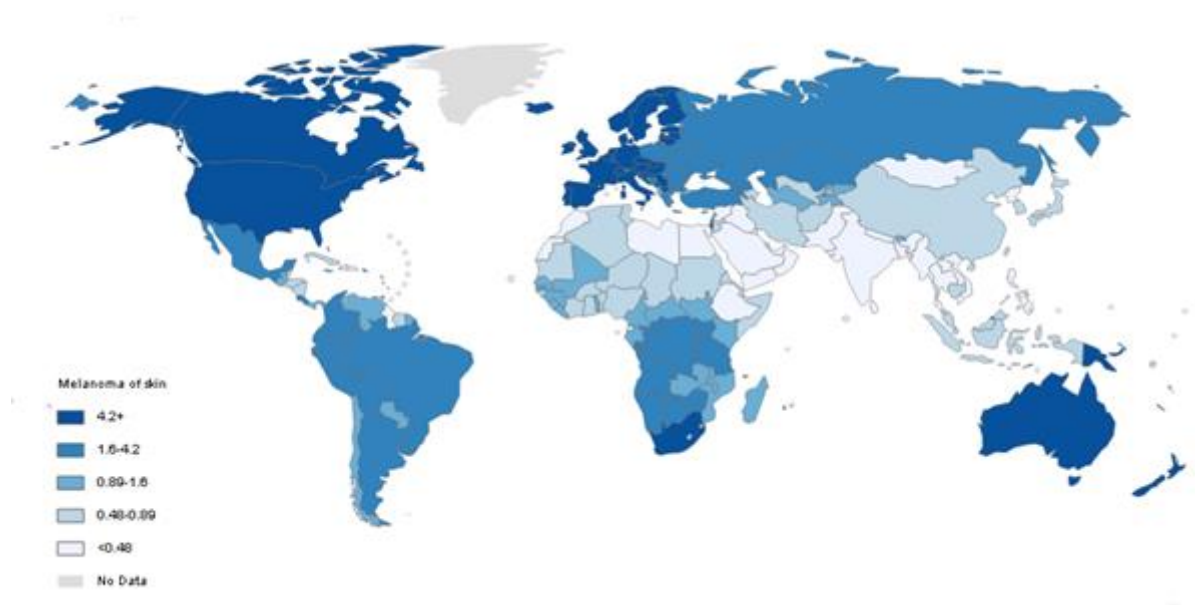


**Figure 1.4 Worldwide prevalence of Malignant Melanoma.** This global map shows that melanoma risk is high in countries with Caucasian populations compared to countries with populations of individuals with darker skin types. (GLOBOCAN, WWW).

### **1.2.3 Animal models of UVA and melanoma**

The ability of UVA to generate melanoma in animal models has been inconclusive and many contradictory studies have been published. Additionally, the validity of the animal models used in such studies has been questioned. When transgenic mice were exposed to UVA or UVB only those exposed to UVB developed melanoma (De Fabo et al., 2004). The *Xiphophorus* fish model previously shown to be susceptible to melanomas following UVA exposure (Setlow et al., 1989) has recently been put under some doubt when a similar but more robust study found that UVA did not induce melanoma formation in the same model (Mitchell et al., 2010). Precursors to melanoma have also been seen to occur in the *Mondelphis domestica* (opossum) after prolonged (81 weeks) exposure to UVA (Ley, 1997) but the suitability of the opossum as model for UVA damage has been put into

question. Opossum have the ability to repair CPD damage by a photolyase enzyme. Photolyases use light as a cofactor to repair CPD damage, with wavelengths between 320nm and 450nm able to activate photolyase (Kusewitt et al., 1991). Photolyase activity is not seen in humans, which makes the suitability of the opossum as a model for any UV carcinogenesis questionable.

A more recent study, (Noonan et al., 2012) utilized HGF (hepatocyte growth factor) transgenic mice (Takayama et al., 1996), which are arguably a better model for human skin; the mice have ectopic extra follicular melanocytes in trunk skin at the dermal/epidermal junction and the epidermis therefore more closely modelling human skin than other animal models used previously. Additionally, the formation of melanoma in these animals also shows significant similarities to the development of melanoma in human skin (Noonan et al., 2000). Noonan et al. (2012) showed that exposure to biologically relevant doses of UVA initiated melanoma formation in HGF transgenic mice but this initiation was dependent on the presence of melanin. UVB initiated melanoma in both the albino and pigmented mice suggesting that UVB induction of melanoma is not dependent on the presence of melanin. This finding suggests the existence of two distinct pathways that could lead to melanoma depending on the type of UV radiation that the individual was exposed to.

The group then went on to examine the DNA damage in the mice exposed to UVA that developed melanoma. They found that the levels of CPDs detected in the mouse skin after exposure was low however 8-oxoG was detected in significant quantities in the nucleus of melanocytes at the dermal epidermal junction but only in the pigmented mice. This suggests that UVA induced melanoma formation may be a consequence of oxidative damage not CPD induced mutagenicity (Noonan et al., 2012), consistent with reports that an oxygen quencher acteylcysteine, delays the onset of melanoma in mice exposed to broadband UV (Cotter et al., 2007)

Further evidence suggesting a role for UVA oxidative stress in melanoma was observed by Mouret et al (2011), who compared the DNA damage profiles of normal melanocytes and keratinocytes when exposed to biologically relevant doses of UVA. They both showed similar levels of CPD induction but the melanocytes accumulated more oxidative damage in the form of oxidised base 8-oxoG. The ratio of CPD: 8-oxoG was 1:4 and 5:2 in melanocytes and keratinocytes respectively. Furthermore, no difference was seen in the yield of single strand breaks in the two cell types a strong suggestion that singlet oxygen is the main mediator of oxidative stress in melanocytes. Singlet oxygen is a high energy form of oxygen present as a single oxygen atom. Singlet oxygen is only able to induce 8-oxoG and does not damage the DNA backbone (Mouret et al., 2011). A further possible detrimental role for melanoma has been seen; UVA induced 8-oxoG production was found to be enhanced by stimulation of melanin synthesis, suggesting a role for either melanin or one of its intermediates in the production of 8-oxoG (Haywood et al., 2006).

Recent work found that nucleotide excision repair is deficient in melanoma following UVA exposure, although further work is needed to establish if this plays a role in melanoma development (Murray et al., 2015). The most recent animal studies are indicative of a role for UVA in the induction of melanoma, but showed that UVA induced melanoma formation is dependent on the presence of melanin, whereas UVB induced melanoma in both albino and pigmented mice. This finding suggests that there are separate pathways for induction of melanoma for UVA and UVB (Noonan et al., 2012). Mouret and co-workers' (2012) recent work has suggested a more prominent role of UVA induced oxidative damage than CPDs in melanocytes.

There are two forms of melanin; eumelanin which is brown/black in colour and pheomelanin which is a reddish yellow colour (Prota, 2000). In general individuals with darker skin have more eumelanin and it is for this reason it is believed they are better protected against UV damage. A black epidermis allows 7.4% of UVB and 17.5% of UVA to penetrate whereas white skin allows 24% UVB and 55% UVA to penetrate (Kobayashi et

al., 1998). Epidemiological evidence shows that the incidence of skin cancer is lower in individuals with darker skin, again pointing at a protective role for melanin. Further evidence comes from the dramatically increased rates of NMSC seen in African albinos, individuals who lack melanin due to defects in the pathways of melanin synthesis. An estimated 1000 fold increase in the development of SCC compared to the normal population is seen in African albinos.

However, evidence also exists to suggest that melanin can have a detrimental role on the health of skin. Pheomelanin is prone to degradation as a result of UV exposure and it is thought that it could contribute to the damaging effects of UV radiation because its degradation produces hydroxide and superoxide anions (Chedekel et al., 1978).

Pheomelanins have also been found to be more oxidative than eumelanin, cells with high levels of pheomelanin were found to have high levels of oxidative damage following UV radiation (Wenczl et al., 1998).

### **1.3 Sources of oxidative stress after UVA**

#### **1.3.1 UVA and photosensitiser reactions**

UVA at a wavelength of between 315nm and 400nm falls outside of the absorption spectra for DNA unlike UVB wavelengths which are readily absorbed. UVC is the most readily absorbed by DNA but is of little relevance when looking at the effects of terrestrial UV exposure and DNA damage because it is fully filtered out by the atmosphere. The absorption spectrum of DNA is shown in Figure 1.5

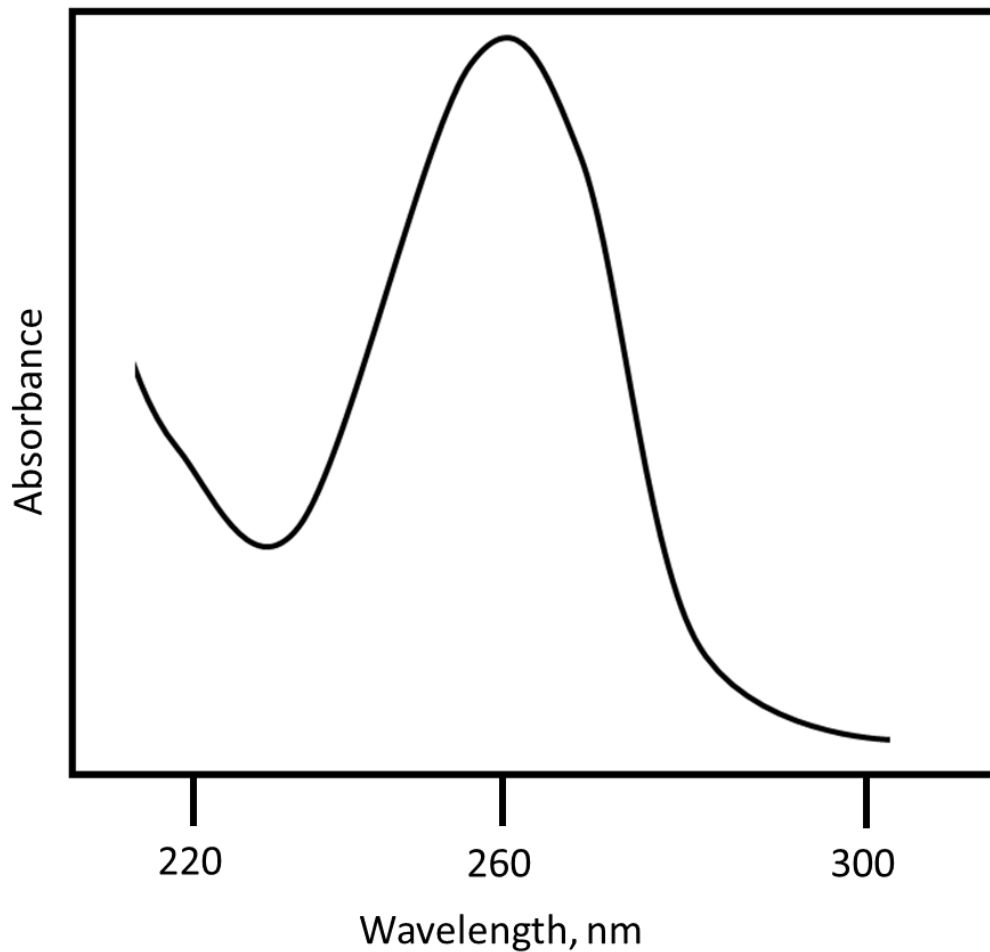


**Figure 1.5 Absorption Spectra of DNA.**

*Shows the absorption spectra for DNA indicating that UVA wavelengths lie outside of those that are readily absorbed by DNA. The DNA maximal absorbs light of wavelength 260nm, which is in the UVC range.*

UVA light is absorbed by endogenous photosensitisers found in tissues; these include riboflavin, flavins and porphyrins (Moreno, 1986). Upon absorption of UVA these sensitisers cross over to a triplet state, due to an electron being transferred to a higher energy orbit (Griffiths et al., 1993). The excitation of these molecules is able to cause cellular damage by two distinct mechanisms each of which allows the photosensitiser to return to its normal state (Straight and Spikes, 1985). Type 1 is electron transfer and hydrogen abstraction processes to yield free radicals; which then go on to produce ROS through reactions with other molecules. Type 2, which can be further split into the major

and minor pathways, the major pathway are the energy transfer from the excited photosensitiser to  $O_2$  to yield the reactive excited state, singlet oxygen (Type II) (Pattison and Davies, 2006). The minor pathway refers to the reaction between a photosensitiser and oxygen to form superoxide or hydroxide molecule (Keyse and Tyrrell, 1990). The type of reaction that takes place upon sensitiser excitation depends on a number of factors including oxygen concentration (Baier et al., 2006).

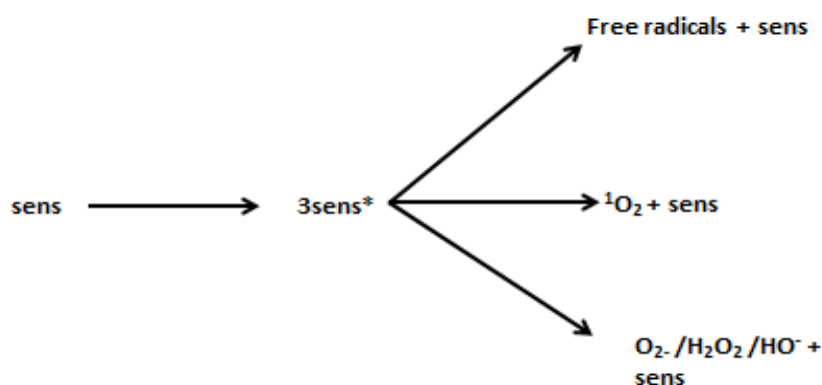


**Figure 1.6 Reaction of UVA with photosensitisers**

*A schematic to demonstrate how UVA causes the formation of ROS by excitation of photosensitisers in the skin which go on to form a number of ROS most notably singlet oxygen.*

**1.3.2 The UVA induction of reactive oxygen species**

Once generated, ROS can go on to cause a number of detrimental effects to the cell; DNA damage; such as single strand breaks and the oxidation of bases as well as lipid peroxidation and the oxidation of proteins. ROS are also known to affect gene regulation as well as signal transduction pathways (Sen and Packer, 1996) and they have the ability

to stimulate some growth factors (Allen and Tresini, 2000). The effects that UVA-induced ROS have on different skin cells will be discussed in the following sections and possible biomarkers for each type of reaction will also be discussed, as well as UVA induced changes seen that are not as a result of ROS production.

### **1.3.3 Singlet Oxygen**

There is significant evidence to suggest that singlet oxygen is the main form of ROS produced by UVA irradiation (Vile and Tyrrell, 1995). The generation of singlet oxygen has been seen to play a role in both UVA-mediated carcinogenesis and photoaging. It has been reported to be involved in a number of events caused by UVA irradiation including cellular death, gene activation (Grether-Beck et al., 1996) activation of protein kinases (Kick et al., 1996), and activation of MAP kinases (Klotz et al., 1997). In addition, the generation of singlet oxygen has been reported to mediate the mitochondrial common deletion that is seen frequently in photoaged skin (Berneburg et al., 1999). The production of singlet oxygen is an event that was first reported in haem oxygenase (HO1) activation (Basu-Modak and Tyrrell, 1993) but has later been seen in a number of other UVA induced genes including Matrix Metalloproteinase 1 (MMP1) (Wlaschek et al., 1994). Singlet oxygen is now considered to be a primary event in UVA mediated gene modulation and is thought to act via generation of oxidised lipids and phospholipids, both of which are powerful signaling molecules (Grether-Beck et al., 2000).

## **1.4 Enzyme mediated processes**

### **1.4.1 NADPH oxidase**

NADPH oxidases (Nox) are a family of membrane associated enzymes. Unlike other cellular enzymes that generate ROS as a by-product of their normal reactions the NADPH oxidases are a direct source of ROS. NADPH oxidases catalyse the reduction of O<sub>2</sub> to superoxide anion using NADH as an electron donor (Lambeth, 2004). The Nox family

modulate a number of redox sensitive intracellular signalling pathways through the generation of ROS, including activation of some transcription factors and the inhibition of some protein tyrosine phosphatases (Bedard and Krause, 2007). Additionally, the Nox family differs from other enzymes in the wide range of stimuli which are able to activate those (Jiang et al., 2010).

These enzymes are multi-unit and the different isoforms can be distinguished by the catalytic subunits (Lambeth, 2004). Isoforms that have been identified are Nox 1-5 and DOX 1/2 and these isoforms have been recognised as mediators of normal physiological functions including signal transduction, innate immunity and biochemical reactions as well as being implicated in a range of pathological conditions including cancer (Lambeth, 2007).

Valencia and Kochevar (2008) examined the effects of a non-cytotoxic dose of UVA (50 kJ/m<sup>2</sup>) on human keratinocytes. They reported that levels of ROS were increased within 5 minutes of exposure to UVA, reaching a peak at 15 minutes and within 60 minutes the ROS levels had returned to that of the non-irradiated cells. They also observed a decrease in ROS following treatments with both DPI, an NADPH oxidase inhibitor and mitochondrial targeted ubiquinone, an antioxidant which becomes localised in the mitochondria. Additionally, they saw that an increase in NADPH oxidase activity was an early event following UVA, and that inhibiting it had little effect on ROS at later time points. This therefore suggests that NADPH oxidase is involved in initial but not prolonged ROS induction following UVA irradiation. Their data suggested a greater role for NADPH oxidase in UVA induced ROS but they also stated that since neither inhibitor fully abrogated UVA-induced ROS there must be another mediator involved.

### **1.4.2 Haem oxygenase**

Haem oxygenase (HO1) is the inducible form of haem oxygenase, a family of enzymes responsible for the degradation of haem to biliverdin and carbon monoxide as well as playing a role in the inhibition of immune responses. *HO1* is the gene whose expression is most significantly up regulated by UVA exposure, it is up-regulated in response to changes in the cells redox status (Lautier et al., 1992), and appears to be triggered by the generation of singlet oxygen (Basu-Modak and Tyrrell, 1993). Lipid peroxidation has also been suggested to play a role in the induction of *HO1* by UVA (Basu-Modak et al., 1996). UVA is able to up-regulate the expression of *HO1* mRNA in human fibroblasts (Keyse and Tyrrell, 1989) although this induction has been found to be cell line dependent and no such induction was observed in keratinocytes (Applegate et al., 1997).

*HO1* appears to play a role in the UVA-induced immune responses (Otterbein and Choi, 2000). The role of UVA in immunosuppression is complex; both the dose and wavelength have been found to play a role in determining the effect that UVA has on immunomodulation. Low doses of long wave UVA between 364 and 385nm has been found to induce immunosuppression but at higher doses this immunosuppression was lost (Matthews et al., 2010). The mechanism behind this bell shaped dose response is currently unclear although it is thought that higher doses of UVA could activate protective mechanisms or inactivate the immunosuppressive pathways activated by lower doses (Byrne et al., 2002). The UVA dose that causes immunosuppression is equivalent to 5 minutes of midday sunlight (Byrne et al., 2006). HO1 activity induced in murine skin by UVA has been shown to be associated with immune-protective effects of UVA against UVB associated immunosuppression, an effect which was abrogated when HO activity was inhibited (Reeve and Tyrrell, 1999; Allanson and Reeve, 2004).

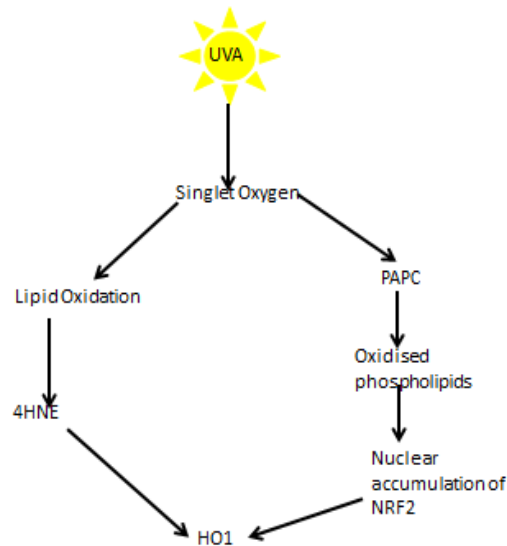


**Figure 1.7 UVA induced expression of HO1**

*Schematic representation of the mechanism behind increased HO1 expression as result of exposure to UVA. Singlet oxygen has been found to mediate this reaction through the oxidation of both lipids and phospholipids.*

Gruber et al (2007) suggested that oxidation products of phospholipid – 1- palmitoyl – 2 arachidonoyl – sn – glycerol – 3- phosphorylcholine (PAPC), a major component of cell membranes and lipoproteins could play a role in HO1 induction. They showed that the oxidation products of PAPC induced *HO1* in both fibroblasts and keratinocytes and the formation of these oxidation products was mediated by UVA exposure. In addition they studied gene expression changes induced by either UVA or UVA induced PAPC oxidation. UVA was found to modulate the expression of over 300 genes, whereas UV-PAPC modulated the expression of 48 genes, indicating that only part of the UVA response is mediated by the signaling of oxidised phospholipids. The genes that were modulated by both treatments were found to be mainly of cytoprotective and detoxifying properties (Gruber et al., 2010).

### **1.5 DNA damage by UV**

Ultraviolet radiation is able to induce a variety of DNA lesions and in turn cause the activation of a variety of DNA repair pathways to repair the lesions. Table 1.1 summarizes the main types of lesion that can occur following exposure to UV and describes the DNA repair pathway activated in each case. The ability of UVA and UVB to induce DNA lesions will be discussed in the following section.

<b>Lesion type</b>	<b>DNA repair pathway activated</b>
CPD/ 6-4PP	Nucleotide Excision repair
8-oxoG	Base Excision repair
Abasic site	Base Excision repair
Double strand break	Homologous recombination / non-homologous end joining
Single strand break	Ligation/ base excision repair.

**Table 1.1 The main DNA repair pathways responsible for repairing each type of DNA lesion**

The nucleotide excision pathway (NER) is the main pathway responsible for the removal of CPDs (Gillet and Schärer, 2006). The NER pathway detects and repairs lesions which cause chemical and structural alterations to the DNA double helix (Batty and Wood, 2000). The damage is detected by two different pathways before they converge to the same pathway. The transcription coupled repair pathway detects lesions occurring in transcribed regions of the DNA, mutations in components of this pathway Excision repair cross complementation group 6 (ERCC6) and Excision repair cross complementation group 8 (ERCC8) result in Cockayne syndrome, a disorder associated with neurological abnormalities but no increase in incidence of skin cancer (Nance and Berry, 1992). The global genome repair pathway detects lesions throughout the whole genome, in both

transcribed and non-transcribed regions, pathological mutations in Xeroderma Pigmentosum, Complementation Group A-E (XPA-XPE) and Damage specific DNA binding protein 2 (DDB2) are seen in Xeroderma Pigmentosum (Cleaver, 1968), a disease characterized by increased risk of skin cancer and increased sensitivity to UV. The disorders associated with nucleotide excision repair deficiency are discussed in more detail by Cleaver et al., (2009)

### **Table 1.1 DNA repair pathways activated by UV-induced lesions**

#### **1.5.1 8-oxoG**

8-oxouanine (8-oxoG) is detected in cells following exposure to all types of ultraviolet light. 8-oxoG is produced indirectly by a photosensitiser mediated reaction in the presence of singlet oxygen (Cheng et al., 1992). It is the most common form of oxidative base damage, guanine being the base with the highest reducing potential and therefore the most susceptible to oxidative damage (Collins et al., 1996). ROS can also act to form both single strand breaks (Kielbassa et al., 1997) and protein cross links although these are much less common than 8-oxoG.

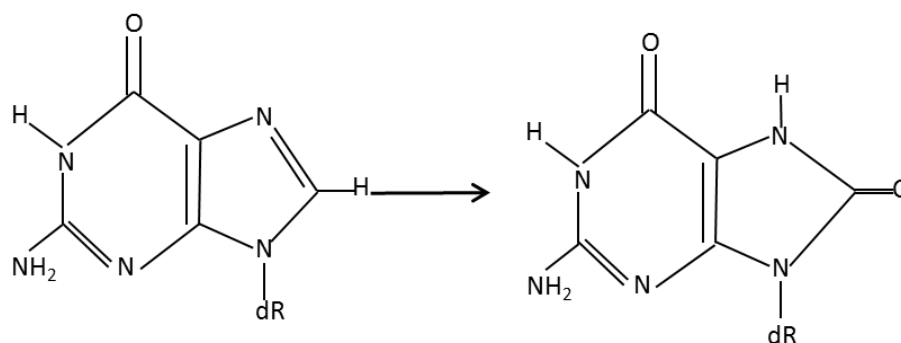


**Figure 1.8 The formation of 8-oxoG from guanine**

There is contradicting evidence as to whether 8-oxoG contributes significantly to the mutagenic properties of UVA. Its hallmark mutation is G to T transversions from the mispairing of 8-oxoG with adenine but these mutations have rarely been seen in UV mutation spectra (Drobetsky et al., 1995). Mice knockouts of 8-oxoG DNA glycosylase (OGG1), the enzyme which removes 8-oxoG, showed no increase in BCC formation following UVA exposure, suggesting that 8-oxoG mutagenicity lacks a role in the initiation of BCC (Kappes et al., 2006). In contrast, decreased levels of human OGG1 were detected in BCC cells, implicating a potential role for 8-oxoG in BCC (Huang et al., 2012).

### **1.5.2 UV and cyclopyrimidine dimers**

The primary DNA lesion following UVB exposure is the formation of CPDs and 6-4 photoproducts (6-4PP), both of which are formed when UVB is directly absorbed by DNA (Cadet et al., 1992). The role of these lesions in UVB induced carcinogenesis will be discussed in greater detail in section 1.11. Originally it was not thought that UVA would induce CPDs but it has now been found that UVA at doses as low as 40 kJ/m<sup>2</sup> is sufficient to induce CPDs. The presence of UVA-induced CPDs has been seen in both cultured cells (Kvam and Tyrrell, 1997; Perdiz et al., 2000; Freeman et al., 1989; Freeman and Ryan, 1990) and skin (Freeman et al., 1989; Young et al., 1998). Even at very low doses CPDs are still present at twice the abundance of 8-oxoG in human skin cells exposed to UVA (Courdavault et al., 2004) and in whole skin (Mouret et al., 2006).

Unlike in response to UVB irradiation, CPDs produced from UVA exposure only form at TT sites not CC or CT sites (Douki et al., 2003; Rochette et al., 2003) and the yield of CPDs from UVA is 10<sup>4</sup> – 10<sup>5</sup> less than that caused by UVB (Kuluncsics et al., 1999). Whilst CPDs are now considered to be the predominant lesion, the ratio of CPD to 8-oxoG depends on radiation conditions and cell and skin types (Rünger and Kappes, 2008).

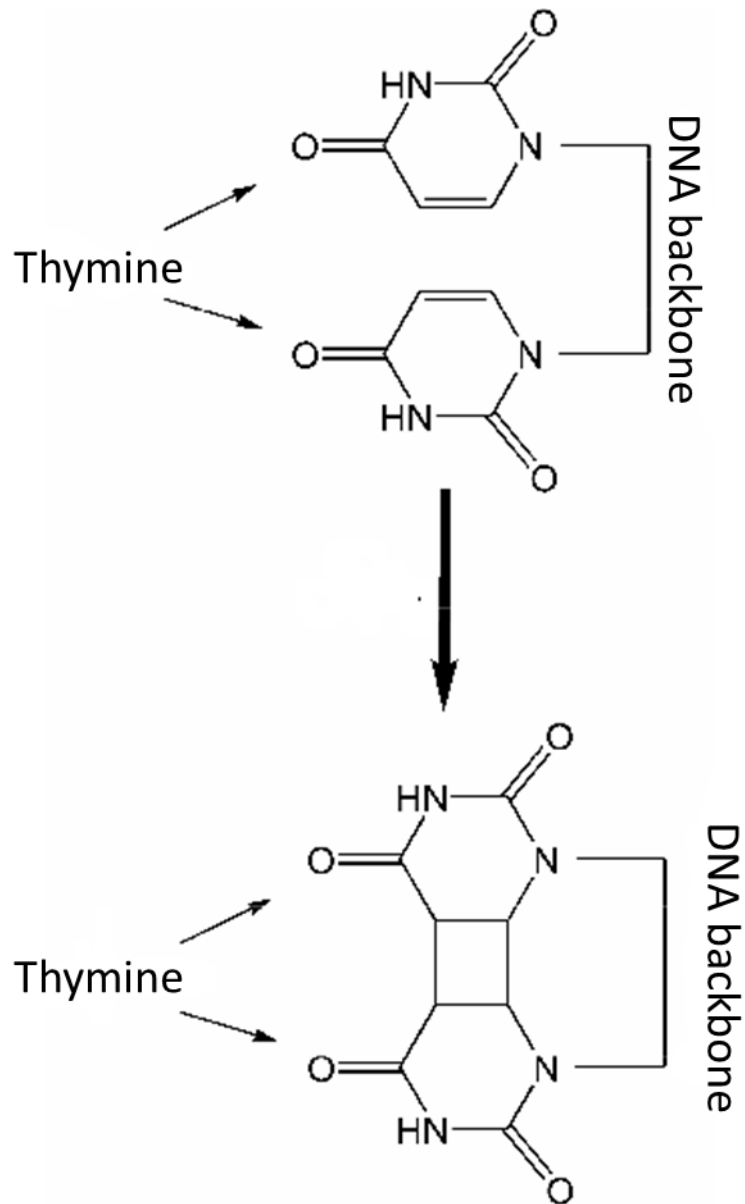


**Figure 1.10 The formation of CPDs**

*A schematic representation of the formation of CPD formation from two adjacent thymine bases.*

As previously mentioned, UVA falls outside of the wavelengths of light that are absorbed by DNA, therefore it is unable to act directly upon DNA, instead inducing effects as a result of photosensitiser mediated mechanisms. However, Jiang et al (2009) detected the presence of CPDs in isolated DNA and suggested that UVA may be able to directly induce CPDs in the absence of photosensitisers. In addition, later work by a different group detected similar yields of CPDs in isolated DNA and human keratinocyte cells after

exposure to UVA (either 500 or 1000 kJ/m<sup>2</sup>). CPDs were also detected in synthetic DNA after exposure to UVA confirming that their presence in isolated DNA was not because of contamination. The CPDs in whole cells and isolated DNA show similarities in both efficiency and their distribution, indicating that the mechanism is the same in each case and there is no photosensitiser involved in UVA induced CPDs (Mouret et al., 2010). Although the doses of UVA used in these studies were higher than those used in earlier work so this could possibly be true only at high doses of UVA.

Intriguingly, a higher ratio of CPD:mutation has been observed following UVA compared to UVB irradiation. Previously it had been suggested that the increased level of mutagenicity is related to oxidative effects of UVA irradiation which cause additional mutations (Enninga et al., 1986). However, the predominance of C to T transitions in UVA irradiated cells suggests that this is not the case (Rünger and Kappes, 2008) and that this increase in mutations following UVA is as a result of unrepaired CPDs. The same group used equi-mutagenic doses of UVA and UVB to irradiate fibroblast cells and measured CPD formation. They found that significantly more CPDs were formed when cells were exposed to UVB, further supporting the idea that repair of CPDs following UVA is less competent than following UVB.

Runger et al (2012) proposed that the higher cellular responses were activated less strongly following UVA than UVB leading to increased persistence of CPDs. Previously it has been reported that p53, a central regulator of the DNA damage responses was significantly less activated following UVA compared to UVB (Kappes et al., 2006). Here they reported on the effects that equi-mutagenic doses of UVA and UVB have on DNA replication, cell cycle progression, DNA repair and apoptosis in human fibroblasts. The group identified UVB to have a much greater effect on DNA replication and repair. Excision repair cross complementation group (XPC) central component of the NER pathway was seen to be more strongly and persistently upregulated following UVB. There

was a more prolonged cell cycle arrest detected at all stages of the cell cycle following UVB compared to UVA. Furthermore UVB irradiation resulted in a greater induction of apoptosis than UVA. They concluded that the difference between cell cycle progression, DNA repair activation and apoptosis induction following UVA and UVB was significant and together, these account for the increased mutagenicity seen from UVA-induced CPDs (Rünger et al., 2012).

Recent work found that nucleotide excision repair is deficient in melanoma cell lines compared to primary melanocytes following UVA exposure. Alterations in the global genome repair pathway were detected in melanoma cell lines following exposure to UVA. These included delayed expression of *XPC*, *DDB1*, *DDB2* and *Tp53*, resulting in a delay in CPD repair in the melanoma cell lines compared to melanocytes. This work was indicative of a role for UVA induced CPDs in melanoma development although further work is needed to confirm these findings (Murray et al., 2015).

### **1.5.3 Dark CPDS**

Recently the induction of delayed CPD formation has been seen in pigmented melanocytes following both UVA and UVB exposure. The formation of CPDs was seen to continue for 3 hours after exposure to UVA, at this point further increase in CPD induction was offset by concurrent repair. Interestingly the predominant form was TC + CT/TT, in contrast to the TT CPDs that are historically associated with UVA exposure (Premi et al., 2015); these are also the mutations that have been seen to occur frequently in sunlight induced melanomas (Brash, 2016).

### **1.6 The ability of UVA to form Double Strand Breaks**

Double strand breaks (DSBs) are considered to be the most dangerous form of DNA damage; repair of DSBs is critical to avoid cell death, chromosomal aberrations, and mutations. In some cases, presence of DSBs can directly initiate pathological events such

as cancers (Mah et al., 2010). The presence of UVA induced, double stranded breaks (DSBs) has been a subject of debate over recent years; particularly since UVA alone is not energetic enough to break the covalent bond directly (Cadet et al., 2009)

While it is now accepted that replication dependent DSBs can occur as a result of UVA exposure (Limoli and Ward, 1994), the data on the existence of replication independent DSBs has been conflicting. Much of the work has focused on detecting upregulation of the DNA damage response (DDR), such as increased  $\gamma$ H2AX to infer the presence of double strand breaks. Some groups finding no existence of DSBs even when using very high doses (400 kJ/m<sup>2</sup>) of UVA (Rizzo et al., 2011) while others have gained data to support the existence of UVA-induced DSBs through the induction of a number of biological endpoints associated with DSBs. These have included micronuclei formation, clonogenic survival (Phillipson et al., 2002) and the formation of  $\gamma$ H2AX foci (He et al., 2005; Greinert et al., 2012b).

The formation of double strand breaks detected by increased number of  $\gamma$ H2AX foci and the neutral comet assay were seen after exposure to UVA has been recently observed in both HaCaT cells and fibroblasts, implying the existence of a common mechanism of DSB formation and not a mechanism dependent on cell line. The addition of antioxidants was found to prevent the formation of DSBs, suggesting a key role for ROS in the induction of DSBs. Additionally, the rate of DSB formation was higher in cells exposed to split doses of UVA when compared to cells exposed to a single irradiation equaling the same total dose. This finding suggests the involvement of a sensitiser that becomes depleted in the cells exposed to single dose UVA and when a split dose of UVA is applied the photosensitiser becomes replenished so is no longer a limiting factor in the UVA induced formation of DSBs (Greinert et al., 2012b).

### **1.6.1 H2AX phosphorylation and the DNA damage response**

The DNA damage response is crucial to maintaining genome instability following changes to chromatin structure. The DNA damage response is a complex network of pathways which prevent DNA lesions causing genomic stability. The DDR comprises of DNA repair mechanisms, made up of specific pathways tailored to process each type of DNA lesion (these are described in table 1.1), as well as activation of cell cycle checkpoints, to slow replication and allow the cell time to repair damage and to prevent damage DNA from being replicated and tolerance processes which allows the bypass of lesions and replication to continue (Hoeijmakers, 2001). There is extensive crosstalk between these pathways which allow for proper repair of lesions, in particular between the DNA repair pathways and the activation of cell cycle checkpoints which allow for additional time to repair the damage (Bartek and Lukas, 2007). The cell cycle position at which the cell is arrested is dependent on the type of damage that has occurred (Zhou and Elledge, 2000).

H2AX is a subtype of histone 2, making up approximately 10% of all H2A molecules in the nucleosomes, it is present in approximately every 5 nucleosomes. However, the ratio of H2A types varies between cell lines, although the reason for this is unknown (Rogakou et al., 1998). The formation of  $\gamma$ H2AX is widely accepted as a marker for measuring activation of the DDR; H2AX is rapidly phosphorylated and recruited to the DNA in response to double strand breaks (Burma et al., 2001) and stalled replication forks (Ward and Chen, 2001). When activated,  $\gamma$ H2AX acts a signaling molecule to downstream effectors, which vary depending on which pathway has been activated.

H2AX phosphorylation ( $\gamma$ H2AX) is thought to contribute to DNA repair and increasing genome stability in a number of ways; the modification increases accessibility to the DNA leading to increased accumulation of DNA repair proteins, sends an epigenetic signal to downstream repair proteins,  $\gamma$ H2AX recruits cohesins that prevent loss of large chromosomal regions where DNA breaks have occurred. At low levels of DNA damage

$\gamma$ H2AX is involved in cell cycle checkpoint responses, however when DNA damage is higher this is not seen suggesting an alternative pathway occurs to manage cell cycle checkpoints at high levels of DNA damage (Mah et al., 2010).

### **1.6.2 Mechanism of H2AX phosphorylation**

As mentioned above H2AX is phosphorylated at serine 139 in response to DSBs; in recent years much research has gone into identifying the mechanism by which this phosphorylation occurs. H2AX is a substrate of several phosphoinositide 3 kinase related protein kinases (PIKKs) including Ataxia telangiectasia mutated (ATM), ataxia telangiectasia and Rad3-related protein (ATR) and DNA dependent protein kinase (DNA-PK). The PI3K family is activated immediately after DNA damage and act as transducer proteins playing a role in the control and progression of the cell cycle, remodeling of chromatin as well as DNA repair (Rogakou et al., 1998). ATM is activated by DSBs (Burma et al., 2001) whereas ATR is recruited to single strand break regions, which arise at stalled replication forks or during the processing of bulky lesions including UV photoproducts (Zou and Elledge, 2003).

The rapid phosphorylation of ATM in response to double strand breaks has been seen to be MRN dependent. In cells expressing mutated MRN or in MRN knockdown cells ATM signaling has been seen to be defective. The MRN complex is made up of MRE11, RAD50 and NBS1 and this complex is associated with the phosphorylation of ATM at serine 1981 as well as its recruitment to DNA damage sites (Lee and Paull, 2005). This was seen in multiple cell lines including HeLa, lymphoblastoid cells and normal fibroblast suggesting that this is likely to be a global mechanism and not a cell line dependent one (Carson et al., 2003; Uziel et al., 2003). The recruitment of the MRN complex to the site of the DSB is a very early event and has been confirmed to act as a sensor of DSBs (Petrini and

Stracker, 2003). Consistent with this work the levels of the MRN complex have been demonstrated to be constant throughout all stages of the cell cycle, further indicative of its role as a damage sensor (Maser et al 1992). In addition to its activation by the MRN complex in response to DSBs. ATM can also be activated by changes in chromatin structure that do not result in the formation of double strand breaks in a MRN independent mechanism. The levels of ATM that are seen in response to changes in chromatin structure initiated by treatment with hypotonic solution are similar to that seen following exposure to ionising radiation (Bakkenist and Kastan, 2003). Additionally, inhibition of histone deacetylases has also been seen to activate ATM (Lee, 2007; Jang et al., 2010).

Phosphorylation of H2AX at serine 139 as well as its recruitment to the sites of damage rapidly follows. As well as acting as a marker for DNA damage  $\gamma$ H2AX plays a crucial role in the DDR and acts to amplify the signal of damage to aid DNA repair. Following its phosphorylation and subsequent recruitment to the damage  $\gamma$ H2AX recruits the Mediator of DNA damage checkpoint 1 (MDC1) (Stucki et al., 2005) to the break, this in turn continues the activation of ATM, generating a positive feedback loop to enhance H2AX phosphorylation (Stucki and Jackson, 2006), this creates the chromatin modification required for the efficient binding of p53 binding protein 1 (53BP1) (Bekker-Jensen et al., 2005). Recruitment of 53BP1 results in recruitment of RNF8 to phosphorylated MDC1, which subsequently results in polyubiquitination of H2AX to recruit BRCA1 (Huang and D'Andrea, 2006). The activation of ATM also leads to the activation of a number of other signaling molecules that play a role in cell cycle progression and DNA repair; these include; p53, Chk2 and Brca1.

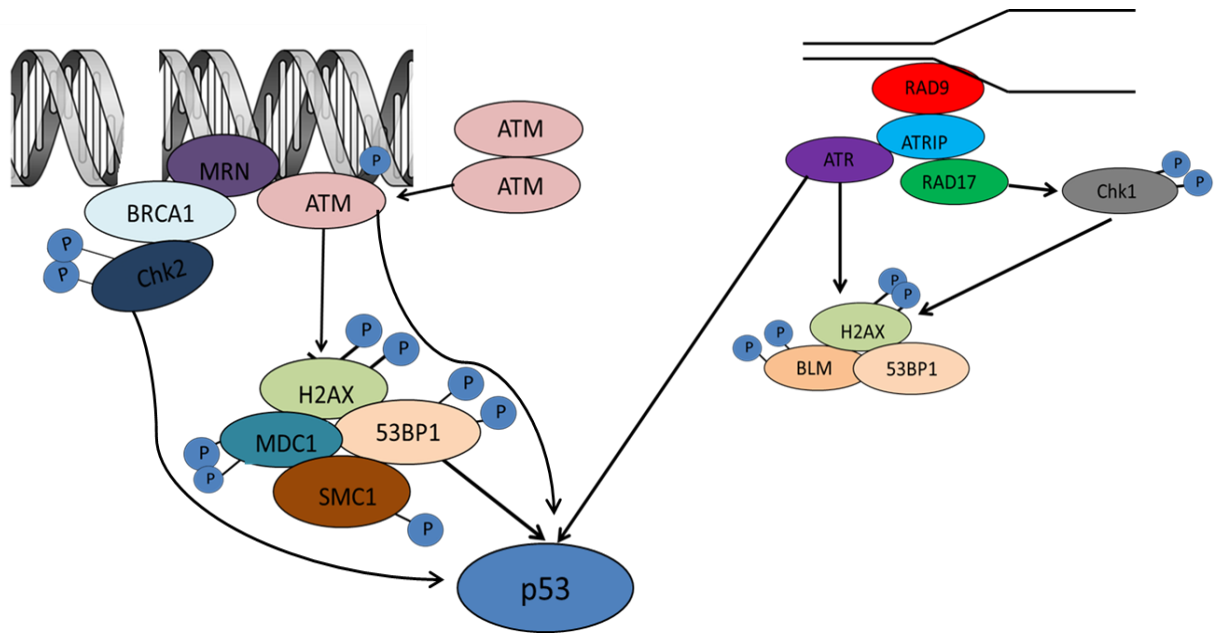


**Figure 1.9 The mechanism behind the phosphorylation of gamma H2AX.**

*This figure demonstrates the two distinct pathways that phosphorylate H2AX following the detection of either double strand breaks or stalled replication forks. Double strand break formation stimulates the recruitment of the MRN (Mre11–Rad50–Nbs1 ) complex, this recruitment stimulates the phosphorylation of ATM at serine 1981 and also its recruitment to the DNA and out of its dimeric form. The phosphorylated ATM then goes on to phosphorylate the histone H2AX and facilitates its recruitment to the site of damage. The presence of stalled replication forks is detected by ATR, which phosphorylates H2AX and other DNA damage response signaling molecules which are distinct from those activated by ATM*

The activation of ATM has been detected following UVA but not UVC irradiation in both mouse and human fibroblast cell lines. UVA induced apoptosis has been found to be dependent on the activation of ATM whereas UVC induced apoptosis is ATM independent. Furthermore, the activation of both UVA induced JNK and p53 has been seen to be dependent on the activation of ATM (Zhang et al., 2002) suggesting that the activation of ATM could be a key mediator in a cells avoidance of UVA induced photo carcinogenesis.

### **1.6.3 H2AX in mitotic cells**

In addition to its role in the repair of double strand breaks  $\gamma$ H2AX has also been seen in un-irradiated cells, where two different populations of foci were seen; one population consisted of large foci that were morphologically similar to those seen detected following ionizing radiation, the other populations were smaller and less intensely stained. The smaller foci were not found to co-localise with proteins associated with DNA repair (McManus and Hendzel, 2005). Cell cycle analysis showed that the abundance of the smaller  $\gamma$ H2AX foci increases as the cell cycle progresses, but instead of peaking in S phase as may be expected the peak was seen in mitotic cells. Efforts have been made to understand the upstream effector of H2AX phosphorylation in untreated cells, but results have been conflicting; with one group finding it to be ATM dependent (McManus and Hendzel, 2005) whereas a conflicting report found that DNA-PKcs was responsible (Tu et al., 2013), and a third group found no role for either ATM or DNA PK in H2AX phosphorylation in cells lacking DNA damage (Ichijima et al., 2005).

### **1.7 UVA and stress response pathways**

UV radiation is considered one of the most important environmental stresses for skin damage (López-Camarillo et al., 2012). Following exposure to UVA and the generation of oxidative cellular stress a number of signaling pathways are activated which could give rise to changes in gene expression of signaling molecules and activation of transcription factors resulting in differential gene expression and protein production which can lead to change in levels of enzyme activation. Of particular importance is the ability of the cell to resist apoptosis in order for the mutations to survive and spread. Better understanding of the pathways involved could give rise to increased understanding of tumour initiation and progression (Zhang and Bowden, 2012) and give rise to better chemotherapeutic drugs (Syed et al., 2006).

### **1.7.1 MAPK**

The Mitogen Activated Protein Kinase (MAPK) signaling pathways are made up of a number of signaling components, they play a vital role in the cell, converting stimuli on cell membrane into a wide range of cellular responses by transfer of the signal to the cell's nucleus (Wagner and Nebreda, 2009). The response initiated by the MAPK is dependent on the stimuli which caused its activation (Winter-Vann and Johnson, 2007). They can be divided into three subsets of pathways; p38 MAPK, JNK and ERK.

The MAPK family can be activated by a wide range of stimuli and their activation is through activation of at least two enzymes upstream. Stimuli activate MAPKKK which phosphorylates and activates the MAPKK, which then causes activation of the MAPK through dual phosphorylation of the Threonine Tyrosine motif on its activation loop (Seeger and Krebs, 1995). The regulation of MAPKs is tightly regulated and this regulation is paramount to the health of the cells as all members of the MAPK family have been seen to play roles in both cell health and cell death. Sustained activation of the MAPK family has been seen to induce adverse effects including increased proliferation and cell death (Winter-Vann and Johnson, 2007).

Although there are conflicting data about the ability of UVA to activate all three pathways: UVA can activate p38 and c-Jun N-terminal kinases (JUN) but not Extracellular signal-regulated kinases (ERK) in fibroblasts (Klotz et al., 2001) but a paper by Zhang et al (2001) suggested UVA activates all 3 pathways. It has since been suggested that activation of different MAPK pathways could be dependent on both dose of UVA and the cell type (López-Camarillo et al., 2012). Activation of these pathways is also wavelength dependent and the pathways activated by UVA vary to those activated by UVB (Syed et al., 2012). MAPKs were not activated in mouse keratinocytes after UVA exposure but have been seen to be activated in human skin, suggesting that a separate component, found in human skin

could play a role in regulation of MAPK activation in human keratinocytes (López-Camarillo et al., 2012).

### **1.7.2 UVA-dependent phosphorylation of ERK**

ERK was the first MAPK characterised it has 8 isoforms, of which ERK1 and ERK2 have been studied extensively (Zhuang and Schnellmann, 2006) . They are widely expressed and play a role in regulation of mitosis and meiosis as well as regulating post mitotic functions of differentiated cells. A great number of stimuli have been found to activate these pathways including cytokines, carcinogens and growth factors, the latter being the pathway that is best understood. Oncogenic Ras has also been seen to activate this pathway leading to increased proliferation as well as the investigation into use of ERK inhibitors as anti-cancer drugs (Johnson and Lapadat, 2002).

An extensive study by He et al (2004) found that UVA activates ERK in a dose and time dependent manner in HaCaT cells. Post irradiation, increased ERK phosphorylation was not detected after 1 hour but a significant increase was seen after 3 hours and up to 15 hours after irradiation. Ras activation was also seen to increase after UVA irradiation in the same time span as ERK and exposure of cells with negative Ras showed a dramatic decrease in ERK activation showing UVA induced ERK activation is Ras dependent. ERK activation was also seen to be dependent on PKC. These results were seen in a number of different cell lines so ERK activation proving ERK activation is not cell line specific (He et al., 2004) in addition sustained ERK activation has been shown to protect cells from photodynamic therapy (Tong et al., 2002). Photodynamic therapy is a form of cancer therapy where patients are treated first with a photosensitiser, which enter all cells, then are later treated with UVA light at a time point where the photosensitiser has left the normal cells but remains present in tumour cells. The reaction between the

photosensitizer and light then produces ROS which kill the neighboring tumour cells (Dolmans et al., 2003).

The activation of p38 and JNK pathways is now thought to be a key event in the UVA response (Zhang and Bowden, 2012). These two pathways are often referred to as stress activated protein kinases due to their sensitive reaction to external stressors such as UV exposure. They both function in a cell context specific and cell type specific manner in order to generate signals which affect a great number of cell functions and are both seen to be deregulated in a number of human cancers (Wagner and Nebreda, 2009). P38 and JNK are activated immediately within 5 minutes after UVA irradiation and reach a peak after 30 – 45 minutes in HaCaT cells (Zhang and Bowden, 2012).

### **1.7.3 UVA activation of p38**

Numerous studies have found p38 to be activated by ROS (Pan et al., 2009) and UVA has been found to activate p38 MAPK in a number of different cell lines, although the dose needed to cause activation does differ (Zhang and Bowden, 2012). Activated p38 has a wide range of substrates, but most interestingly it has been seen to cause both anti-apoptotic and pro-apoptotic effects. The apoptotic effects of p38 after UVB irradiation are well established but recently Zhang and Bowden (2012) gained data that showed p38 had anti apoptotic effects in UVA irradiated HaCaT cells; Inhibition of p38 of irradiated HaCaTs showed a great increase in apoptosis. The non-functional p53 (Lehman et al., 1993) in HaCaTs has been suggested as a possible explanation for this controversial finding. Activation of p38 causes increased expression of Cox-2 through the increased stability of mRNA leading to increased expression (Bachelor and Bowden, 2004a) and B-cell lymphoma-extra large (Bcl-XL). Animal models of p38 $\alpha$  have proved tricky, p38 $\alpha$

knockout mice are non-viable. However a skin specific knockout has been developed and shows a significant inhibition in tumourigenesis (Bachelor and Bowden, 2004b).

Activation of MAPK by UVA-generated ROS has been heavily implicated in playing a role in regulation of gap junction intercellular communication (GJIC). This area has gained interest in recent years because the pathways involved have been suggested as good targets for combating the detrimental effects of UVA including carcinogenesis and photoaging. The disruption of GJIC is widely believed to have a role in tumour development and progression as GJIC is involved in a number of keratinocyte processes including differentiation and growth (Provost et al., 2003).

P38 MAPK reduces GJIC via phosphorylation of protein connexin 43 (cx43) which compromises its expression. Phosphorylation of cx43 has a number of effects relating to GJIC, it affects opening and closing of the channels as well as affecting the number of active channels via its effects on the synthesis of cx43 which through a positive feedback mechanism further increases the expression of cx43. The cumulative effects are seen in aberrant GJIC (Wu et al., 2011). A role for ROS in GJIC has been heavily implicated; a strict correlation has been observed between free radical production and decreased GJIC. In keratinocytes treated with N-acetylcysteine, a free radical scavenger, the decrease in GJIC was partially prevented further suggesting a role for ROS in the decrease GJIC (Bellei et al., 2008).

#### **1.7.4 UVA activation of JNK**

The JNK family are also activated in response to stress including UV, in the case of UVA; they are activated by the presence of singlet oxygen as proven by an increased activation of JNK in the presence of deuterium oxide which increases the lifetime of singlet oxygen

(Klotz et al., 1997). The major target for JNK signalling is the activation of activator protein 1 (AP1) via the phosphorylation of subunit JUN. It is the activation of AP1 that is considered the prime oncogenic function of JNK.

Activation of JNK can have diverse effects on the cell, in some cases promoting apoptosis (Sluss et al., 1994) and in some proliferation (Schwabe et al., 2003), these effects are thought to be dependent on stimuli and the strength of JNK activation (Lin and Dibling, 2002). The effects have also been seen to be dependent on the member of the JNK family that has been activated; JNK2 has been linked to degradation of JUN whereas JNK1 phosphorylates JUN leading to activation of AP1 and has also been linked to senescence via p53. AP1 is a transcription factor complex comprised of two heterodimers Fos and Jun. It is well established that MAP kinases are able to directly phosphorylate the proteins of the AP1 complex therefore directly affecting its activity (Whitmarsh and Davis, 1996). Activation of JNK family are also linked to expression of cytokines which control inflammation and cancer although not as strongly as seen by p38. Mutations of JNK have also been seen in human cancers.

The MAPK family are responsible, in part for the increased expression of C-JUN in response to UVA exposure. MAPK enzymes are situated directly upstream of C-JUN in a number of pathways which lead to increased expression of C-JUN and therefore an increase in AP1 which directly initiates the increase in MMPs, enzymes which play a critical role in photoaging of the skin. C-JUN has been suggested as a good potential biomarker for photoaging.

### **1.7.5 UVA activation of AP1 and its role in carcinogenesis**

There is increasing evidence to suggest that UVA increases AP1 activation in multiple cell lines, but the MAP kinase responsible for the observed increase has been observed to vary between cell lines (Bachelor and Bowden, 2004b). AP1 has been shown to be involved in both skin tumour promotion and progression; increased levels of AP1 have been seen in tumour promotion sensitive cells compared to tumour promotion resistant cells (Bernstein and Colburn, 1989) and AP1 levels have been observed to be higher in malignant tumours compared to benign (Domann et al., 1994).

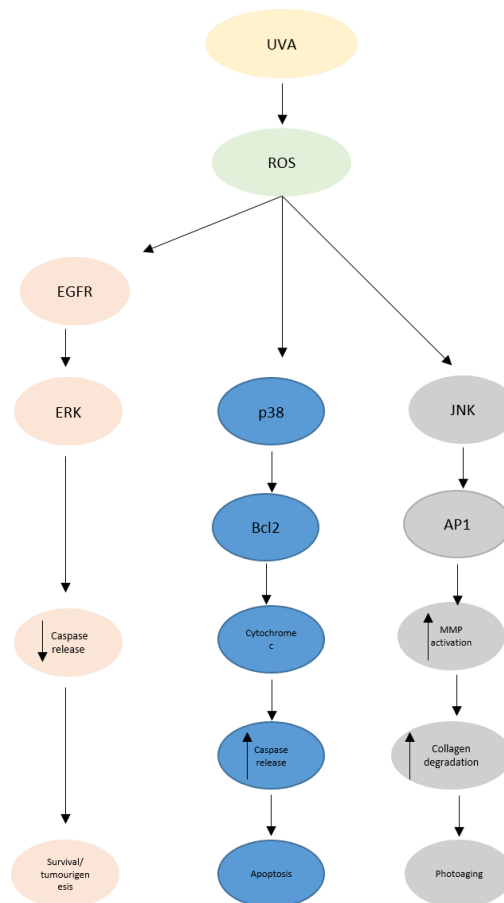


**Figure 1.12 UVA activation of MAPkinases**

*A schematic representation of MAPK activation by UVA radiation. Demonstrating that activation of MAP kinases by UVA can lead to effects which contribute to both photoaging and carcinogenesis.*

## **1.8 UV induction of apoptosis**

When the DDR is unable to fully repair the DNA lesions that have been induced, the stress pathways can respond by inducing apoptosis. There are two main pathways by which apoptosis are induced, the extrinsic and intrinsic pathways which are also referred to as the death receptor and the mitochondrial pathway. The intrinsic pathway is activated from inside the cell by members of the B-cell lymphoma 2 (BCL-2) protein family; the extrinsic pathway is activated from outside the cell by the binding of pro-apoptotic ligands that bind to death receptors on the cells surface reviewed in detail by (Green, 2000). The activation of either of these pathways ultimately results in upregulation of caspases, important effector molecules which play a prominent role in apoptosis (Earnshaw et al., 1999).

The pathways through which UV radiation trigger apoptosis in cells have been shown to be both dose and cell line dependent (Lee et al., 2013). A number of pathways have been reported to play a role in UVA induction of apoptosis, which include the activation of the p53 signaling pathway following DNA damage (Ziegler et al., 1994) activation of death receptor pathway (Aragane et al., 1998) and the mitochondrial pathway (Kulms and Schwarz, 2002).

The pathways leading to the initiation of apoptosis following exposure to UV are still not fully understood. It has been suggested that the formation of photoproducts plays a substantial role; NER deficient cells have been shown to have increased susceptibility to UV induced cell killing (Dunkern et al., 2001). Furthermore, it is thought that formation of CPDs plays a more prominent role in apoptosis induction than 6-4PPs, at least in NER proficient cells because of the speed at which the latter are repaired (Mellon et al., 1987). Although not confirmed, it has been suggested that the presence of 8-oxoG does not contribute significantly to apoptosis following UVA induction. It has long been shown that

CPDs and not 8-oxoG are the primary lesion following UVA (Courdavault et al., 2004) and secondly that, 8-oxoG when compared to other DNA lesions has little effect on blocking either replication or transcription (Larsen et al., 2004).

There is also evidence to suggest that UVA is able to induce apoptosis independently of DNA damage. The increase in ROS following UVA exposure have been shown to cause damage to proteins, lipids and saccharides within the cell (Pattison and Davies, 2006), This can cause damage to both the cell membrane and the mitochondrial membrane, resulting in the release of cytochrome c, a pivotal part of the intrinsic apoptosis pathway (Li et al., 2000).

ATM has been reported to play a role the cellular decision to trigger p53- and c-Jun N-terminal kinase (JNK)-dependent apoptotic pathways in response to UVA, however in ATM deficient cells apoptosis following UVA was not completely abrogated suggesting the involvement of another pathway (Zhang et al., 2002). This is consistent with in vivo evidence that AT cells have a high tendency towards malignant transformation as a result of increased resistance to apoptosis, resulting from deficient ATM signaling (Westphal et al., 1997).

Both UVA and UVB induce apoptosis in melanocytes through p53 dependent pathways but the pathways that activate the p53 are different. The melanocytes showed high levels of oxidative stress but no increase in p53 expression; however, translocation of p53 to the mitochondria was detected. This translocation was dependent on oxidative stress; the addition of N-acetylcysteine blocked it. Downstream, mitochondrial release of cytochrome c and consequent caspase activation were observed as well as the translocation of the BCL-2 family to the mitochondria. This indicates that the p53 mediated apoptosis following UVA may be transcription independent, at least in some cell lines. UVB also

initiated the translocation of p53 to the mitochondria, but this was seen alongside an increase in expression, and both of these events were seen to be independent of oxidative stress, indicating that UVB-mediated apoptosis is a transcription dependent event (Wäster and Ollinger, 2009). The clear role for p53 in apoptosis induction following both UVA and UVB exposure suggests that the intrinsic apoptosis pathway is activated in response to both UVA and UVB wavebands. Interestingly it has also been demonstrated that UVA irradiation protects cells from UVB mediated apoptosis (Ibuki et al., 2007).

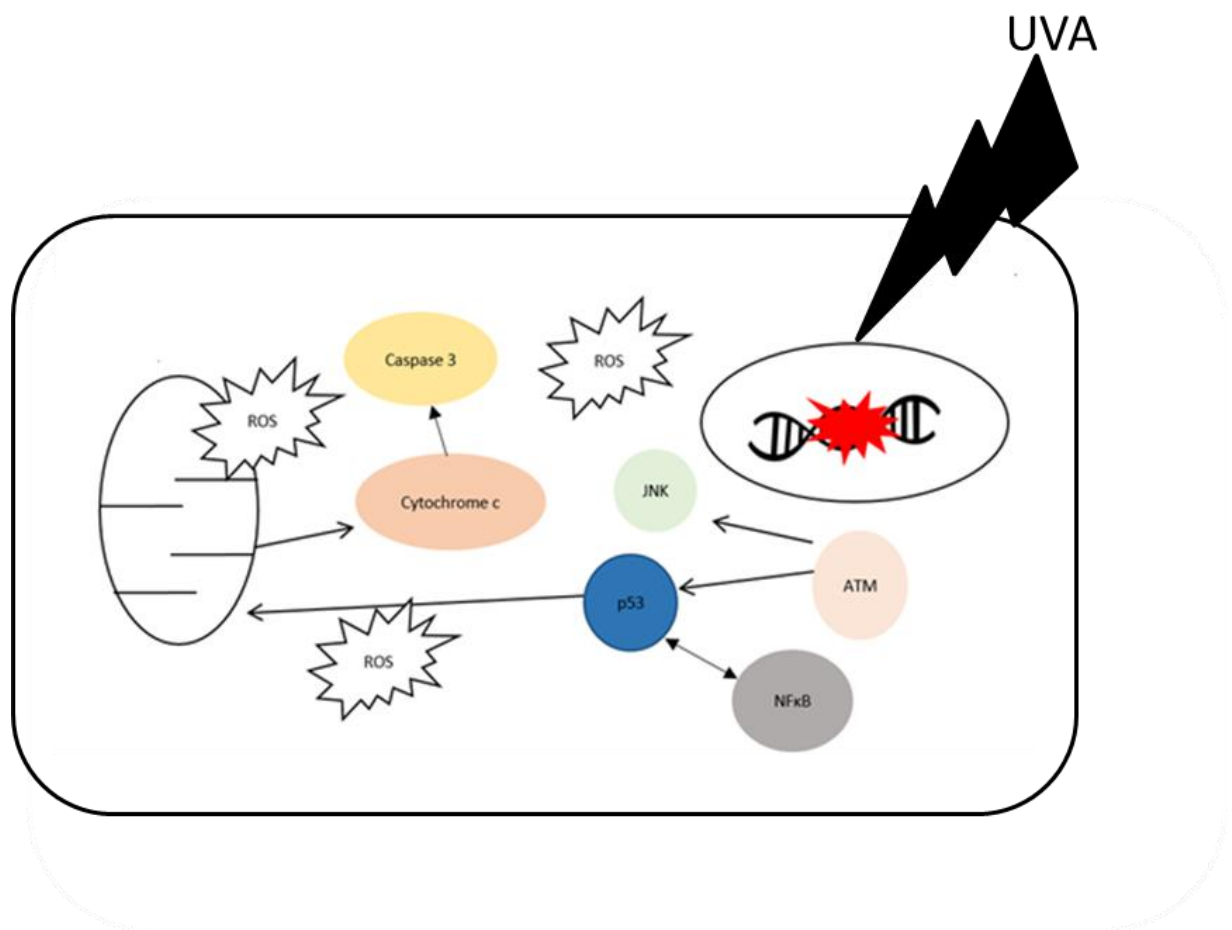


**Figure 1.11 UVA induced pathways of apoptosis**

*Schematic representation of pathways involved in apoptosis induction following exposure to UVA; pathways exist which are able to initiate apoptosis in the absence of DNA damage as well as pathways that are initiated by DNA damage.*

### **1.8.1 Mitochondrial Membrane Potential and Apoptosis**

It has previously been described that the mitochondria play a central role in the induction of apoptosis via both the intrinsic pathway and extrinsic pathways. The involvement of mitochondria in a number of apoptotic pathways is well established, resulting in their release of cytochrome c and in turn the activation of caspases, which in turn induces apoptosis, see Desagher and Martinou for review (Desagher and Martinou, 2000). In particular, discussion has focused on the mitochondrial membrane potential and its possible role in apoptosis induction; although there remains some debate as to whether mitochondrial membrane potential is an initiator or an effect of apoptosis. A number of groups have seen loss of mitochondrial membrane potential prior to nuclear feature of apoptosis (Vayssiere et al., Zamzami et al., 1995). Loss of mitochondrial membrane potential has also been seen to be independent of caspase activation and has been seen as a requirement for cytokine induced apoptosis (Barbu et al., 2002).

In contrast, a number of studies have found a lack of early loss of mitochondrial membrane potential; instead they have seen it occurring late on as a result of nuclear alterations and activation of the intrinsic apoptotic pathway. (Desagher and Martinou, 2000). This has led to some suggestion that the loss of mitochondrial membrane potential may be as a consequence of apoptosis induction, but it may serve as an amplification method to initiate further apoptosis .

### **1.9 Dose rate response**

The effect of dose rate response of UVA is of great interest because of its biological relevance. The intensity at which individuals are exposed to UVA can vary greatly depending on time of day, time of year and geographical location. The Bunsen-Ruscoe Law of Reciprocity states that if the cumulative dose of radiation administered remains

constant then the biological effect of the radiation is the same regardless at the intensity at which the exposure occurs. Much of the earlier data characterised the biological end points for a dose of UVA exposure assuming the biological effect was independent of the dose rate at which the UVA was administered. However, a number of studies now exist which challenge this law and dose rate response has been found to affect a number of biological end points.

Merwald et al (2005) hypothesised that due to the complex effect that exposure to UV radiation has on the cell the Bunsen Roscoe Law of Reciprocity law is unlikely to hold true for these photochemical reactions. They reported that fractionated UVA doses increased the rate of apoptosis compared to one single dose as well as inducing a greater decrease in rate of proliferation and cells exposed to fractionated UVA exposure showed greater membrane damage. The increased ability of UVA to cause a variety of cellular damage at fractionated doses was true of intervals between doses of up to 4 hours, longer than this and a decrease in damage was seen, perhaps indicative of an antioxidant response occurring at this time point (Merwald et al., 2005).

Shorrocks et al (2008) demonstrated an inverse dose rate response relationship for micronuclei formation and membrane damage. They also demonstrated that irradiation at a lower dose rate resulted in a higher rate of apoptosis over the 7 day time course (Shorrocks et al., 2008). Greinert et al (2012) have reported an increase in DSBs when irradiated with fractionated UVA compared to a single dose.

### **1.10 Long term consequences of UVA**

It is now recognised that not all biological effects are as a direct result of radiation exposure. Irradiated cells have been seen to maintain a level of instability for some time post irradiation. This instability can result in new chromosomal damage, an increase in spontaneous mutations, membrane damage and an increased rate of apoptosis. These

characteristics can lead to the cells developing a hypermutator potential and later on becoming carcinogenic (Dahle and Kvam, 2003)

Evidence for long term effects of UVA radiation is increasing. As seen in ionising radiation changes in the cellular survival rate and an increase in mutations have been seen in the progeny and cells surrounding irradiated cells. These long term changes are often referred to as persistent genome stability and the bystander effect which has been found to occur in UVA irradiated cells is thought to be one of the main causes.

### **1.10.1 Persistent Genome Instability**

Persistent genome instability (PGI) was first characterised in ionising radiation (Little et al., 1990) and is defined as persistent DNA and cellular damage in progeny of irradiated cells for multiple generations post irradiation. It refers to a cellular phenotype which expresses an increase in both cell death and spontaneous mutations at both the nucleotide and chromosomal level (Phillipson et al., 2002). Genomic instability has been linked to almost all cancers and has been suggested as the first step in radiation induced carcinogenesis (Selvanayagam et al., 1995). Skin cancer in particular is highly genetically unstable both at the chromosomal and the nucleotide level (Dahle et al., 2005).

O'Reilly and Mothersill (1997) demonstrated an increase in delayed cell death following UV irradiation. Other groups have since looked at the effects of UVA on other characteristics of PGI; they reported that UVA induced an increase in delayed cell death confirming previous work, delayed spontaneous mutations and induction of micronuclei, representing chromosomal damage. They also found that incubation in catalase prior to UVA irradiation decreased the above effects, suggesting that hydrogen peroxide plays a role in PGI induction (Phillipson et al., 2002)

UVA causes fewer immediate mutations than UVB (Wells and Han, 1984) but induces more genomic instability than both UVB radiation and X radiation (Dahle and Kvam,

2003). The same laboratory later found that whilst long term mutations induced by UVB were significantly decreased with incubations in catalase, superoxide dismutase (SOD) or glutathione (GSH), only GSH significantly inhibited the long term mutations caused by UVA (Dahle et al., 2005). Their finding indicates that the generation of ROS plays a great role in the induction of long term mutations of both UVA and UVB. GSH decomposes a wider range of ROS than the other enzymes. Furthermore GSH can be broken down by membrane enzymes, the by-products of this are then able to pass into the cell and stimulate GSH production inside the cell suggesting a more prominent role for gap junction intercellular signaling than signal release into media (Dahle et al., 2005). Furthermore, they attempted to investigate both the time course and the mechanism behind UVA induced PGI. They showed a significant increase in delayed mutations in the UVA-irradiated cells for up to 21 generations post irradiation. Their results also suggested that the so called bystander effect plays a role in the increase in delayed mutations induced by UVA but to a lesser extent than UVB. The bystander effect is defined as the induction of DNA and cellular damage in cells which have not been directly irradiated, but as a result of signals released from directly irradiated cells. The bystander effect will be discussed further in chapter 4.

### **1.11 UV mutations in cancer**

To gain further insight into UVR carcinogenesis the mutation spectrum of skin cancers has been studied, looking for the presence of mutations associated with CPDs, 8-oxoG and other UV DNA lesions. CPDs formed following UVB are associated with C-T transitions. The presence of CPDs distorts the structure of the DNA double helix (Kim et al., 1995) and presents a challenge for replication and transcription, therefore must be repaired before these processes can continue. In most cases CPDs are readily repaired by the NER pathway (Thoma, 1999) however, if undetected these lesions are then targeted by the translesion polymerase pol $\eta$  which, unlike transcription polymerases is able to insert

nucleotides opposite to the dimer. This is non mutagenic when the CPD does not contain cytosine but can cause a C-T mutation in cytosine containing lesions, due to the tendency for these to undergo hydrolytic deamination to uracil lesions. These C-T or CC-TT mutations are often referred to as the UV signature mutation (Ziegler et al., 1994). In addition to formation of CPDs UV, in particular UVA also causes the oxidation of bases, in particular 8-oxoG (Cheng et al., 1992).

Earlier work focused on the mutation spectrum of single genes however this has changed drastically in recent years as next generation sequencing has become affordable and is now readily utilised. In 2010 the mutation spectrum of a malignant melanoma was published (Plesance et al., 2010) and subsequent studies have confirmed the mutation spectrum described in their work. However challenges still remain, skin cancers have the highest mutational load of all cancers, which can make it difficult to distinguish between driver and passenger mutations.

#### **1.11.1 UV mutations in Non-melanoma skin cancer**

*Tp53* is a tumour suppressor gene of key importance in the DNA damage response pathways; it is mutated in at least 50% of all cancers (Zhang et al., 2007). Mutation of *Tp53* is strongly associated with UVB irradiation and non-melanoma skin cancers; it has been stated that *Tp53* is mutated in 90% of SCC (Brash et al., 1996) and 50% of BCC (Nataraj et al., 1995). The link between UVB irradiation and mutations of *Tp53* are well known and it is considered a key player in UVB induced skin carcinogenesis. An early study analysing *Tp53* mutations in SCC to internal tumours found distinct differences in the mutations in the *Tp53* gene suggesting UV induced cancers harbour distinct mutations. Wavelengths in the UVB range were found to contribute most significantly to mutations of *Tp53* seen in the squamous cell carcinoma, 58% of mutations in the *Tp53* gene were found to be CT or CC-TT transition mutations, (Brash et al., 1991).

Mutations of p53 occur early in UV carcinogenesis as well as being detected in non-cancerous UV exposed skin. Mouse model studies have identified the *Tp53* mutation to be an early response to UVB occurring far before a tumour is observed (Berg et al., 1996). The *Tp53* mutation is believed to play a pivotal role in the development of skin cancer, causing the cell to be genetically unstable and opening it up to more mutations (de Gruijl, 2002). In contrast to the effects of UVB, exposure to UVA does not increase expression of *Tp53* in melanocytes and only causes a slight increase in expression in keratinocytes, approximately half of the increase seen by the same dose of solar simulation compared to non-irradiated controls.

Patched gene (*PTCH*) is a tumour suppressor gene which is believed to play a role in the development of BCC. It encodes for a regulatory protein that forms part of the sonic hedgehog pathway (Stone et al., 1996). Inactivation of this pathway has been seen to play a crucial role in oncogenic transformation. Inactivation of *PCTH* is the most common cause of inappropriate Hedgehog signaling leading to oncogenic transformation. Mutations of *PTCH* have been seen to commonly occur in BCC (Hahn et al., 1996; Uden et al., 1996) and are seen equally in minute and larger tumours. The most common mutations seen in *PTCH* are UV signature mutations (Gailani et al., 1996).

As mentioned above next generation sequencing is becoming increasingly used to study the mutation spectrum of tumours on a global scale; recent work sequencing the whole exome of tumour and normal DNA from 12 BCC patients found that BCCs are the most highly mutated cancer, with a mutation rate of 75.8 mutations /Mb (Jayaraman et al., 2014), which was double that seen in SCC (33.3 mutations/Mb) (Durinck et al., 2011). They additionally found that tumours arising from areas associated with chronic rather than intermittent UV exposure had a greater number of mutations.

This methodology confirmed much of the early work looking at specific genes; *PCTH* and *Tp53* were mutated in 75% and 66 % of the tumours respectively. Furthermore, three

mutational hotspots were also identified which had not previously been strongly associated with cancer. The UV signature mutation C-T was seen in the same loci in multiple tumours in signal transducer and activator of transcription 5B (*STAT5B*), Crooked Neck Pre-mRNA Splicing Factor 1 (*CRNKL1*) and Nebulette (*NEBL*) (Jayaraman et al., 2014).

### **1.11.2 UV signatures in Melanoma**

It is now accepted that melanomas display an elevated level of base mutations compared to other solid tumours (Plesance et al., 2010), which is almost entirely attributable to the observed increase in C-T mutations associated with UV exposure. The two genes most commonly mutated in melanoma are *BRAF*, which has been found to be mutated in over 50% of melanomas (Davies et al., 2002) and *NRAS* which is mutated in up to 30% of melanomas (van 't Veer et al., 1989). Mutations in these two oncogenes are mutually exclusive (Rajagopalan et al., 2002) and melanomas negative for a *BRAF* mutation often contain a *NRAS* mutation. The mutations which activate these two oncogenes are not the C-T transitions that are associated with UV DNA lesions. Although, in the case of *BRAF* this has been disputed; the most common mutation seen in *BRAF* is V600E, resulting from a T to A transversion (Davies et al., 2002). Although, there have been suggestions that this mutation could be as a result of error prone replication repair following UV damage (Thomas et al., 2006).

The increased use of genome wide analysis has allowed further insight into the mutation spectrum of melanoma rather than looking at individual genes. Plesance et al (2010) used next generation sequencing to establish the catalogue of somatic mutations in COLO-829, a cell line derived from a malignant melanoma. The most common mutation observed was C-T transition, which is associated with the formation of CPDs following exposure to UV light. They additionally reported that the second most common class of mutations were G to T transversions, suggesting that 8-oxoG formation could play a larger

role in mutagenesis than has been indicated by animal models. However, a study focusing on the driver genes involved in melanoma progression found that 46% of mutations in driver genes were UV signature mutations, but only 9% of these were G-T mutations associated with UVA, the remainder were UVB signature mutations. They also found that the percentage of UV mutations in driver genes increased when the oncogenes *BRAF* and *NRAS*, which are activated by non UVB signature mutations, were excluded, suggesting that UV may play substantial role in melanomas without *BRAF* or *NRAS* mutation (Hodis et al., 2012).

In recent years a number of studies have sequenced both the whole genome (WGS) and exome (WES) of melanoma tumours, metastases and cell lines to gain further insight into the mutational landscape of melanoma. Novel genes identified in these studies have been summarized in the below table and are reviewed in more detail in (Zhang et al., 2016).

Further insight into the genomic landscape of melanoma has great potential for development of new, more targeted therapies and potential to improve patient outcome.

The studies summarized in the table focused on either a single platform analyzing a large number of samples or utilized multiple platforms on fewer samples.. The Cancer Genome Atlas Project used multiple platforms on a large (333) number of samples in the most comprehensive genome analysis of melanoma to date. In this work they proposed that there are four genomic subtypes of melanoma; *BRAF*, *RAS*, *NF1* and triple wildtype. They defined the tumours as having a UV signature if over 60% of total mutations were either C-T or CC-TT transitions; interestingly they saw that only 30% of the wild type tumours had a UV signature, compared to over 90% in the three other genomic subtypes. In addition the wild type tumours also harbored *Tp53* mutations less frequently (Network, 2015).

### **1.11.3 UV mutations in TERT**

Telomerase reverse transcriptase (TERT) is responsible for maintaining telomere length and its reactivation is strongly associated with carcinogenesis (Günes and Rudolph, 2013). Mutations in the promotor region of TERT are common in a number of cancers including gliomas and thyroid cancers (Landa et al., 2013; Killela et al., 2013) but have been seen to be particularly common in skin cancers, and result in increased TERT activation and therefore decreased telomere wearing. Activating mutations in the promoter region of TERT have been seen in 56% of BCCs, 50% of SCCs and up to 70% of melanomas. The mutations display a UV signature indicating a causative role for UV radiation (Horn et al., 2013; Huang et al., 2013; Griewank et al., 2013).

<u>Authors</u>	<u>Study Type</u>	<u>Patient Number</u>	<u>Sample type</u>	<u>Novel genes</u>	<u>Mutation Prevalence</u>
(Wei et al., 2011)	WES	14	Metastases	<i>GRIN2A</i>	42.9%
(Stark et al., 2012)	WES	8	Cell lines	<i>MAP3K9</i>	15%
(Nikolaev et al., 2012)	WES	7	Cell lines	<i>MAP2K1</i>	6.3%
(Berger et al., 2012)	WGS	23	Metastases	<i>PREX2</i>	44%
(Hodis et al., 2012)	WES	121	15 primary tumour 30 Metastases 76 cultures derived from metastases	<i>PPP6C</i>	9.1%
				<i>ARID2</i>	9.1%
(Krauthammer et al., 2012)	WES	73	Metastases and cultures derived from metastases	<i>RAC1</i>	9.8%
				<i>PPP6C</i>	13.1%
				<i>ARID2</i>	18%
				<i>DCC</i>	34.4%
				<i>PTPRK</i>	19.7%
(Mar et al., 2013)	WES	34	Primary tumours	<i>NF1</i>	17.7%
(Gartner et al., 2013)	WES	29	Metastases	<i>BCL2L12</i>	3.4%
	WGS				
(Aydin et al., 2014)	WES	8	Metastases	<i>FBXW7</i>	8.1%
(Wong et al., 2015)	WES	20	Cell lines	<i>RQCD1</i>	4%
(Ding et al., 2014)	WGS	20	Cell lines	<i>EPHA3</i>	25%
(Krauthammer et al., 2015)	WES	117	Primary tumours, metastases and cell lines derived from each0	<i>SOS1</i>	6.6%
(Shain et al., 2015)	WES and WGS	20	Primary tumours	<i>PAK3</i>	19%

**Table 1.2 Mutations identified in Melanoma**

A table summarizing recent work identifying mutations in melanoma utilizing both whole genome sequencing (WGS) and whole exome sequencing (WES).

### **1.12 UV, COX2 and tumorigenesis**

In addition to p53 mutations there are a number of other UV induced events which are considered critical for the progression of skin cancer. One of which is the upregulation of COX2 expression, an enzyme belongs to the cyclooxygenase (COX ) family, which is undetectable in normal healthy tissues, including skin. COX2 has been found to be elevated in a number of human cancers (Hull, 2005). There is substantial evidence to suggest a role for COX2 in the promotion of skin tumours following UVB irradiation. Elevated levels of COX2 have been seen in SCCs, benign papillomas and metastatic tumours of the skin (An et al., 2002; Kagoura et al., 2001), Furthermore the inhibition of COX2 has been seen to have detrimental effects on the growth and survival of UVB skin cancers reviewed in (Rundhaug and Fischer, 2008) Similarly, to what is seen with p53, the upregulation of COX2 has been shown to be an early event in UV induced carcinogenesis (An et al., 2002). At a molecular level, a number of pathways have been reported to lead to the upregulation of COX2 seen in response to UV irradiation, these include the p38MAPK pathway, activation of epidermal growth factor receptor (EGFR), p53 pathway and upstream stimulatory factors 1 and 2, see review by Rundhaug and Fisher for more detail (Rundhaug and Fischer, 2008).

UVA has also been seen to upregulate COX2 and it has been hypothesised that 70% of solar light induced COX2 is as a result of UVA irradiation (Mahns et al., 2004). The UVA upregulation of COX2 is mainly through increased ROS signaling, leading to lipid peroxidation. In addition, singlet oxygen activation of p38 has been seen to stabilise COX2 mRNA and lead to increased protein levels (Bachelor et al., 2002). A role for JNK signaling also become apparent when a selective JNK inhibitor blocked upregulation of COX2 in UVA irradiated artificial epidermis (Mahns et al., 2004). Therefore, it seems likely that UVA like UVB leads to the upregulation of COX2 through a number of different pathways.

### **1.13 General Aims**

The broad research aims of this project were to identify markers of UVA exposure that could be used to assess efficacy of sun creams in a more biologically relevant methodology than those that are currently used. Current methods of assessing UVA protection are a 5 star system that measure the amount of UVA that is blocked by a sun cream compared to UVB, that is, a ratio of UVA: UVB sun protection offered. Identification of markers of UVA damage would allow the direct measurement of UVA protection afforded by application of a sun cream.

#### **1.13.1 The ability of UVA and UVB to induce the DNA damage response**

Chapter 3 aimed to look for upregulation of the DNA damage response following biologically relevant equitoxic doses of UVA and UVB.

#### **1.13.2 Initiation of a DNA damage response in UVA bystander cells**

There is accumulating evidence supporting the ability of UVA to induce a bystander effect, but the majority of this work focuses on a decrease in survival or increase in apoptosis of the bystander populations. Here I aimed to study the existence of a DNA damage response in bystander cells, once again using  $\gamma$ H2AX as a marker in the first incidence.

#### **1.13.3 Activation of MMPs in response to UVA**

As well as being a class one carcinogen UVA plays a role in induction of photoaging. At a molecular level MMPs have been described to be important in the increased turnover of collagen that is characteristic of photoaging. In chapter 5, I aimed to look for the increased activation of MMPs following UVA irradiation.

# **Chapter 2 Materials and**

# **Methods**

## **2.0 Methods**

### **2.1.1 Materials**

All tissue culture media and additives were obtained from Lonza unless stated otherwise.

Keratinocyte Growth medium was purchased from PromoCell.

Cell culture T75 flasks were obtained from NUNC and all cell culture dishes were from Greiner Bio-one.

FBS was purchased from Labtech.

KOSR serum replacement was purchased from Invitrogen.

Trypsin EDTA and 0.5M EDTA pH 8 was obtained from Gibco.

PBS tablets – Gibco

### **2.1.2 Buffers and Solutions**

**Unless otherwise stated buffers were made up in water.**

**3x SDS loading Buffer** – 150 mM Tris, pH 6.8, 30% Glycerol 0.6% SDS, 0.3M DTT 0.02%

Bromphenol blue

**10X TBST** – 0.5 M Tris, 1.5 M NaCl, 0.5% Tween 20, pH 7.4

**10X TG** – 0.25 M Tris, 1.9M Glycine

**10X TGS** – 0.25M Tris, 1.9M Glycine, 1% SDS

**Coomassie Stain** – 2.5g/l brilliant Blue R250 40% Methanol 10 % Acetic acid

**Destaining Buffer** - Methanol: acetic acid : water 40:10:50

**Developing buffer** - 50 mM Tris-Cl, pH 8 5 mM CaCl<sub>2</sub> 0.02% sodium azide

**Incubation buffer** – 0.5% bovine serum albumin (BSA) in 1X PBS.

**Phosphate – buffer saline** – 0.14 M NaCl, 0.01 M NaPO<sub>4</sub>, buffer, 3 mM KCl

**RIPA** – 0.05 M Tris, pH 7.4, 5 M NaCl, 1% Igepal (CA 630) 0.1% SDS, 0.12 M sodium deoxycholate.

**Resolving Tris** - 1.5 M Tris, pH6.8

**Stacking Tris** – 0.5 M Tris, pH 6.8

**Staining Buffer** -5 mM potassium ferricyanide, 5 mM potassium ferrocyanide, 2 mM magnesium chloride,10% dimethyl sulphoxide (DMSO) buffer stabilizer PBS

**Transfer buffer**- 10% Methanol, 1 X TG

### **2.1.3 Antibodies**

**Table 2.1 Antibodies used in Western Blotting**

<b><u>Primary Antibody</u></b>	<b><u>Supplier</u></b>	<b><u>Incubation conditions</u></b>	<b><u>Secondary</u></b>	<b><u>Supplier</u></b>	<b><u>Incubation conditions</u></b>
Anti-gamma H2A.X (phospho S139) antibody	Abcam (ab26350)	1/2000 for 1 hour at RT	Shp pAb to mouse (ab6808)	Abcam	1/1000 for 1 hour at RT
Purified Mouse Anti-Human p53 Clone DO-1	BD Bioscience (554293)		Shp pAb to mouse (ab6808)	Abcam	1/1000 for 1 hour at RT
TIMP1					
Beta Actin		1/200 for 1 hr at RT	Shp pAb to mouse (ab6808)	Abcam	1/1000 for 1 hour at RT

**Table 2.2 Antibodies used in Immunofluorescence**

<b><u>Primary Antibody</u></b>	<b><u>Supplier</u></b>	<b><u>Incubation conditions</u></b>	<b><u>Secondary antibody</u></b>	<b><u>Supplier</u></b>	<b><u>Incubation conditions</u></b>
Anti-gamma H2A.X (phospho S139) antibody	Abcam (ab 26350)	1/4000 for 1 hour at RT	Goat anti-Mouse IgG (H+L) Secondary Antibody, Alexa Fluor® 488 conjugate	Thermo Fisher Scientific	1/1000 for 1 hour at RT
53BP1	GeneTex	1/500 Overnight at 4°C	Goat anti-Rabbit IgG (H+L) Secondary Antibody, Alexa Fluor® 568 conjugate	Thermo Fisher Scientific	1/1000 for 1 hour at RT
Anti-ATM (phospho S1981) antibody	Abcam (ab79891)	1/1000 Overnight at 4°C	Goat anti-Rabbit IgG (H+L) Secondary Antibody, Alexa Fluor® 568 conjugate	Thermo Fisher Scientific	1/1000 for 1 hour at RT
Phospho-Chk1 (Ser345) (133D3) Rabbit mAb	Cell Signalling	1/250 Overnight at 4°C	Goat anti-Rabbit IgG (H+L) Secondary Antibody, Alexa Fluor® 568 conjugate	Thermo Fisher Scientific	1/1000 for 1 hour at RT

**Table 2.3 Antibodies used in Flow Cytometry**

<b><u>Primary Antibody</u></b>	<b><u>Supplier</u></b>	<b><u>Incubation conditions</u></b>	<b><u>Secondary</u></b>	<b><u>Supplier</u></b>	<b><u>Incubation conditions</u></b>
Anti-gamma H2A.X (phospho S139) antibody	Abcam (ab26350)	1/1000 for 1 hour at RT	Goat anti-Mouse IgG (H+L) Secondary Antibody, Alexa Fluor® 488 conjugate	Thermo fisher scientific	1/1000 for 1 hour at RT

**Table 2.4 Inhibitors used.**

<b><u>Name</u></b>	<b><u>Substrate</u></b>	<b><u>Supplier</u></b>	<b><u>Working Concentration</u></b>	<b><u>Incubation time</u></b>
KU-55933	ATM	Selleckchem (S1092)	1µM	1 hour prior to irradiation
VE-821	ATR	Selleckchem (S8007)	1µM	1 hour prior to irradiation
Mirin	MRN complex	Abcam (ab141182)	100 µM	1 hour to irradiation
Catalase	Hydrogen peroxide	Sigma (C-9322)	250 units/ml	Immediately after irradiation for the duration of the experiment
<u>Diphenyleneiodonium (DPI)</u>	NADPH oxidase		2µM	18 hours prior to irradiation. Media was changed immediately after combination of feeder and bystander cells

## **2.2 Cell culture**

### **2.2.1 HaCaT cell culture**

HaCaT cells were obtained from ATCC. HaCaTs were grown in DMEM + 10%FBS (Foetal bovine serum) +penicillin (100U/ml) and streptomycin (100µg/ml) in T75 cell culture flasks and incubated at 37 °C and 5%CO<sub>2</sub> in a humidified incubator. To split the cells medium was removed and the cells were washed in 5ml Phosphate Buffered Saline (PBS) (Gibco) before 5ml of PBS-EDTA (0.05%) (Gibco) was added to the flask and incubated at 37 °C, 5% CO<sub>2</sub> for 10-12 minutes. 2ml Trypsin was added to a T75 flask and incubated for 2 minutes at 37 °C or until the cells had detached. The trypsin was then neutralised with 3ml of complete DMEM media and the cells re - suspended. For maintenance of cell culture 1ml of cells was then added to 11ml of fresh media in a T75 flask.

### **2.2.2 NHEK cell culture**

NHEK cells were obtained from Life Technologies. To make up the complete keratinocyte medium the Supplement mix was added to the basal medium along with Calcium chloride solution. The final supplement concentrations are shown in the below table.

**Table 2.5 Concentrations of supplements in NHEK media**

Supplement	Final Concentration
Bovine Pituitary extract	0.004ml / ml
Epidermal Growth Factor (recombinant human)	0.125ng / ml
Insulin (recombinant human)	5µg / ml
Hydrocortisone	0.33µg / ml
Epinephrine	0.39 µg / ml
Transferrin	10 µg / ml
CaCl <sub>2</sub>	0.06 mM

NHEK cells were passaged using the Detach Kit (PromoCell).

**Table 2.6 The NHEK Detatch kit**

Constituent	Composition
HEPES-BSS	30 mM HEPES, D-Glucose, NaCl, KCl, Na-phosphate and phenol red
Trypsin EDTA Solution	0.04% trypsin 0.03% EDTA
Trypsin Neutralising Solution	0.055 trypsin Inhibitor 0.1% BSA

The PromoCell Detach Kit was allowed to equilibrate to room temperature prior to passaging the cells. Medium was aspirated from the NHEK cells and 100 µl of HEPES per cm<sup>2</sup> of culture vessel surface was added to the flask to wash the cells. The vessel was agitated for 30 seconds before the HEPES solution was removed. 100µl of Trypsin/EDTA solution per cm<sup>2</sup> of surface area of flask was added to the cells and the cells were visualised under the microscope until they had detached from the flask. Once the cells had detached 100 µl per cm<sup>2</sup> of surface area of Trypsin neutralising solution was added. The cell suspension was transferred to a centrifuge tube and centrifuged at 220 x g for 3 minutes. After centrifugation the supernatant was discarded and the cells were re-suspended in 1ml of the appropriate media and counted. Cells were then seeded at the required density either for experiments or for maintenance of culture. The cells were routinely maintained at 37 °C 5% CO<sub>2</sub>.

### **2.2.3 Dermal Fibroblast Cell Culture**

Normal human dermal fibroblast cells were purchased from Life Technologies. The cell culture methods used for this cell line were identical to section 2.2.1, but the PBS EDTA incubation prior to trypsinisation was omitted.

#### **2.2.4 Bystander cell culture**

For the bystander effect experiments both a trans-well system and the exchange of conditioned media methods were used depending on the experimental demands. The 6 well plates and inserts (1µm pore size) were purchased from Greiner. The 60mm culture dishes used for the media exchange experiments were purchased from NUNC. The trans-well system was used for all immunofluorescence experiments and the media transfer method was used for flow cytometry or western blotting.

For all bystander experiments the feeder cells were grown on the permeable insert and the bystander cells were grown on coverslips in the 6 well plate. Cells were seeded at densities of 10,000 cells per insert and 50,000 cells per well. The inserts were placed into a 6 well dish containing media but no cells in the wells. Both plates were incubated overnight at 37° and 5% CO<sub>2</sub>. The feeder cells were irradiated with UVA as described in section 2.3.1 and immediately after irradiation the inserts containing both the irradiated and control feeder cells were placed into a six well plate containing the bystander cells. The co-incubation was maintained at 37°C and 5% CO<sub>2</sub> until the time at which the cells were required to be harvested for analysis, typically 48 hours. Both HaCaT and dermal fibroblast cells were used for bystander cells: the experiments were set up as in table 2.7

**Table 2.7 Bystander Set up**

Feeder Cells	Bystander Cells
HaCaT	HaCaT
HaCaT	Dermal fibroblasts

### **2.3 UV Irradiation**

The cells were irradiated in phenol red free DMEM + L-glutamine, unlike a number of other studies which have carried out their irradiations in PBS. Phenol red also known as phenolsulfonephthalein is a pH indicator included in many culture mediums. Phenol red free media was used because phenol red has been seen to be photoactive and therefore media containing phenol red is not a suitable choice for an irradiation media.

The phenol red free media in which the cells were irradiated did not contain antibiotics. In a previous study by Le Gall et al (2005) antibiotics have been found to affect the susceptibility of fibroblasts to UVA irradiation. They found that streptomycin could at least partially protect the cells against UVA induced mortality as well as causing a decrease in lipid peroxidation. A role for the antibiotics in ROS scavenging was also suggested. Therefore, it is undesirable to have antibiotics present in the media when the cells are irradiated with UVA. The study also found that culturing the cells without antibiotics for 24 hours prior to UVA exposure was long enough to abrogate the effects of antibiotic on UVA irradiation and so our cells were routinely maintained in medium containing streptomycin and penicillin but upon trypsinisation and seeding the cells for experimentation the cells were cultured in antibiotic free medium for 24 hours prior to irradiation with UVA.

#### **2.3.1 UVA irradiation**

UVA irradiations were carried out using Pro-lite Plus 240V 25W UVA bulbs. These tubes had a small UVB output which was quenched using Mylar filter. Measurement of the output of the bulb was done prior to each irradiation using a Spectroradiometer (MACAM Photometrics Model SR9910PC). Output readings gained was used to calculate the irradiation time required to irradiate cells with the desired dose of UVA. Outputs from the bulb were between 75-85W/m<sup>2</sup>/s with a peak output at 37

The rig was kept at a constant temperature in order to prevent change of temperature being a factor in any changes seen to cells. The cooling system Grant RC 400 set to 25 °C and this was sufficient to maintain the temperature at 37 °C for the duration of all UVA irradiation doses used. Control cells were kept in the incubator in which they were cultured.

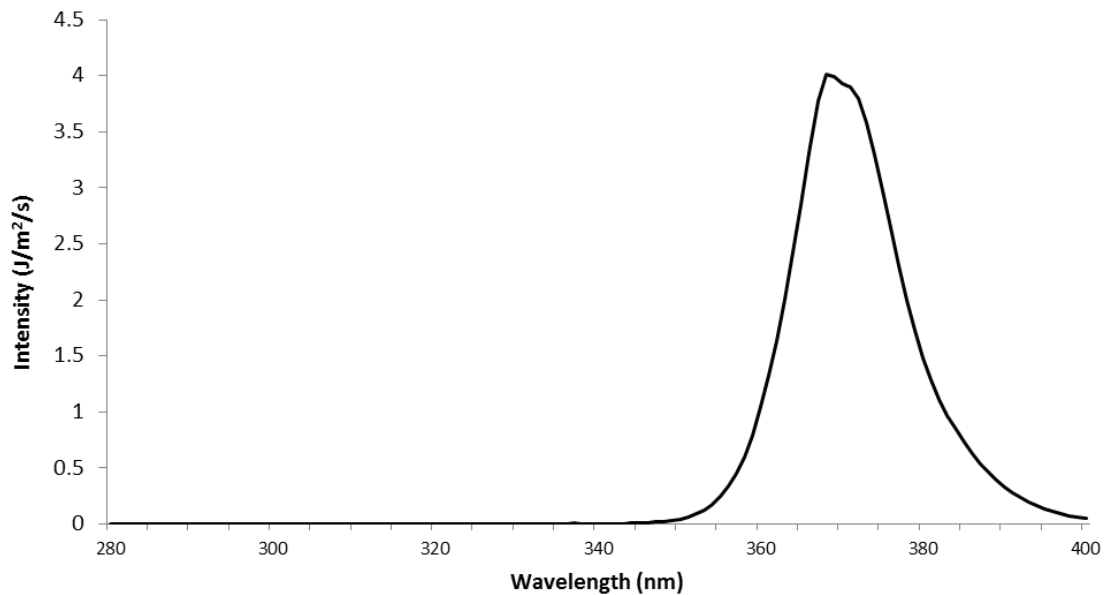


**Figure 2.1 UVA output**

### **2.3.2 UVB irradiations**

UVB irradiations were performed using Phillips T140 UVB bulbs (Starna Ltd) at 37 °C. The outputs were measure using Spectroradiometer (MACAM Photometrics Model SR9910PC) and readings gained were used to calculate the irradiation time needed to achieve the desired dose. UVB doses ranged from 25 J/m<sup>2</sup> to 200 J/m<sup>2</sup> depending on the experiment. The doses that were used were used because they have equal to the UVA doses that had been used in the UVA clonogenic survival experiments. There was no need for the use of a chiller to maintain the temperature of the cells because the time of irradiation was short

enough to not cause any substantial dip in temperature of the media the cells were cultured in.

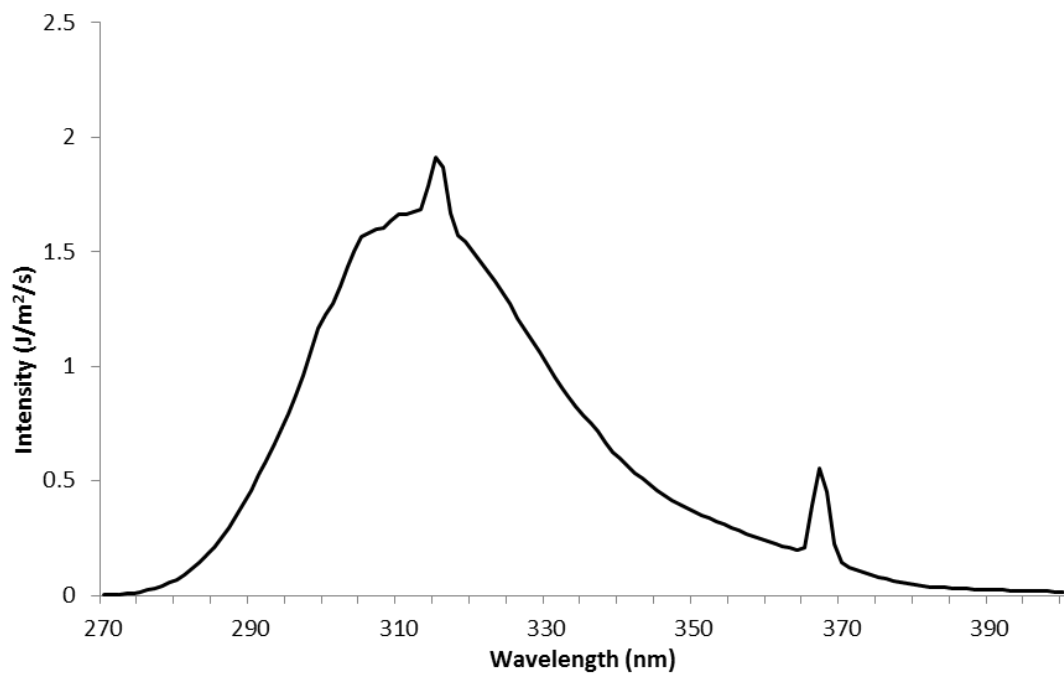


**Figure 2.2 UVB Output**

## **2.4 Clonogenic Assay Method**

250 HaCaT cells were seeded in 4ml of phenol red free DMEM medium +10 %FBS + L-glutamine into 60mm cell culture dishes. The cells were incubated at 37 and 5% CO<sub>2</sub> for approximately 6 hours to allow them to adhere to the culture dish but not replicate. The cells were then either sham irradiated or exposed to UVA irradiation at one of the following doses; 25kJ/m<sup>2</sup>, 50kJ/m<sup>2</sup>, 100kJ/m<sup>2</sup> or 200kJ/m<sup>2</sup>. When looking at the effects of UVB via the clonogenic assay doses of UVB that were equitoxic the doses of UVA were used and cells were irradiated with 25 J/m<sup>2</sup>, 50 J/m<sup>2</sup>, 100 J/m<sup>2</sup> or 200 J/m<sup>2</sup>. Each dose including the sham irradiation was carried out in triplicate.

Following irradiation, the phenol red free DMEM was removed and 4ml complete DMEM was added to the cells. This was done to prevent infections occurring in the cells. The cells were then left to proliferate in the incubator in the same conditions as described above. After 9 days the cells were fixed in 70% ethanol for 20 minutes, followed by staining in 5% Giemsa for 20 minutes. The Giemsa stain was then removed, the plates were rinsed with PBS and the cells were allowed to dry before the colonies formed were counted, and an average taken for each condition.

The plating efficiency was then calculated as follows;

$$\text{(Colony number / number of cells seeded) x 100.}$$

Using the plating efficiency the percentage survival for each condition was calculated;

$$\text{(Treated plating efficiency / control plating efficiency) x 100.}$$

The same methodology was repeated increasing the seeding density to 500 cells to establish if the previous result was seen because the cells were seeded at such a low density.

## **2.5 Western blotting**

### **2.5.1 Protein isolation**

1.5 X 10<sup>6</sup> HaCats or NHEKS were seeded in a 100mm culture dish, allowed to adhere overnight at 37°C and 5% CO<sub>2</sub> prior to UVA/UVB irradiation. Post irradiation the media was removed, cells washed in PBS and proteins isolated using RIPA and protease inhibitors (Proteases complete Ultra tablets Roche) and phosphatase inhibitors (and Phos STOP Roche). RIPA extracts were collected at the following time points post UVA / sham irradiation; 0 hour, 1hour, 3hours, 24hours and 48 hours. The RIPA extracts were centrifuged at 13300rpm for 10 minutes at 4 °C.

### **2.5.2 Protein concentration measured using Bradford assay.**

Protein standards of 1mg/ml 0.5 mg/ml and 0.25mg/ml of BSA (Sigma) were made up and 30µl of each standard was added to 2.5µl of RIPA. A blank was made up from 2.5µl of RIPA and 30µl of PBS. To analyse protein content of samples 2.5µl of each sample was added to 30µl of PBS. 960µl of Bradford reagent was added to each sample, the standards and the blank. Each tube was mixed and incubated at room temperature for 5minutes. The solutions were transferred to cuvettes and the spectrophotometer was blanked using the blank made up. Absorbance of the standards and unknown solution was read at 600nm. A standard curve was drawn using results gained from the standards and the equation of the line was used to calculate the concentrations of protein in the unknown samples. The concentrations of proteins were used to calculate the volume needed to load 20µg of protein into the gel for Western Blot analysis. 20µg of each RIPA extract was added to PBS to a total volume of 10µl and this was then mixed in a ratio of 2:1 with 3 x SDS PAGE loading buffer and boiled at 95 °C for 3 minutes. The sample was then vortexed whilst hot.

### **2.5.3 SDS PAGE gel**

Protein samples were run on 4 -14% gradient gels (BioRad). The protein marker, Precision Plus Protein Standards All Blue (BioRad) was loaded into one of the lanes and the samples were loaded. The gels were run in 1 x TGS buffer at 200V for 35 minutes using the Mini -PROTEAN ®Tetra Vertical Electrophoresis Cell setup.

### **2.5.4 Gel transfer system**

The Thermo Scientific™ Pierce™ Power Blotter was used to transfer the proteins onto Immobilon® PVDF Membrane (Millipore). The membrane was soaked in methanol to hydrate it. The membrane and 4 sheets of blotting paper were then soaked in Pierce™ 1-Step Transfer Buffer. The required settings were selected according to how many gels were being transferred and the size of the proteins of interest for that experiment.

### **2.5.5 Detection of proteins**

Following irradiation the membrane was washed once with 1X TBST and blocked in 5% w/v BSA in 1X TBST. Antibody incubations were carried out as described in table 2.1.

The membrane was visualised using Super Signal West Pico reagent (Thermo Fisher), 0.5 ml of each substrate was mixed together before coating the membrane and incubating for 2minutes, the membrane chemiluminescence was visualised with a BioRad Chemidoc XRS+ Imaging System. The exposure time adjusted accordingly depending on band strength/ background signal.

## **2.6 Immunofluorescence.**

### **2.6.1 Cell culture and irradiation for immunofluorescence**

9 X 10<sup>4</sup> HaCaT cells in 1.5ml of phenol red free DMEM + 10% FBS + 1mM L- glutamine were seeded onto 25mm cover slips in culture dishes and incubated overnight at 37 °C and 5%CO<sub>2</sub>. The cells were then exposed to UVA as previously described in section 2.3.

### **2.6.2 Processing of coverslips for detection of $\gamma$ H2AX**

Post irradiation the cells were washed once with PBS and fixed with 4% PFA at room temperature for 20 minutes. Cells were fixed at various points post irradiation according to the experimental demands. After fixation the cells were washed 3X in PBS and permeabilised in 0.5% Triton X-100 and washed 3X in PBS. After washing the coverslips were removed from individual culture dishes and placed onto labelled Parafilm in a humidified dish. Fresh 3% BSA made up in PBS was used to block the cells for 1hour at room temperature, followed by incubation with the appropriate antibodies as described in table 2.2.

Following incubation with the fluorescently labelled secondary antibody coverslips were then washed five times in PBS and then rinsed with ddH<sub>2</sub>O. Excess water was drained off the coverslips and they were mounted onto slides using Vectashield (Vector Labs). Once dried the slides were sealed with clear nail varnish and stored at 4 °C in the dark ready for visualisation by microscopy.

### **2.6.3 EdU labelling**

Cells were pulse labelled by incubation with EdU at a concentration of 10 $\mu$ M for 30 minutes at 37 degrees and 5%CO<sub>2</sub>. The cells were then fixed with 4%PFA for 20minutes at room temperature, washed twice with 3%BSA and permeabilised in 0.5% Triton X-100 for 20 minutes at room temperature. the coverslips were again washed twice and transferred to a humidified chamber. The coverslips were then incubated in 1 X Click-iT®

reaction cocktail made up as shown in table 2.8 for 30 minutes in the dark. The coverslips were then washed once in 3% BSA and antibody incubation steps were carried out. Following incubation with the reaction cocktail all further incubations were carried out in the dark to minimize photobleaching.

**Table 2.8 EdU Reaction cocktail**

Reaction Component	Volume ( $\mu$ l)
1 X Click it reaction buffer (Life Technologies)	430
CuSO <sub>4</sub>	20
Alexa Fluor 555 azide	1.2
Reaction Buffer Additive	50
Total Volume	500

#### **2.6.4 Confocal Microscopy**

In chapter 3 Images were taken using a Zeiss LSM510 confocal microscope.

In chapter 4 images were taken using a Zeiss LSM880 confocal microscope.

#### **2.6.5 Image J analysis of fluorescence**

In order to establish whether UVA or UVB causes a significant difference in fluorescence quantification of the fluorescence of each nucleus needed to be carried out. Image J was used to establish the fluorescence intensity of each nucleus. Or, the average number of foci per nucleus, for analysis of 53BP1. At least 100 nuclei were analysed for each condition across a number of fields of view. The average intensity per nuclei was then calculated for each time point for both the UVA irradiated and un-irradiated HaCaT cells. From this the relative intensity for each condition was calculated relative to the fluorescence seen in the control cells at zero hours. Box plots were then plotted to illustrate the median and the spread of fluorescence intensity. Either one way ANOVA or paired t- tests were carried

out to establish if the differences in fluorescence were significant for any of the conditions.

### **2.6.6 ZEN analysis of fluorescence**

In chapter 4, image analysis was carried out using ZEN imaging software. In this chapter EdU was utilized to identify S phase cells, and the fluorescence of EdU +ve and -ve cells was analysed separately. At least 100 nuclei were analysed for each condition across a number of fields of view for 3 biologically independent replicates. The average intensity per nuclei was then calculated for each time point and EdU status for both the UVA bystander and un-irradiated HaCaT cells or dermal fibroblast cells. From this the relative intensity for each condition was calculated relative to the fluorescence seen in the EdU control cells.

Box plots were then plotted to illustrate the median and the spread of fluorescence intensity for each experimental group. Either one way ANOVA or paired t tests were carried out to establish if the differences in fluorescence were significant for any of the conditions.

## **2.7 Flow cytometry**

Cells were seeded in phenol red free DMEM in a 100mm dish at a density of  $1 \times 10^6$  incubated overnight at 37 °C and 5% CO<sub>2</sub>. The cells were then either exposed to UVA or UVB irradiation as previously described in section 2.3 or were treated as control cells. The cells were then harvested by incubation in PBS EDTA followed by trypsinisation, neutralisation in media and centrifugation down to form a pellet. The cell pellet was then fixed in 100µl of 1% PFA, vortexing the pellet as the PFA was added drop by drop, and incubated for 10 minutes at room temperature. The above steps were timed so that the cells were fixed 1 hour after irradiation with UVA so that t time points were directly comparable with immunofluorescence and Western blots.

After fixation, 1 ml of 0.1% Triton X-100 was added to the cells, the pellet was re-suspended and centrifuged at 500g for 5 minutes. After pelleting a further 100µl of 0.1% Triton was added to the pellet, again using vortexing to mix and incubated for 10 minutes at room temperature. The pellet was then washed by centrifugation and re-suspension in PBS three times before the pellet was then re-suspended in 100µl of 3% BSA and blocked in this for 30 minutes at room temperature. The pellet was then washed by centrifugation and re-suspension in PBS three times. Following the blocking step the primary antibody for γH2AX was added at 1µg/  $10^6$  cells and incubated for 1 hour at room temperature. The cells were then rinsed as before the secondary was added at 1/1000 in incubation buffer. The cells were then rinsed as before and finally re-suspended in 1ml of PBS ready for analysis. Once re-suspended in PBS 1µl of propidium iodide was added to the sample as a DNA stain to allow for analysis of the cell cycle. Samples were analysed on a BD FACSCanto II flow cytometer immediately after re-suspension in PBS. Data from a total of 10,000 cells was recorded and subsequently analysed.

Graphs drawn from the analysis of the flow cytometry data were: Forward scatter vs side scatter followed propidium iodide width vs propidium iodide stained area (doublet

discrimination). These two graphs were gated in order to avoid including cell fragments or clumps of cells in the analysis which could affect the interpretation of the data. Posts gating the following graphs were also drawn from the analysed sample; FITC stain vs count, propidium iodide stain vs count and FITC stain vs Propidium Iodide stain.

## **2.8 Analysis of mitochondrial membrane potential**

JC1 was used to detect changes in mitochondrial membrane potential in UVA and UVB irradiated HaCaT and dermal fibroblast cells. This was analysed by both flow cytometry and confocal microscopy, the general methods for each are described below. JC1 accumulation in the mitochondria is indicated by a fluorescence emission shift from green to red. Loss of mitochondrial potential, results in a lack of JC1 accumulation in the mitochondria and a consequent decrease in the ratio of red: green staining that can be seen.

### **2.8.1 Flow cytometry**

HaCaT cells were seeded in phenol red free media in 60mm dishes and incubated overnight at 37°C and 5% CO<sub>2</sub>. Cells were irradiated with 100 kJ/m<sup>2</sup> UVA or 100 J/m<sup>2</sup> UVB or sham irradiated. Cells were then either incubated for 3 or 24 hours before the media was removed and kept, the cells were harvested by incubation with PBS EDTA for 12 minutes followed by trypsinisation and the harvested cells along with the media removed were pelleted by centrifugation at 500g for 5 minutes. The cells were then resuspended and washed once with PBS before once again being centrifuged and resuspended in fresh PBS. JC1 was added to the suspension cells at a concentration of 1µg/ml and incubated for 20 minutes at 37 °C before analysis by flow cytometry.

For dermal fibroblasts the the irradiation conditions were identical but the harvesting of the cell did not require the EDTA incubation and the JC1 incubation was at 0.3µg/ml for 1 hour at 37 °C before analysis by flow cytometry.

Flowing software 2.5.1 ([Cell Imaging Core, Turku Centre for Biotechnology](#)) was used to construct histograms and overlay histograms to demonstrate the shift in FITC staining between the UVA irradiated and the control samples.

## **2.8.2 Immunofluorescence**

HaCaT or dermal fibroblast cells were seeded in phenol red free DMEM on coverslips in 35mm culture dishes and incubated overnight at 37° and 5%CO<sub>2</sub>. The cells were irradiated and JC1 was added at either 3 or 24 hours post irradiation in the directly irradiated experiments or at either 24 or 48 hours post co-incubation for bystander experiments. The concentrations remained the same as for the flow cytometry analysis. The coverslips were imaged using confocal microscopy and the images analysed using ZEN 2012 software. The intensity of both red and green staining was measured for each cell and the ratio of red:green staining was calculated. The average ratio for each condition was then calculated normalised to the control and a box plot constructed to demonstrate the median and the spread of the data.

## **2.9 Substrate Zymography**

### **2.9.1 Sample preparation**

3 x 10<sup>5</sup> HaCaT cells were seeded in 2 ml of phenol red free DMEM media+20%KOSR +1mM glutamine in 35mm cell culture dish. The cells were incubated overnight at 37 °C, 5% CO<sub>2</sub> in a humidified incubator and irradiated or sham irradiated as previously described in section 2.3. Samples of the culture media were collected at 0, 1, 3, 24 and 48 hours post UVA irradiation or sham irradiation and stored at -80 °C. The protein content of the samples was calculated using the Bradford assay as described previously (section 2.5.2) and the volume of sample needed to load desired amount into the gel was calculated.

### 2.9.2 Casein Zymography

A 10% resolving gel containing 2mg/ml casein was made up and a 4% stacking gel was made up as shown in table 2.1. Gels were poured using 1.0mm empty gel cassettes (Invitrogen).

The gel was pre-run in 1X TGS for 15 minutes at 125V. The samples and a sample of the phenol red free media +20% KOSR were diluted 1:1 with non-reducing 2 x loading buffer, incubated at room temperature for 30 minutes and then loaded into the gel along with molecular marker. The gel was ran at 125V for 90 minutes or until the tracking dye had reached the bottom of the gel. The gel was then removed from the cassette and placed into a clean container. The gel was washed twice for fifteen minutes with 2.5% Triton X-100 with constant agitation.

**Table 2.9 Recipe for Casein SDS-PAGE gel**

<b>10 % Resolving gel</b>		<b>4 % Stacking Gel</b>	
<b>Reagent</b>	<b>Volume</b>	<b>Reagent</b>	<b>Volume</b>
<b>Acrylamide</b>	2.5ml	<b>Acrylamide</b>	0.27ml
<b>1.5M TrisHCl pH 8.8</b>	1.88ml	<b>0.5M Tris pH 6.8</b>	0.5ml
<b>10% SDS</b>	75µl	<b>10% SDS</b>	20µl
<b>dd H<sub>2</sub>O</b>	2.99ml	<b>dd H<sub>2</sub>O</b>	1.19ml
<b>APS</b>	45µl	<b>APS</b>	10µl
<b>TEMED</b>	15µl	<b>TEMED</b>	5µl

Developing buffer was added to the gel and incubated with gentle agitation for 30 minutes at room temperature. The buffer was then removed, replaced with fresh developing buffer and incubated overnight at 37 °C. The gel was then washed three times with distilled water before being stained with 0.25% Coomassie blue for 1 hour and de-stained with 40% methanol 10% acetic acid until clear bands were seen. The gel was then washed with distilled water to remove any background staining in unstained regions.

### **2.9.3 Collagen zymography**

Collagen zymography, like casein zymography was carried out using 10% SDS PAGE gels containing 2ml of a 1mg/ml collagen solution. Collagen solution consisted of rat tail type 1 collagen (sigma) and a 0.1M acetic acid solution. Samples were prepared and the gel was run as described in 2.7.2. The gel was then washed twice for 30 minutes in 2.5% Triton. The gel was incubated in developing buffer for 30 minutes at room temperature the developing buffer was then replaced with fresh developing buffer and the gel incubated overnight after initial experiments with a 4 hour incubation time resulted in gels with no digested areas. The gel was then rinsed and stained and de-stained as described in 2.7.2.

### **2.9.4 Casein digesting activity in confluent irradiated cells.**

HaCaT cells were grown to confluence in 35mm culture dishes in phenol red free DMEM + 20% KOSR. Prior to irradiation 20µl of media was removed as an un - irradiated control. The cells were then irradiated with 100kJ/m<sup>2</sup> UVA. Further samples of the conditioned media were taken at 0, 24 hours post irradiation. Protein content was analysed using Bradford assay and MMP activity analysed by casein zymography as previously described in 2.7.2.

### **2.9.8 Analysis of Zymograms with Image J**

Once the zymograms have been imaged Image J was used to assess the relative density of each of the bands that are seen on the gel. The lanes were selected and the profiles of each

lane plotted. Straight lines were drawn across the plot to enclose each of the peak and from the size of the peak the percentage of the total area was calculated. This was done separately for each of the 3 bands that were seen on the gel. Once the area and percentage had been calculated the percentage value was used to calculate the relative density for each of the bands compared to the bands that were generated by the control 0 hours sample which was normalised to 1. This analysis was carried out for each of the 3 biological repeats and an average and standard error values were calculated. A bar chart was then plotted showing the conditions and the average.

### **2.10 Analysis of RT-PCR data**

RT – PCR data previously generated in the laboratory was reanalysed. The original method of analysis is described below.

- The Mean Ct and Standard deviation was calculated for each irradiated sample and time matched control (this was repeated for 3 biological replicates)
- Delta Ct was calculated by subtracting the Ct of the gene of interest from the control. The standard deviation was calculated by adding the square
- Delta delta Ct was calculated by subtracting the delta Ct of the treated sample from the time matched untreated sample. The relative gene expression was then calculated as follows:

$$\text{Relative gene expression} = 2^{-\Delta\Delta Ct}$$

- The range of expression was calculated using the delta delta Ct plus or minus the SD of delta delta Ct.
- The relative expression was expressed relative to the expression of the time matched control which was normalised to 1.

The data was reanalysed as follows:

- The Mean Ct and Standard deviation was calculated for each irradiated sample and time matched control (this was repeated for 3 biological replicates)
- Delta Ct was calculated by subtracting the Ct of the gene of interest from the control. The standard deviation was calculated by adding the squared of the SD of the gene of interest to the square of the SD for the control. The square root of this value was then calculated.
- Delta delta Ct was calculated by subtracting the delta Ct of the treated sample from the untreated sample at time 0 hours. The relative gene expression was then calculated as follows:

$$\text{Relative gene expression} = 2^{-\Delta\Delta Ct}$$

- The range of expression was calculated using the delta delta Ct plus or minus the SD of delta delta Ct.
- The relative expression was expressed relative to the expression of the control o time point which was normalised to 1.

**Chapter 3- The**  
**timeframes and kinetics**  
**of H2AX phosphorylation**  
**following UVA and UVB**  
**irradiation**

### **3.1 Introduction**

UVA causes a wide variety of cellular damage and DNA lesions, the majority of which come through its reactions with photosensitisers. UVA at wavelengths of between 315nm and 400nm falls outside of the wavelengths that are readily absorbed by DNA; instead UVA initiates DNA damage through its reactions with photosensitisers and consequent ROS production. The ability of UVA to induce CPDs, oxidised bases and single strand breaks is well accepted, these DNA lesions by looking for the presence of CPDs or 8-oxoG directly.

The ability of UVA to cause replication dependent double strand breaks is well established. However, the ability of UVA to initiate formation of double strand breaks remains controversial, some groups finding no evidence to suggest UVA is able to initiate DSB formation even at very high doses, which are arguably no longer biologically relevant (Rizzo, Dunn et al. 2011). Another group saw the induction of DSBs following UVA irradiation at a biological dose; furthermore, they suggested a role for antioxidants and photosensitiser reactions in the observed DSB formation (Greinert, Volkmer et al. 2012). The measurement of more complex breaks, such as DSNs that occur both independently of replication and those dependent on replication are often assessed by measuring the activation of the DDR pathways.

The DDR is crucial to maintaining genome stability following changes to chromatin structure. The DDR is a complex network of pathways which prevent DNA lesions causing genomic stability. The DDR comprises of DNA repair mechanisms, made up of specific pathways tailored to resect each type of DNA lesion as well as cell cycle checkpoints, to slow replication and allow the cell time to repair damage and to prevent damage DNA from being replicated and tolerance processes which allows the bypass of lesions and replication to continue (Hoeijmakers, 2001). There is extensive crosstalk between these pathways which allow for proper repair of lesions, in particular between the DNA repair

pathways and the activation of cell cycle checkpoints which allow for additional time to repair the damage (Bartek and Lukas, 2007). The cell cycle position at which the cell is arrested is dependent on the type of damage that has occurred (Zhou and Elledge, 2000).

### **3.2 Aims**

Although there is some evidence to suggest that UVA is able to induce double strand breaks independently of replication (Greinert et al., 2012b) this still remains controversial. Additionally, when H2AX phosphorylation has been looked at, the mechanism has not been further studied, nor have the comparative abilities of UVA and UVB to initiate a DNA damage response. This data looks at the up regulation of  $\gamma$ H2AX in response to either UVA or UVB irradiation; It is well established that  $\gamma$ H2AX foci are formed both in response to DSBs (Rogakou, Pilch et al. 1998) and stalled replication forks arising, but the pathways by which  $\gamma$ H2AX is activated in response to either damage type vary.  $\gamma$ H2AX foci formation is activated via the phosphorylation of ATM in response to double strand breaks (Burma et al., 2001) and by activation of ATR in response to stalled replication forks (Ward and Chen, 2001). A number of other signalling molecules such as cell cycle checkpoint kinases Chk1 and Chk2 vary depending on the type of damage that caused the response (Bartek and Lukas, 2003).

The results show the different time frames in which  $\gamma$ H2AX are up regulated in response to equi-toxic doses of UVA and UVB irradiation. The data also suggests possible mechanisms of double strand break formation through the use of ATM and ATR inhibitors as well as possible mechanism by which the damage is repaired.

### **3.3 Results**

#### **3.3.1 Clonogenic survival of HaCaT cells following UVA and UVB**

The clonogenic survival assays were carried out in order to determine the effects of UVA or UVB irradiation on the survival of HaCaT cells grown in a monolayer and irradiated in phenol red free medium. HaCaT cells are commonly used in the literature to study the effects of a variety of stressors on skin cells and are well established as a fair representational model for human keratinocytes. The choice of model for studying the reaction of skin to exposure of UV radiation remains a challenge but for the initial experiments this cell line and model type was thought to be suitable. The doses of UVA to which the cells were exposed are all biologically relevant doses with the largest dose of 200 kJ/m<sup>2</sup> being equivalent to approximately 60 minutes of midday sun, so not a dose that is unrealistic to be achieved by individuals who spend time outdoors. The doses used were all biologically relevant (Sola and Lorente, 2015).

##### **3.3.1.1 UVA clonogenic survival experiments**

Either 250 or 500 HaCaT cells were seeded in phenol red free DMEM media incubated for 6 hours so that the cells had attached to the culture plate but not replicated and then the cells were irradiated with doses of UVA varying from 25 kJ/m<sup>2</sup> to 200 kJ/m<sup>2</sup>. Colonies that had formed 9 days' post UVA irradiation were fixed in 70% ethanol allowed to dry and stained in 5% Giemsa. The colonies were then counted ensuring that only colonies with over 50 cells were included in the count to prevent the inclusion of smaller colonies where the cells had become senescent as a result of UVA exposure. Senescent cells are no longer able to proliferate and therefore should not be included in a count for percentage survival. The plating efficiencies were then calculated as discussed in section 2.5. From the plating efficiencies the percentage survival of the irradiation groups was calculated in comparison to the un- irradiated groups. The plating efficiency of the un-irradiated cells

was about 15% at each of the seeding densities that were used therefore confirming that the lower seeding density of 250 cells did not cause a decrease in cell survival due to sparseness of plating. The average seeding density at each dose of UVA was calculated as was the standard error and these values were plotted on the graph shown in figure 3.1. The doses of UVA and UVB that were used for these clonogenic studies have been previously used in other studies by other groups and are accepted as being roughly equal cytotoxicity and of equal physiological relevance. The clonogenic survival experiments aimed to show that in the model utilized for this work, which does vary from other models that have been used previously, the doses still had the same effect.

Figure 3.1 shows the percentage survival of HaCaT cells after exposure to increasing, but still biologically relevant doses of UVA. The percentage survival was greatly decreased in response to any of the doses of UVA that were used showing that exposure to UVA does have an effect on the ability of HaCaT cells to survive and proliferate. A strong dose-response relationship was seen, with even a dose of 25 kJ/m<sup>2</sup> causing a 20% decrease in cell survival and the highest dose of 200 kJ/m<sup>2</sup> UVA resulting in a survival rate of just 7%. The error bars on the graph show that there was little difference in the percentage survival of the HaCaT cells between the repeats of the experiment. The repeats were carried out at different seeding densities, but the lack of difference in survival shows that increasing the seeding density of the cells has no effect on their survival after UVA irradiation. This shows that there is reproducibility in the results even when the amount of cells that are seeded is varied.

The ED<sub>50</sub> was then calculated, and it was determined that a dose of 47.6 kJ/m<sup>2</sup> UVA irradiation would result in a 50% cell survival rate. It is this figure that could be used to compare the survival rate between different models or to compare efficacy of UVA filters in the current cell culture model.

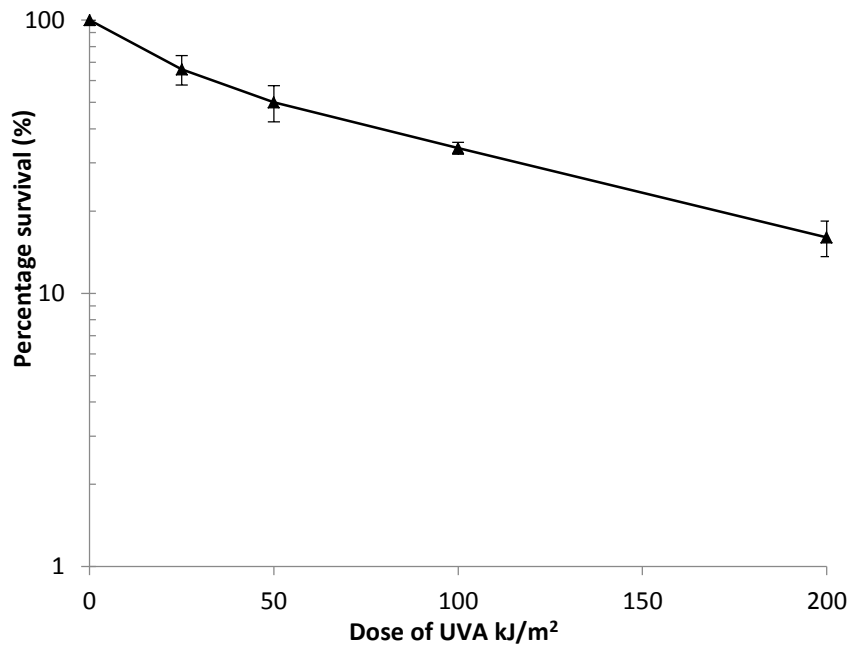


**Figure 3.1 Clonogenic cell survival assays of HaCaT cells following UVA exposure.**

*250 HaCaT cells were seeded in a 60mm culture dish and allowed to adhere for 6 hours. The cells were then irradiated with doses of UVA between 25 kJ/m<sup>2</sup> and 200 kJ/m<sup>2</sup> and then allowed to proliferate for 9 days at 37°C and 5%CO<sub>2</sub>. After 9 days' colonies were fixed in 70% ethanol, stained with 5% Giemsa and colonies of 50 cells or larger were counted. The percentage survival for each dose of UVA relative to the un-irradiated group was calculated and a scatter graph illustrating this was constructed. The error bars represent the standard deviation.*

### **3.3.1.2 UVB Clonogenic survival experiments**

UVB clonogenic survival experiments were also carried out to demonstrate the effect of UVB irradiations on survival of HaCaT cells in our model. The doses of UVB used were between 25 J/m<sup>2</sup> and 200 J/m<sup>2</sup>. These doses are commonly accepted to be equally cytotoxic to the doses of UVA that had been previously used in the clonogenic survival experiments however, our experimental set up was different to those that have been utilised before so to ensure, that in our model these doses showed equal cytotoxicity.

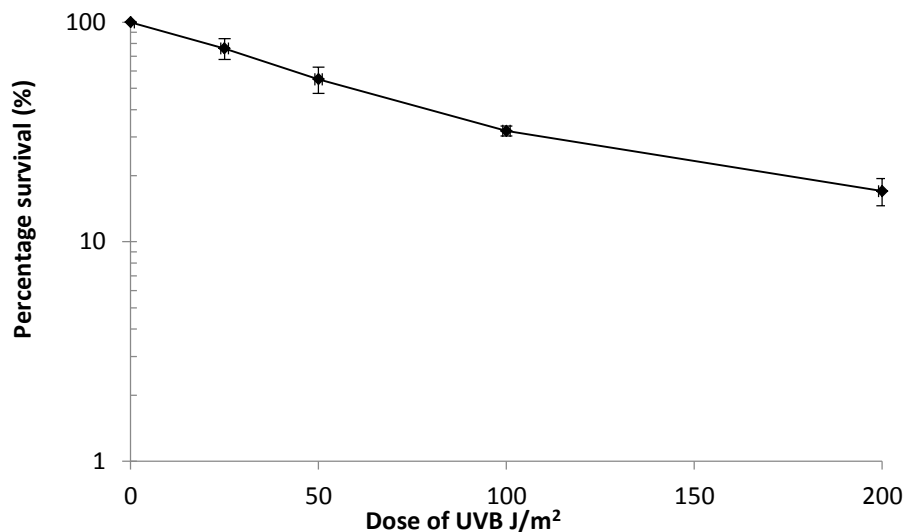


**Figure 3.2 Clonogenic cell survival assays of HaCaT cells following exposure to UVB.**

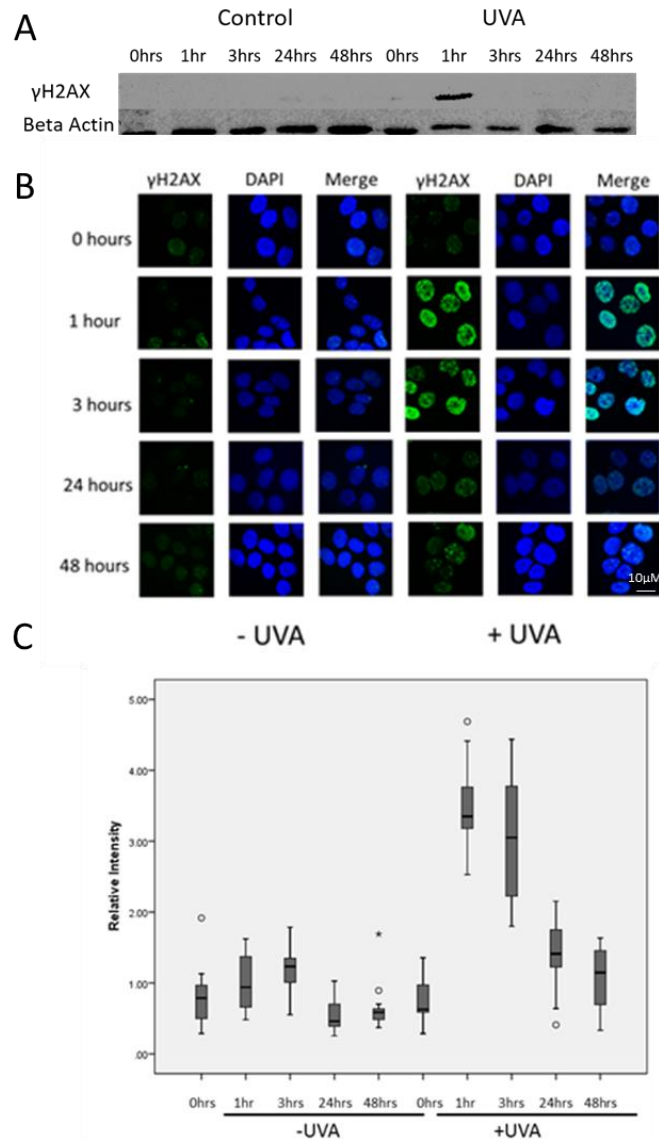
*250 HaCaT cells were seeded in a 60mm culture dish and allowed to adhere for 6 hours. The cells were irradiated with doses of UVB between 25 J/m<sup>2</sup> and 200Jm<sup>2</sup> and then allowed to proliferate for 9 days. After 9 days colonies were fixed in 70% ethanol, stained with 5% Giemsa and colonies which contained over 50 cells were counted. Percentage survival for each dose of UVB was calculated relative to the un-irradiated control and a graph illustrating this was constructed. The error bars represent the standard deviation.*

Figure 3.2 demonstrates that there is a dose response relationship between survival of HaCaT cells and the dose of UVB with which they are irradiated. The lowest dose results in one third of HaCaT cells unable to survive and the highest dose of 200 J/m<sup>2</sup> results in a survival rate of 16%. The ED<sub>50</sub> was calculated and it was found that a dose of approximately 50 J/m<sup>2</sup> was sufficient to result in a 50% decrease in survival of the HaCaT cells.

The ED<sub>50</sub> values calculated from these clonogenic survival experiments confirmed that the ranges of doses of UVA and UVB that had been utilized are of approximately equal cytotoxicity despite the changes in experimental methodology that have made from previous work. Therefore, doses in this range were utilized for further work on the DDR.

### **3.3.2 Time course of H2AX phosphorylation following UVA or UVB irradiation**

The initial experiment aimed to compare the timeframes within which  $\gamma$ H2AX foci were formed in asynchronous HaCaT and NHEK cells following exposure to equitoxic and biologically relevant doses of UVA or UVB. For this time course experiment a dose of 100kJ/m<sup>2</sup> UVA and 100J/m<sup>2</sup> UVB were used. These are both biologically relevant doses that individuals could be readily exposed to with normal environmental exposure (Sola and Lorente, 2015). The formation of  $\gamma$ H2AX foci was observed at a number of time points that varied from immediately after irradiation up to 48 hours after the exposure. These time points were chosen in an attempt to establish if  $\gamma$ H2AX foci formation following either UVA or UVB were early or late occurring events following irradiation and the  $\gamma$ H2AX foci persisted once formed. The fluorescence of each nucleus was measured and the intensity relative to the control 0 time point was calculated for all other time-points. Box plots of the data were constructed to demonstrate the median and spread of the data, the middle line demonstrates median and the outline of the box demonstrates the interquartile range.



**Figure 3.3 The phosphorylation of H2AX is an early event following exposure to UVA irradiation in HaCaT cells** The cells were irradiated with 100kJ/m<sup>2</sup> UVA, or sham irradiated.

- A) Western blot analysis of protein extracts harvested and probed for γH2AX (ser139) and HRP-conjugated Sheep polyclonal antibody to mouse.
- B) Cell seeded on coverslips were fixed at 0, 1, 3, 24 or 48-hour post irradiation. The coverslips were processed using an antibody to γH2AX (ser139) and Alexa Fluor 488 conjugated anti mouse secondary. The nuclei were counterstained using DAPI. A representative confocal image (n=3) taken using Zeiss LSM 510 confocal microscope is shown.
- C) Fluorescence of at least 100 nuclei per condition was measured using Image J software and normalized to the control 0-time point. A box plot was constructed to demonstrate the median and the spread of the data. The box represents the median and interquartile ranges and the whiskers show the 95 percentiles.

To demonstrate that this early up-regulation of  $\gamma$ H2AX is seen in normal cell lines as well as in the immortalized keratinocyte cell line used in the first experiments the time course was repeated in NHEK cells, the same dose of UVA and time points were used.

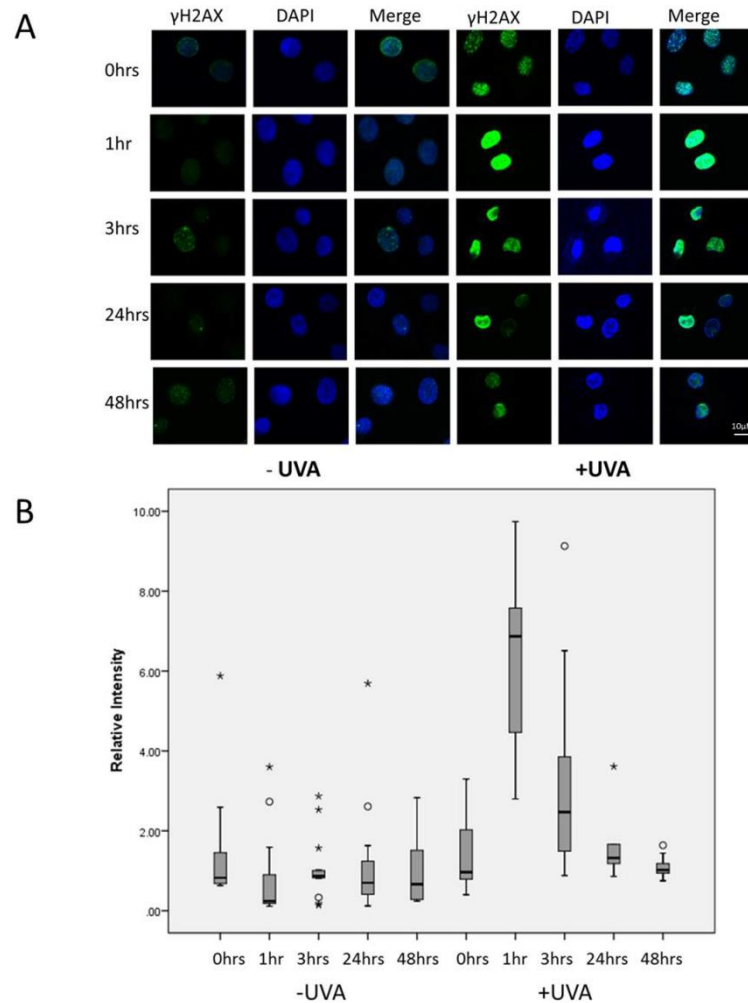


**Figure 3.4 H2AX phosphorylation is an early event in NHEK cells exposed to a biologically relevant dose of UVA**

*NHEK cells were seeded on coverslips, exposed to 100 kJm<sup>2</sup> UVA and fixed at 0, 1, 3, 24 or 48-hour post irradiation. The coverslips were processed using an antibody to  $\gamma$ H2AX (ser139)) and Alexa Fluor 488 conjugated anti mouse secondary. The nuclei were counterstained using DAPI.*

- A) *Representative confocal image (n=3) taken using Zeiss LSM 510 confocal microscope.*  
 B) *Fluorescence of at least 100 nuclei per condition was measured using Image J software and normalized to the control 0-time point. A box plot was constructed to demonstrate the median and the spread of the data. The box represents the median and interquartile ranges and the whiskers show the 95 percentiles.*

Following UVA irradiation  $\gamma$ H2AX phosphorylation was seen to peak at 1-hour post irradiation where a significant ( $P < 0.001$ , One-way ANOVA) 3.8-fold increase in average fluorescence per nuclei was seen in the UVA irradiated group compared to the control. At three hours the fluorescence remains significantly increased ( $P < 0.01$  One-way ANOVA) although a greater spread of intensity of fluorescence is seen indicating that at this time some repair of DNA damage has occurred. This is also shown in the immunofluorescence images where some cells show higher levels of  $\gamma$ H2AX staining. In addition, at these early time points all the cells were positive for  $\gamma$ H2AX foci. The data shown in figures 3.3 and 3.4 indicates that the phosphorylation of H2AX following UVA is due to the formation of double strand breaks caused by a direct mechanism rather than a replication dependent one. This finding was seen in both immortalized and normal keratinocytes, indicating that it is unlikely to be a cell line dependent observation.

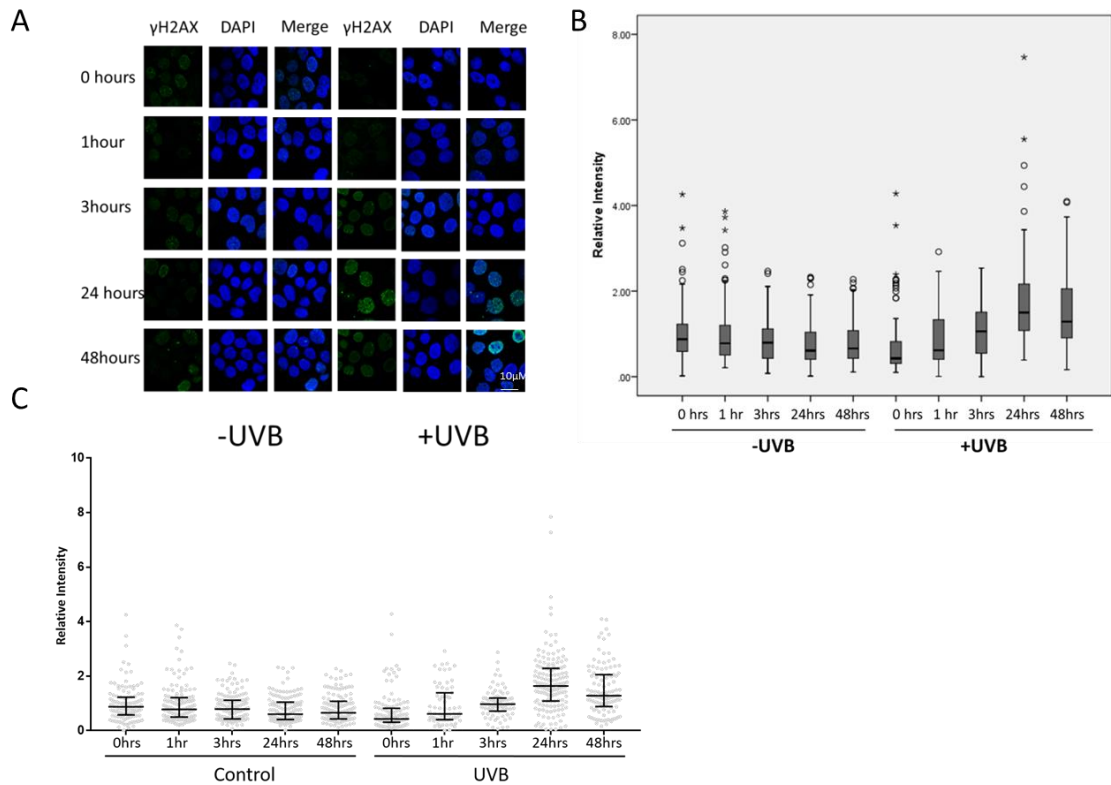


**Figure 3.5 The phosphorylation of H2AX is a late event following exposure to UVB irradiation**

*HaCaT cells were seeded onto glass coverslips and allowed to adhere overnight at 37°C and 5%CO<sub>2</sub>. The cells were then irradiated with 100 J/m<sup>2</sup> UVB, or sham irradiated and fixed at 0, 1, 3, 24 or 48-hour post irradiation. The coverslips were processed using an antibody to γH2AX and Alexa Fluor 488 conjugated anti mouse secondary. The nuclei were counterstained using DAPI*

- A) Representative confocal image (n=3) taken using Zeiss LSM 510 confocal microscope
- B) Fluorescence of at least 100 nuclei per condition was measured using Image J software and normalized to the control 0-time point. A box plot was constructed to demonstrate the median and the spread of the data. The box plot represents the median and the interquartile ranges and the whiskers show the 95 percentiles.
- C) A categorical scatter plot to further demonstrate the spread of the data. The median and interquartile range is demonstrated.

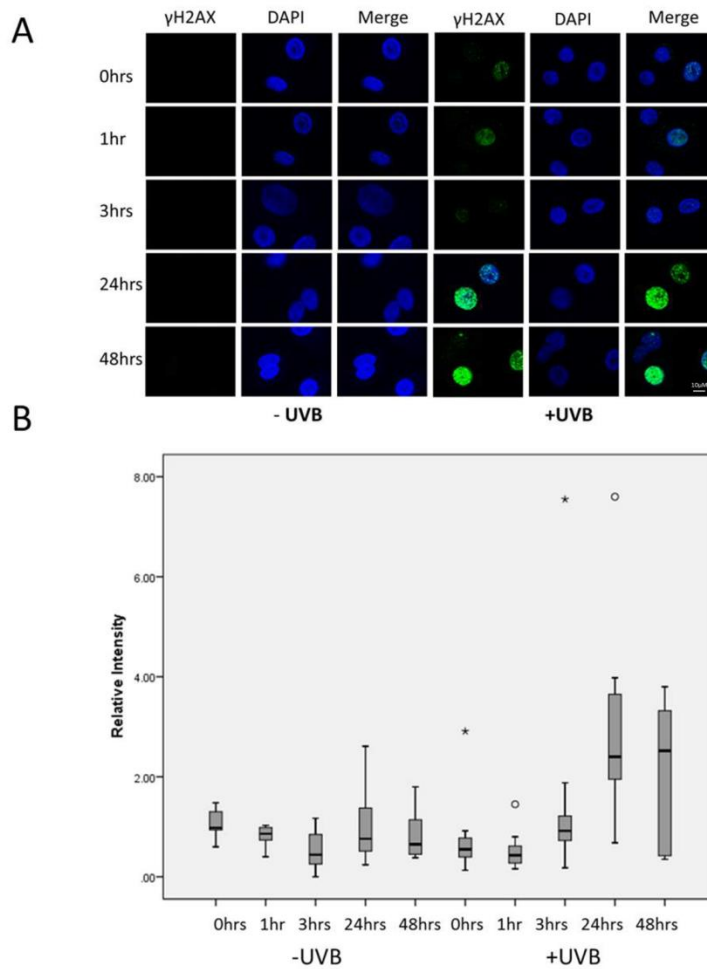


**Figure 3.6 The phosphorylation of H2AX is a late occurring event in NHEK cells exposed to UVB**

*NHEK cells were seeded on coverslips, exposed to 100Jm<sup>2</sup> UVB and fixed at 0, 1, 3, 24 or 48-hour post irradiation. The coverslips were processed using an antibody to  $\gamma$ H2AX (ser139) and Alexa Fluor 488 conjugated anti mouse secondary. The nuclei were counterstained using DAPI.*

- A) *Representative confocal image (n=3) taken using Zeiss LSM 510 confocal microscope.*  
 B) *Fluorescence of at least 100 nuclei per condition was measured using Image J software and normalized to the control 0-time point. A box plot was constructed to demonstrate the median and the spread of the data. The box plot represents the median and the interquartile ranges and the whiskers show the 95 percentiles.*

Post UVB irradiation the peak in average fluorescence per nuclei is seen at 24 hours post-irradiation where the average fluorescence was increased 2.2 fold compared to the control 0-time point, this was a significant ( $P < 0.01$ , One-way ANOVA) increase; however even at this time point not all the cells are positive for  $\gamma$ H2AX foci. A slight decrease was seen in the median staining intensity at 48 hours, but this remained a significant increase ( $P < 0.05$ , One-way ANOVA) compared to the control. At both of these time points two sub-populations were clear, indicating a sub-population of the cells is more susceptible to H2AX phosphorylation than others. This was demonstrated further in the analysis of the fluorescence; the spread of the data shows increases of up to four fold of the control. This is a larger spread than had been detected in response to UVA irradiation. This was seen in both HaCaT (Figure 3.5) and NHEK (Figure 3.6) cells which indicates that the mechanism involved in H2AX phosphorylation following UVB is likely to be conserved between keratinocyte cell lines and not a unique mechanism in the immortalized HaCaT cell line. The categorical box plot shown in figure 3.5 shows the relative fluorescence of each nucleus and clearly demonstrates the existence of two populations at both 24 and 48 hours post UVB.

In contrast to what was observed following UVA irradiation, no increase in fluorescence is seen at the earlier time points when compared to the un-irradiated controls. These initial experiments are indicative of a different mechanism involved in the phosphorylation of  $\gamma$ H2AX following UVA irradiation compared to UVB.

### **3.3.3 Dose response relationship between UVA, UVB and $\gamma$ H2AX foci formation.**

The initial time course experiment demonstrated that both UVA and UVB, at a biologically relevant dose are able to induce H2AX phosphorylation but the time frames within which  $\gamma$ H2AX is upregulated are markedly different, indicating a different mechanism underpinning the formation of  $\gamma$ H2AX foci following each waveband. Next, the existence of any dose-response relationship between H2AX phosphorylation and dose of UVA/UVB

the cells were exposed to was investigated. The doses used were the same as those used in the earlier described clonogenic survival experiments, therefore allowing for direct comparison between  $\gamma$ H2AX and decrease in clonogenic survival. The time points that were studied were 1 and 24 hours post UVA/UVB irradiation, which were the time points where peak levels of  $\gamma$ H2AX following exposure to each waveband had been detected in the time course experiments.

Figure 3.7 shows a partial dose response relationship between phosphorylation of H2AX and dose of UVA; a significant ( $P < 0.05$ , One-way ANOVA) increase in  $\gamma$ H2AX was detected following the 25 kJ/m<sup>2</sup>, a further increase was seen between 25 and 50 kJ/m<sup>2</sup>, but increasing the dose of UVA further showed no further increase in  $\gamma$ H2AX. These doses showed a marked ability to cause H2AX phosphorylation in the cells; however, they induced just a 20% decrease in clonogenic survival. The higher doses of UVA showed highly significant ( $P < 0.01$ , One-way ANOVA) increases in H2AX phosphorylation. This shows further potential dangers of UVA, in particular at lower doses because it initiates high levels of DNA damage at doses that do not result in a substantial decrease in cell survival. Figure 3.9 shows that similar to what was seen in the HaCaT cells the NHEK cells also show a partial dose response relationship between dose of UVA and H2AX phosphorylation. Again no further increase of H2AX phosphorylation was seen at doses above 50 kJ/m<sup>2</sup>.

Looking at the 24-hour time point following UVA, there is no increase from the un-irradiated sample to the 50 kJ/m<sup>2</sup> suggesting that DNA repair is able to fully repair the damage that has occurred at these doses. For the two higher doses some cells remain positive for  $\gamma$ H2AX foci at the 24-hour time point indicating that at the higher doses DNA repair pathways are unable to fully repair the damage within a 24-hour period. Here the level of H2AX phosphorylation remained significantly ( $P < 0.05$ , One-way ANOVA) higher than that seen in the control.

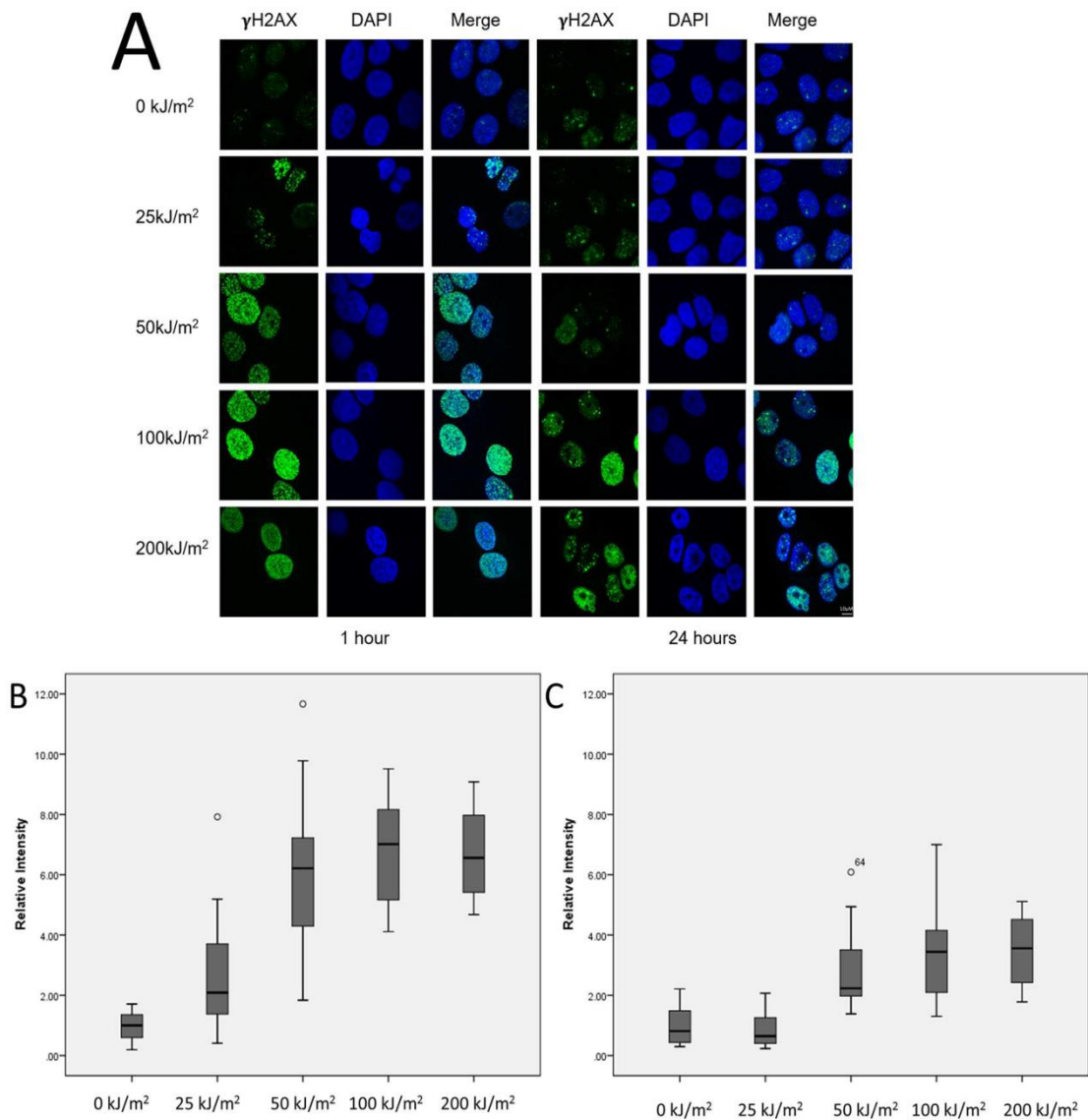


**Figure 3.7 Phosphorylation of H2AX following UVA irradiation shows a partial dose response**

*HaCaT cells were seeded onto glass coverslips and allowed to adhere overnight at 37°C and 5%CO<sub>2</sub>. The cells were then irradiated with a dose of UVA ranging from 0 to 200 kJ/m<sup>2</sup>, the cells were then fixed either 1 or 24 hours post irradiation. The coverslips were processed using an antibody to  $\gamma$ H2AX (ser139) and Alexa Fluor 488 conjugated anti mouse secondary. The nuclei were counter stained with DAPI.*

*A) Representative confocal image (n=3) taken using Zeiss LSM 510 confocal microscope.*

*B) Fluorescence of at least 100 nuclei per condition was measured using Image J software and normalized to the untreated control at each time point. A separate box plot is shown for the intensity of  $\gamma$ H2AX at B) 1 hours post irradiation and C) 24-hour post irradiation. The box plot indicates the median and the interquartile ranges of the data. The whiskers demonstrate the 95% percentile.*

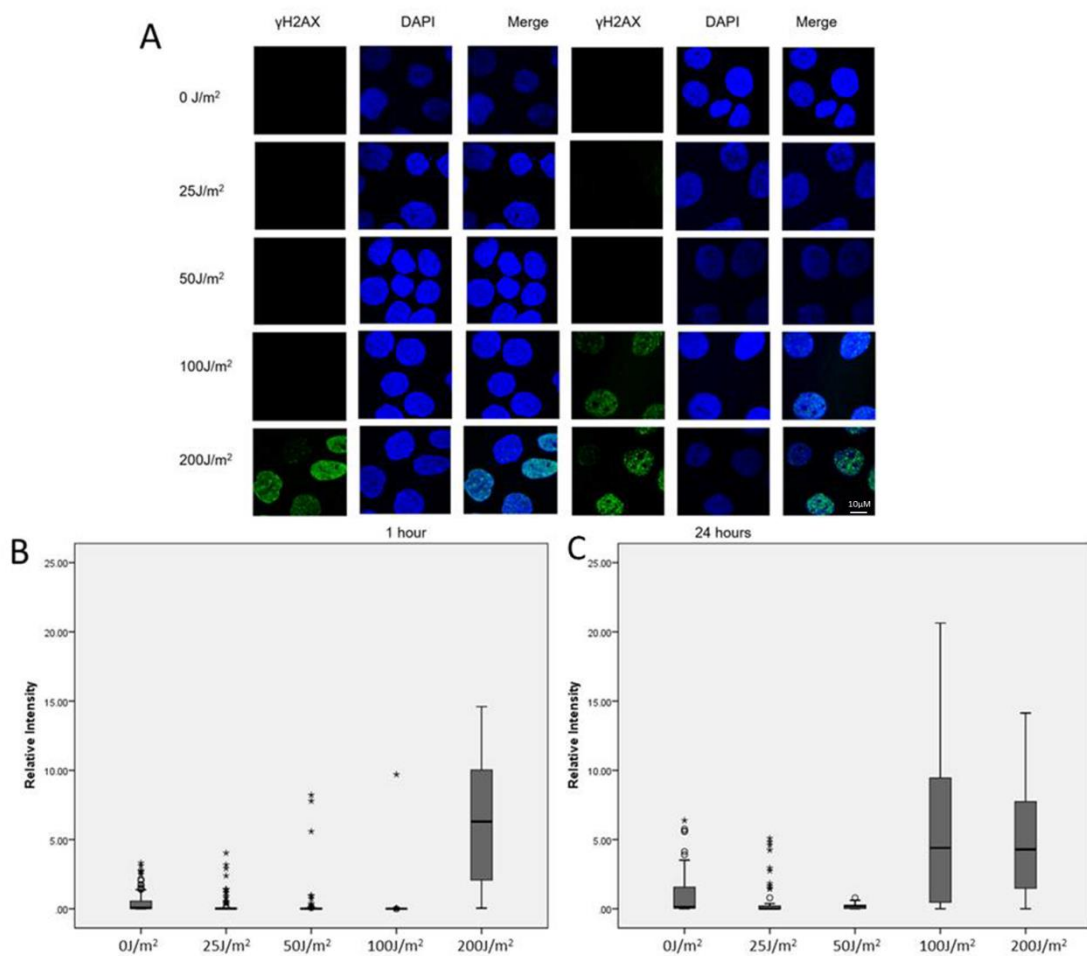


**Figure 3.8 Phosphorylation of H2AX following UVB irradiation shows a threshold response**

*HaCaT cells were seeded onto glass coverslips and allowed to adhere overnight at 37°C and 5%CO<sub>2</sub>. The cells were then irradiated with a dose of UVB ranging from 0 to 200 J/m<sup>2</sup>, the cells were then fixed at either 1 or 24 hours post irradiation. The coverslips were processed using an antibody to γH2AX (ser139) and Alexa Fluor 488 conjugated anti mouse secondary. The nuclei were counter stained with DAPI*

A) *Representative confocal image (n=3) taken using Zeiss LSM 510 confocal microscope.*

*Fluorescence of at least 100 nuclei per condition was measured using Image J software and normalized to the untreated control at each time point. A separate box plot is shown for the intensity of γH2AX at B) 1 hours post irradiation and C) 24-hour post irradiation. The box plot indicates the median and the interquartile ranges of the data. The whiskers demonstrate the 95% percentile.*

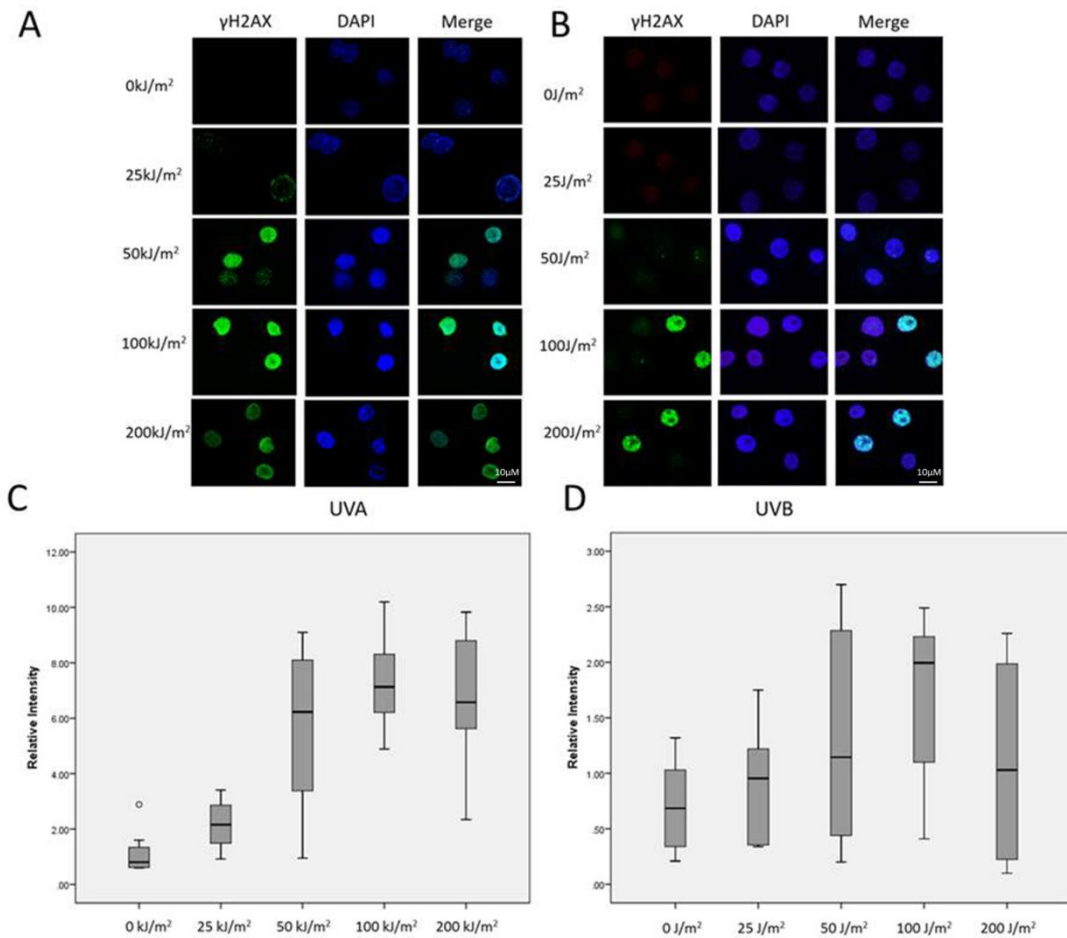


**Figure 3.9 NHEK cells show similar dose response relationship of H2AX phosphorylation following UVA/UVB than the immortalised HaCaT**

*NHEK cells were seeded on coverslips and exposed to varying doses of UVA or UVB irradiation, the cells were then fixed at either 1 hour (UVA) or 24 hour (UVB). The coverslips were processed using an antibody to  $\gamma$ H2AX (ser139) (ab26350) and Alexa Fluor 488 conjugated anti mouse secondary. The nuclei were counterstained using DAPI. Representative confocal image (n=3) taken using Zeiss LSM 510 confocal microscope for A) 1 hour post UVA and B) 24 hours post UVB.*

*Fluorescence of at least 100 nuclei per condition was measured using Image J software and normalized to the untreated control at each time point. A separate box plot is shown for the intensity of  $\gamma$ H2AX at C) 1 hours post UVA- irradiation and D) 24-hour post UVB-irradiation. The box plot indicates the median and the interquartile ranges of the data. The whiskers demonstrate the 95% percentile.*

Figure 3.8 shows that there is a dose- response relationship between UVB and  $\gamma$ H2AX upregulation when looking at the 24-hour time point. The lowest dose that was able to induce an increase in  $\gamma$ H2AX compared to the control was 100J/m<sup>2</sup> and a further increase in H2AX phosphorylation was also detected with the 200J/m<sup>2</sup> dose. When looking at  $\gamma$ H2AX foci formation at 1-hour post UVB irradiation very few foci are detected following any dose of UVB except the largest dose used. Figure 3.9 demonstrates that in the NHEKs the lowest dose of UVB that resulted in a detectable increase of H2AX phosphorylation was 100J/m<sup>2</sup>, showing a similar dose response relationship in the two cell lines.

When looking at figures 3.7 and 3.8 alongside the clonogenic survival experiments data shown in figure 3.1 and 3.2 it is possible to conclude that a lower relative cytotoxicity of UVA compared to UVB is able to induce detectable formation of  $\gamma$ H2AX foci in the utilized model. This was indicated by significant increases in  $\gamma$ H2AX staining relative to the un-irradiated control occurring at a lower relative dose following UVA compared to UVB irradiation. These dose response experiments and the time frame experiments further indicate a different mechanism in H2AX phosphorylation following each irradiation type.

#### **3.3.4 Investigating the effect of cell cycle progression on the ability of UVB to form $\gamma$ H2AX foci formation.**

To further confirm that the  $\gamma$ H2AX foci formed by UVA and UVB irradiation are caused by the activation of different mechanisms flow cytometry techniques were utilised to show the position in the cell cycle distribution of  $\gamma$ H2AX positive cells. This could indicate whether there was any dependence on replication for the formation of  $\gamma$ H2AX foci following either irradiation type. For these experiments the same time points that had previously shown the highest levels of H2AX phosphorylation following both UVA and UVB were used. A time matched control was used for each irradiation sample. The data was analysed using Flowing Software to construct dot plots of FITC staining against PI staining, a quadrant was then constructed onto each box plot to highlight FITC positive and negative populations and to distinguish between G1 and S-phase cells. The

percentage of positive or negative cells for each condition was calculated for three independent replicates.

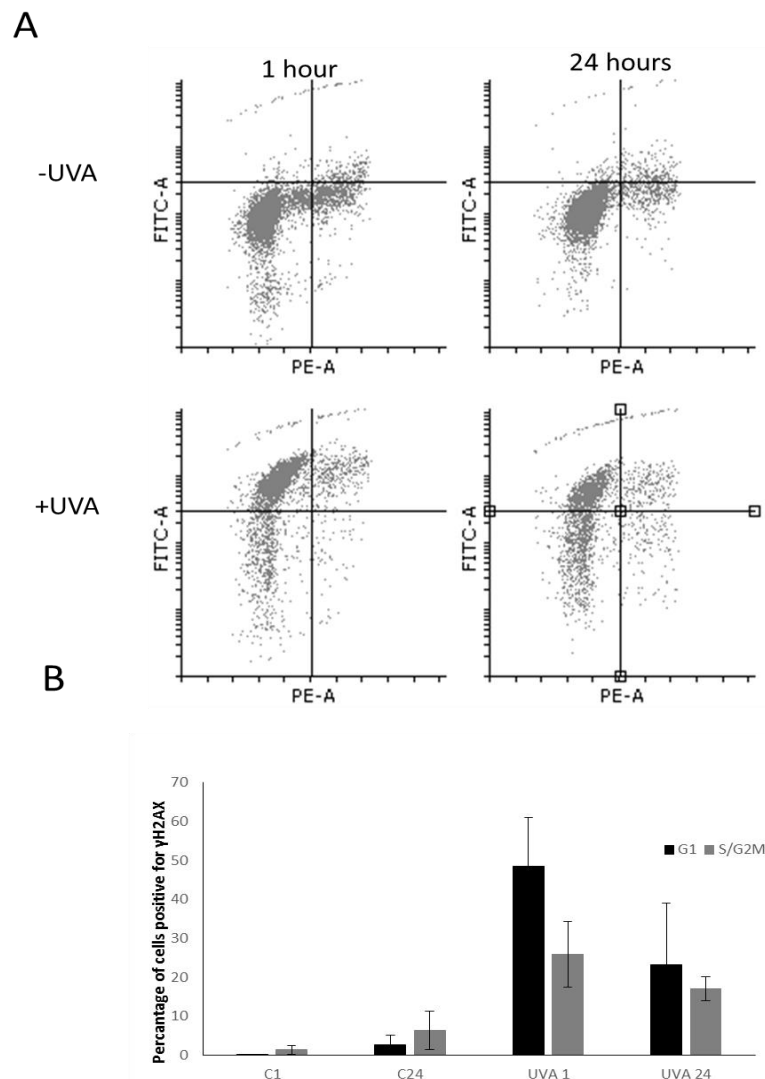


**Figure 3.10 UVA induced  $\gamma$ H2AX is independent of replication.**

*HaCaT cells were exposed to 100kJ/m<sup>2</sup> UVA; the cells were harvested by trypsinisation, pelleted by centrifugation and washed once in PBS before fixation. The cells were fixed at either 1 or 24 hours post irradiation. The cell suspension was processed using an antibody to  $\gamma$ H2AX (ser139) and Alexa Fluor 488 conjugated anti mouse secondary. Propidium iodide was added to the samples immediately before analysis to determine the DNA content of each cell. The samples were analysed using BD FACSCanto II flow cytometer; the data was according to the PI signal area and width to exclude the presence of doublets.*

*A) Flowing Software was used to create a dot plot of FITC staining vs PI staining, and a quadrant was drawn identify FITC positive cells and cell cycle stage*

*B) The average percentage of cells in each of the 4 quadrants for three biologically independent replicates was calculated, a bar graph was plotted to show the percentage of  $\gamma$ H2AX positive cells at each stage of the cell cycle for each time point. Error bars represent the standard deviation.*

Figure 3.10 A) shows that there are  $\gamma$ H2AX foci in all cells independent of cell cycle stage following UVA irradiation when the cells were fixed for analysis at 1-hour post irradiation. At 1 hour post UVA irradiation 74% (+/-4.7%) of the cell population was detected to be positive for H2AX phosphorylation. A decrease in fluorescence was detected at 24 hours post UVA compared to 1 hour post UVA, when 43%(+/- 13%) of the cell population was positive for H2AX phosphorylation. This is consistent with the data gained from the immunofluorescence in Figure 3.3 the data shown here in figure 3.10 suggests that the formation of  $\gamma$ H2AX foci following UVA irradiation is independent of replication, consistent with what was found by Greinert et al (2012) who saw the presence of H2AX phosphorylation in G1 synchronised cells following UVA irradiation.

Quantitation of the flow cytometry analysis shown in Figure 3.10 B) demonstrates a striking increase is seen in  $\gamma$ H2AX positive cells 1 hour after UVA irradiation in both stages of the cell cycle. The increase in positive cells in G1 phase at 1-hour post UVA is significant ( $P < 0.05$ , One-way ANOVA) increased compared to the time matched control. A significant ( $P < 0.05$ , One-way ANOVA) decrease is seen in the  $\gamma$ H2AX positive cells at 24 hours post UVA compared to 1-hour post UVA indicating that between these time points DNA repair has successfully dealt with the damage occurred and that the cells are able to successfully deal with damage at that level.

In contrast figure 3.11 shows that following UVB irradiation, positive cells were only seen in cells in S phase and later and not in the G1 phase. Consistent with earlier data (Figure 3.5) positive cells were not seen 1-hour post UVB irradiation showing that H2AX phosphorylation is a delayed event following UVB irradiation. This indicates that the formation of  $\gamma$ H2AX foci following UVB irradiation is dependent on replication, a further indication that these foci are as a result of stalled replication forks and not through double strand breaks arising directly.

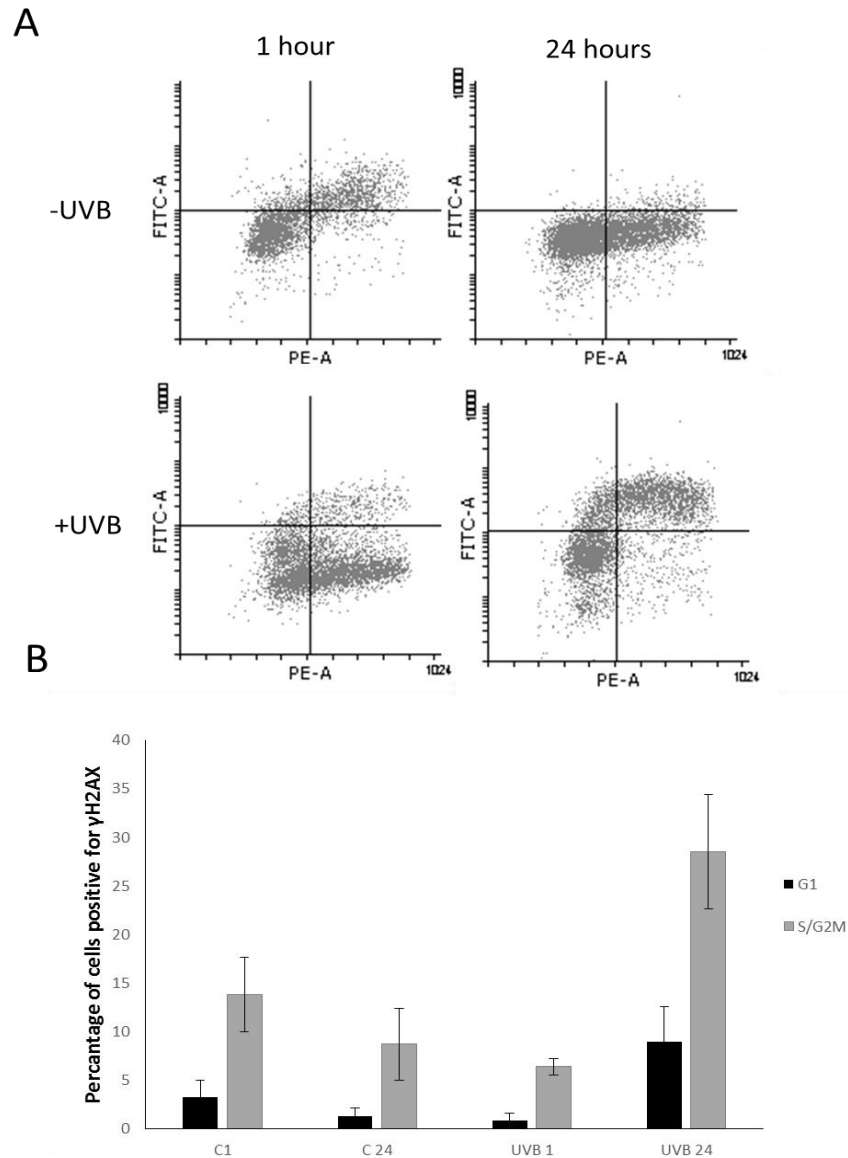


**Figure 3.11 H2AX phosphorylation following exposure to UVB irradiation is dependent on cell cycle progression**

*HaCaT cells were exposed to 100J/m<sup>2</sup> UVB; the cells were harvested by trypsinisation, pelleted by centrifugation and washed once in PBS. The cells were fixed at either 1 or 24 hours post irradiation. The cell suspension was processed using an antibody to  $\gamma$ H2AX (ser139) and Alexa Fluor 488 conjugated anti mouse secondary. Propidium iodide was added to the samples immediately before analysis. The samples were analysed using BD FACSCanto II flow cytometer. The data was gated according to the PI signal area and width to avoid any doublets being included in the analysis.*

*A) Flowing Software was used to create a dot plot of FITC staining vs PI staining, and a quadrant was drawn identify FITC positive cells and cell cycle stage*

*B) The average percentage of cells in each of the 4 quadrants for three biologically independent replicates, a bar graph was blotted to show the percentage of  $\gamma$ H2AX positive cells at each stage of the cell cycle. Error bars represent the standard deviation.*

Unlike what was seen following UVA irradiation there was no significant increase in  $\gamma$ H2AX at 1-hour post UVB in either G1 or S-phase cells ( $P=0.248/P=0.149$ , One-way ANOVA). Additionally, there was no increase in positive cells in G1 phase at 24 hours post UVB ( $P=0.203$ , One-way ANOVA), a significant ( $P<0.05$ , One-way ANOVA) increase in positive cells was seen in S-phase cells at 24 hours post UVB. For each of the un-irradiated time points a slight increase in  $\gamma$ H2AX positive cells in S-phase cells compared to G1 was detected. This was not an unexpected observation as DNA damage occurs routinely in cells so it is inevitable to see low levels of  $\gamma$ H2AX and other DNA repair proteins, in particular in S phase as a result of the occurrence of stalled replication forks.

### **3.3.5 Activation of ATM following UVA and UVB irradiation**

It is well established that  $\gamma$ H2AX foci can be formed in response to both double strand breaks (Burma et al., 2001) and the presence of stalled replication forks (Ward and Chen, 2001). The earlier data generated in the time course experiments showed different time frames of  $\gamma$ H2AX foci formation following UVA compared to UVB irradiation and indicated that the formation of foci following UVB was replication dependent.

Therefore, in order to further establish the mechanism by which H2AX is phosphorylated following each type of irradiation, activation of ATM was probed for within the time frames where H2AX phosphorylation had previously been detected. A time matched control was also carried out. Activation of ATM would suggest that the foci are formed as a consequence of double strand breaks rather than stalled replication forks.

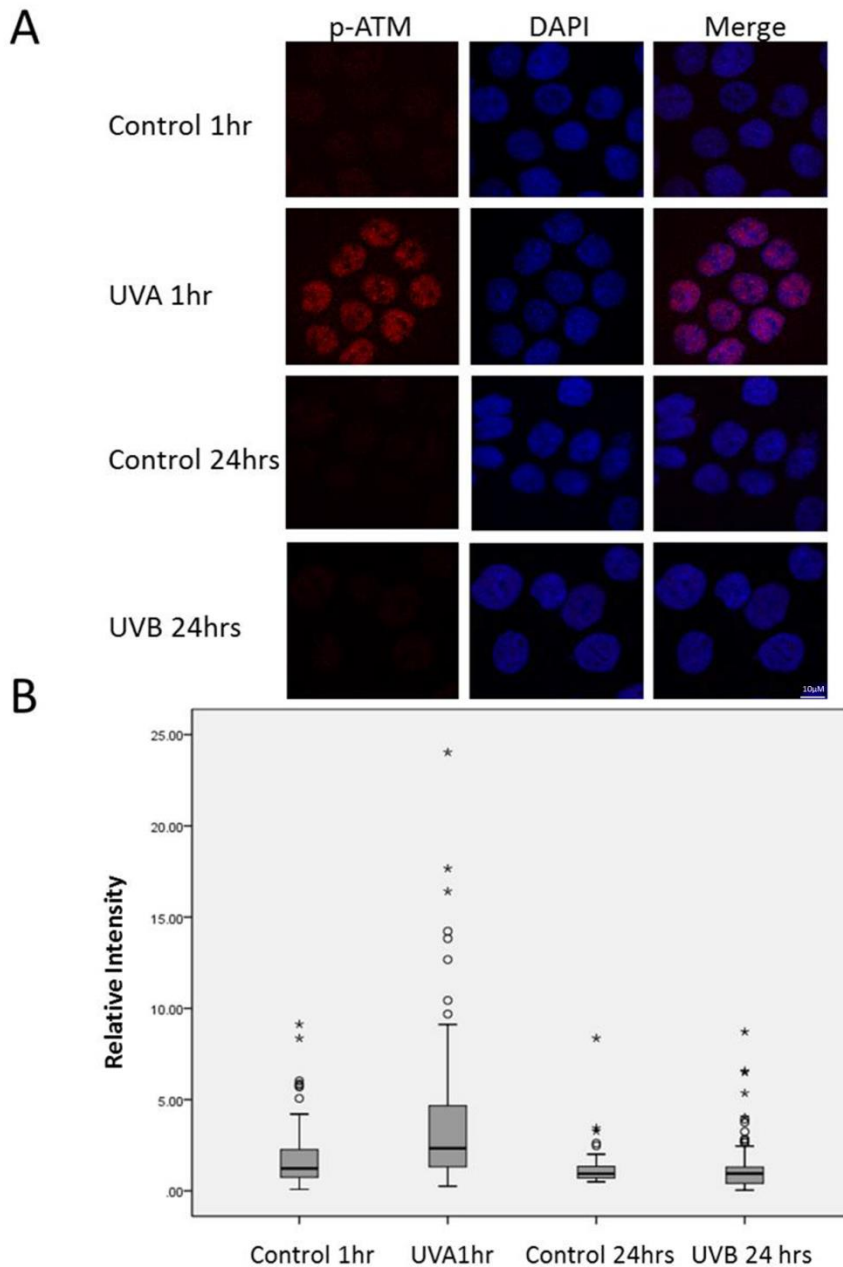


**Figure 3.12 UVA but not UVB is able to induce phosphorylation of ATM**

*HaCaT cells were grown on a coverslip and irradiated with either 100kJ/m<sup>2</sup> UVA or 100J/m<sup>2</sup> UVB. The cells were fixed at 1hour (UVA) or 24 hours post irradiation (UVB). The cells were then permeabilised, blocked in 5% BSA and incubated with anti ATM and anti-mouse antibodies. The nuclei were counter stained with DAPI and the slides were visualised using a Zeiss LSM 510 confocal microscope.*

- A) *A representative confocal image (n=3) of HaCaT cells showing staining for p-ATM (red) and DAPI nuclear staining (blue)*
- B) *The intensity of staining per nuclei was measured using ImageJ software, the staining of each nucleus was normalized to that of the average staining of the control group and a box plot was constructed to represent the median and the spread of the data. The box represents the median and interquartile range and the whiskers show the 95 percentiles.*

Figure 3.12 showed that ATM was phosphorylated following UVA but not UVB exposure. ATM was seen to be significantly ( $P < 0.01$ , One-way ANOVA) activated at 1-hour post UVA irradiation compared to the time matched control. Conversely there was no significant increase ( $P = 0.816$ , One-way ANOVA) in ATM phosphorylation following UVB irradiation at the 24-hour time point where I had previously shown H2AX phosphorylation to be significantly increased.

The experiments carried out thus far indicated strikingly different mechanisms and kinetics of H2AX phosphorylation following exposure to either UVA or UVB irradiation. Therefore, going forward the two irradiation types would be looked at separately in order to allow further investigation into the mechanisms of foci formation following each.

### **3.3.6 Validation of PIK inhibitors**

Following the observation of phospho - ATM in response to UVA but not UVB or sham irradiation; I wanted to identify if the  $\gamma$ H2AX foci formation was dependent on ATM or ATR for each of irradiation types. Pharmacological inhibitors to ATM and ATR were used to identify any H2AX phosphorylation dependence following UVA or UVB. The selectivity and specificity of the inhibitors used is described in table 3.1.

Name of inhibitor	Primary target	IC <sub>50</sub>	Cross reactivity IC <sub>50</sub>
VE-821	ATR	13 nM	ATM = 16 nM DNA-PK = 2.2 nM PI3K = 3.9 nM
KU-55933	ATM	12.9 nM	PI3K = 16.6 nM DNA-PK = 2.5 nM

### **Table 3.1 Pharmacological inhibitors of PIKKs**

Prior to the use of the inhibitors in any experimental work they were first validated to ensure that they could abrogate  $\gamma$ H2AX signal following chemical treatments where the mechanism of H2AX phosphorylation is well defined. Zeocin treatment was used to induce double strand breaks in the cells, which would cause ATM dependent phosphorylation of H2AX. Aphidicolin was used to induce stalled replication forks, which would result in ATR dependent H2AX phosphorylation. In each case the inhibitors were used at a dose of 1  $\mu$ M and the cells were treated with the inhibitors for 1 hour prior to treatment with zeocin or aphidicolin as appropriate.

These doses were below the IC<sub>50</sub> of any cross reactivity, therefore unlikely to knock down any pathways other than their primary substrate, but considerably higher than the IC<sub>50</sub> of their substrate. These doses were chosen to ensure that both ATR and ATM were fully inhibited by their specific inhibitor. The inhibitors were added to the cells for 1 hour prior to treatment with the respective DNA damaging agents; this time frame was decided because the activation of ATM and ATR are well characterized to be very early events in response to double strand break and stalled fork formation respectively.

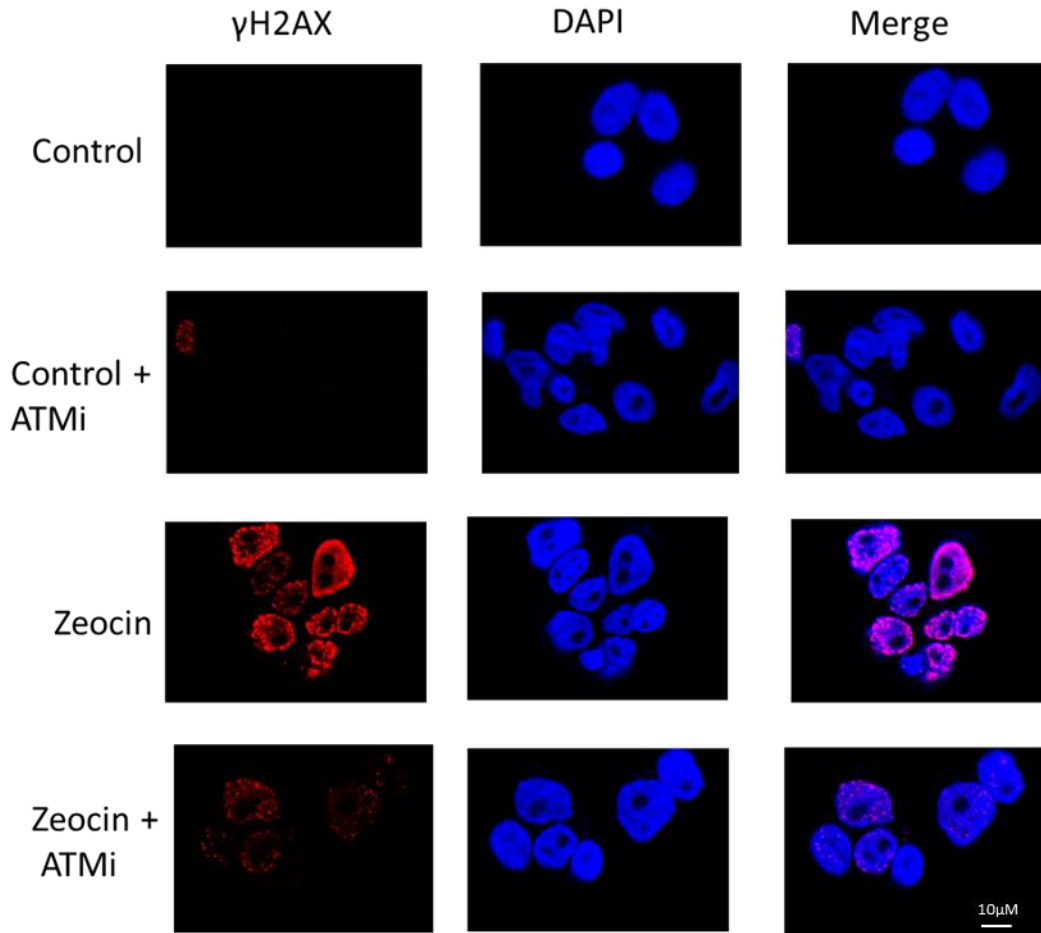


**Figure 3.13 an inhibitor to ATM abrogates H2AX phosphorylation following treatment with zeocin.**

*HaCaT cells were seeded onto glass coverslips, allowed to adhere before pre-treatment with or without an inhibitor to ATM at a concentration of 1 $\mu$ M. Zeocin was added 1-hour post inhibitor treatment at a concentration of 100 $\mu$ g/ml. 1 hour post treatment the cells were fixed and processed using an antibody to  $\gamma$ H2AX (ser139) and Alexa Fluor 488 conjugated anti mouse secondary antibody. DAPI was used to counterstain the nuclei and the cells were visualized using a Zeiss 510 LSM confocal microscope.*

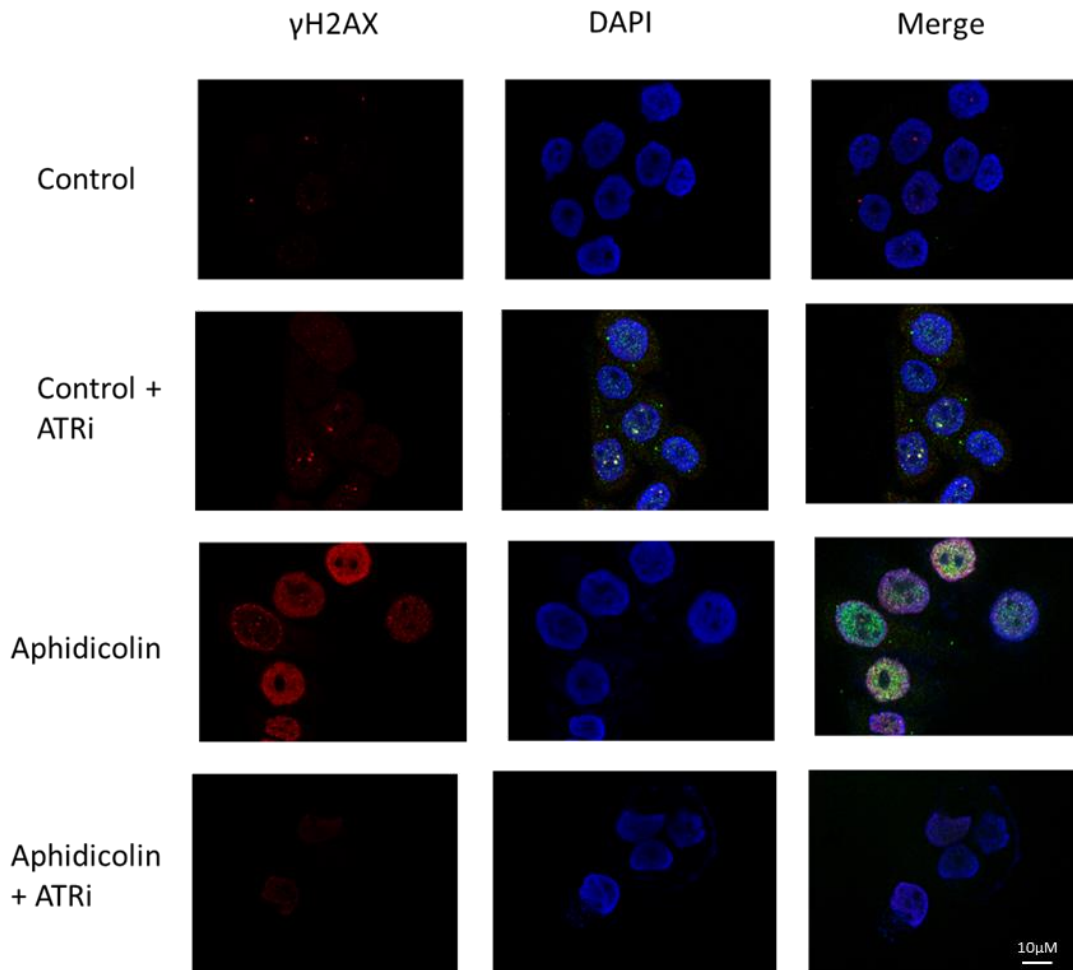


**Figure 3.14 An inhibitor to ATR abrogates H2AX phosphorylation following aphidicolin treatment.**

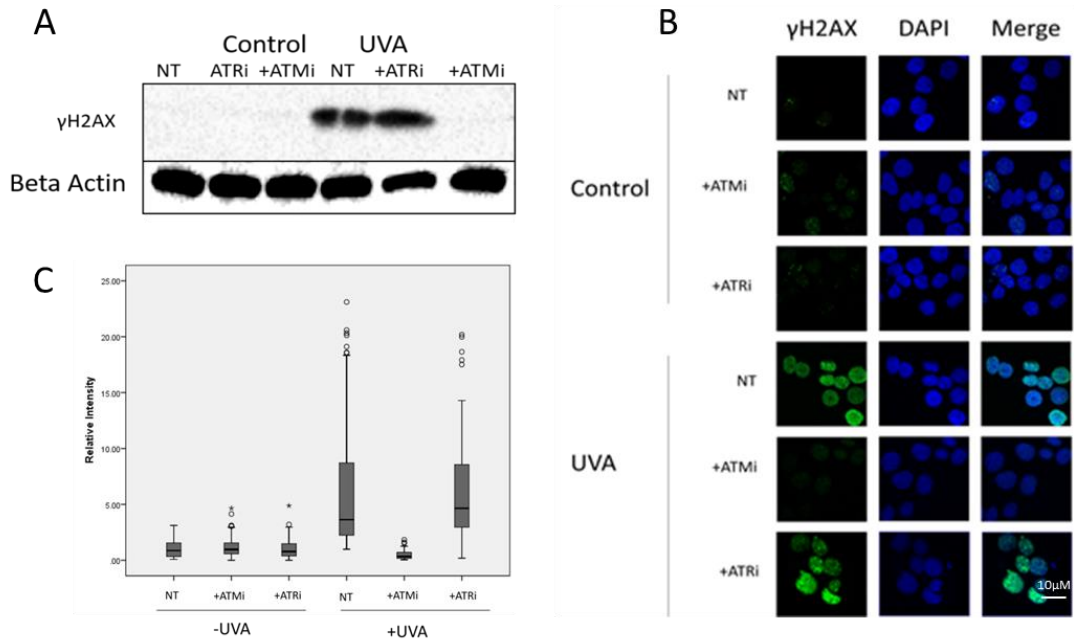
*HaCaT cells were treated with an inhibitor to ATR at a concentration of 1 $\mu$ M for 1 hour prior to treatment with aphidicolin at a concentration of 1 $\mu$ g/ml for 16 hours, after which the cells were fixed and processed using an antibody to  $\gamma$ H2AX (ser139) and Alexa Fluor 488 conjugated anti mouse secondary antibody. DAPI was used to counterstain the nuclei and the cells were visualized using a Zeiss 510 LSM confocal microscope.*

Figure 3.13 shows that pre-incubation of the cells with an ATM inhibitor prior to treatment with zeocin resulted in a marked decrease in H2AX phosphorylation compared to cells which were treated with zeocin only, therefore confirming that the ATM inhibitor KU-55933 is able to prevent the ATM dependent phosphorylation of H2AX following double strand break formation. Importantly no changes in morphology in the control cells treated with KU-55933 was seen and there was no change in H2AX phosphorylation.

Figure 3.14 shows that that the use of an inhibitor to ATR caused a decrease in H2AX phosphorylation in aphidicolin treated cells compared to the cells treated with aphidicolin alone. This confirms that the inhibitor VE-821 was able to block ATR-dependent phosphorylation of H2AX following stalled fork formation. Again, no changes in morphology of the cells was detected as a result of treatment with the inhibitor.

### **3.3.7 Mechanism of H2AX phosphorylation following UVA irradiation.**

Initially the effect of each of the previously described inhibitors on the ability of UVA to induce  $\gamma$ H2AX foci was investigated. The inhibitors to ATM or ATR were added to the cells to a final concentration of 1 $\mu$ M for 1 hour prior to irradiation. The irradiation conditions and the time point at which the cells were fixed remain the same as were used for previous experiments.



**Figure 3.15 An inhibitor to ATM abrogates the  $\gamma$ H2AX response of UVA HaCaT cells** were incubated with either an inhibitor to ATM or ATR at a final concentration of  $1\mu\text{M}$  for 1 hour prior to irradiation. Cells were then irradiated with UVA ( $100\text{kJ}/\text{m}^2$ ) or sham irradiated.

- A) Western blot analysis of protein extracts harvested at 1-hour post UVA-irradiation. The membrane was probed for  $\gamma$ H2AX (ser139) and HRP-conjugated Sheep polyclonal antibody to mouse.
- B) The cells were fixed at 1-hour post irradiation processed using an antibody to  $\gamma$ H2AX (ser139) and Alexa Fluor 488 conjugated anti mouse secondary and imaged using a Zeiss LSM 510 confocal microscope. A representative confocal image is shown ( $n=3$ ).
- C) Average fluorescence per nucleus was quantified using Image J, the fluorescence was normalised to the untreated control and a box plot constructed, where the box represented median and interquartile ranges of the data and the whiskers showed the 95 percentiles.

The data in figure 3.15 shows that the addition of the ATM inhibitor to the media for 1 hour prior to irradiation at a concentration of 1  $\mu$ M significantly decreases ( $P < 0.001$ , One-way ANOVA) the foci formation following UVA irradiation compared to the un-treated UVA irradiated cells. In this group the intensity of  $\gamma$ H2AX staining is similar to that of the control ( $P = 0.730$ , One-way ANOVA). The addition of the ATR inhibitor has no significant effect on foci formation ( $P = 0.842$ , One-way ANOVA). Importantly the addition of either inhibitor to the un-irradiated group had no effect on the intensity of  $\gamma$ H2AX staining ( $P = 0.99$ , One-way ANOVA).

However, in addition to ATM, DNA-PK is also activated in response to double strand breaks and there is evidence to suggest that there is some overlap between ATM and DNA-PK, cell lines deficient in either ATM or DNA-PK were found to phosphorylate H2AX in equal quantities to proficient cell lines following ionising radiation. Although there was a delay in H2AX phosphorylation detected in the ATM deficient cells suggesting that ATM plays the more prominent role than DNA-PK when both are present (Stiff et al., 2004).

It is unlikely that the decrease in  $\gamma$ H2AX staining that was observed following pre-treatment with ATM inhibitor is as a result of changes in the level of DNA-PK, the dose of inhibitor used was 2.5 times lower than the  $IC_{50}$  for DNA-PK. To further show that the previous results were as a result of ATM inhibition and not DNA-PK, Mirin, an inhibitor to the MRN complex was utilized. The MRN complex is well established to play a vital role in the recruitment of ATM but not DNA-PK to double strand breaks (Uziel et al., 2003). The recruitment of ATM and DNA-PK to double strand breaks is depicted in figures 3.16 and 3.17 respectively.

Furthermore, ATM can be phosphorylated in response to both double strand breaks (Burma et al., 2001) and changes in chromatin structure therefore the data generated up until this point does not tell us for certain that the increase in  $\gamma$ H2AX foci formation that

have been detected in response to UVA irradiation are as a result of the occurrence of double strand breaks.

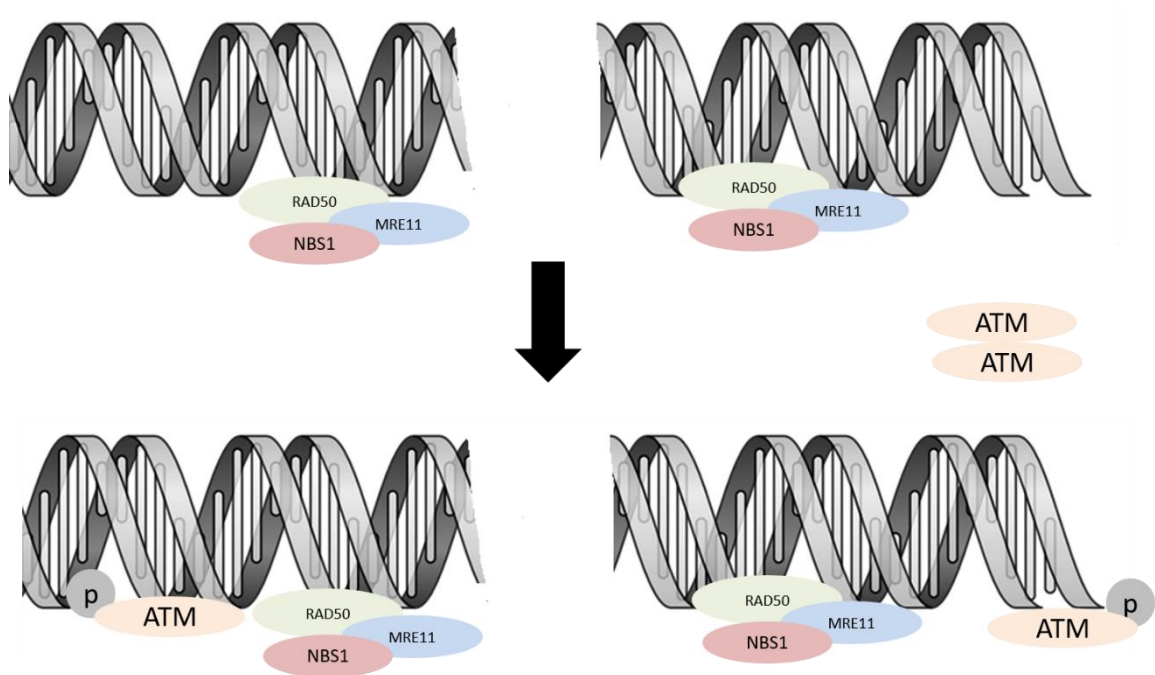


**Figure 3.16 The recruitment of ATM to double strand breaks is dependent on the MRN complex.**

*Schematic representation of recruitment of ATM to the sites of double strand breaks by the MRN complex; inactive ATM exists as an inactive dimer, which becomes phosphorylated on serine 1981 following double strand break formation and is recruited to the site of breaks in its active monomer form within seconds of the break formation.*

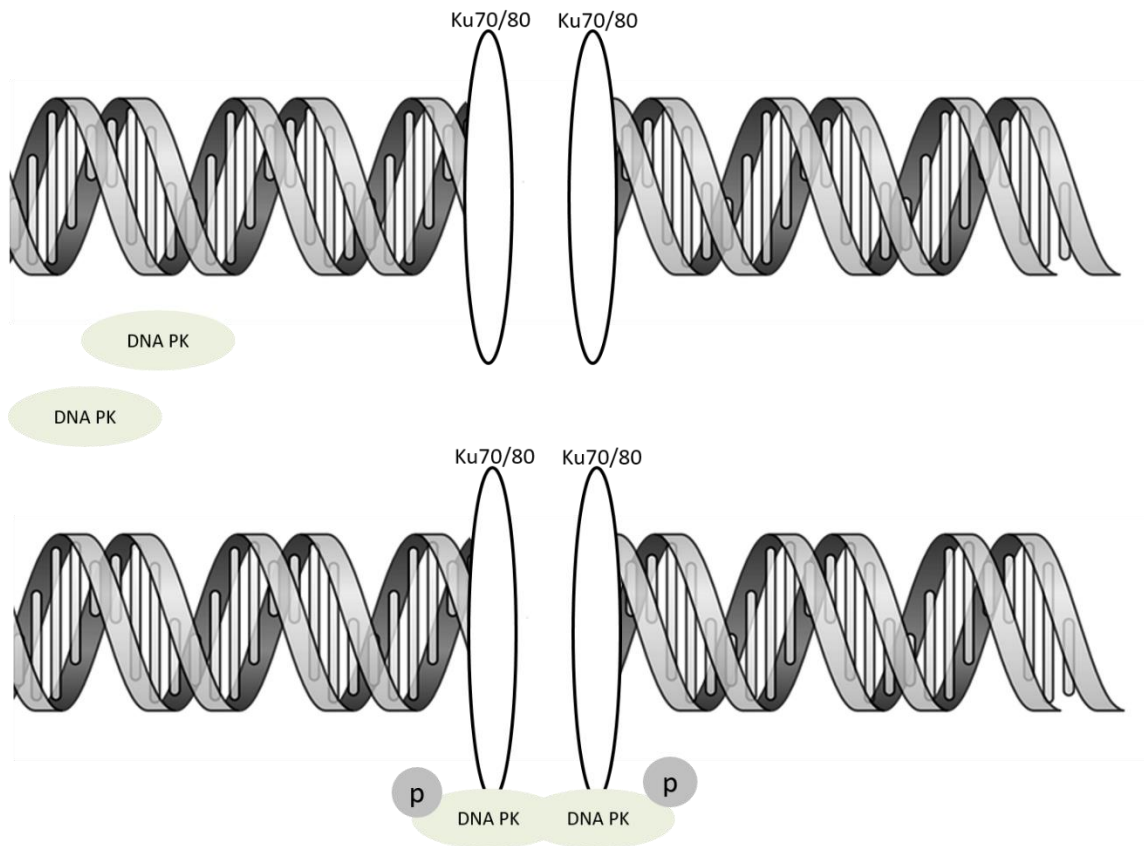


**Figure 3.17 DNA -PK is recruited to DNA ends of double strand breaks by Ku70/80**

*Schematic representation of DNA PK recruitment to double strand breaks, DNA-PK is rapidly phosphorylated and recruited to the sites of double strand breaks by Ku70/80.*

Figure 3.18 demonstrated that the addition of Mirin at a concentration of 100  $\mu\text{M}$  for 1 hour prior to UVA irradiation causes a decrease in  $\gamma\text{H2AX}$  foci formation to a similar level as that of the un-irradiated control. The decrease in H2AX phosphorylation in the group pre-treated with Mirin was significant ( $P < 0.01$ , One-way ANOVA) compared to the untreated UVA-irradiated group. Therefore, indicating that the phosphorylation of H2AX following UVA is an MRN dependent event. The addition of Mirin had no detectable effect on presence of  $\gamma\text{H2AX}$  foci in the in irradiated control. Additionally, and importantly, Mirin had no effect on the morphology of the cells.

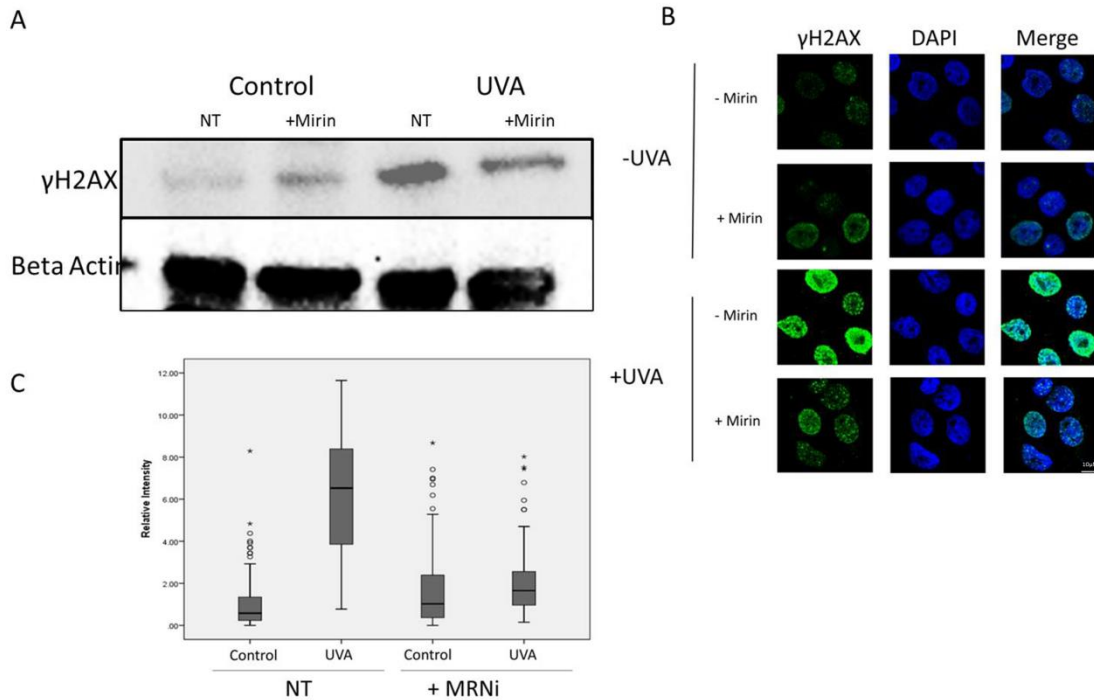


**Figure 3. 18 The formation of  $\gamma$ H2AX foci can be abrogated by pre incubation with a MRN inhibitor**

*HaCaT cells were incubated with MRN inhibitor Mirin at a final concentration of 100  $\mu$ M for 1 hour prior to UVA or sham irradiation.*

- A) *Western blot analysis for  $\gamma$ H2AX, extracts were collected at 1-hour post irradiation and probed for  $\gamma$ H2AX (ser139) and HRP-conjugated Sheep polyclonal antibody to mouse.*
- B) *The cells were fixed 1-hour post UVA irradiation processed using an antibody to  $\gamma$ H2AX (ser139) and Alexa Fluor 488 conjugated anti mouse secondary, the nuclei were counter stained using DAPI and the slides imaged using a Zeiss LSM 510 confocal microscope. A representative image is shown (n=3).*
- D) *Average fluorescence per nucleus was quantified using Image J, the fluorescence was normalised to the untreated control and a box plot constructed to represent the median and spread of intensity, where the box represented median and interquartile ranges of the data and the whiskers showed the 95 percentiles.*

### **3.3.8 Detection of 53BP1 in UVA-irradiated cells**

To further indicate the presence of DSBs in the UVA irradiated cells the upregulation of other markers of the DDR were looked for in addition to those shown thus far in this chapter; in particular, the redistribution of 53BP1 to form distinct foci, which is well established to be a mediator of great importance in the response to double strand breaks. There is evidence to suggest that the presence of 53BP1 foci are a strong indication of DSBs; 53BP1 foci have been detected following treatment with agents known to induce DSBs such as ionizing radiation but not in response to agents that induce replication stress or other DNA lesions (Schultz et al., 2000). 53BP1 contains interaction surfaces for numerous DSB responsive proteins and is involved in multiple functions following the occurrence of a DSB, such as; checkpoint signaling (Fernandez-Capetillo et al., 2002) recruitment of DSB responsive proteins, synapsis of distal DNA ends during NHEJ (Huen et al., 2010; Silverman et al., 2004) as well as influencing DNA repair pathway choice (Bunting et al., 2010).

53BP1 is rapidly redistributed to sites of DSBs, however the interaction between 53BP1 is complex and bimodal, the immediate accumulation of 53BP1 at the site of a DSB requires direct interaction between the Tudor domain of 53BP1 and dimethylated lysine on histone 3. This chromatin modification is present in DNA lacking double strand breaks and it was postulated that the presence of a DSB unmasks the modification, therefore allowing the interaction with 53BP1. After the initial contact has occurred, the retention of 53BP1 at the site of damage is dependent on the ATM mediated phosphorylation of H2AX.

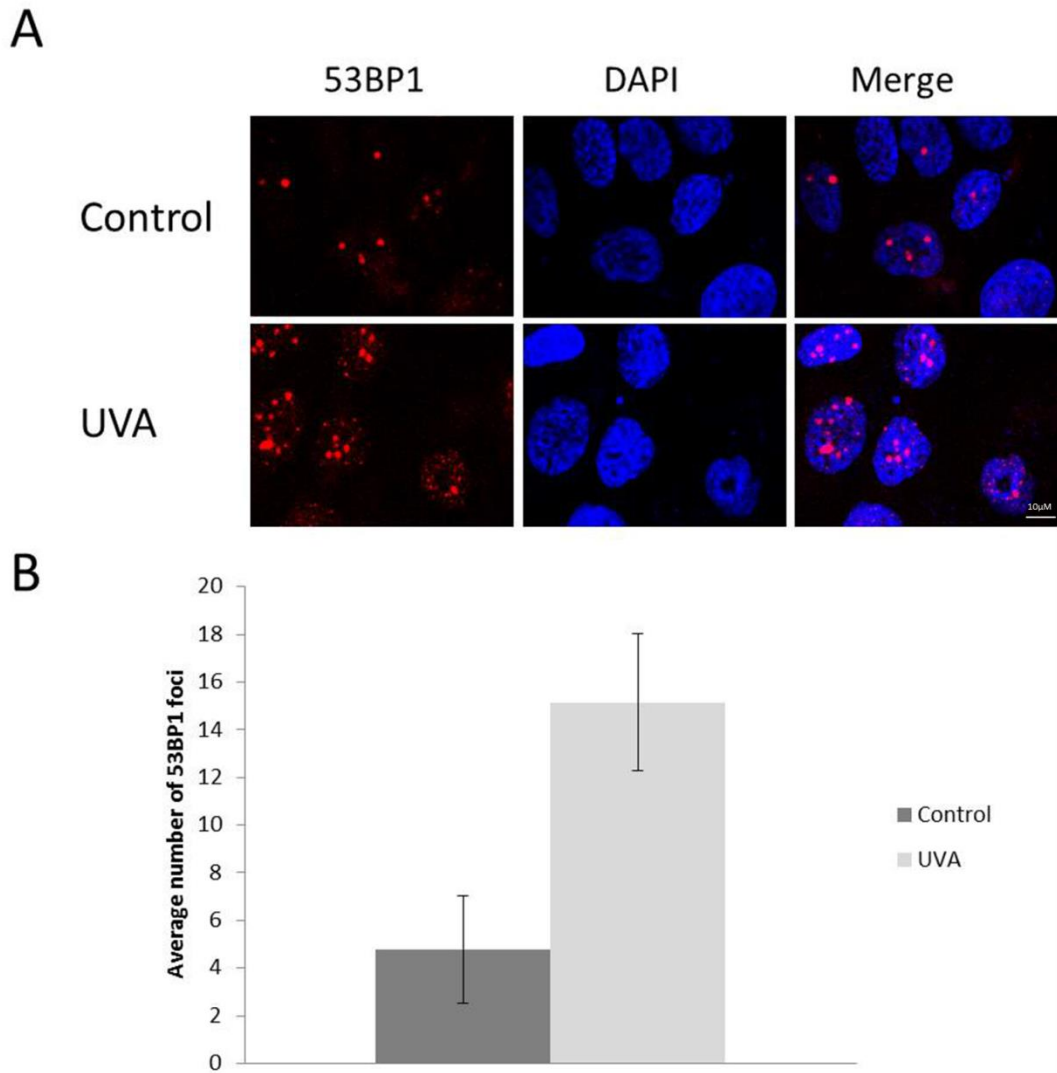


**Figure 3.19 UVA induces an increase in 53BP1 within the same time frames as H2AX phosphorylation**

A) HaCaT cells were seeded onto glass coverslips and allowed to adhere overnight at 37°C and 5%CO<sub>2</sub>. The cells were then irradiated with 100kJ/m<sup>2</sup> UVA, or sham irradiated. The cells were fixed 1-hour post UVA irradiation, processed using an antibody to 53BP1 (GENE TEX) and Alexa Fluor 555 conjugated anti rabbit secondary, the nuclei were counter stained using DAPI and the slides imaged using a Zeiss LSM 510 confocal microscope. A representative image is shown (n=3).

B) Average foci count per nucleus was quantified using Image J, and a bar chart was constructed to show the average number of foci and the error bars represent the standard deviation.

Figure 3.19 demonstrates that an increase in average number of 53BP1 foci per nucleus was detected in the UVA irradiated cells at 1-hour post irradiation. This was the time point in which H2AX phosphorylation had been seen to peak following exposure to UVA. This is consistent with published work that has described 53BP1 to co-localise with  $\gamma$ H2AX and ATM in response to DSBs.

### **3.3.9 Mechanism of H2AX phosphorylation following UVB**

As previously described following on from the UVA irradiation experiments pharmacological inhibitors to either ATM or ATR were added to the cells prior to UVB irradiation and the intensity of  $\gamma$ H2AX staining was analysed to investigate the effect of either on inhibitor on the cells ability to respond to DNA damage following UVB irradiation.

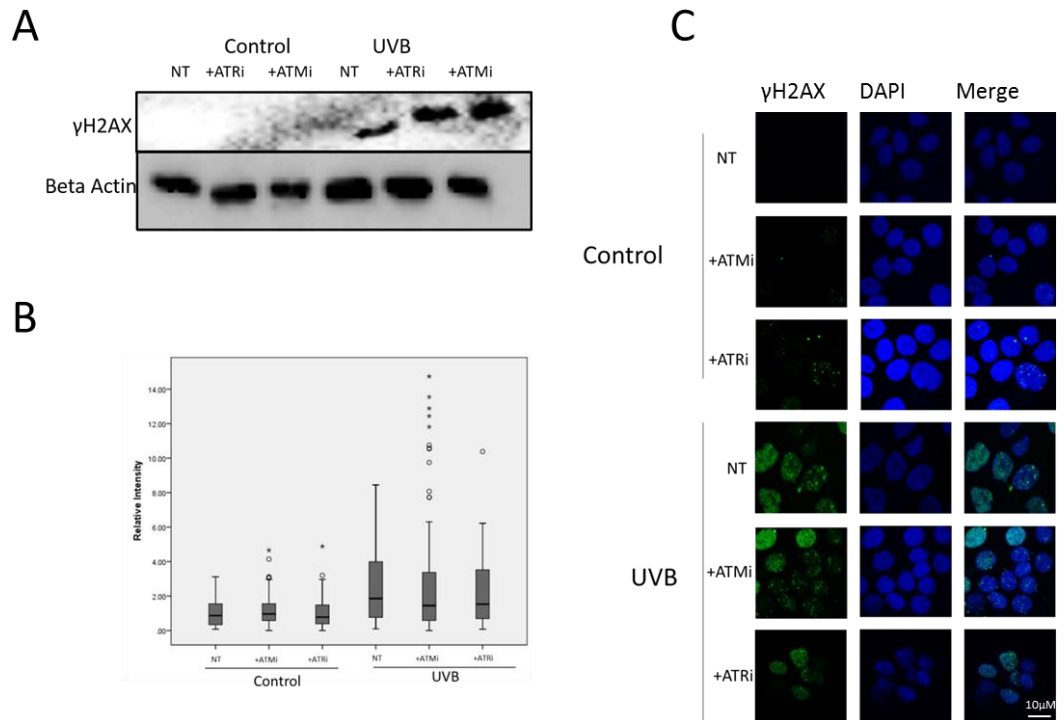


**Figure 3.20 Neither an inhibitor to ATM or ATR result in a decrease in H2AX phosphorylation following UVB irradiation.**

*HaCaT cells were incubated with either an inhibitor to ATM or ATR at a final concentration of 1  $\mu$ M for 1 hour prior to irradiation. Cells were then irradiated with UVB (100J/m<sup>2</sup>) or sham irradiated.*

- A) Western blot analysis of protein extracts collected at 24 hours post irradiation. The blot was probed for  $\gamma$ H2AX (ser139) and HRP-conjugated Sheep polyclonal antibody to mouse.*
- B) The cells were fixed at 24 hours post irradiation processed using an antibody to  $\gamma$ H2AX (ser139) and Alexa Fluor 488 conjugated anti mouse secondary, the nuclei were counterstained using DAPI and imaged using a Zeiss LSM 510 confocal microscope. A representative Image is shown (n=3).*
- C) Average fluorescence per nucleus was quantified using Image J, the fluorescence was normalised to the untreated control and a box plot constructed to represent the median and spread of intensity. The box represents the median and interquartile range of the data and the whiskers represent the 95% percentile.*

Figure 3.20 demonstrates that the addition of neither an inhibitor to ATM (KU-55933) or ATR (VE-291) caused a detectable decrease in the H2AX phosphorylation following UVB irradiation compared to the un-treated group. The intensity of H2AX phosphorylation staining was significantly increased in all three UVB treated groups regardless of pre-treatment with an inhibitor ( $P < 0.05$ , One-way ANOVA). No significant difference was seen in the H2AX staining of the UVB irradiated cells treated with an inhibitor to ATM ( $P = 0.666$ , One-way ANOVA) or ATR ( $P = 0.399$ , One-way ANOVA) compared to the untreated UVB group. This demonstrates that neither ATM nor ATR are solely responsible for the phosphorylation of H2AX following UVB irradiation. It was postulated that it was possible that there is some redundancy between ATM and ATR in response to stalled replication forks following UVB irradiation and that inhibiting the activity of only one of them was not sufficient to block a response. Therefore, the two inhibitors were combined, each at a concentration of  $1 \mu\text{M}$  and levels of H2AX phosphorylation investigated.

Figure 3.21 demonstrates a significant decrease ( $P < 0.001$ , One-way ANOVA) in staining for  $\gamma\text{H2AX}$  following UVB irradiation when the cells were pretreated with a combination of the ATM and ATR inhibitors. The level of  $\gamma\text{H2AX}$  in the treated cells was the same as that of the control ( $P = 0.435$ , One-way ANOVA), demonstrating full abrogation of a response to stalled forks and further suggesting some redundancy between ATM and ATR in response to the formation of stalled replication forks following exposure to UVB irradiation.

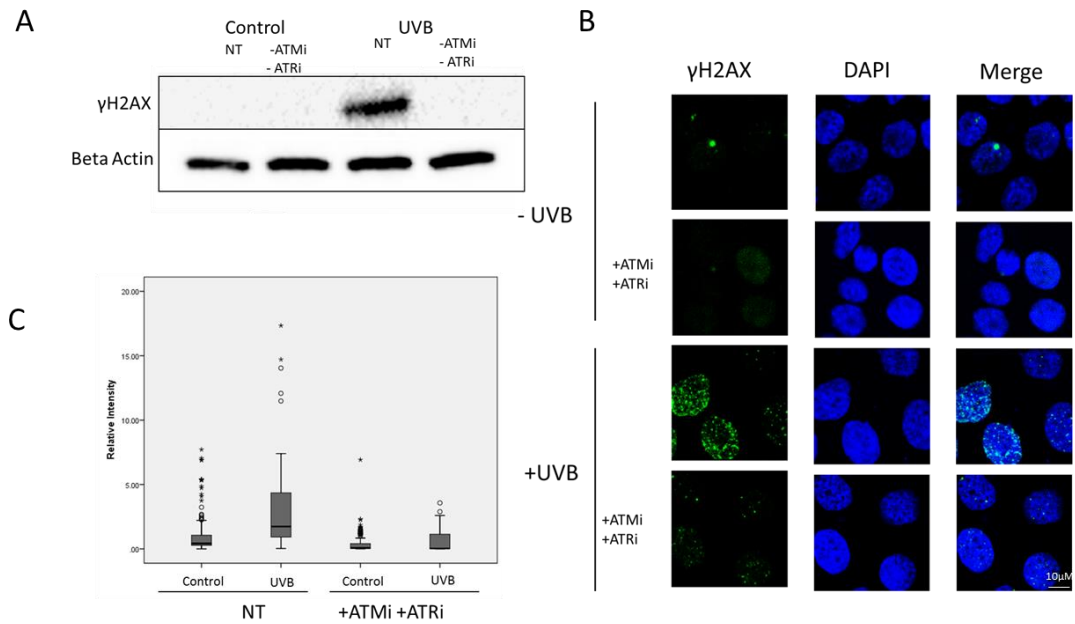


**Figure 3.21 Combination of inhibitors to ATM and ATR result in abrogation of  $\gamma$ H2AX foci formation following UVB irradiation.**

*HaCaT cells were incubated with either both an inhibitor to ATM or ATR at a final concentration of  $1\mu\text{M}$  for 1 hour prior to irradiation. Cells were then irradiated with UVB ( $100\text{J}/\text{m}^2$ ) or sham irradiated*

- A) *Western blot analysis of protein extracts collected at 24 hours post irradiation. The blot was probed for  $\gamma$ H2AX (ser139) and HRP-conjugated Sheep polyclonal antibody to mouse.*
- B) *The cells were fixed at 24 hours post irradiation processed using an antibody to  $\gamma$ H2AX (ser139) and Alexa Fluor 488 conjugated anti mouse secondary antibody, the nuclei were counterstained using DAPI and imaged using a Zeiss LSM 510 confocal microscope. A representative Image is shown (n=3).*
- C) *Average fluorescence per nucleus was quantified using Image J, the fluorescence was normalised to the untreated control and a box plot constructed to represent the median and spread of intensity. The whiskers show the 95 percentiles.*

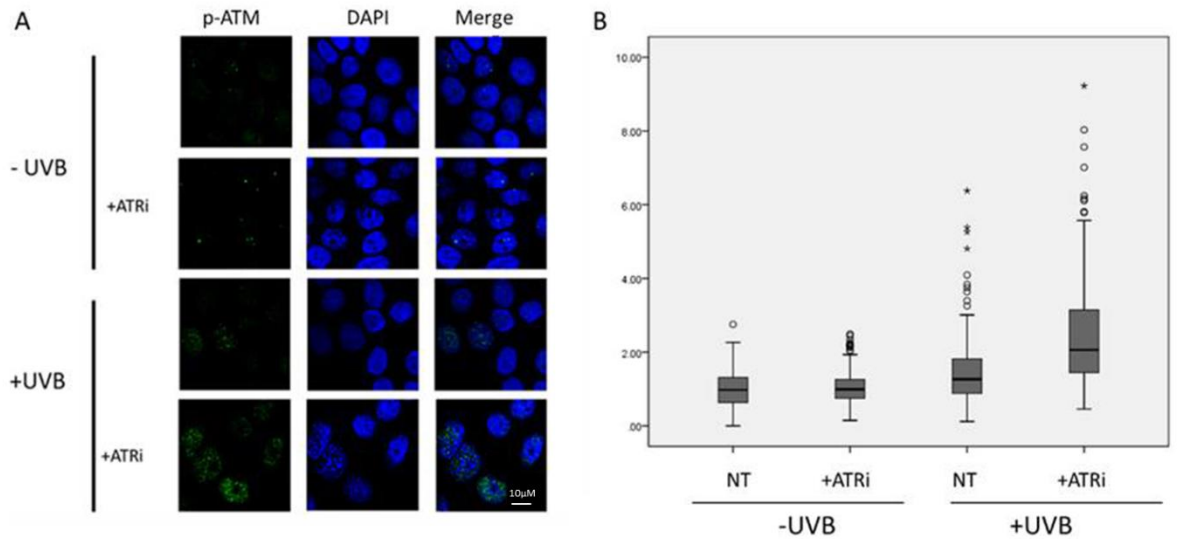


**Figure 3.22 Upregulation of ATM phosphorylation is seen following UVB when cells are pre-treated with an inhibitor to ATR**

*HaCaT cells were grown on a coverslip, then treated with 1 µM ATR (VE-821) for 1 hour prior to irradiation with 100J/m<sup>2</sup> UVB. The cells were fixed at 24 hours post irradiation.*

- A) *Representative confocal image (n=3) showing staining for p-ATM (Ser1981) (green) and DAPI (blue).*
- B) *Quantitation of  $\gamma$ H2AX fluorescence intensity of Control and UVB irradiated cells with or without prior incubation with an inhibitor to ATR. Staining intensity of p-ATM was measured using Image J software, at least 100 nuclei per condition were analysed and the experiment was repeated with 3 biologically independent replicates. The relative fluorescence compared to the control group was calculated and a box plot of the data was plotted. The box shows the median and the interquartile range of the data and the whiskers represent the 95 percentiles.*

Figure 3.22 demonstrates that the use of an ATR inhibitor results in a significant ( $P < 0.01$ , One-way ANOVA) increase in upregulation of p-ATM following UVB irradiation. This upregulation was seen within the same times that H2AX phosphorylation had previously been detected following UVB irradiation. In addition, again similar to what was detected with  $\gamma$ H2AX not all the cells in the population were positive for p-ATM. This is reflected in the quantitation, when a greater spread of intensity of staining is seen for the UVB +ATRi group compared to the three experimental groups. This data along with figures 3.20 and 3.21 suggest that ATM and ATR may function redundantly to phosphorylate H2AX following exposure to UVB and only when both ATM and ATR are inhibited is a decrease in DNA damage, as measured by H2AX phosphorylation detected.

### **3.3.10 Induction of apoptosis in UVA/UVB irradiated cells as indicated by a loss of mitochondrial membrane potential.**

In addition to looking into the DNA damage response in cells exposed to UVA or UVB irradiation changes to the mitochondrial membrane potential, an indicator of apoptosis in our cell populations were also looked at. There is significant evidence to suggest that there is a decrease in mitochondrial membrane potential associated with apoptosis induction and it is well established that mitochondria play a prominent role in apoptosis through the release of cytochrome c which, in turn leads to activation of the caspase cascade.

Changes in mitochondrial membrane potential can be measured by the commercially available dye JC-1 using the ratio of red: green staining that is seen in the mitochondria. Accumulation of JC1 in the mitochondria is indicated by a fluorescence emission shift from green to red. Loss of mitochondrial potential results in a lack of JC1 accumulation in the mitochondria and a consequent decrease in the ratio of red: green staining that can be seen (Perelman et al., 2012).

Initially, confocal microscopy was utilised to detect changes in the mitochondrial membrane potential of cells exposed to either UVA or UVB at either 3 or 24 hours post irradiation. These time points were chosen so to establish if immediate or delayed apoptosis was being induced in the cells exposed to either UVA or UVB (Godar et al., 1994). Immediate apoptosis will be induced within 3 hours, so a change in mitochondrial membrane potential should be detectable at this time point. Delayed apoptosis occurs within 24 hours and so a change in mitochondrial potential would be detectable at 24 hours if this had been induced.

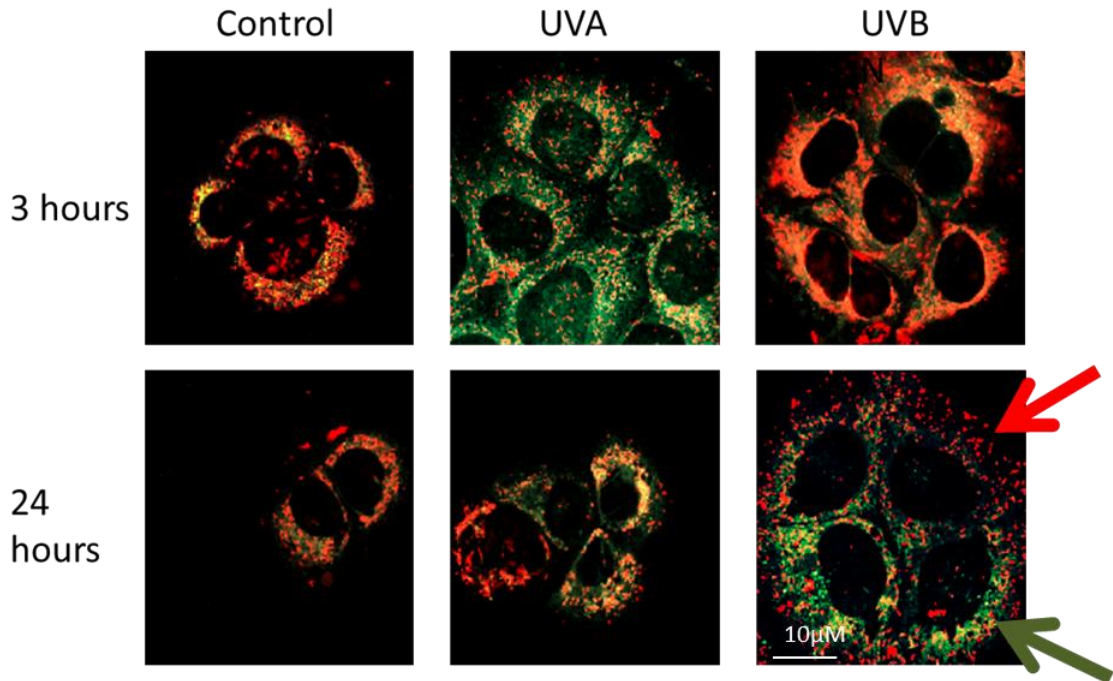


**Figure 3.23 A decrease in mitochondrial membrane potential is an event that can be detected earlier following UVA irradiation compared to UVB irradiation.**

*HaCaT cells were seeded onto glass coverslips and incubated at 37 and 5%CO<sub>2</sub> overnight. The cells were then irradiated with 100kJ/m<sup>2</sup> UVA or 100J/m<sup>2</sup> UVB. JC1 was added to the cells at a concentration of 1µg/ml at either 3 or 24 hours post irradiation and incubated for 20 minutes at 37 °C before analysis by confocal microscopy. A representative image of HaCaT cells following UVA/ UVB treatment and JC1 incubation is shown (n=3).*

Figure 3.23 demonstrates that loss of mitochondrial membrane potential occurs earlier in the HaCaT cell line following UVA compared to UVB similar to the activation of the DDR shown earlier in this chapter. A loss in mitochondrial membrane potential, as indicated by a loss of red: green staining is seen at 3 hours following UVA but not UVB, indicating that immediate apoptosis is triggered following UVA but not UVB irradiation. At 24 hours post irradiation a decrease in mitochondrial membrane potential is seen in the UVB irradiated cells. In addition, in the UVB irradiated cells, at the 24-hour time point there are two clear populations of cells, marked with arrows. Some cells showing a decrease in mitochondrial membrane potential compared to the control as indicated by the green arrow and the others showing less of a difference in mitochondrial membrane potential compared to the time matched control, an example of this indicated by the red arrow.

Somewhat surprisingly, at the 24 hour time point there does not appear to be a decrease in mitochondrial potential in the cells exposed to UVA compared to the time matched control, but it is possible that this is because, at the 24 hour time point some of the UVA irradiated cells could now be in late stages of apoptosis and have detached from the coverslip and therefore changes in the mitochondrial membrane potential of these cells is not detected by the confocal microscopy techniques that had been utilized here. So, flow cytometry techniques were utilised, which allowed collection the medium containing detached cells before harvesting the adherent cells by trypsinisation and then incubation with JC-1 and analysis by flow cytometry. The same time points were studied that had been used for the confocal microscopy approach.

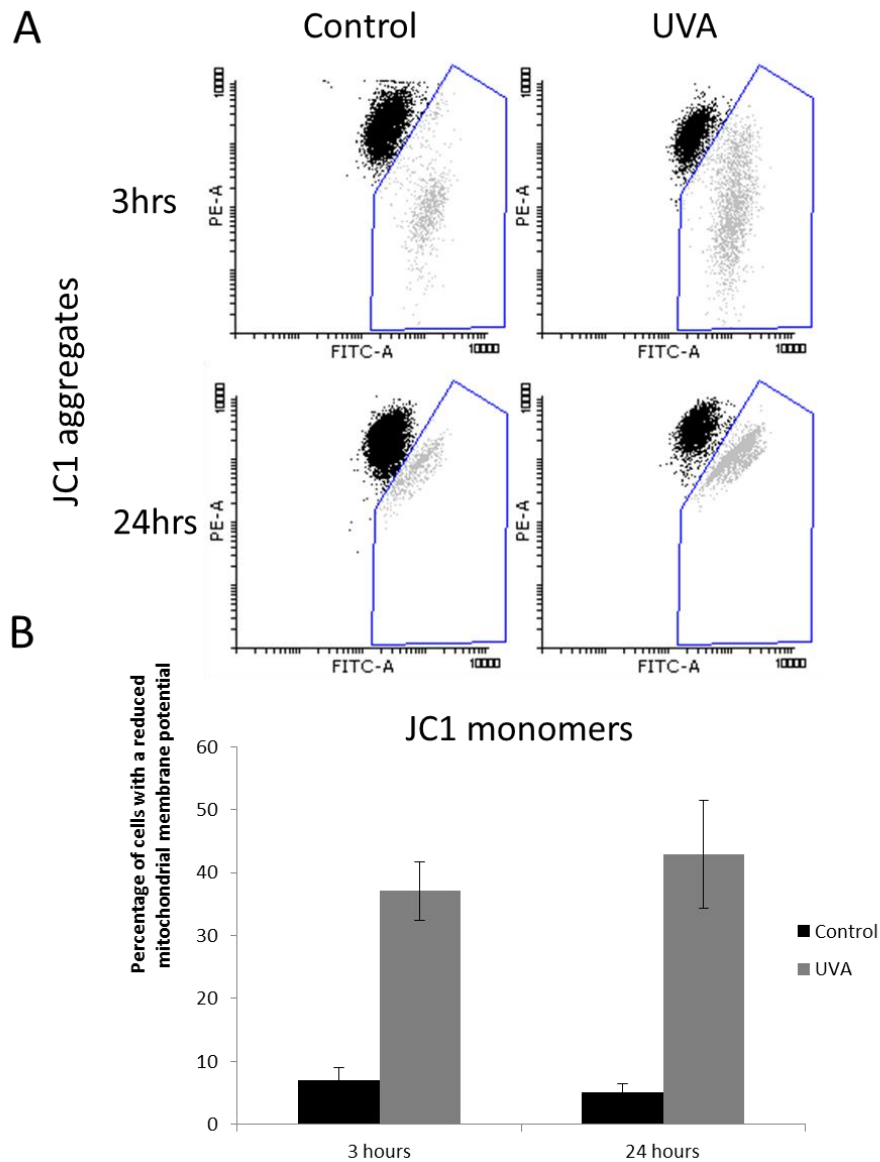


**Figure 3.24 Mitochondrial membrane potential is decreased at 3 hours following UVA irradiation**

*HaCaT cells were grown in a 60 mm culture dish and irradiated with 100 kJ/m<sup>2</sup> UVA. At either 3 or 24 hours post irradiation the media was collected, the cells were then trypsinised and the trypsinised cells were added to the previously collected media. JC1 was added to the suspension of cells at a concentration of 1µg/ml and incubated for 20 minutes at 37 °C before analysis on a BD FACSCanto II flow cytometer.*

- A) *Representative images (n=3) demonstrating JC1 staining; the gated population represents cells with decreased presence of JC1 aggregates.*
- B) *A bar graph to show the average percentage of cells in the gated (apoptotic) population. Error bars show the standard deviation.*

Figure 3.24 A) demonstrates that there is a decrease in mitochondrial membrane potential as measured by loss of JC1 aggregates present in HaCaT cells at 3 hours post UVA irradiation. At 3 hours post irradiation an average of 40.7% of the population of the cells showed a decrease in mitochondrial potential, this was compared to 6.95% in the time matched control, this was a significant increase ( $P < 0.01$ , One-way ANOVA). There was no further increase in percentage of cells with a decreased mitochondrial membrane potential seen at 24 hours ( $P = 0.986$ , One-way ANOVA), when the average percentage of cells with a decrease in mitochondrial membrane potential was 43%. This was consistent with what had been using confocal microscopy techniques and taken together this data indicates that immediate apoptosis rather than delayed apoptosis occurred on our cell line following UVA irradiation. Importantly, there was no difference seen in the mitochondrial membrane potential of the two control groups ( $P = 0.990$ , One-way ANOVA) indicating that the loss of mitochondrial membrane potential demonstrated was as a result of UVA irradiation and not due to culture conditions.

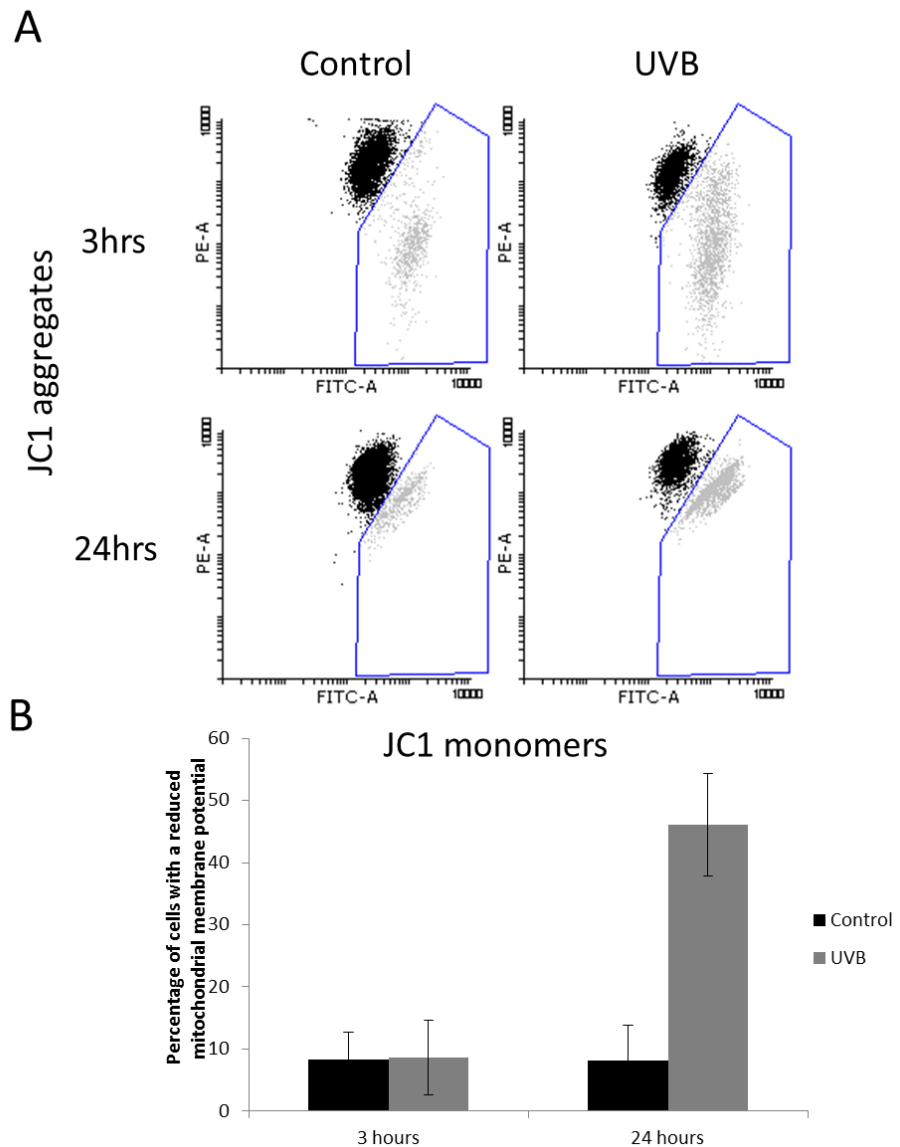


**Figure 3.25 Exposure to UVB initiates a decrease in mitochondrial membrane potential 24 hours post exposure**

*HaCaT cells were grown in a 60 mm culture dish and irradiated with 100J/m<sup>2</sup> UVB. At either 3 or 24 hours post irradiation the media was collected, the cells were then trypsinised and the trypsinised cells were added to the previously collected media. JC1 was added to the suspension of cells at a concentration of 1µg/ml and incubated for 20 minutes at 37 °C before analysis on a BD FACSCanto II flow cytometer.*

- A) *Representative images (n=3) demonstrating JC1 staining, the gated population represents cells with decreased presence of JC1 aggregates.*
- B) *A box plot to show the average percentage of cells in the gated (apoptotic) population. Error bars show the standard deviation.*

Figure 3.25 shows that consistent with what was demonstrated using confocal microscopy techniques there was no decrease in mitochondrial membrane potential in the HaCaT cells at 3 hours post UVB irradiation utilising flow cytometry techniques. There was an average of 7.69% of cells with a shift in mitochondrial membrane potential at 3 hours post UVB irradiation compared to 7.64% A decrease was seen in mitochondrial membrane potential of the UVB irradiated cells at 24 hours post exposure, there was an average of 46.1% of cell in the cell population showing a shift in mitochondrial membrane potential, this was a significant increase ( $P < 0.05$ , One-way ANOVA) demonstrating that at 24 hours post UVB there is a significant increase in apoptotic cells.

Comparatively, this data demonstrated that loss of mitochondrial membrane potential is an earlier event following UVA compared to UVB, an increase in cells with an altered mitochondrial membrane at 3 hours post UVA, whereas there was no decrease in mitochondrial membrane potential detected at this time point for UVB irradiated cells. At 24 hours both populations of cell showed an increase in the percentage of cells with altered mitochondrial potential, the percentage of cells with altered mitochondrial potential were 5.85 and 6.07 times that of the time matched control for UVA and UVB respectively at 24 hours post each irradiation type, therefore indicating that although UVA initiates a change in mitochondrial membrane potential earlier than UVB at alter time points the percentage of cells with a decreased mitochondrial membrane potential is similar for each irradiation type. This is in agreement with the clonogenic survival experiments data shown in figure 3.1 and 3.2 where clonogenic survivals of 34% and 32% were seen following treatments of UVA and UVB respectively. The doses of UVA and UVB were the same in these two experimental approaches.

### **3.3.11 Mechanism of apoptosis induction following UVA or UVB irradiation**

After establishing the strikingly different time frames at which apoptosis is seen following UVA and UVB irradiation, attempts were made to establish the mechanism behind the induction of apoptosis following each waveband. Apoptosis can be induced through two main pathways, either as a result of high levels of DNA damage that the cell is unable to repair efficiently or as a result of increased ROS which initiate apoptosis through mitochondrial release of cytochrome c and initiation of the caspase cascade.

The relationship between DNA damage signalling and apoptosis initiation in each case was examined. In this chapter it has previously shown that H2AX phosphorylation is ATM dependent following UVA irradiation and that there is cross talk between ATM and ATR involved in H2AX phosphorylation following UVB. It is well established that both ATM and ATR play a vital role in initiating apoptosis in response to DSBs and stalled replication forks respectively when the quantity of DNA lesions is too high for efficient repair to occur.

These experiments aimed to examine the effect on mitochondrial membrane potential loss of an ATM inhibitor prior to UVA irradiation and of both inhibitors (ATM and ATR) to UVB irradiation. The inhibitors were added to the cells 1 hour prior to irradiation at a concentration of 1  $\mu$ M. These were the same conditions for which previously a significant effect on the DNA damage response had been detected and so would be a good indication of DNA damage dependent apoptosis. There have been suggestions that following UVA apoptosis is initiated independently of DNA damage, and that UVB initiates apoptosis following DNA damage, this work was carried out in blood lymphocytes so this work aimed to confirm this in our cell line to establish if their finding was a cell line dependent finding or if this is a conserved mechanism for UVA apoptosis.

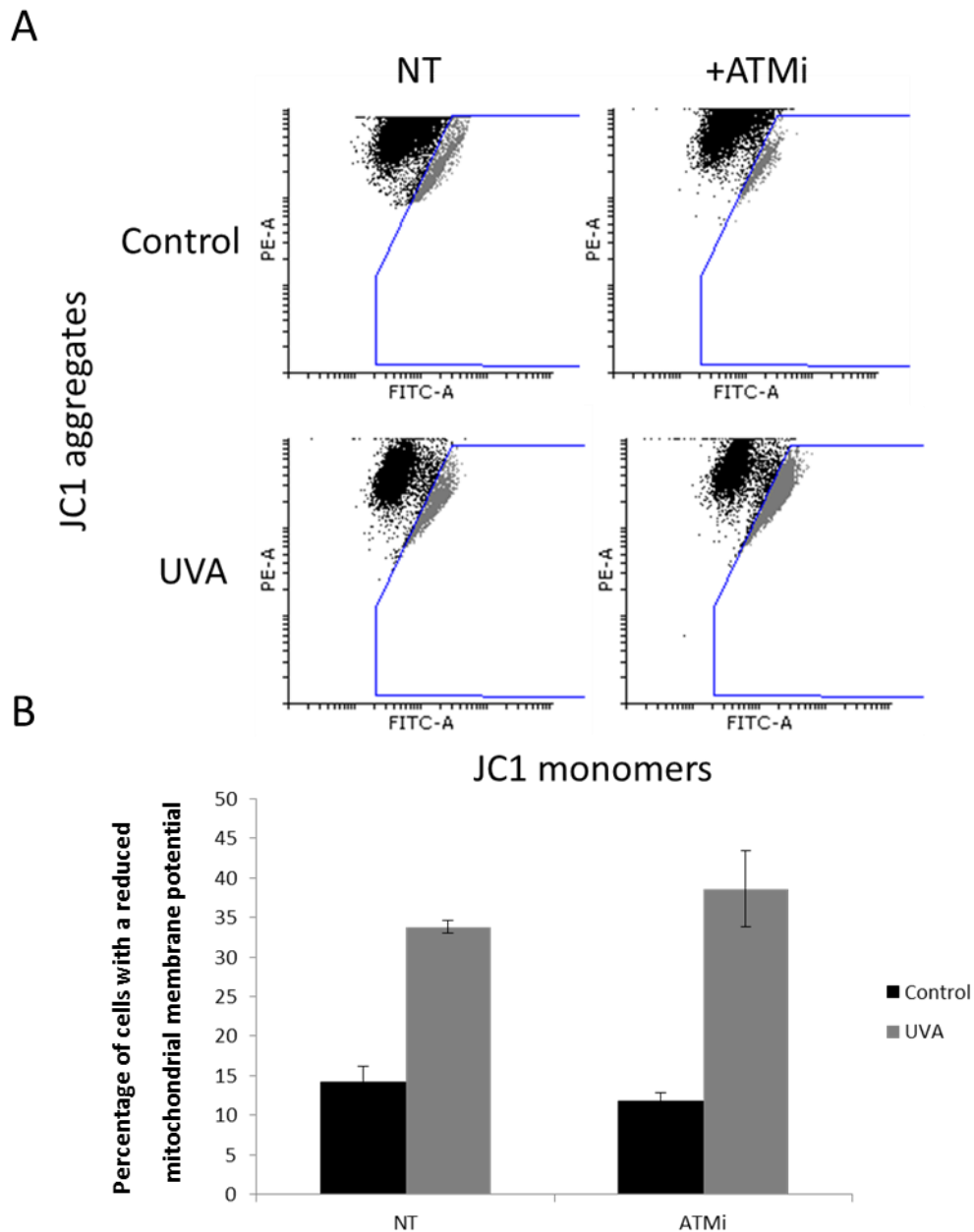


**Figure 3.26 Apoptosis induction following UVA is independent of ATM activation**

*HaCaT cells were grown in a 60mm culture dish, pretreated for 1 hour with the ATM inhibitor KU55933 at a concentration of 1  $\mu$ M and irradiated with 100kJ/m<sup>2</sup> UVA. At 3 hours post irradiation the media was collected, the cells were then trypsinised and the trypsinised cells were added to the previously collected media. JC1 was added to the suspension of cells at a concentration of 1 $\mu$ g/ml and incubated for 20 minutes at 37  $^{\circ}$ C before analysis on a BD FACSCanto II flow cytometer.*

- A) Representative images (n=3) demonstrating JC1 staining, the gated population represents cells with decreased presence of JC1 aggregates.
- B) A bar graph to demonstrate the average percentage of cells in the gated population. Error bars show the standard deviation.

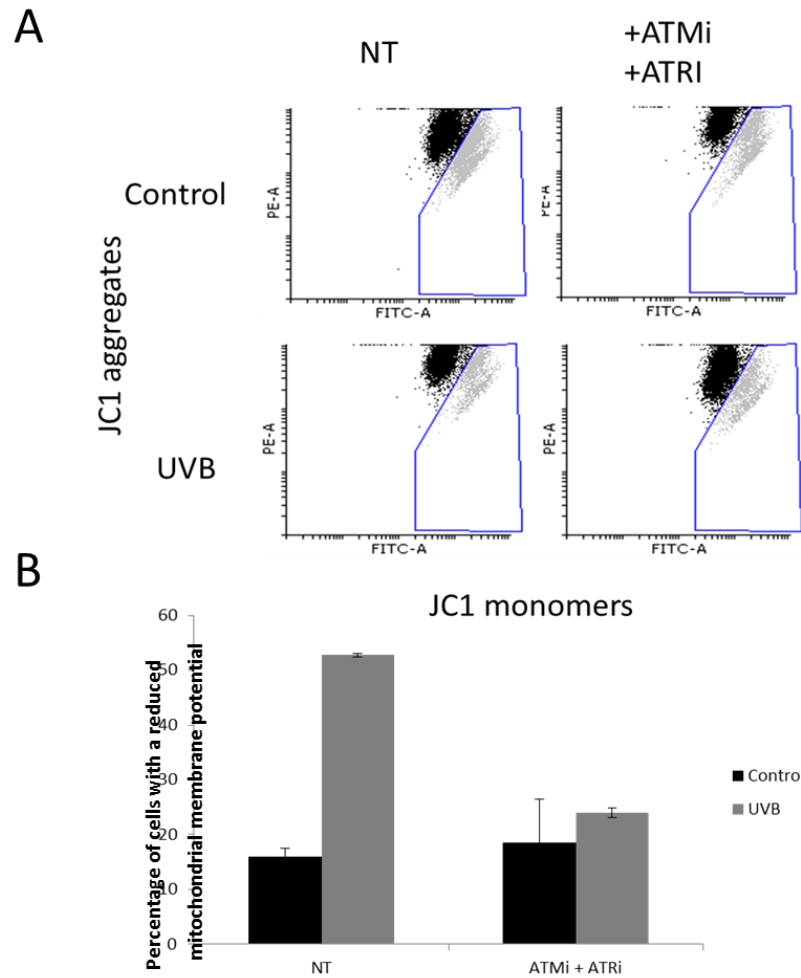


**Figure 3.27 Apoptosis induction following UVB is dependent on activation of the DDR**

*HaCaT cells were grown in a 60mm culture dish, pretreated for 1 hour with the ATM inhibitor KU55933 and the ATR inhibitor VE-821 each at a concentration of 1  $\mu$ M and irradiated with 100J/m<sup>2</sup> UVB. At 24 hours post irradiation the media was collected, the cells were then trypsinised and the trypsinised cells were added to the previously collected media. JC1 was added to the suspension of cells at a concentration of 1 $\mu$ g/ml and incubated for 20 minutes at 37  $^{\circ}$ C before analysis on a BD FACSCanto II flow cytometer.*

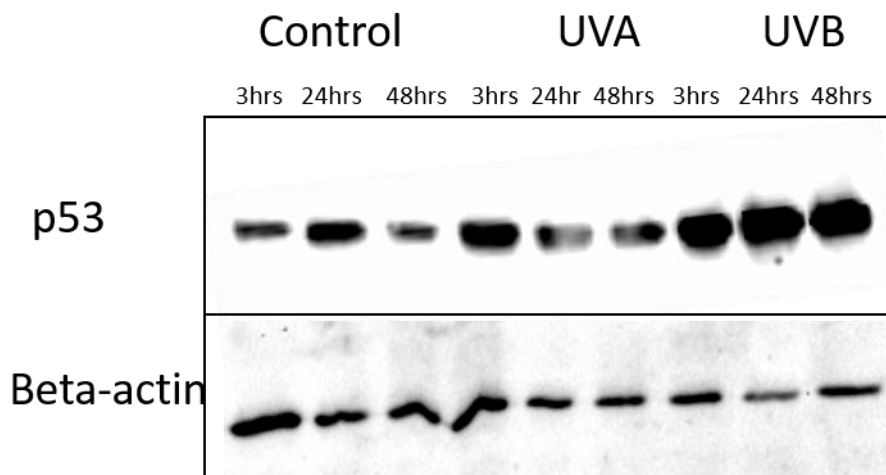
- A) *Representative images (n=3) demonstrating JC1 staining, the gated population represents cells with decreased presence of JC1 aggregates.*
- B) *A bar graph to demonstrate the average percentage of cells in the gated population. Error bars show the standard deviation.*

Figure 3.26 shows that the pre-treatment of an ATM inhibitor prior to UVA irradiation does not result in a significant change ( $P=0.67$ , Students T-test) in the percentage of cells with a decreased mitochondrial membrane potential. The mean percentage of cells with a decrease in altered mitochondrial membrane potential was 34% in the un-treated UVA irradiated cells compared to 38% for the ATMi treated UVA-irradiated cells. This indicated that apoptosis at 3 hours following UVA is not dependent on activation of the DNA damage response pathways. Importantly there was no significant effect ( $P=0.92$ , Students T-test) of the inhibitor to the percentage of cells with altered mitochondrial membrane potential in the control groups. It is likely that the induction of apoptosis following UVA irradiation is as a result of the mitochondrial initiated pathway, due to increased ROS.

Figure 3.27 shows that addition of both the ATM and ATR inhibitors prior to UVB irradiation results in a significant decrease ( $P<0.05$ , One-way ANOVA) of cells with a decrease mitochondrial membrane potential from 52% in the untreated UVB-irradiated cells to 24% in the cells pre treated with the inhibitors, which allow though still an increased percentage to compared to the control is no longer a significant ( $P=0.655$ , One-way ANOVA). Importantly, the inhibitors had no significant ( $p=0.976$ , One-way ANOVA ) effect on the percentage of cells with an altered mitochondrial membrane potential in the control groups. Taken together, these results indicate that in addition to different time frames of apoptosis induction following UVA and UVB wavebands there are also different mechanisms underpinning the apoptosis induction in each case, Our data indicates that following UVA irradiation the apoptosis induction is DNA damage independent, this is in contrast to work carried out on mouse embryonic fibroblasts, where they demonstrated that apoptosis induction following UVA was ATM dependent (Zhang et al 2002). There is considerable dispute as to whether ATM is involved in induction of apoptosis and it could be dependent on cell lines. Whereas the data shown here suggests that apoptosis induction following UVB is dependent on DNA damage.

### **P53 Accumulation following UVA/UVB irradiation.**

The accumulation of p53 in response to both UVA and UVB irradiation was studied next. The p53 accumulation at 3, 24 and 48 hours post UVA/UVB irradiation as well as in a time matched control was examined. These timeframes were chosen to fit with the JC1 data presented earlier. P53 accumulation is seen in apoptosis



**Figure 3.28 UVB but not UVA induces robust p53 accumulation**

*Western blot analysis of cell extracts from HaCaT cells exposed equi-toxic doses of UVA or UVB, extracts were collected at 3, 24 or 48 hours post irradiation. The blot was probed using antibodies to p53 and an anti-mouse. Beta actin was used as a loading control.*

Figure 3.28 shows that UVB irradiation results in increased accumulation of p53 at all the time points that were looked at, demonstrating that this is a long lasting effect. Conversely an increase in p53 accumulation was detected only at 3 hours following UVA irradiation, at the later time points the p53 levels were the same as that seen in the un-irradiated control suggesting just a transient accumulation of p53 occurs in response to UVA irradiation. The demonstrated accumulation of p53 is within the same time frame that have previously shown a decrease in mitochondrial membrane potential suggesting a possible role for p53 in UVA induced

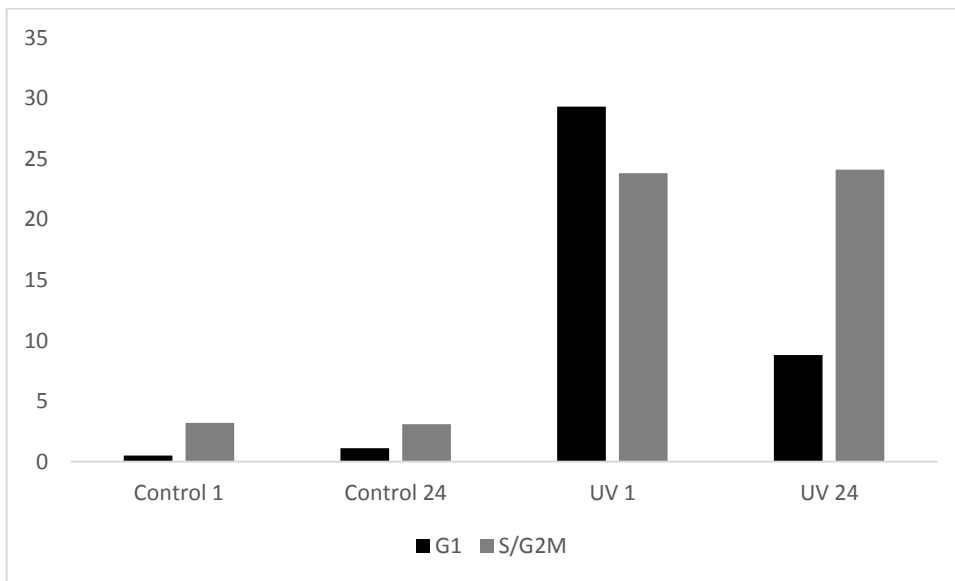
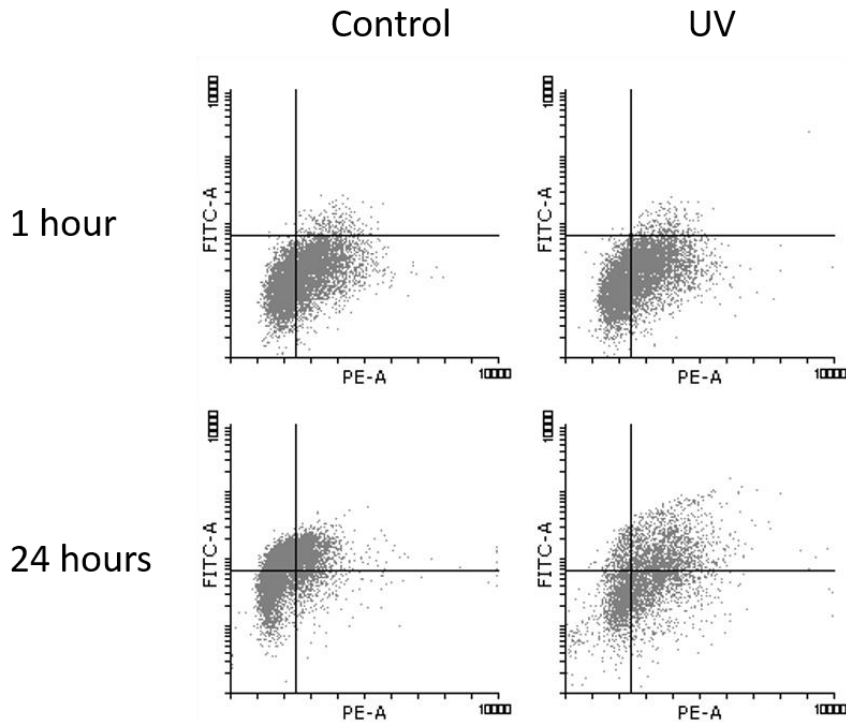


**Figure 3.29 induction of  $\gamma$ H2AX in UV (solar simulated) irradiated cells.**

*HaCaT cells were exposed to 100J/m<sup>2</sup> UVB; the cells were harvested by trypsinisation, pelleted by centrifugation and washed once in PBS. The cells were fixed at either 1 or 24 hours post irradiation and processed using The cell suspension was processed using an antibody to  $\gamma$ H2AX (ser139) (ab26350) and Alexa Fluor 488 conjugated anti mouse secondary. Propidium iodide was added to the samples immediately before analysis. The suspension was strained using cell strainer (Greiner). The samples were analysed using BD FACSCanto II flow cytometer. The data was gated in the PI channel to avoid any doublets being included in the analysis.*

Figure 3.29 shows that there is an increase in  $\gamma$ H2AX positive cells in all stages of the cell cycle at 1 hour following UV irradiation, however at 24 hours post UV irradiation an increase in positive cells is only seen in s-phase. This indicates a possible bi-phasic increase in  $\gamma$ H2AX following UV irradiation as a result of UVA and UVB phosphorylating H2AX at very different time frames. Once again a small increase in positive cells is seen in S phase in control cells however this level was still significantly below the levels of  $\gamma$ H2AX seen in the UV irradiated cells.

### **3.4 Discussion**

#### **3.4.1 Clonogenic survival of HaCaT cells following biological relevant doses of UVA or UVB**

The clonogenic survival experiments data (figures 3.1 and 3.2) showed that the doses of UVA and UVB that were used had similar effects on the cells ability to survive and proliferate; the ED<sub>50</sub> for UVA was 48 kJ/m<sup>2</sup> and for UVB 50 J/m<sup>2</sup> showing that the doses used were of equal cytotoxic effect. These doses had previously been used as doses of equal mutagenicity in studies looking at the effects of UVA and UVB on DNA (Rünger et al., 2012) but the model used in this body of work varied slightly from the one used in that experiment therefore clonogenic survival experiments were used to validate that the doses used were of equal toxicity. There was no significant difference between the ED<sub>50</sub>s of the UVA and UVB doses used therefore it was concluded that these doses were suitable doses for future experiments relating to the ability of both UVA and UVB to cause DNA damage and would allow for comparison between the ability of UVA and UVB at doses of equal relative cytotoxicity to induce H2AX phosphorylation .

#### **3.4.2 The ability of UVA and UVB to induce DNA damage detected by $\gamma$ H2AX**

Initial experiments looked for the presence of  $\gamma$ H2AX following exposure to equitoxic, biologically relevant doses of UVA or UVB. Both short and long term time points were looked at. Figures 3.3-3.6 show that both UVA and UVB are able to initiate the formation of  $\gamma$ H2AX in normal and immortalized keratinocyte cell lines but the timeframes within which this occurs are markedly different. In addition the pattern of staining for  $\gamma$ H2AX that were seen following irradiation with each wavelength was strikingly different. Following UVA all cells were positive for  $\gamma$ H2AX, whereas only a subset of cells was seen to be positive following UVB.

Following UVA exposure  $\gamma$ H2AX foci are formed within one hour, there is a decrease at 3 hours although some foci remain. 24 hours post UVA irradiation the level of  $\gamma$ H2AX foci

had returned to that of the un-irradiated control. The ability of UVA to cause double strand breaks independently of replication remains controversial with recent studies contradicting one another (Rizzo et al., 2011; Greinert et al., 2012b). By using  $\gamma$ H2AX as a marker of double strand breaks work shown in this chapter indicates that a biologically relevant doses of both UVA and UVB irradiation is able to induce an increase in the formation of  $\gamma$ H2AX foci in both normal and immortalized keratinocyte cell lines in culture using much lower dose of UVA than a previous study which had found no formation of H2AX foci following UVA irradiation (Rizzo et al., 2011).

Both the data generated from looking at the timeframes of  $\gamma$ H2AX foci formation (figures 3.3 and 3.4) in response to UVA and from flow cytometry (figure 3.10) suggest that UVA is able to initiate  $\gamma$ H2AX foci formulation in cells at all stages of the cell cycle. This further supports the finding made by Greinert et al (2012) who found that UVA was able to induce  $\gamma$ H2AX foci formation in G1 synchronized HaCaTs and fibroblasts. Their data and mine both indicate that H2AX phosphorylation following UVA was not dependent on replication. However, in work presented here a higher level of foci than they did in their study. This could be due to a number of differences in experimental design. The previous study irradiated cells in PBS whereas here the cells were irradiated in phenol red free DMEM media. Removing the cells from media for the duration of the UVA irradiation could have an effect on their signalling pathways and this could explain the difference in foci formation between this study and theirs. In addition, they also used G1 synchronised cells whereas for this body of work the cells were asynchronous. It is well accepted that G1 cells are more protected from DNA damage because the DNA is tightly coiled at this point in the cell cycle (Rancourt et al., 2002).

Following UVB exposure there is no increase in  $\gamma$ H2AX foci at any of the early time points however an increase is seen in foci formation at both 24 and 48 hours post UVB

irradiation. In addition, H2AX phosphorylation following UVB irradiation is seen in only a subset of cells (figures 3.5 and 3.6). This, along with the different time frames of foci formation following the two irradiation types suggested that different pathways could play a role in  $\gamma$ H2AX foci formation following UVA and UVB.

### **3.4.3 Dose response relationship between UVA/UVB and $\gamma$ H2AX foci formation**

Figures 3.7-3.9 demonstrated that a lower relative dose of UVA (25 kJ/m<sup>2</sup>) compared to UVB (100 J/m<sup>2</sup>) was able to when comparing the  $\gamma$ H2AX foci at the time points which induced highest levels of H2AX phosphorylation. Even the lowest dose of UVA that was used (25kJ/m<sup>2</sup>) caused an increase in foci relative to the control, this dose is equivalent to less than 10 minutes of exposure to midday summer sunlight therefore indicating that relatively small amounts of UVA can cause DNA damage to cells.

In addition, when the two highest doses of UVA were used there was incomplete repair of the damage at 24 hours post irradiation, suggesting that when a large number of double strand breaks are formed the cells repair machinery is unable to repair this damage within a 24-hour time point. Despite the damage remaining un-repaired from the flow cytometry data (figure 3.10) there did not appear to be any decrease in cell cycle progression compared to the time matched control suggesting that the cells containing DNA damage are still being replicated. This is consistent with data looking at the cell cycle progression following UVA and UVB, which saw that there is a less efficient cell cycle arrest following exposure to UVA and UVB (Rünger et al., 2012).

#### **3.4.4 Mechanism of H2AX phosphorylation following UVA and UVB.**

Figure 3.10 shows that UVA induced  $\gamma$ H2AX is independent of replication, the flow cytometry data showed that cells were positive for  $\gamma$ H2AX independent of cell cycle stage and therefore the formation of foci is a replication independent event. Again, this is supportive of the work by Greinert et al (2012) who saw foci formation in G1 stalled cells. In contrast, our data suggests that the formation of  $\gamma$ H2AX foci following UVB is dependent on replication. The flow cytometry data showed that only cells in S-phase or later of the cell cycle were positive for foci, suggesting that the foci seen in this case are as result of stalled replication forks rather than as a result of double strand breaks arising.

It is already established that the formation of  $\gamma$ H2AX foci is an early event that occurs in response to DNA damage including double strand breaks (Burma et al., 2001) and stalled replication forks (Ward and Chen, 2001). Having seen  $\gamma$ H2AX foci formed following both UVA and UVB irradiation but in contrasting time frames it was likely that the stimuli formed following UVA was formed immediately after exposure, the event was likely to occur later following exposure to UVB.

Figure 3.12 showed that UVA but not UVB induced the phosphorylation of ATM.

Additionally, pre-incubation with a selective inhibitor to ATM but not an inhibitor to ATR abrogated the foci formation in UVA (figure 3.16). Furthermore, Figure 3.19 demonstrated that an MRN complex inhibitor resulted in a significant decrease in H2AX phosphorylation in UVA irradiated cells. This data is strongly suggestive that UVA is causing double strand breaks and not stalled replication forks. Therefore, this indicates that UVA is able to induce what our data suggests to be DSBs at a biologically relevant dose. Furthermore, there is evidence to show that not all of the damage is repaired at 24 or even 48 hours, indicating that the DDR is insufficient to repair all damage that has occurred. This further highlights the importance of an increased understanding of mechanism of UVA damage.

Neither an ATM nor an ATR inhibitor alone had a significant effect on the formation of foci following UVB (figure 3.20), however when the two inhibitors were combined there was a significant decrease in foci formation (figure 3.21). This suggests that there is a compensatory effect in which either ATM or ATR can initiate the formation of  $\gamma$ H2AX foci following UVB irradiation. Cross talk between ATM and ATR in response to stalled fork replication has previously been described; ATM and ATR have been shown to function together to prevent the collapsing of stalled forks (Trenz et al., 2006). Furthermore, it was demonstrated the upregulation of phosphorylated ATM following UVB irradiation of cells treated with an ATR inhibitor prior to irradiation (figure 3.22) perhaps suggesting that ATR is preferentially phosphorylated following UVB irradiation but in cells lacking ATR function ATM can initiate a DDR.

#### **3.4.5 Mitochondrial membrane potential following UVA and UVB irradiation.**

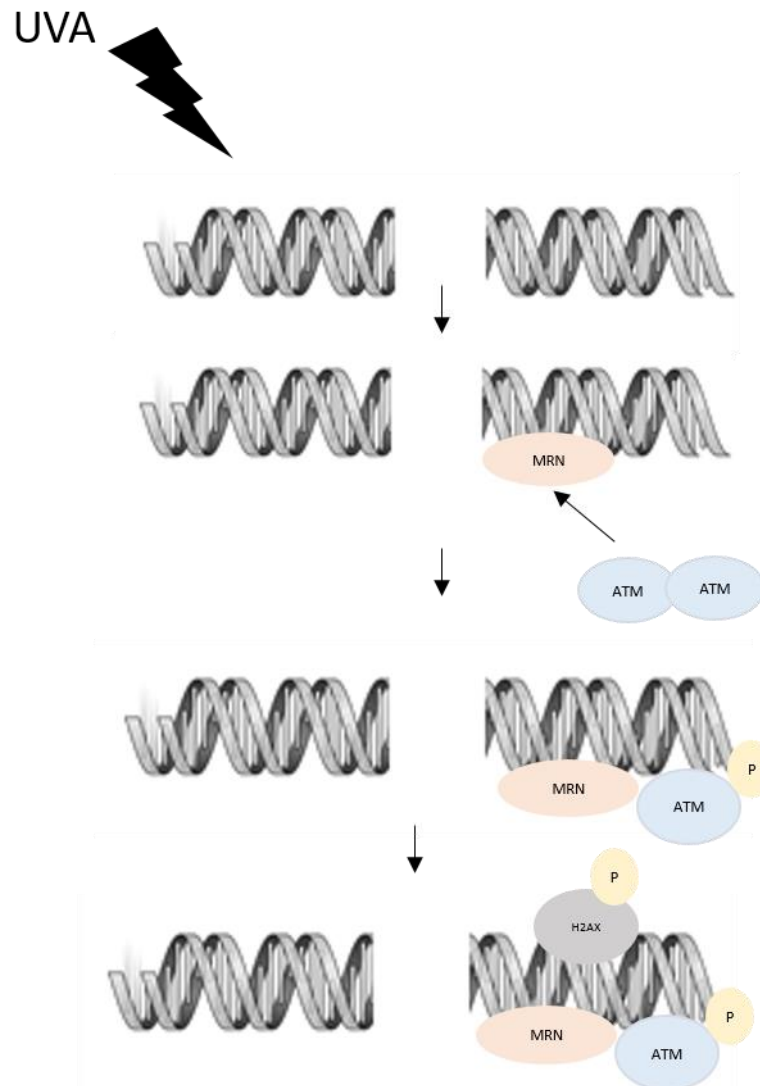
In this chapter, in addition to assessing the DDR following both UVA and UVB changes in mitochondrial membrane potential, an early indicator of apoptosis were assessed. Much like what had been observed with the DDR, the data indicated that loss of mitochondrial membrane potential was an earlier event following UVA than UVB, a significant increase in the percentage of cells with a decrease in mitochondrial membrane potential was seen at 3 hours following UVA irradiation (figures 3.23 and 3.24), but not UVB irradiation. A significant increase in cells with a decreased mitochondrial membrane potential was seen at 24 hours post UVB irradiation (figures 3.23 and 3.25). Therefore, these results suggested that UVA initiates apoptosis much earlier than UVB following exposure, this is consistent with earlier work carried out on T cells (Breuckmann et al., 2003) and lymphoma cells (Godar et al., 1994) and it has been suggested that UVA is able to initiate immediate apoptosis as a result of membrane damage whereas UVB initiates delayed apoptosis following DNA damage (Godar and Lucas, 1995).

Further to this, the mechanism underpinning the apoptosis induction of each waveband was examined. The single inhibitors and combinations of inhibitors that had previously had a significant effect on the DDR as measured by  $\gamma$ H2AX intensity were utilized once again. The effect of these inhibitors on mitochondrial membrane potential to indicate DNA damage dependence of apoptosis was assessed. Figure 3.26 demonstrated that the use of an ATM inhibitor had no effect on the percentage of cells with a decreased mitochondrial membrane potential at 3 hours post irradiation. This suggests that apoptosis induction following UVA irradiation is not dependent on activation of the DDR. Conversely pre-treatment with inhibitors to ATM and ATR resulted in a significant decrease of cells with a decreased mitochondrial membrane potential (figure 3.27); this suggests that following UVB irradiation apoptosis induction is dependent on activation of the DDR. Additionally p53 accumulation in UVA and UVB irradiated cells was assessed, it was found that UVB initiated a more robust accumulation of p53, spanning from 3-48 hours post irradiation. In contrast UVA resulted in a transient increase of p53 accumulation; I detected an increase in p53 at 3 hours, but not at the later time points. This is consistent with what work demonstrated in figures 3.25 and 3.26.

### **3.4.6 Conclusions**

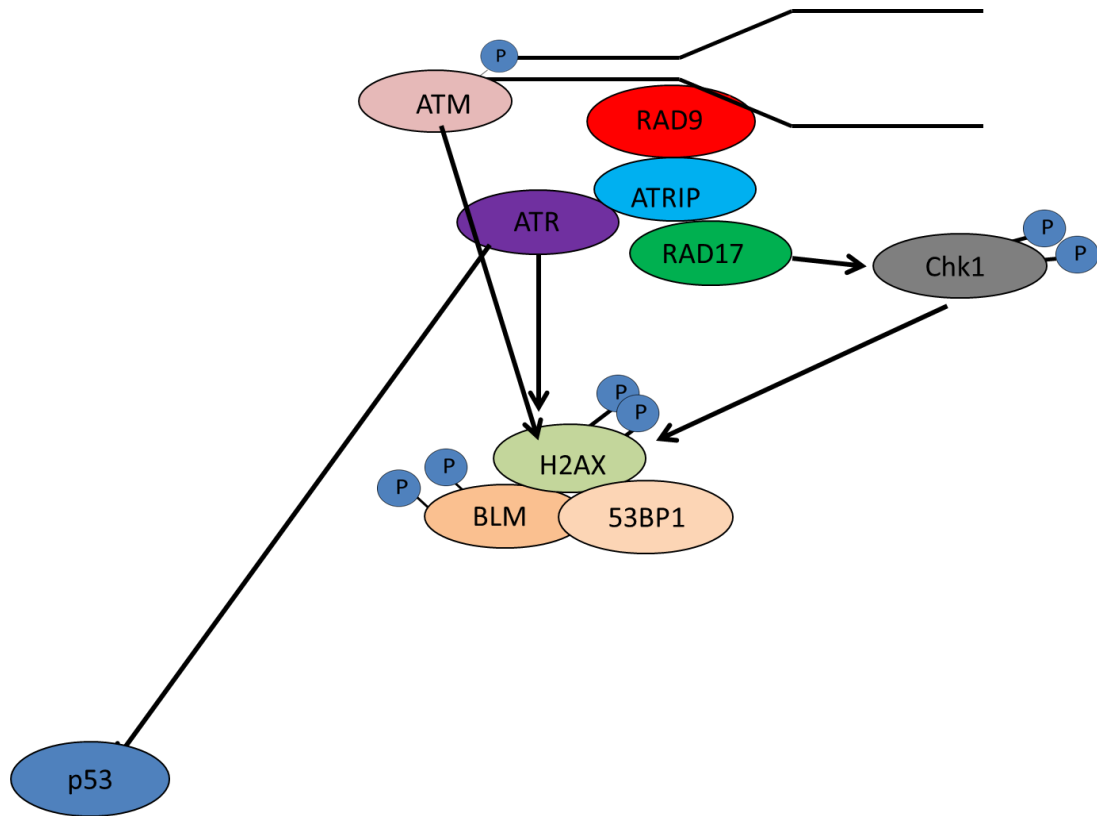
In conclusion work shown in this chapter has indicated that both UVA and UVB are able to initiate the formation of  $\gamma$ H2AX foci, but the kinetics and mechanism behind the formation in response to each irradiation type are markedly different. Two different models for H2AX phosphorylation depending on which irradiation type the cells were exposed to were proposed. The data shown in this chapter indicated that the phosphorylation of H2AX following UVA exposure is independent of replication but dependent on ATM phosphorylation at serine 1981 and dependent on prior recruitment of the MRN complex.

The response to UVA irradiation is suggesting double strand break formation or at least damage that is being recognised by the MRN complex as a double strand break.



**H2AX phosphorylation following UVA irradiation is both MRN and ATM dependent.**

In contrast neither an inhibitor to ATM nor ATR resulted in a significant decrease in H2AX phosphorylation following UVB irradiation however a significant decrease was seen when the two inhibitors were combined. Additionally, although an increase in ATM phosphorylation following UVB irradiation alone was not detected, an increase in ATM activation when the cells were pretreated with an ATR inhibitor. Taken together this suggested the following model, that there is a level of cross talk between ATM and ATR following UVB irradiation, which means that they can function redundantly to phosphorylate H2AX in response to UVB irradiation.



**H2AX phosphorylation following UVB irradiation involves cross talk between ATM and ATR.**

Additionally it was detected that there are different time frames of apoptosis induction following UVA and UVB wavebands, UVA was seen to induce immediate apoptosis and this was seen to be independent of activation of the DDR. In contrast data indicated that UVB induced delayed apoptosis at 24 hours post irradiation and that apoptosis induction was dependent on activation of the DDR. UVB was also seen to induce a longer lasting accumulation of p53 than UVA.

### **3.4.7 Further work**

There is now some evidence to suggest that UVA is able to induce clustered DNA damage, previously thought to be unique to ionising radiation. Clustered DNA damage is also referred to as multiple damage sites and is defined as the induction of two or more DNA lesions located within a few helices. The clustered damage can be tandem, where the lesions are on the same DNA strand or bi-stranded where the lesions occur on opposite strands. The complexity of clustered damage that is induced has been seen to increase with increased densities of ionising radiation.

Clustered damage is of particular interest because repair of clustered lesions is less efficient than in single lesions and therefore has a higher rate of mutations. The rate of repair compromise is dependent on a number of factors; the lesions within the cluster, and the orientation of the lesions to each other.

In addition to their work identifying the presence of double strand breaks in UVA irradiated cells Greinert et al also showed that UVA is able to induce clustered DNA damage. This is the first study that demonstrated the ability of non ionising radiation to induce this type of damage. Their work differed from ours in a few experimental details; the cells were arrested in G1, the irradiations took place in PBS and the doses they used to induce H2AX were higher than those that were utilized. They detected H2AX phosphorylation at lower levels than demonstrated here, this could be due to the irradiation occurring in PBS. They stated that the irradiation took around 40 minutes, removing media and serum from the cells for this time period could cause the difference in efficacy of H2AX phosphorylation that have seen between their results and ours. Additionally, the cells they used were in G1 phase whereas in this work synchronous population was used. Cells in G1 have been shown to be more protected from DNA damaging agents.

It would be interesting to examine the ability of UVA to induce clustered DNA damage in our model, the dose that the previous study used was 600kJ/m<sup>2</sup>, which is 6 times higher

than the dose routinely used to induce H2AX phosphorylation in our work and perhaps at a level which is arguably no longer biologically relevant.

The ability of UVA to induce clustered DNA damage is of great interest because of the possible consequences it could have on human health, it is well established that the repair of clustered lesions is less efficient than if damage occurs as single lesions in particular it has been demonstrated that the presence of 8-oxoG in a clustered lesion is one of the main types of clustered lesion that are difficult to repair. Therefore, there is an increased possibility that this type of lesion would remain unrepaired until the DNA is replicated.

In terms of the work on apoptosis induction following UVA and UVB, it would be useful to attempt to further understand the mechanism by which cells undergo apoptosis following UVA irradiation in our model. It is likely that ROS play a critical role in this so a good approach would be to test the effect of antioxidants and ROS scavengers on the mitochondrial membrane potential loss seen in our model. Additionally, other markers of apoptosis could be assessed such as the annexin V assay to further confirm the induction of apoptosis that is indicated through the work shown on mitochondrial membrane in this chapter.

**Chapter 4 The ability of  
UVA to induce a DNA  
damage response in  
bystander cells**

## **4.1 Introduction**

### **4.1.1 Transmission of bystander signals**

The radiation induced bystander effect is broadly defined as the induction of cellular and DNA damage in cells which have not been directly irradiated; instead the damage is seen as a consequence of signals released from directly targeted cells. Experimental evidence was first seen by Nagasawa and Little (1992) in CHO (Chinese Hamster Ovary) cells when they used alpha particles to transverse 1% of nuclei of a confluent monolayer cell population but found that 30% of cells showed an increase in sister chromatid exchanges. This experimental design allowed for direct cell to cell contact, therefore it was hypothesised that signals from irradiated cells were passed to the bystander cells through gap junction intercellular communication (GJIC).

It was later found that cell to cell contact was not required for induction of the bystander effect; medium taken from irradiated cells was able to induce the bystander effect in un irradiated cells as seen by an increase in cell death in the bystander populations (Mothersill and Seymour, 1998). Additionally it has been shown that cytoplasmic extracts from irradiated cells can initiate an increase in DNA fragmentation in un-irradiated cells (Kurihara et al., 1998). Direct targeting of the cytoplasm has also been seen to induce bystander effects such as cell killing and increase mutations in bystander cells (Wu et al., 1999). These data suggest that it is not only the irradiation of the nuclei that can cause the release of bystander signals. The current model for the transfer of signals from target to bystander cells is shown in figure 4.1.

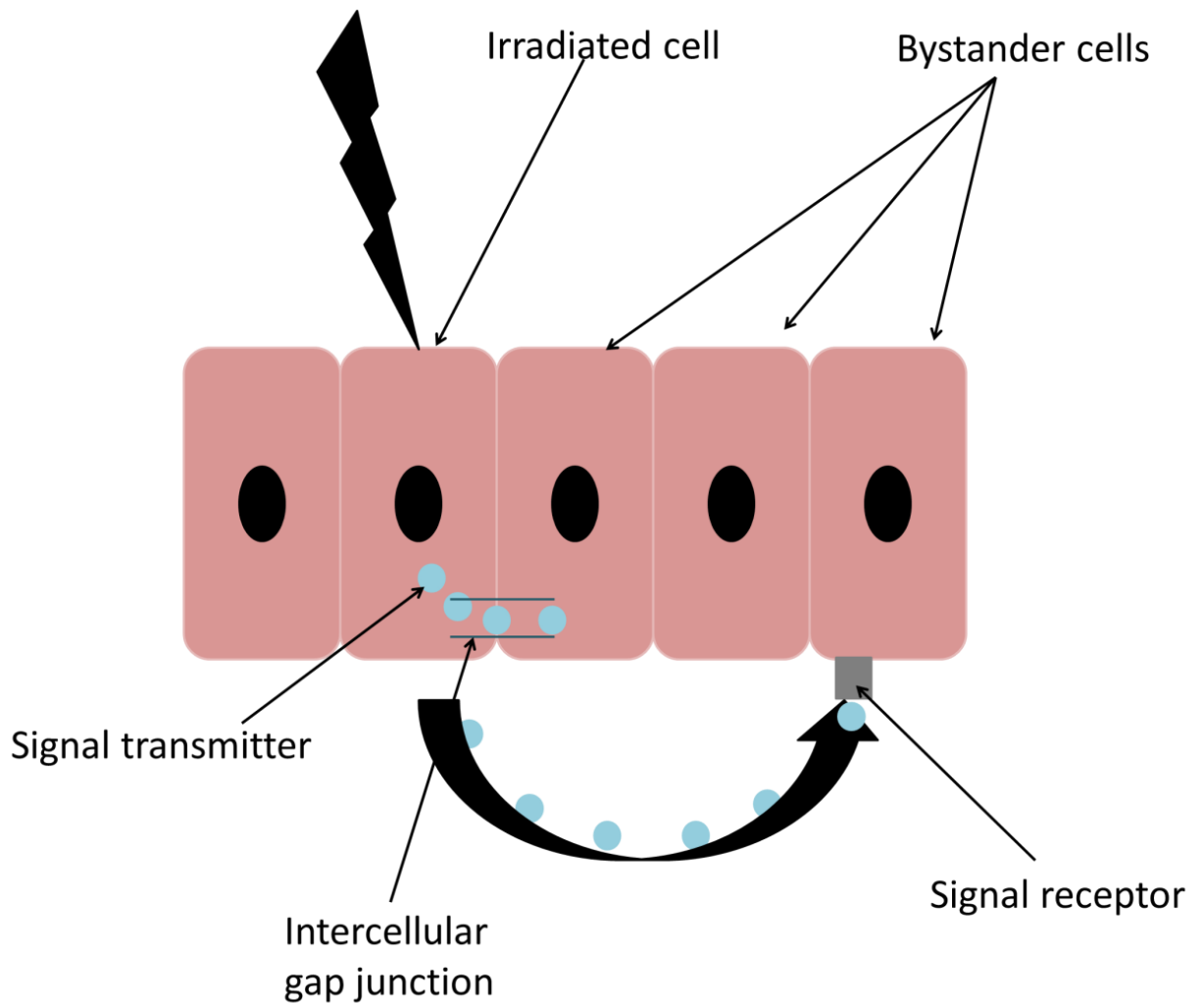


**Figure 4.1 Methods of signal transmissions in the bystander effect**

*Schematic depiction of the ability of irradiated cells to release signals which can be transferred to bystander cells either through gap junctions or please into the media and binding of signals onto the cell membrane of bystander cells.*

The response of cells to bystander signals has found to be distinct from the responses observed in directly irradiated cells; an increase in mutations has been observed in bystander cells, but the mutations observed did not resemble the mutations that were seen in the directly irradiated cells. The bystander cells showed a majority of point mutations whereas the directly irradiated cells displayed mainly large or partial gene deletions (Nagasawa and Little, 1999). The mutation spectrum seen in the bystander cells showed high similarities to that seen in unstable progeny of irradiated cells (Little et al.,

1997) and the high proportion of point mutations is consistent with ROS-mediated damage (Little et al., 2002).

Increased interest in this area has led to a number of other endpoints being studied in bystander cells such as: increased occurrence of micronuclei formation (Prise et al., 1998), increased apoptosis (Belyakov et al., 2001) and decreased clonogenic survival of bystander cells (Sawant et al., 2002). In addition, a wide number of cell lines have been studied, including normal human lung fibroblasts (Zhou et al., 2005b), normal human keratinocytes, (Mothersill and Seymour, 1998), MRC5 cells and immortalised cell lines such as HaCaTs (Whiteside and McMillan, 2009). It has been demonstrated that not all cell lines release the signals which produce the bystander effect and not all cells are equally susceptible to the bystander signals (Mothersill et al., 2001). There are data to suggest that rapidly dividing cells are more vulnerable to bystander signals (Shao et al., 2008) and that cells in S phase are the most susceptible to bystander signals (Burdak-Rothkamm et al., 2007).

Interestingly, it has been shown that there is no dose response relationship in the bystander effect. Experiments have both increased the number of particle traversals per cell (Zhou et al., 2001) and the total dose of irradiation (Hu et al., 2006) without an increase in the bystander effect being recorded; again highlighting differences between the mechanism of damage in directly irradiated cells and bystander cells.

#### **4.1.2 The mechanism of the bystander effect**

Despite increased interest in this phenomenon the exact mechanism for the bystander effect remains unknown. The use of a number of pharmacological inhibitors and ROS scavengers has resulted in a decrease in the demonstrated bystander effects. However, the inhibition of one single pathway or ROS component have not fully abrogated

bystander effects making it likely that the bystander effect is a consequence of the activation of multiple pathways and increased ROS initiated by signal release from irradiated cells (Hei et al., 2008). Three independent mechanisms behind the induction of the bystander effect have been described: direct cell to cell communications through gap junctions; the release of factors by the irradiated cells which affect bystander cells; and the immune response, such as cytokine release from the irradiated cells. Hei et al (2008) reviewed the mechanism involved and suggested a model unifying a number of signalling pathways involved in radiation induced bystander effects. These have been summarized schematically in figure 4.2.

#### **4.1.2.1 Intercellular gap junction communication**

Despite it being well established that gap junctions are not the only way to transmit signals from donor to bystander cells there is evidence to suggest a role for gap junction intracellular communication (GJIC) in mediating bystander effects. When monolayer cell cultures are studied for bystander effects, increased cell density results in an increase in bystander effects (Agarwal and Sohal, 1994), implying the importance of cell: cell contact and therefore gap junctions.

Cells deficient in GJIC did not show a bystander response. In addition, the use of GJIC inhibitors such as lindane has also been seen to cause a decrease in the bystander response (Azzam et al., 2001; Zhou et al., 2001). However, inhibitors such as lindane are nonspecific and initiate wide ranging effects on the cell, not just acting on gap junctions alone so it is difficult to draw conclusions from this.

The effect of dominant negative mutations in connexins on the ability of cells to form bystander responses has been studied as a more specific and direct way to understand the importance of gap junctions in the induction of bystander effects. Connexins are the principal protein component of gap junctions and there is evidence to suggest that connexins alone are responsible for the generation of gap junctions (Bruzzone and Meda,

1988) (Kumar and Gilula, 1992). The principal connexin in gap junctions is connexin 43. Dominant negative connexin 43 cells have been found to lack the ability to respond to bystander signals in monolayer populations (Zhou et al., 2001), indicating a role for connexin 43 and therefore gap junctions in the transmission of the bystander effect.

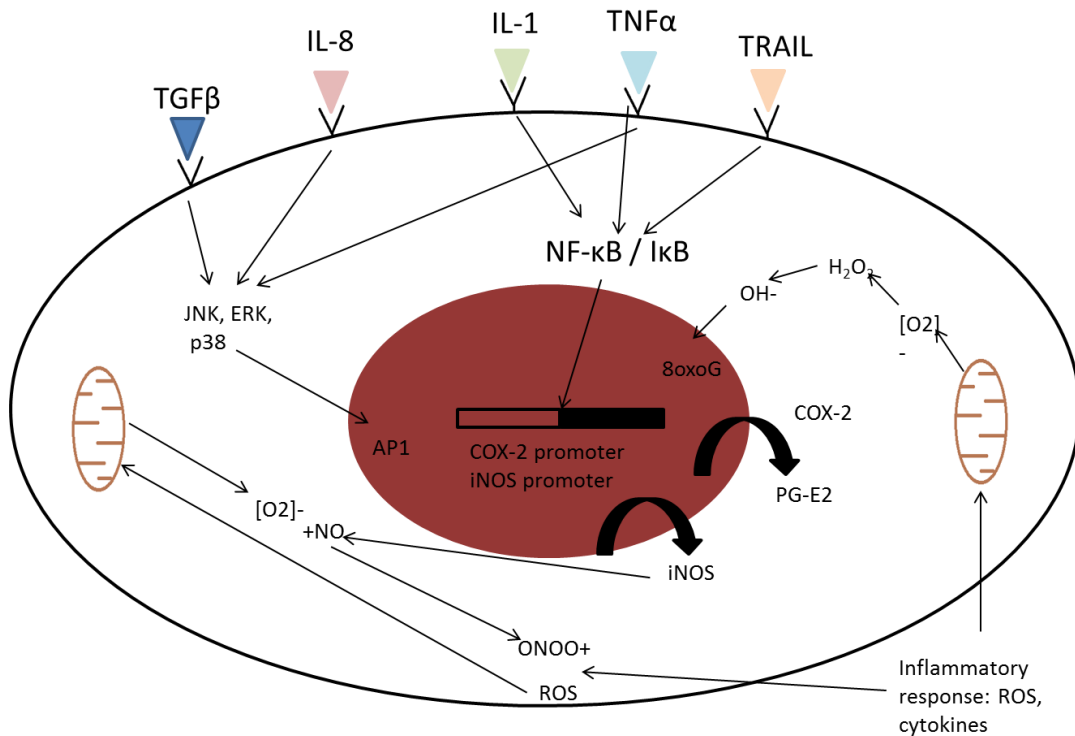


**Figure 4.2 Mechanism of the bystander effect**

*Cytokines are secreted from targeted cells and bind to receptors on the membrane of neighbouring non targeted cells..This leads to stimulation of MAPK pathways, activation of AP1 and consequently up regulation of COX2, which stimulates NO production. Additionally NF-κB is released, enters the nucleus and caused additional up regulation of COX2 and inducible nitric oxide synthase, both resulting in increase in NO. This activation of COX-2 provides a continual supply of ROS for the propagation of further bystander signals. Mitochondrial damage results in release of ROS. Adapted from Hei et al (2008)*

#### **4.1.2.2 A role for ROS in the bystander effect**

A role for ROS in the initiation of the bystander effect was hypothesised by Nagasawa and Little (1992), in their pioneering study, showing the first evidence for a radiation induced bystander effect. This was then demonstrated by Lehnert and Goodwin (1997) who observed the inhibition of sister chromatid formation in bystander cells when pre-incubated with superoxide dismutase (SOD). This effect was seen both in cells directly neighboring irradiated cells and those incubated with conditioned medium from irradiated cells, indicating a universal role for ROS in the induction of the bystander response.

Increased levels of both hydrogen peroxide and superoxide anions have been seen in both directly irradiated and bystander cells. These increased levels of ROS were seen in both bystander cells cultured with irradiated cells and those incubated in media from irradiated cells (Narayanan et al., 1997). Further attention to this area showed that the addition of superoxide dismutase (SOD) or catalase caused a decrease in bystander effects but neither of them fully inhibit the bystander effect, suggesting that both hydrogen peroxide and superoxide anions both play a role in the initiation of the bystander effect but neither are solely responsible (Azzam et al., 2002). There is some evidence to suggest that superoxide may play a more dominant role. Catalase was seen to have less of an effect on the bystander response than SOD (Little et al., 2002).

Reactive oxygen species have short half-lives, therefore in order for them to induce the demonstrated bystander effects it is likely that they would need to be generated constantly in bystander populations. A role for the reactive oxygen species generator NADPH oxidase has been suggested. The use of Diphenyleneiodonium (DPI), which inhibits NADPH oxidase activity has resulted in decreased bystander effects being detected (Azzam et al., 2002). Additionally, the inactivation of NADPH oxidase was seen to cause a greater decrease in bystander effects than was seen when catalase or SOD were

added to bystander populations (Little et al., 2002), possibly suggesting a greater role for NADPH oxidase than superoxide or hydrogen peroxide.

An increase in levels of nitric oxide has been seen in the medium of irradiated cells and was detected at a micromolar level in conditioned media. This led to an increase in the radio-sensitivity of the bystander cells, an observation that was abrogated through the addition of 2-(4-carboxyphenyl)-4,4,5,5-tetramethyl-imidazole-1-oxyl-3-oxide a specific nitric oxide scavenger (C-PTIO) (Matsumoto et al., 2001). Furthermore the addition of C-PTIO also eliminated the observed increase in MN in bystander cells using both glioma and primary fibroblast cell lines (Shao et al., 2003)

#### **4.1.2.3 A role for mitochondria in bystander effect**

The possible role for mitochondria in the bystander effect was first postulated when it was demonstrated that nuclear targeting of cells is not essential for the release of bystander signals and that targeting of cytoplasm was able to induce a bystander effect. This study also showed increased mitochondrial damage (Wu et al., 1999). It has been demonstrated that both mtDNA depleted cells (Zhou et al., 2008) and those with inhibitors to the mitochondrial respiratory chain are less sensitive to bystander effects (Chen et al., 2008). The same group later suggested that mitochondria generated ROS were involved in the early stages of bystander effect initiation when an increase in ROS was observed within 10 minutes of irradiation in target normal cells but not mtDNA depleted cells (Chen et al., 2009).

It has been observed that bystander cells are able to induce both point mutations and the common 4977-bp deletion occurring between two 13-bp repeats from position 8470–13,447 in the mitochondrial genome. The bystander signals were able to induce the mutations with a similar efficacy to that of directly irradiated cells although the

occurrence of the mutations was later in the bystander cells: 24 hours following exposure compared to 12 hours for the directly irradiated cells. Moreover, as is typical of bystander effects no dose response was seen in the bystander cells (Murphy et al., 2005).

#### **4.1.2.4 Contribution of the immune system in bystander effect induction**

Much work has been carried out with the aim of gaining understanding of what the signals released by the targeted cells are that bring about the demonstrated bystander effects. In particular increased levels of cytokines including Interleukin 8 (IL8), Interleukin 2 (IL2), Tumour necrosis factor alpha (TNF $\alpha$ ) and Transforming growth factor beta (TGF $\beta$ ) have been detected in medium collected from the targeted cells (Facoetti et al., 2006). Similarly, *in vivo* evidence shows that irradiation of primary tumours has long range effects on un-irradiated tissues or organs and it has been proposed that these effects are mediated by the immune system and cytokines.

#### **4.1.2.5 NF- $\kappa$ B**

The NF- $\kappa$ B network is thought to play a key role in the bystander effect. Bay 11-2082, a pharmacological inhibitor of NF- $\kappa$ B caused a significant decrease in mutation frequency in bystander cells (Zhou et al., 2008). In addition global gene expression of alpha particle exposed primary fibroblasts was compared to that of their bystander equivalents and similarities were seen between the expressions of NF- $\kappa$ B regulated genes suggesting that bystander cells have a full NF- $\kappa$ B response that has been induced (Ghandhi et al., 2008).

Zhou et al (2005) examined the difference in gene expression levels between bystander and control cells. COX-2 was found to be consistently up-regulated by at least 3 fold in bystander cells. In addition, the use of COX-2 inhibitor NS-398 was seen to suppress bystander mutagenesis as demonstrated by mutations in the *HPRT* locus. The same group also saw a consistent 7 fold decrease in expression of insulin growth factor binding

protein. This decrease would increase the binding of insulin growth factor to cell receptors and lead to the initiation of a number of downstream signalling pathways including the MAPK pathways. A sustained up regulation of phospho-ERK was also observed, the ratio of ERK: phospho-ERK increased from 2 to 13 in the bystander cells. The addition of an inhibitor specific to MEK –ERK (PD98059) was seen to suppress bystander effects further indicating a role for these pathways in the bystander effect.

#### **4.1.3 Activation of the DDR in bystander cells**

More recently work has focused on the DNA damage response in bystander cells and in particular the up regulation of  $\gamma$ H2AX in bystander cells. Phosphorylation of histone 2A at serine 139 occurs as an early response to the presence of double strand breaks (Mah et al., 2010) caused both directly and indirectly (Toyooka et al., 2011), and also in response to replication stress such as stalled replication forks (Ward and Chen, 2001).

$\gamma$ H2AX has been seen as an early event in bystander cells co-incubated with feeder cells that were exposed to ionising radiation. However, the formation of foci in bystander cells was seen after 18 hours co-incubation in contrast to the 30 minute time point at which it is seen in directly-exposed cells. It was suggested that the phosphorylation of H2AX could be a trigger for further downstream and later events of the bystander effect (Sokolov et al., 2007).

It has also been shown that whilst ATM, DNA-PK (Stiff et al., 2004) and ATR (Ward and Chen, 2001) have all been reported to play a role in  $\gamma$ H2AX phosphorylation following ionising radiation, with ATM and DNA-PK having been demonstrated to function redundantly (Stiff et al., 2004) it is likely that ATR plays the most significant role in  $\gamma$ H2AX foci formation in bystander cells. ATR- mutated cells showed no  $\gamma$ H2AX phosphorylation in bystander cells, but inhibitors to neither ATM or DNA-PK had any effect on foci

formation in either normal or tumour bystander cell lines, despite the irradiated cells showing foci formation. Additionally only bystander cells in S phase were positive for the presence of  $\gamma$ H2AX foci suggesting a dependence on cell cycle progression of DNA damage response (DDR) in bystander cells. This further implies that the H2AX phosphorylation detected in bystander populations is likely to be as a result of stalled replication forks and not the direct formation of double strand breaks. This is suggestive of different mechanisms behind foci formation in directly irradiated and bystander cells (Burdak-Rothkamm et al., 2007).

However another group found the activation of DDR in bystander cells outside of S phase (Dickey et al., 2009). The same group later hypothesised that cells with high DNA metabolism may represent the population that is most vulnerable to bystander signalling. This would include cells that were transcriptionally active as well as replicating cells. They used non replicating cells with varying transcriptional activities and exposed them to ionising radiation. They found that the cells with higher transcriptional activity were more susceptible than those with low transcriptional activity, demonstrating for the first time that transcriptionally active cells as well as replicating cells show increased susceptibility to bystander signals. Additionally, these cells showed no dose response relationship (Dickey et al., 2012).

#### **4.1.4 UV and the bystander effect**

The bystander effect has now been seen to be induced by a number of other stressors which include UV irradiation (Whiteside and McMillan, 2009; Dahle et al., 2001; Dahle et al., 2005). A number of endpoints have been studied, which include micronuclei formation, the formation of delayed mutations (Dahle and Kvam, 2003; Dahle et al., 2005), a decrease in clonogenic survival (Whiteside and McMillan, 2009) and increased apoptosis (Banerjee et al., 2005).

Additionally, the timeframes of the UVA bystander response have been studied, using clonogenic survival as the endpoint for bystander effect. It was shown that the signal release from the UVA irradiated cells was a delayed event and that the irradiated cells continue to release signals that can induce a bystander effect long after they have been exposed to UVA irradiation (at least 72 hours) (Whiteside et al., 2011).

A more recent paper compared the abilities of UVA, UVB and UVC to induce the bystander effect in human dermal fibroblasts using a trans-well co-incubation system. UVA was seen to be the most effective in producing a bystander response, in particular in decrease of cell survival, when the survival of the bystander cells was lower than that of directly UVA-irradiated cells and in the ability to produce ROS in the bystander cells. An increase in the cytokine IL-6 was observed for all 3 wavebands and this was seen to be higher in the bystander cells than in the directly irradiated cells (Widel et al., 2014).

These findings were in contrast to previous work where UVB at a dose of 400J/m<sup>2</sup> was not seen to induce a bystander effect in keratinocytes (Whiteside and McMillan, 2009) but the dose used in the later study was significantly higher at 10kJ/m<sup>2</sup>. The experimental evidence surrounding the ability of UVB to induce the bystander effect is inconclusive, with contradictory results obtained in different cell lines and different studies; it could be that the ability of UVB to induce bystander effects is cell line dependent.

There are some data to suggest that the UVA bystander effect is ROS-mediated. In experiments on HaCaT cells a decrease in clonogenic survival as a result of UVA irradiation was abrogated by DPI, an inhibitor to NADPH oxidase (Whiteside and McMillan, 2009). Glutathione, SOD and catalase were also seen to prevent the induction of delayed mutations following UVA irradiation (Dahle et al., 2005).

## **4.2 Aims**

It is well accepted that UVA is able to induce a bystander effect, much of the earlier work has focused on the effect of UVA on clonogenic survival of bystander cells and little evidence exists on the upstream effectors of this, such as the occurrence of DNA damage and consequent activation of the DDR. In this chapter the ability of UVA at a biologically relevant dose activate a DDR has been studied. Primarily through detection of up regulation of  $\gamma$ H2AX in bystander cells .The mechanisms of H2AX phosphorylation in bystander populations have been studied as well as the effects of ROS scavengers and inhibitors to up- stream effectors on the up regulation of  $\gamma$ H2AX in bystander cells.

## **4.3 Results**

### **4.3.1 Formation of $\gamma$ H2AX in UVA bystander cells**

Previously, our laboratory has shown that UVA but not UVB is able to induce the bystander effect in both keratinocyte (HaCaT) and fibroblast (MRC5) cell lines (Whiteside and McMillan, 2009). This was demonstrated using clonogenic survival as the biological endpoint. A decrease in clonogenic survival was seen in the UVA bystander cells compared to the control. A delay in release of signals which caused the bystander effect was also shown; decrease in clonogenic survival of bystander cells was only detected when co-incubated with UVA irradiated feeder cells for 48 hour or more. No decrease in clonogenic survival was seen when the co-incubation time was 24 hours, suggesting a time lapse between the irradiation of the feeder cells and their release of signals which cause the bystander effect (Whiteside et al., 2011).

The experimental set up used the BD bioscience multi-well insert system with inserts with a pore size of 1 $\mu$ m. This did not allow for direct cell to cell contact, but any signal released from the UVA irradiated cells would be able to readily pass through the membrane to reach the bystander populations. The feeder cells were irradiated with 100 kJ/m<sup>2</sup> UVA in each of the experiments; this was a donor cell line that had previously been shown to be able to induce H2AX phosphorylation in directly irradiated cells see chapter 3. The dose is biologically relevant, equivalent to approximately 30 minutes of midday summer sun exposure (Kimlin et al., 2002).

The formation of  $\gamma$ H2AX has been seen to be one of the earliest events in bystander cells following ionising radiation (Hu et al., 2006). Immunofluorescence techniques were utilised to detect the presence of  $\gamma$ H2AX in the UVA bystander cells, the nuclei were counter stained with DAPI. The intensity of 100 nuclei was measured and the median intensity per nuclei was calculated for each experimental condition.

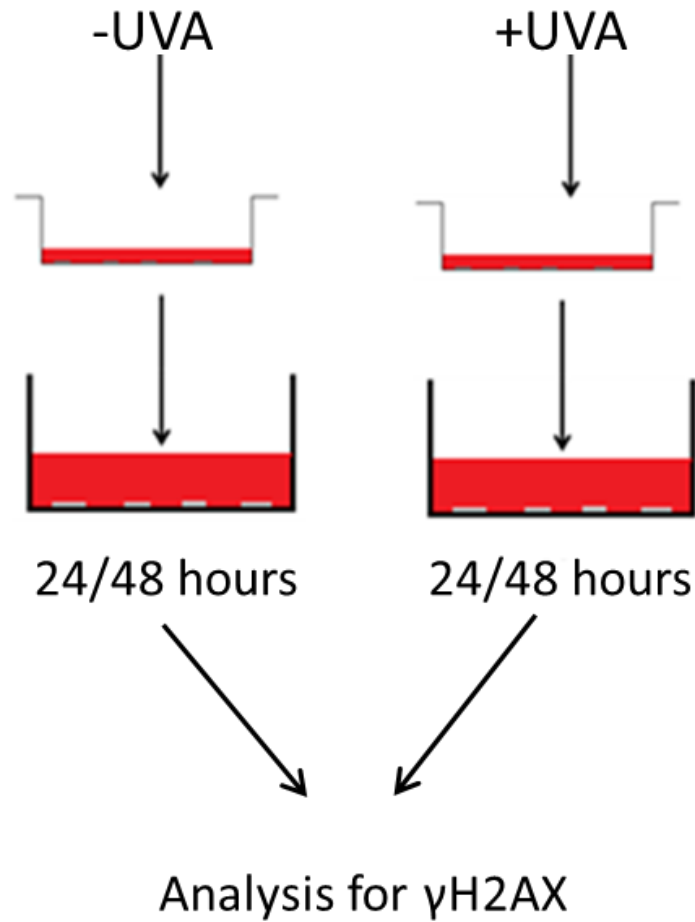


**Figure 4.3 The setup used in bystander experiments**

*Feeder cells were grown on membranes of a multi well insert system with pore size  $1\mu\text{m}$ . The feeder cells were either un-irradiated or irradiated with  $100\text{kJ}/\text{m}^2$  UVA. Immediately after irradiation both the control and irradiated feeder cells were placed into a 6 well plate containing bystander cells seeded onto glass coverslips. The feeder and bystander cells were co-incubated for either 24 or 48 hours before analysis.*

The initial experiment aimed to detect the formation of  $\gamma$ H2AX in bystander cells that had been incubated with UVA irradiated cells for either 24 or 48 hours prior to fixation and processing (Figure 4.4). These time points were chosen because previous work in our laboratory has shown that there is a delay in the release of bystander signals following UVA irradiation (Whiteside et al., 2011). The bystander experiments were carried out using both HaCaT and normal human dermal fibroblast cells as the bystander cells. The donor cells were always HaCaT cells. The combination of the two different skin cell lines was used to see whether irradiated keratinocytes could affect fibroblasts which lie deeper in the skin, in the dermal layer.

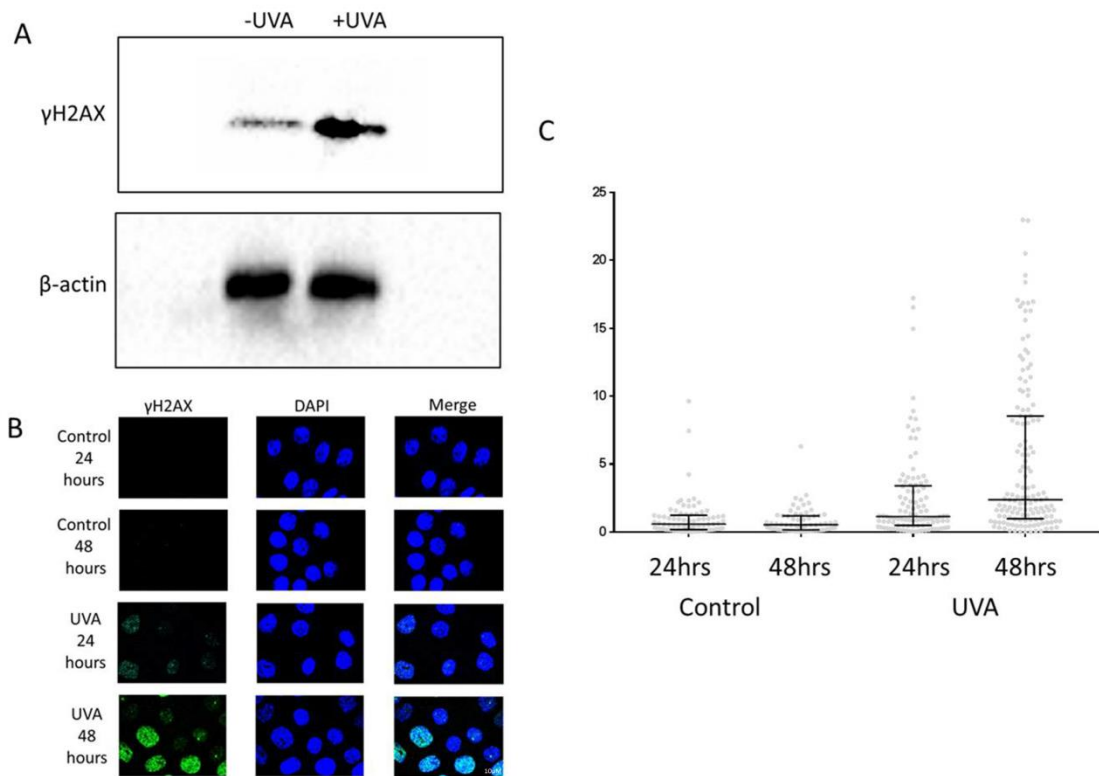


**Figure 4.4 UVA irradiation is able to induce the formation of  $\gamma$ H2AX in bystander cells when they are incubated with cells that have been exposed to UVA irradiation**

*A) Western blot analysis of cell extracts from bystander cells Treated with conditioned medium collected from either UVA irradiated or control donor cells 48 hours after irradiation for 24 hours.*

*B) HaCaT cells were grown on a membrane or on a coverslip in a 6 well dish. The cells grown on the membrane were either irradiated with UVA or sham irradiated. The irradiated cells were added to the recipient cells immediately after irradiation. The recipient cells were then fixed at either 24 or 48 hours post co-incubation and processed as has been scribed previously. A representative Image is shown (n=3).*

*C) The fluorescence intensity of the Control and UVA bystander cells was measured using Image J software, at least 100 cells per condition were analysed and the experiment was repeated with 3 biologically independent replicates. The relative fluorescence compared to the control group was calculated and a categorical scatter plot was plotted. The median and interquartile range is shown.*

Figure 4.4 (A) shows that a modest increase in  $\gamma$ H2AX was detectable in the UVA bystander populations compared to the time matched control by western blot, here, looking at 48 hours post combination of bystander and medium from irradiated/control donor cells. Loading control was demonstrated by blotting for beta actin.

Figure 4.4 (B) shows that  $\gamma$ H2AX was detected in the bystander cells that were co-incubated with UVA irradiated feeder cells for both 24 and 48 hours following irradiation. There was no detectable  $\gamma$ H2AX for the recipient cells that were co incubated with un-irradiated donor cells demonstrating that it is the UVA irradiation of the donor cells and not their mere proximity that causes the increase seen in  $\gamma$ H2AX. A small increase in staining intensity is seen in the UVA 24 hour group however the levels of  $\gamma$ H2AX are greater at 48 hours compared to 24 hours, indicating that there is an increase in  $\gamma$ H2AX formation the longer they are incubated with the UVA irradiated donor cells. Interestingly, not all the bystander cells were positive for  $\gamma$ H2AX at either time point. In addition, the  $\gamma$ H2AX detected in bystander cells was seen as distinct foci. Both of these observations are in contrast to what is observed in directly UVA irradiated cells see (figure 3.3).

Figure 4.4 (C) shows that in the bystander cells at 24 hours there is a slight increase in median relative intensity of  $\gamma$ H2AX staining, but this increase was not significantly different to the time matched control ( $p=0.139$ , One-way ANOVA); however, there is an increase in the upper quartile and 95<sup>th</sup> percentile. There is a slight increase seen in the median of the 48 hour UVA bystander cells compared to the time matched un-irradiated controls and a further increase is seen in the upper quartile and 95<sup>th</sup> percentile. Overall a larger spread is seen in the relative intensity of  $\gamma$ H2AX in the UVA bystander cells compared to their time matched controls, some cells are not stained for  $\gamma$ H2AX whilst some cells show very strong staining.

Together the data shown in figure 4.5 demonstrate that, although from the IF data it suggests that there is an increase in  $\gamma$ H2AX in UVA bystander cells compared to the

control recipient cells this increase is masked to some degree by the existence of two distinct populations. Some cells are clearly more sensitive than others to the bystander signals. For subsequent experiments the UVA bystander cells and the control recipient cells, will be co-incubated with the appropriate donor cells for 48 hours prior to analysis. This co-incubation time was selected because it was at this time an increase in H2AX phosphorylation was detected.

#### **4.3.2 The effect of cell cycle position on $\gamma$ H2AX foci formation in UVA bystander cells**

The appearance of a mixed  $\gamma$ H2AX-positive and  $\gamma$ H2AX-negative population in UVA bystander cells led to the hypothesis that cell cycle status could have an effect on the formation of  $\gamma$ H2AX foci in UVA bystander cells. To investigate this the experiment was repeated, labelling actively replicating cells by incorporation of the nucleotide analogue 5-ethynyl-2'-deoxyuridine (EdU) to identify S phase. A cell cycle dependence of H2AX phosphorylation has been demonstrated in bystander cells exposed to cells targeted by IR see section 4.1.3. This work has also shown a cell cycle dependence of  $\gamma$ H2AX following UVB irradiation in figure 3.11.

The immunofluorescence images were then analysed for intensity of  $\gamma$ H2AX staining, with  $\gamma$ H2AX fluorescence being separately quantitated for actively replicating and non-replicating populations, as determined by EdU status and the relative fluorescence calculated by dividing the fluorescence by the average fluorescence of a control EdU-negative cell. A categorical scatter plot of the data was constructed to demonstrate the median intensity per nuclei and the spread of fluorescence intensity for each experimental group.

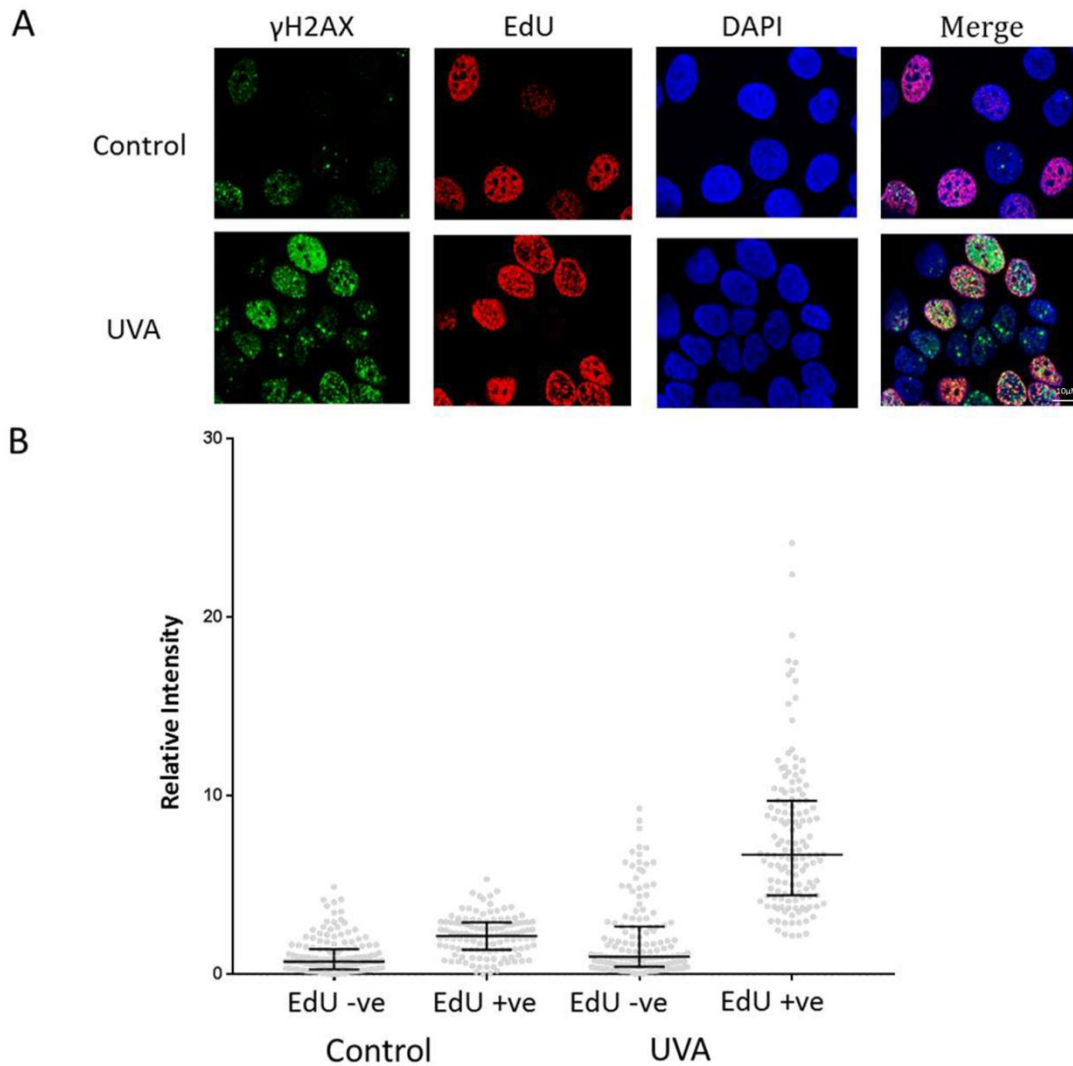


**Figure 4.5 UVA bystander cells that are positive for  $\gamma$ H2AX are the actively replicating cells.**

*HaCaT keratinocytes were grown on a membrane insert and either irradiated with UVA (100kJ/m<sup>2</sup>) or sham irradiated. The inserts were then immediately transferred to wells containing recipient HaCaT cells cultured on coverslips. Recipient cells were fixed and processed 48 hours later, having been treated with EdU for the final hour of incubation.*

*A) Representative confocal microscopy images (n=3) of recipient keratinocytes showing immunofluorescent detection of  $\gamma$ H2AX (green) and fluorescent labelling of EdU (red)*

*B) The  $\gamma$ H2AX fluorescence of EdU-positive and -negative populations in both control and UVA recipients was measured using Zeiss LSM 510 software. At least 100 cells per condition were analysed and the experiment was repeated with three biologically independent replicates. The relative fluorescence compared to the control EdU-negative group was calculated and a categorical scatter plot of the data is shown. The median and interquartile ranges are indicated.*

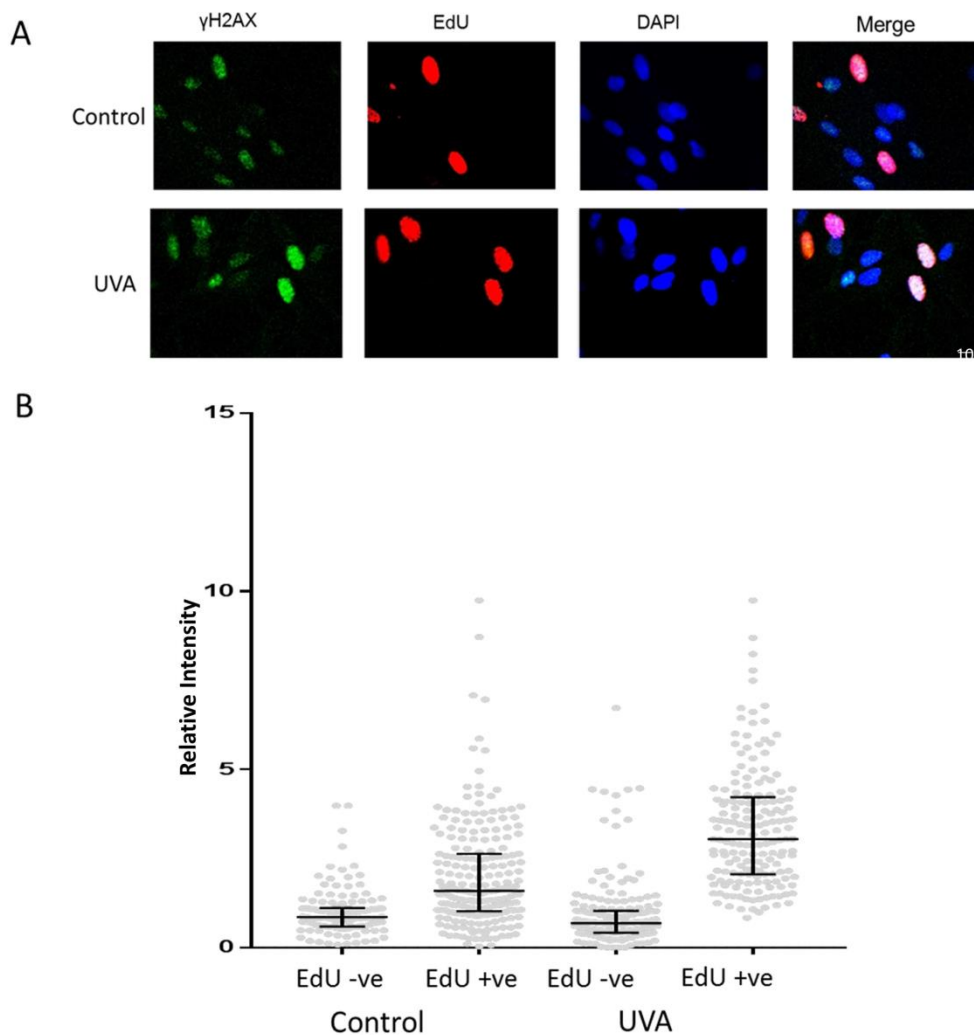


**Figure 4.6 Replicating fibroblasts are also susceptible to the UVA bystander effect**

*HaCaT cells were grown on a membrane and recipient fibroblasts were grown on a coverslip in a 6 well dish. The cells grown on the membrane were either irradiated with UVA (100kJ/m<sup>2</sup>) or sham irradiated. The irradiated cells were added to the recipient cells immediately after irradiation. EdU was added to the cells 1 hour prior to fixation 48 hours post co-incubation*

- A)** *Representative confocal microscopy images (n=3) of recipient fibroblasts showing immunofluorescent detection of  $\gamma$ H2AX (green) and fluorescent labelling of EdU (red)*
- B)** *The  $\gamma$ H2AX fluorescence of EdU-positive and -negative populations in both control and UVA recipients was measured using Zeiss LSM 510 software. At least 100 cells per condition were analysed and the experiment was repeated with three biologically independent replicates. The relative fluorescence compared to the control EdU-negative group was calculated and a categorical scatter plot of the data is shown. The median and interquartile ranges are indicated.*

Figures 4.5 and 4.6 show a slight increase in fluorescence was seen in the EdU positive control compared to the EdU negative control. This increase in  $\gamma$ H2AX is likely to be as a result of spontaneous DNA damage and stalled replication forks and was not an unexpected observation.

Figure 4.5 was carried out with HaCaT cells as both the donor and the recipient cells. The data shows that only the cells that were positive for EdU staining were positive for  $\gamma$ H2AX foci; indicating that only the cells that were in S-phase or later at the time of fixation were positive for foci. By analysing the EdU positive and negative cells separately the difference between the UVA bystander cells and the control is much more apparent than in the original analysis. The median of the EdU positive UVA bystander cells was 6.7 time greater than for the control EdU negative in the HaCaT cells, which is far greater than when the EdU positive and EdU negative cells were analysed together, the median increase was 2.3 in that case.

Previous work had shown bystander effects on clonogenic survival could be induced between different cell types, with keratinocytes and fibroblasts both able to induce the bystander effect in each other (Whiteside and McMillan, 2009). The experiment was therefore repeated to investigate whether UVA-irradiated keratinocytes could induce a DNA damage response in dermal fibroblasts and whether any observed induction was dependent on replicative status. Figure 4.6 demonstrates an increase in  $\gamma$ H2AX was also seen in the fibroblast cell line in the S phase populations, however, at only three times that of the EdU negative un-irradiated control, the fibroblasts showed a diminished  $\gamma$ H2AX bystander response compared to the HaCaT cell line.

### **4.3.3 Assessment of EdU uptake in bystander populations**

The data shown in figures 4.4, 4.5 and 4.6 indicate that it is likely that stalled replication forks are occurring in the bystander cells as a result of exposure to bystander signalling from the UVA irradiated populations. To further investigate this the EdU staining of the control populations relative to the EdU staining in the UVA bystander cells was analysed. The proportion of S-phase positive cells in each population was calculated and the intensity of EdU staining of all EdU positive cells across three independent replicates was analysed. This was carried out for both the HaCaT and dermal fibroblast bystander populations. In the presence of stalled replication forks it would be expected to see a higher proportion to S-phase cells, due to slowed replication as a result of stalled forks, the EdU incorporation would also be diminished as a result of inhibited replication. Forks expose single stranded DNA, which becomes coated in RPA and triggers the recruitment of ATR, which mediates Rad53 phosphorylation. The activation of Rad53 is require for full replication checkpoint response, activation of the replication checkpoints are crucial for retaining cell viability following replication stress.

Figure 4.7 shows that in the bystander HaCaT cells there is a significant ( $P < 0.01$ , Students T-test) increase in proportion of cells in S-phase, as demonstrated by the proportion of EdU positive cells. The data additionally demonstrated a significant ( $P < 0.05$ ) decrease in intensity of EdU staining in the UVA bystander population as demonstrated by a decrease in median shown in figure 4.7b. Figure 4.8 demonstrates that in dermal fibroblast cell lines there is a significant ( $P < 0.01$ , Students T-test) increase in S-phase cells in the UVA bystander population, this was demonstrated by an increase in EdU positive cells in the UVA bystander population. Additionally, a significant ( $P < 0.05$ , Students T-test) decrease in average EdU intensity per nucleus was seen in the dermal fibroblast bystander cells. Together the data shown in figures 4.7 and 4.8 are further indication that the increase in H2AX phosphorylation detected in the UVA bystander populations is a consequence of the presence of stalled replication forks,

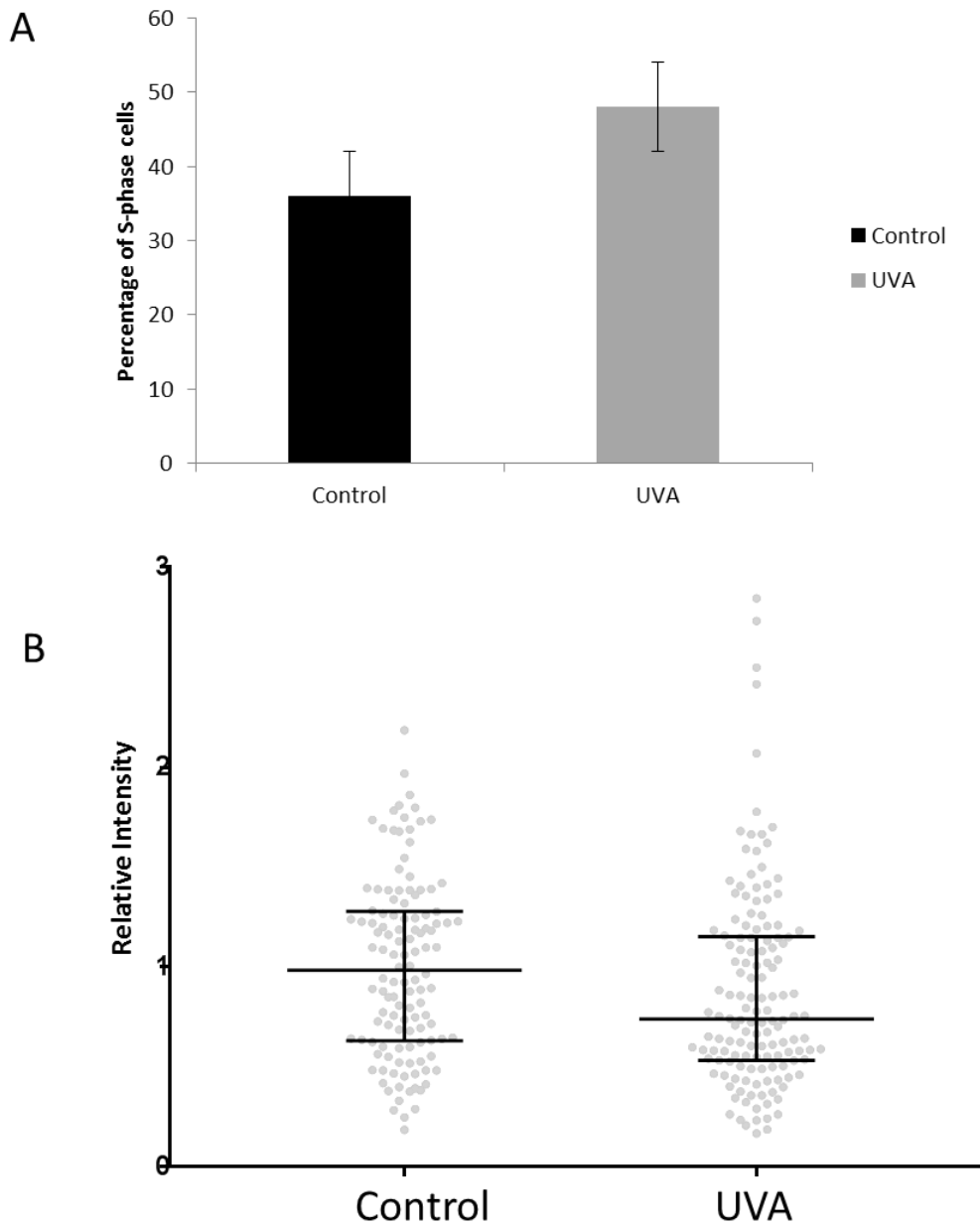


**Figure 4.7 EdU incorporation is decreased in UVA bystander keratinocytes.**

*HaCaT cells were grown on a membrane (donor) or on a coverslip (recipient) in a 6 well dish. The cells grown on the membrane were either irradiated with UVA (100kJ/m<sup>2</sup>) or sham irradiated. The donor cells were added to the recipient cells immediately after irradiation as before, fixed at 48 hours post co incubation and processed.*

- A) Bar chart to demonstrate the percentage of S-phase in the control and the UVA bystander groups. Error bars represent the standard deviation.*
- B) Categorical scatter plot to demonstrate the relative EdU staining intensity of control and UVA bystander cells. The median and interquartile range is indicated.*

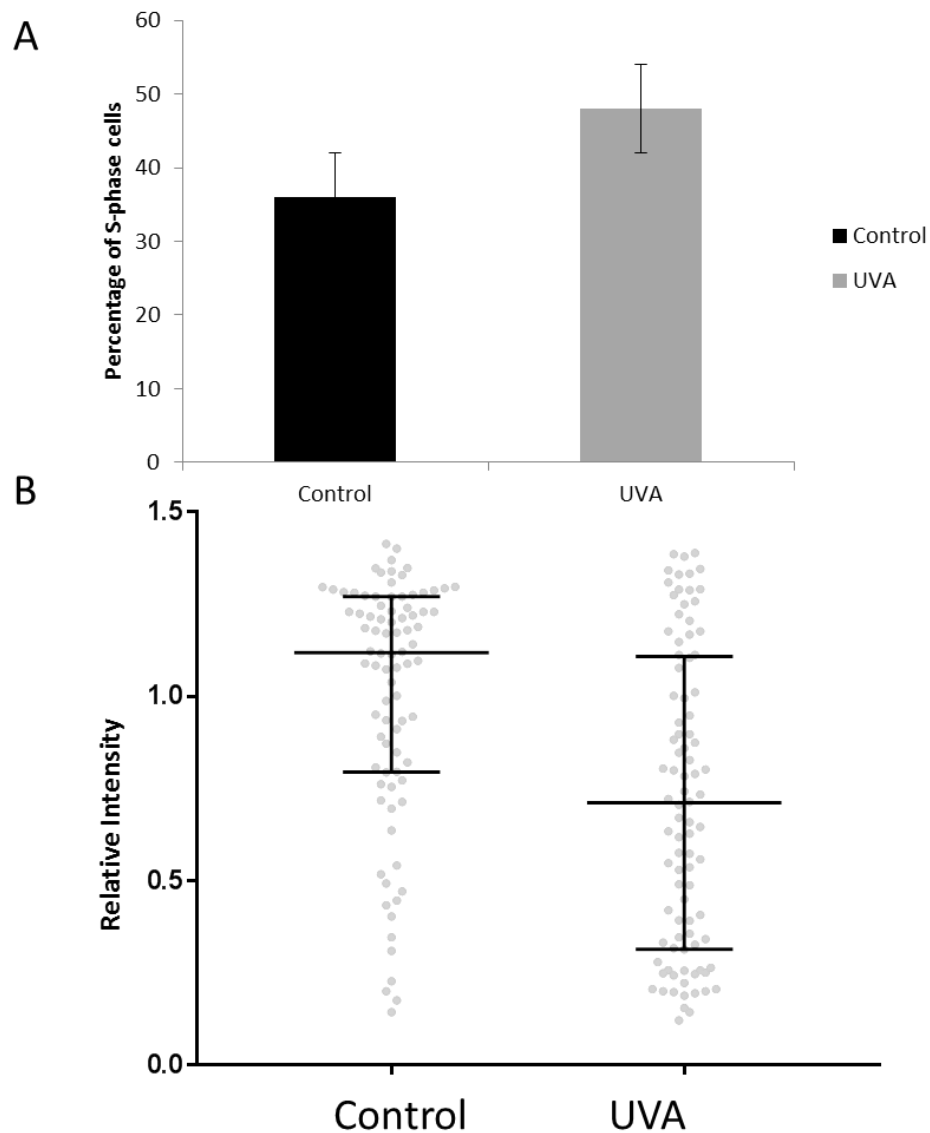


**Figure 4.8 EdU incorporation is decreased in UVA bystander fibroblasts.**

*HaCaT cells were grown on a membrane (donor) and dermal fibroblasts were grown on a coverslip (recipient) in a 6 well dish. The cells grown on the membrane were either irradiated with UVA (100kJ/m<sup>2</sup>) or sham irradiated. The donor cells were added to the recipient cells immediately after irradiation as before, fixed at 48 hours post co incubation and processed.*

- A) Bar chart to demonstrate the percentage of S-phase in the control and the UVA bystander groups. Error bars represent the standard deviation.*
- B) Categorical scatter plot to demonstrate the relative EdU staining intensity of control and UVA bystander cells. The median and interquartile range is indicated.*

#### **4.3.4 Phosphorylation of Chk1 in UVA bystander cells**

It is well accepted that  $\gamma$ H2AX is seen to be upregulated following both double strand breaks (Rogakou et al., 1998) and stalled replication forks (Ward and Chen, 2001) see figure 1.9. The pathway that has been activated can be determined by identifying other signalling molecules that have been activated. In this case it has already been shown that  $\gamma$ H2AX occurs only in S phase cells, and that there is an increased proportion of S-phase cells and decreased EdU staining in the UVA bystander populations indicating that  $\gamma$ H2AX up regulation is likely to be as a result of stalled replication forks. To further show this, the up regulation of p-Chk1 (Ser345) in bystander cells was examined. The upregulation of p-Chk1 (Ser345) is seen primarily in cells challenged by stalled replication forks (Feijoo et al., 2001) whereas the up regulation of p-Chk2 (Thr68) is seen following the formation of true double strand breaks (Matsuoka et al., 1998). The same time frames and experimental set-up used previously in this chapter were used here.

Figure 4.9 demonstrates that there is an upregulation of phosphorylated Chk1 in the UVA bystander cells relative to the control but similar to what was seen with  $\gamma$ H2AX staining was only seen in a subset of UVA bystander cells. Although a low level of p-Chk1 was seen in the remaining population of UVA bystander cells and in the control bystander cells. Quantification revealed a greater spread of intensity of staining in the UVA bystander population similar to what was observed with  $\gamma$ H2AX. Part C shows confirmation that the p-Chk1 positive cells were the EdU positive population further highlighting that it is likely that the increase in H2AX phosphorylation that is detected in the UVA bystander populations is as a result of the occurrence of stalled replication forks.

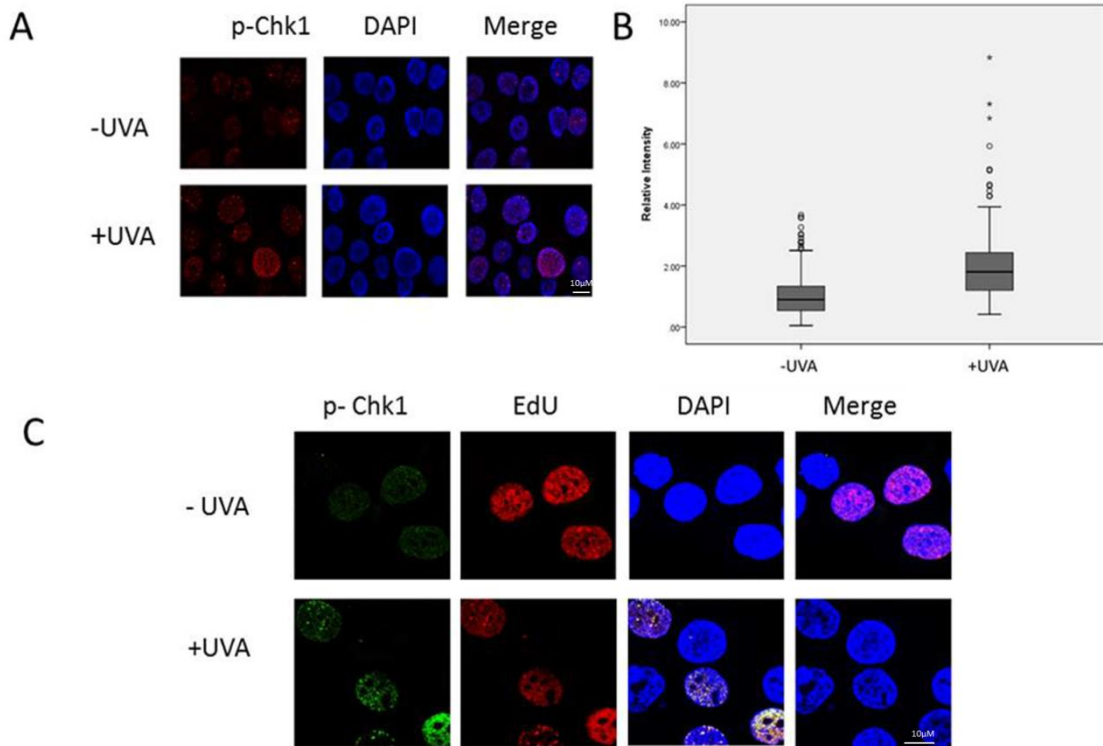


**Figure 4.9 Chk1 is phosphorylated in UVA bystander cells**

*HaCaT cells were grown on a membrane (donor) or on a coverslip (recipient) in a 6 well dish. The cells grown on the membrane were either irradiated with UVA (100kJ/m<sup>2</sup>) or sham irradiated. The donor cells were added to the recipient cells immediately after irradiation as before, fixed at 48 hours post co incubation and processed.*

- A) *Representative confocal microscopy images (n=3) of recipient keratinocytes showing immunofluorescent detection of pChk1, detected with a primary rabbit antibody against Chk1Ser345 and an AlexaFluor563 conjugated secondary antibody*
- B) *Quantitation of  $\gamma$ H2AX fluorescence intensity of Control and UVA bystander cells measured using Zeiss LSM510 software. At least 100 nuclei per condition were analysed and the experiment was repeated with 3 biologically independent replicates. The relative fluorescence compared to the control group was calculated and a box plot of the data is shown. The box represents the median and interquartile range and the whiskers show the 95 percentiles.*
- C) *Representative confocal image (n=3) to demonstrate pChk1 (green) and EdU (red) staining.*

#### **4.3.5 The effect of PIKK inhibitors on $\gamma$ H2AX foci formation in bystander cells**

The finding that the formation of  $\gamma$ H2AX foci in bystander cells occurred only in S phase suggested that the formation of foci could be due to stalled replication forks rather than the immediate formation of double strand breaks. Pharmacological inhibitors specific to ATM (KU-55933) and ATR (VE-821) were used to indicate whether either of these had an effect in the formation of  $\gamma$ H2AX foci in the bystander populations. In the initial experiment the inhibitors were added to both the feeder cells and the recipient cells at a concentration of 1 $\mu$ M for 1 hour prior to irradiation. The inhibitors were left on the cells for the duration of the experiment. Each of the inhibitors have been previously validated at the concentrations used as described see figures 3.14 and 3.15. Once again the nuclei were counterstained using labelling actively replicating cells by incorporation of the nucleotide analogue 5-ethynyl-2'-deoxyuridine (EdU) to identify S phase populations.

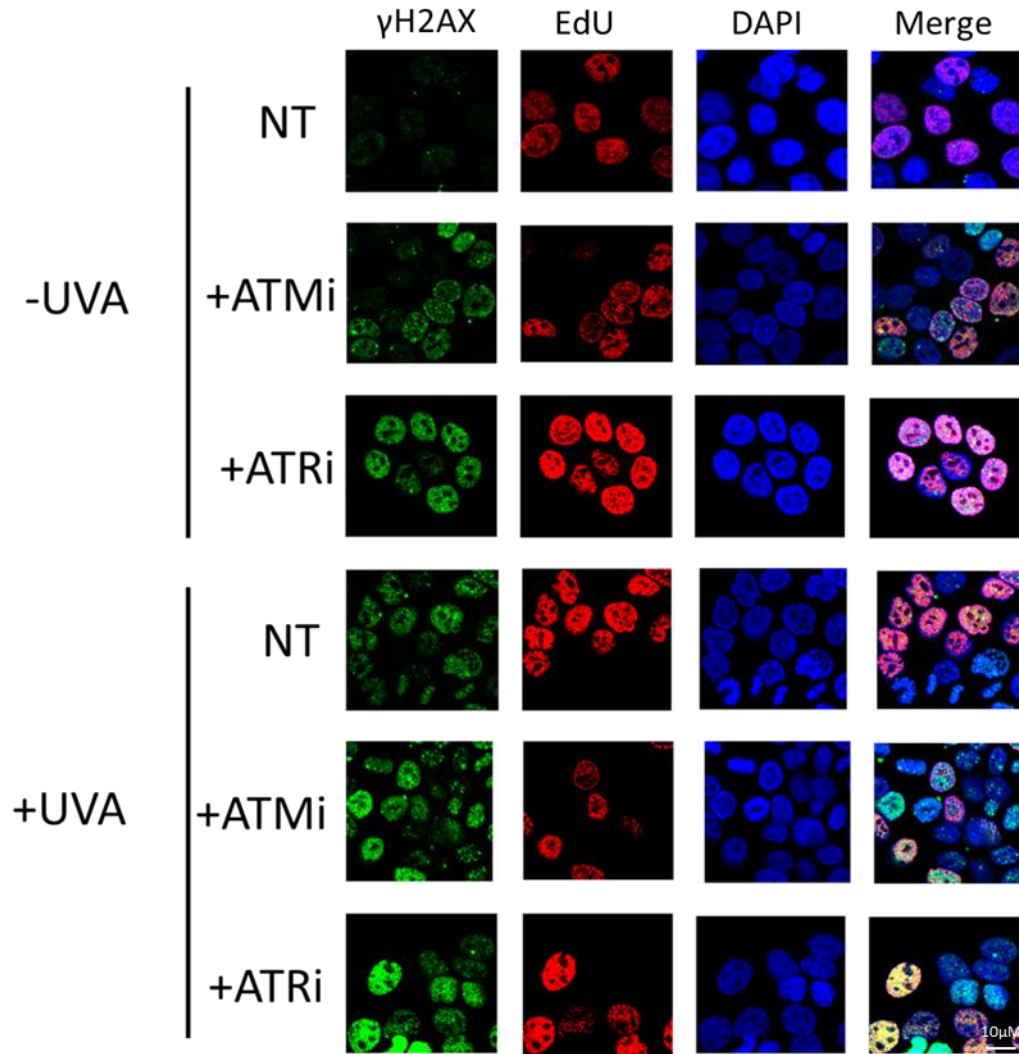


**Figure 4.10 Inhibitors to ATM and ATR increase H2AX phosphorylation following prolonged incubation**

*HaCaT cells were grown on a membrane or on a coverslip in a 6 well dish. The cells grown on the membrane were either irradiated with UVA (100kJ/m<sup>2</sup>) or sham irradiated. An inhibitor to either ATM (KU-55933) or ATR (VE-821) was added to both the control and UVA bystander cells 1 hour prior to co-incubation with the respective donor cells. The irradiated cells were added to the recipient cells immediately after irradiation as before. Recipient cells were fixed and processed 48 hours later, having been treated with EdU for the final hour of incubation.*

Figure 4.10 shows that the addition of either the ATM or ATR inhibitor caused a detectable increase in the levels of  $\gamma$ H2AX in both the control and the UVA bystander cells. The HaCaT cells were incubated with the inhibitors for 48 hours, this is longer than the inhibitors had been used on the cells in experiments in chapter 3. This suggests that prolonged incubation with the inhibitors caused an increase in activation of the DDR in the bystander cells. In each case the increase in H2AX phosphorylation appears to be limited to S phase cells. Interestingly the staining appeared to be different depending on which inhibitor the cells had been treated with, treatment with an ATM inhibitor resulted in an increase in distinct foci, whereas the ATR inhibitor resulted in an increase in pan nuclear staining. These two distinct patterns of staining indicate that it is likely that two separate mechanisms underpin the increased  $\gamma$ H2AX in the un-irradiated control cells treated with the inhibitors.

Next the inhibitors were added to the combined donor and recipient cells 24 hours after the donor cells were first added. This incubation time was chosen because when cells were incubated with the inhibitors for the whole duration (48 hours) as above, resulted in a detrimental effect on control cells. In previous experiments in chapter 3 the maximum time cells were incubated with the ATM or ATR inhibitors was 24 hours. This length of incubation had no negative effect on cells. It has also been established that there is a delay in the release of signals that cause the formation of  $\gamma$ H2AX in the bystander cells as demonstrated in figure 4.5 which showed only an increase in  $\gamma$ H2AX in bystander cells 48 hours after co-incubation with irradiated donor cells and not at 24 hours.

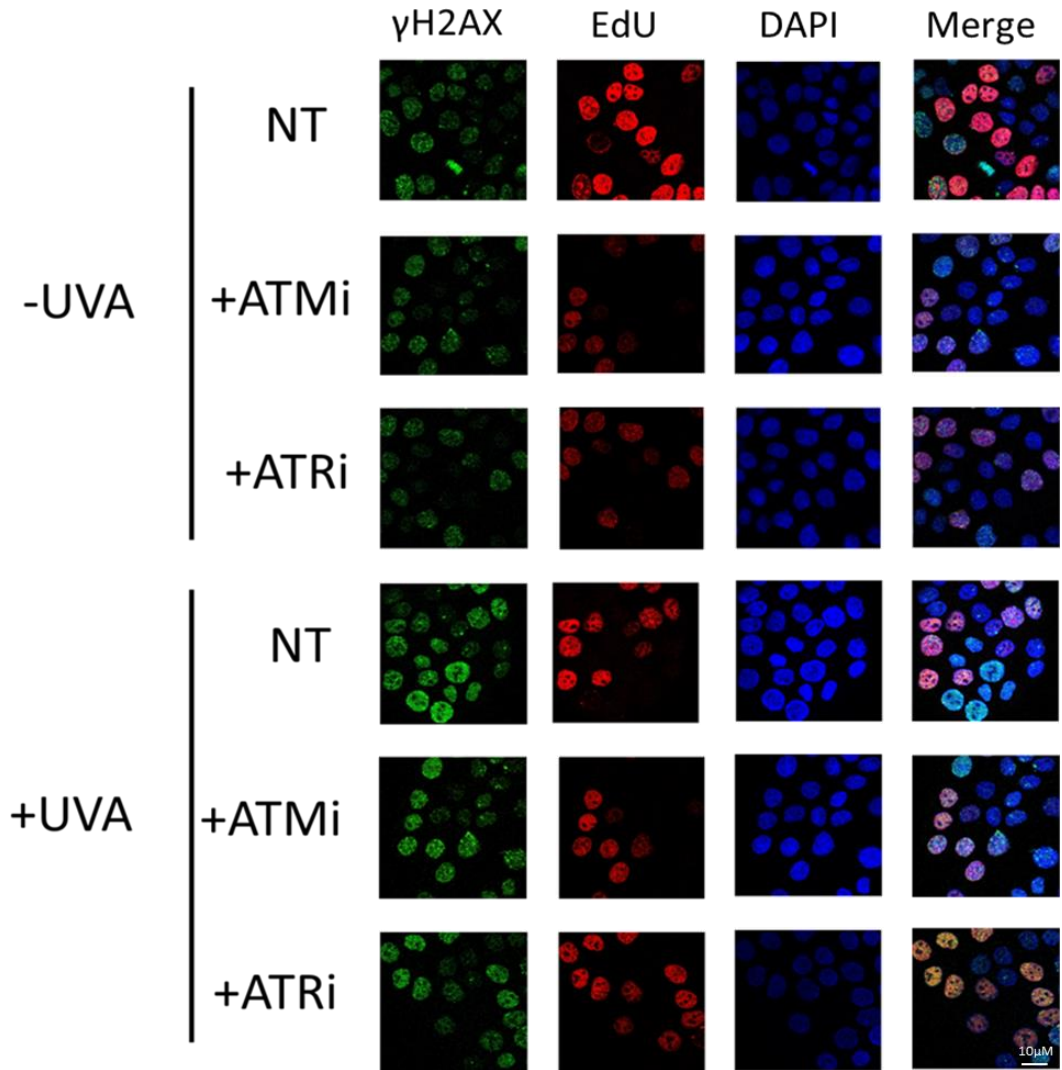


**Figure 4.11 Neither an inhibitor to ATM or ATR have an effect on the formation of  $\gamma$ H2AX in bystander cells**

*HaCaT cells were grown on a membrane or on a coverslip in a 6 well dish. The cells grown on the membrane were either irradiated with UVA (100kj/m<sup>2</sup>) or sham irradiated. The irradiated cells were added to the recipient cells immediately after irradiation as before; an inhibitor to either ATM or ATR was added to both the control and UVA bystander cells after 24 hours of co-incubation with the respective donor cells. Recipient cells were fixed and processed 48 hours later, having been treated with EdU for the final hour of incubation. Representative confocal microscopy images (n=3) are shown.*

Figure 4.11 shows that neither the ATM or ATR inhibitor caused an increase in H2AX phosphorylation in the control recipient cells indicating that the use of inhibitors for this incubation time had no detectable detrimental effect on the cells. However, there was no detectable decrease seen in H2AX phosphorylation in the UVA bystander cells treated with the inhibitors, indicating that neither ATM nor ATR play an exclusive role in  $\gamma$ H2AX foci formation in the UVA bystander populations.

#### **4.3.6 The role of ROS in $\gamma$ H2AX foci formation in bystander cells**

A role for reactive oxygen species in the induction of bystander effects is well established, the role of ROS in bystander effects has been repeatedly implicated in medium mediated bystander experiments using a variety of biological endpoints (Yang et al., 2005b; Hu et al., 2006; Azzam et al., 1998).

Previously in our laboratory a role for catalase has been identified in the induction of the bystander effect as measured by clonogenic survival of bystander cells. Therefore, the effect of catalase on H2AX phosphorylation in our UVA bystander populations was studied next. Catalase was added to cells immediately after irradiation and combination of the donor and recipient populations and remained on the cells for the duration of the experiment thereafter.

Figures 4.12 and 4.13 show that the addition of catalase immediately after irradiation caused a decrease in the formation of  $\gamma$ H2AX in both HaCaT (Figure 4.12) and fibroblast (figure 4.13) recipient cell lines. However, while there was a detectable decrease in  $\gamma$ H2AX intensity in the catalase-treated UVA bystander cells the levels remained higher than that of the time-matched un-irradiated control. Significant decreases of 32% and 48% ( $p < 0.01$ , One-way ANOVA), in median  $\gamma$ H2AX intensity were seen in the catalase-treated HaCaT and dermal fibroblast cell lines respectively.

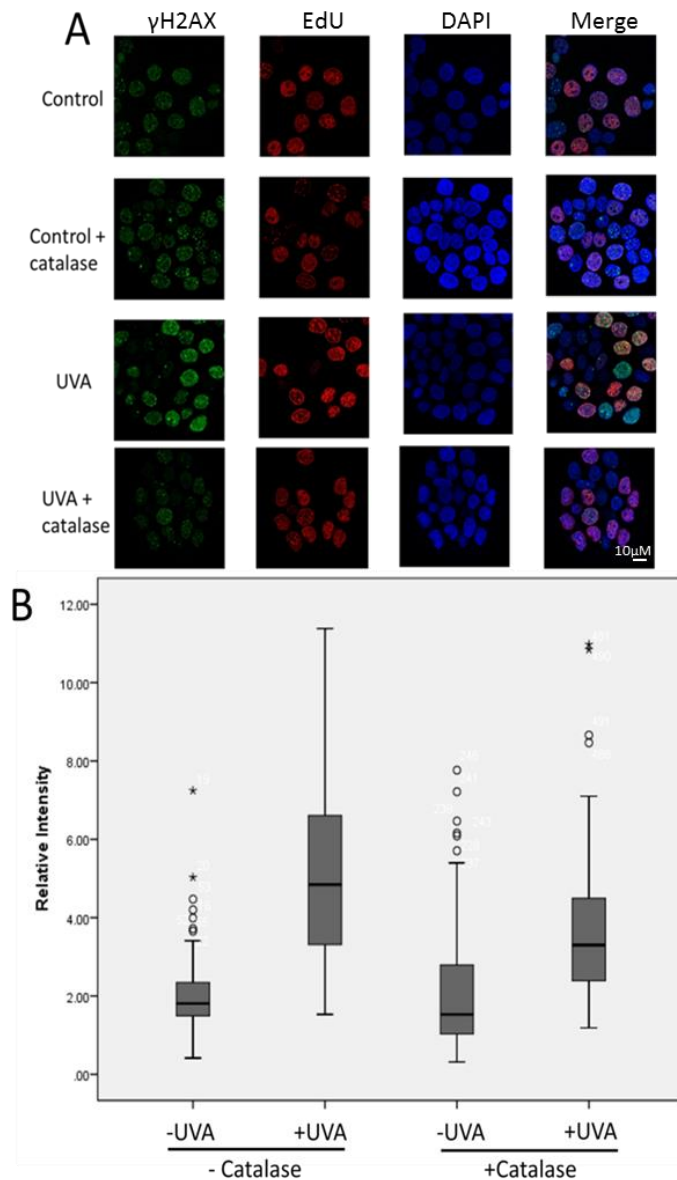


**Figure 4.12 Catalase causes a decrease in  $\gamma$ H2AX in bystander keratinocytes**

- A) HaCaTs were grown on a membrane insert and either irradiated with UVA ( $100\text{kJ}/\text{m}^2$ ) or sham irradiated. The inserts were then immediately transferred to wells containing HaCaTs cultured on coverslips. Catalase was added to both chambers to a final concentration of 250 U/ml. Recipient cells were fixed and processed 48 hours later, having been treated with EdU for the final hour of incubation. A representative ( $n=3$ ) image is shown.
- B)  $\gamma$ H2AX fluorescence intensity per nucleus was measured with Zeiss LSM510 software and the relative intensity compared to the average intensity of the control EdU-negative group was calculated and a box plot constructed to demonstrate the median and spread of the staining intensity. The box represents the median and interquartile range and the whiskers show the 95 percentiles.

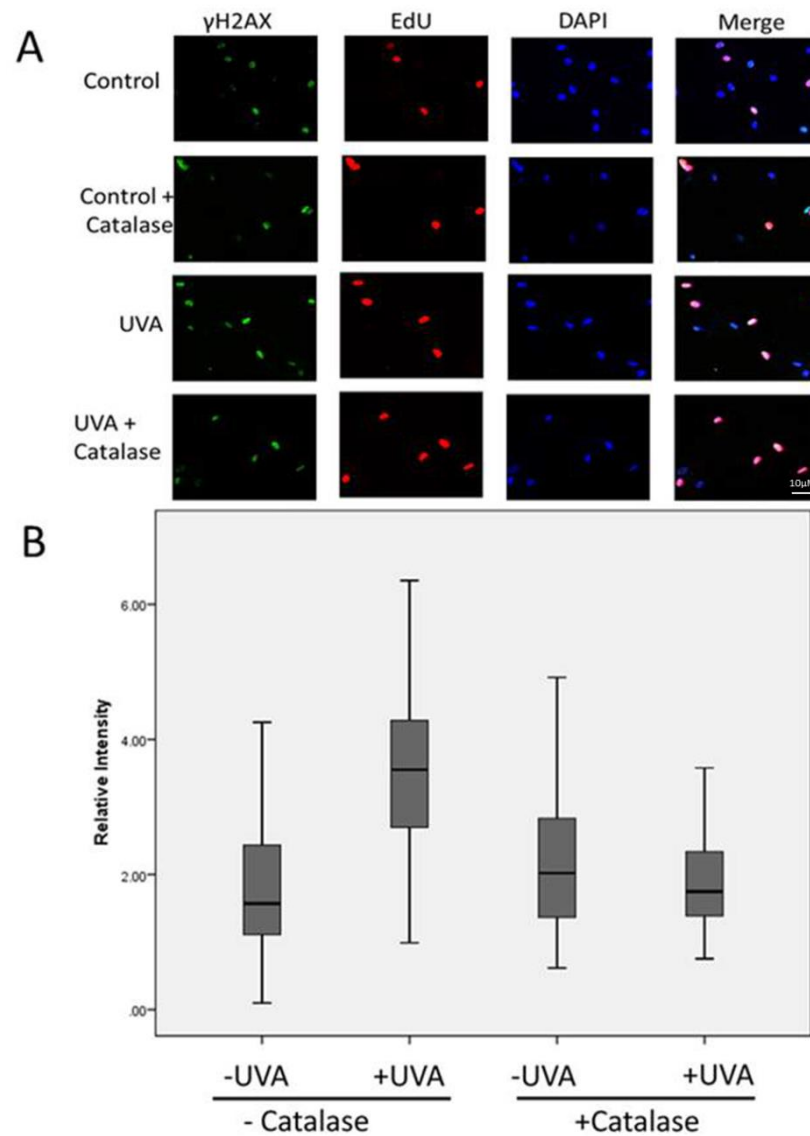


**Figure 4.13 Catalase causes a decrease in  $\gamma$ H2AX in bystander fibroblasts**

- A) HaCaTs were grown on a membrane insert and either irradiated with UVA ( $100\text{kJ}/\text{m}^2$ ) or sham irradiated. The inserts were then immediately transferred to wells containing normal human dermal fibroblasts cultured on coverslips. Catalase was added to both chambers to a final concentration of  $250\text{ U}/\text{ml}$ . Recipient cells were fixed and processed 48 hours later, having been treated with EdU for the final hour of incubation. A representative ( $n=3$ ) image is shown.
- B)  $\gamma$ H2AX fluorescence intensity per nucleus was measured with Zeiss LSM510 software and the relative intensity compared to the average intensity of the control EdU-negative group was calculated and a box plot constructed to demonstrate the median and spread of the staining intensity. The box represents the median and interquartile range and the whiskers show the 95 percentiles.

#### **4.3.6.2 The effect of DPI on H2AX phosphorylation in UVA bystander cells**

Previous work from our laboratory found that pre-incubation of HaCaT keratinocytes with the NADPH oxidase inhibitor DPI is able to attenuate the cytotoxic effects caused by co-incubation with UVA-irradiated cells (Whiteside 2006). DPI was added to both donor (HaCaT) and recipient (either HaCaT or dermal fibroblasts) cells for 18 hours prior to donor cell irradiation. The media was changed on both the donor and recipient cells to medium without DPI immediately prior to irradiation followed by 48 hours co-incubation. The samples were analysed as before to determine if DPI has any effect on the formation of  $\gamma$ H2AX foci in the bystander cells.

Figures 4.14 and 4.15 show that NADPH oxidase inhibitor DPI caused a significant decrease ( $P < 0.01$ , One-way ANOVA) in the formation of  $\gamma$ H2AX foci in the bystander cells suggesting a role for ROS, in particular superoxide anions in the UVA bystander response. Little difference was recorded between any of the EdU negative groups.

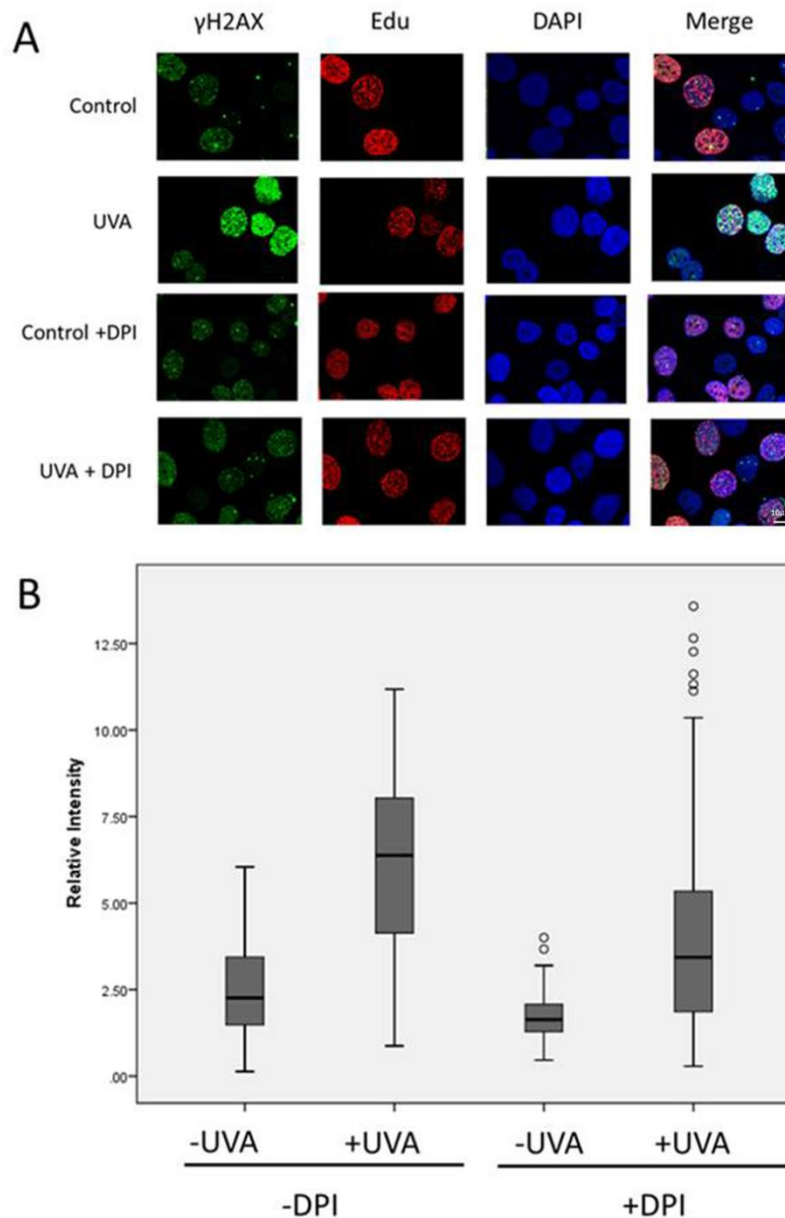


**Figure 4.14 Preincubation with NADPH oxidase inhibitor DPI causes a decrease in the formation of  $\gamma$ H2AX foci in bystander keratinocytes**

- A) HaCaT keratinocytes were grown on a membrane insert and pre-incubated with DPI (2  $\mu$ M) for 18 hours. They were then either irradiated with UVA (100kJ/m<sup>2</sup>) or sham irradiated. The inserts were immediately transferred to wells containing HaCaT cells cultured on coverslips and that had also been pre-incubated with DPI for the same time. Recipient cells were fixed and processed after 48 hours co-incubation, having been treated with EdU for the final hour of incubation. A representative (n=3) image is shown.
- B)  $\gamma$ H2AX fluorescence intensity per nucleus was measured with Zeiss LSM510 software and the relative intensity compared to the average intensity of the control EdU-negative group was calculated and a box plot constructed to demonstrate the median and the spread of intensity. The box represents the median and interquartile range and the whiskers show the 95 percentiles.

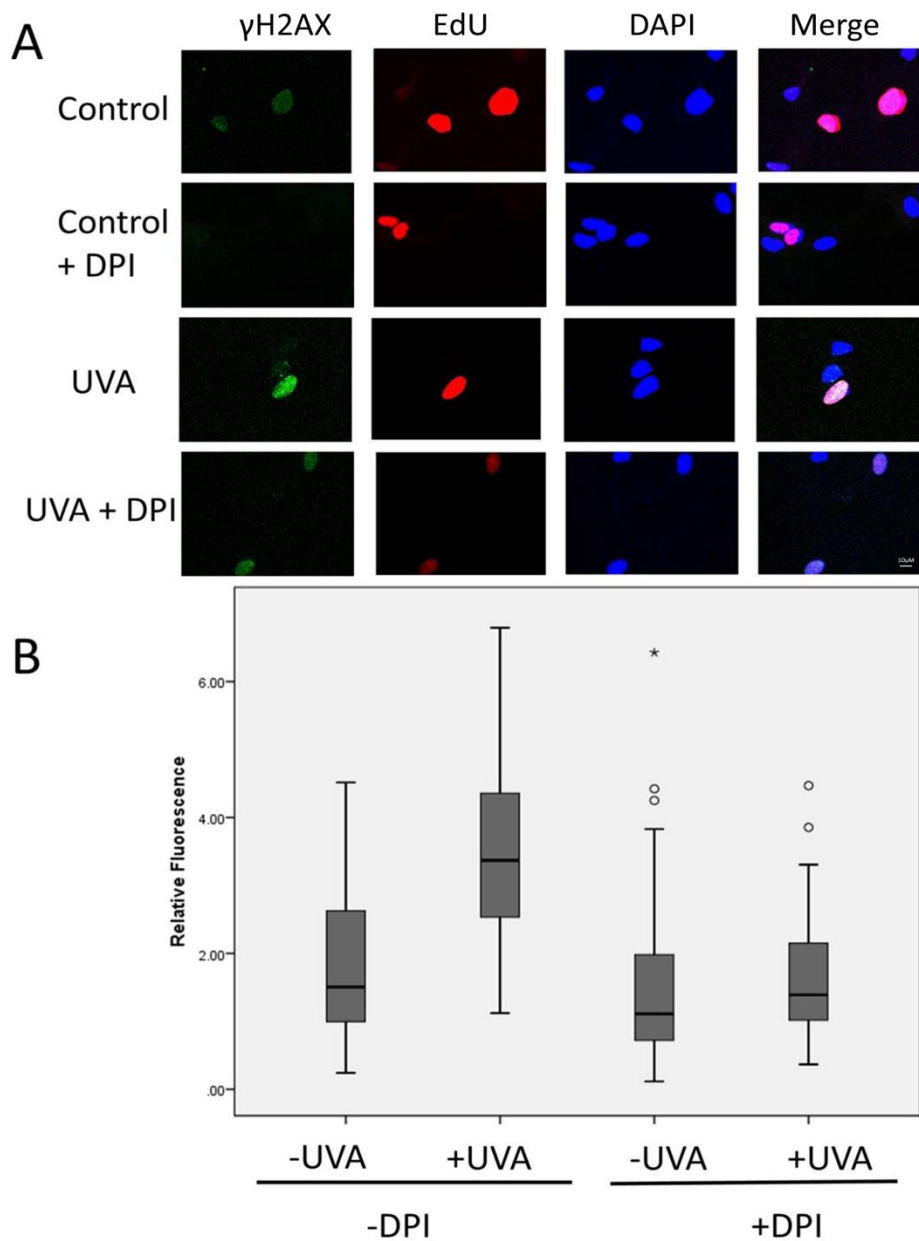


**Figure 4.15 Preincubation with NADPH oxidase inhibitor DPI causes a decrease in the formation of  $\gamma$ H2AX foci in bystander fibroblasts.**

- A) HaCaT keratinocytes were grown on a membrane insert and pre-incubated with DPI (2  $\mu$ M) for 18 hours. They were then either irradiated with UVA (100kJ/m<sup>2</sup>) or sham irradiated. The inserts were immediately transferred to wells containing normal human dermal fibroblast cells cultured on coverslips and that had also been pre-incubated with DPI for the same time. Recipient cells were fixed and processed after 48 hours co-incubation, having been treated with EdU for the final hour of incubation. A representative (n=3) image is shown.
- B)  $\gamma$ H2AX fluorescence intensity per nucleus was measured with Zeiss LSM510 software and the relative intensity compared to the average intensity of the control EdU-negative group was calculated and a box plot constructed to demonstrate the median and the spread of intensity. The box represents the median and interquartile range and the whiskers show the 95 percentiles.

#### **4.3.7 Apoptosis induction in bystander cells**

In addition to looking into the DNA damage response in bystander cells the induction of apoptosis in bystander cells was assessed using JC1, a marker of mitochondrial membrane potential. As discussed in chapter 3, JC1 can be used to measure mitochondrial membrane potential by measuring the ratio of red: green staining that is seen in the mitochondria.

Conditioned media was collected from UVA irradiated cells at either 24 or 48 hours post irradiation and incubated with bystander populations for a further 24 hours before cells were analysed by flow cytometry. To assess the mitochondrial membrane potential, the presence of JC1 aggregates (PI channel) and monomers (FITC channel) in the bystander cells was measured. There was a population of cells showing a shift towards JC1 monomers present in all samples analysed, demonstrating a decrease in mitochondrial membrane potential. This population was gated and the percentage of total cells present in this sub population was calculated.

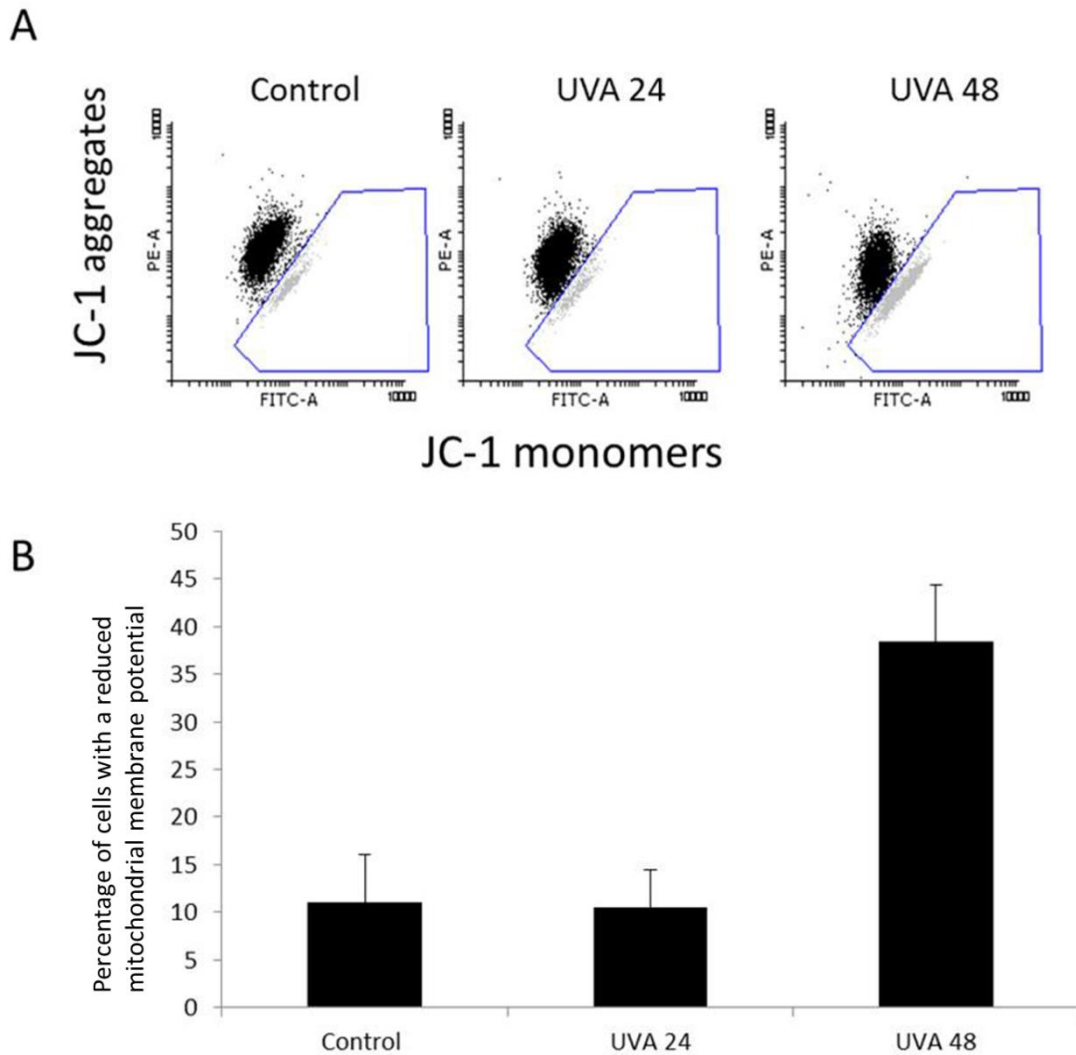


**Figure 4.16 A decrease in mitochondrial membrane potential is seen in UVA bystander cells at 48 but not 24 hours of co-culture with irradiated feeder cells**

*HaCaT cells were grown in a 60mm culture dish and irradiated with 100kJ/m<sup>2</sup> of UVA. Media was collected from the irradiated cells either 24 or 48 hours after irradiation and the bystander cells were cultured in the conditioned media. After 24 or culture in the conditioned media the cells were harvested by trypsinisation and JC1 was added to the suspension of bystander cells at a concentration of 1µg/ml and incubated for 20 minutes at 37 °C before analysis by flow cytometry.*

- A) *Representative images (n=3) demonstrating JC1 staining, the gated population represents cells with decreased presence of JC1 aggregates and therefore a decreased mitochondrial membrane potential.*
- B) *A bar chart to demonstrate the average percentage of cells in the gated population. Error bars show standard deviation.*

Figure 4.16 demonstrates that the conditioned media collected 48 hours after the feeder cells were exposed to UVA was able to induce a loss of mitochondrial membrane potential in the bystander cells. There was no change seen in the mitochondrial membrane potential of the bystander cells exposed to conditioned media of sham irradiated cells or conditioned media collected from targeted cells 24 hours post irradiation. This is consistent with our earlier data (figure 4.4) where 24 hour bystander cells showed no increase in H2AX phosphorylation but the 48 hour bystander cells did and with published work on the timeframes of the UVA bystander effect (Whiteside et al., 2011). In addition, figure 4.4 shows two distinct populations of cells when exposed to 48 hour conditioned media, illustrating that only a sub-population of bystander cells had a decrease in mitochondrial membrane potential, demonstrating that some cells are more susceptible to bystander signals. The increase in the number of cells in the sub population was seen to significantly ( $P < 0.01$ , One-way ANOVA) increase in the bystander 48 hour populations. This was a 4 fold increase of cells showing an altered mitochondrial membrane potential compared to the control and the UVA 24 hour group.

Additionally, confocal microscopy was used to further demonstrate changes in mitochondrial membrane potential in the bystander population. For this analysis the trans-well system that had been utilised for the work shown earlier in this chapter was used. For this analysis the mitochondrial membrane potential of bystander cells co-incubated with UVA irradiated cells for 48 hours and measure the red and green fluorescence of each cell. The ratio of red / green staining was then calculated and a box plot was plotted to demonstrate the red/green ratios of each population.

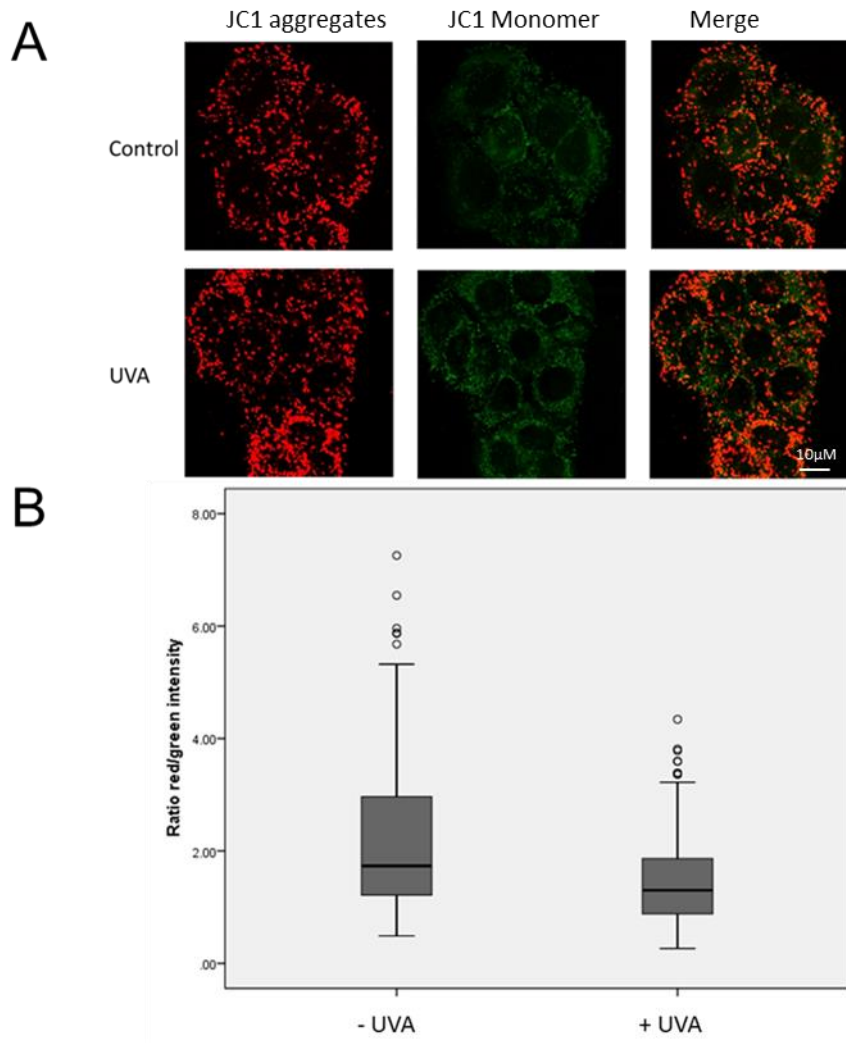


**Figure 4.17 A decrease in mitochondrial membrane potential can be detected in UVA bystander cells.**

*HaCaT cells were grown on a trans-well insert (pore size 1.0µm), irradiated with 100kJ/m<sup>2</sup>, immediately after irradiation the irradiated or sham irradiated cells were co-cultured with bystander cells grown on glass coverslips on a six well plate. After 48 hours of co-culture JC1 was added to the bystander cells at a concentration of 1µg/ml and incubated for 20 minutes at 37 °C before analysis by confocal microscopy.*

- A) *Representative confocal image (n=3) demonstrating the red (JC1 aggregates) and green (JC1 monomers) staining.*
- B) *The intensity of red and green intensity was measured using Zeiss LSM510 software, the ratio of red green intensity was calculated for each cell and normalised to the average red/green ratio of a control bystander cell. Box plots of the data were plotted to demonstrate the median and spread of the data. The box represents the median and interquartile range and the whiskers show the 95 percentiles.*

Figure 4.16 (A) demonstrates a decrease in the ratio of red/green staining in the UVA bystander cells compared to the control. In addition, two populations of cells can be seen in the UVA bystander cells, a substantial decrease in red staining is seen in some of the UVA bystander cells compared to others in the same population and the control bystander cells. This is similar to what was seen when detecting H2AX phosphorylation in UVA bystander cells, not all cells are equally vulnerable to bystander signals, and it appears that this finding may be a universal characteristic of bystander effect.

A box plot (figure 4.16 B) was constructed to demonstrate the median ratio of red: green staining and it demonstrates a significant ( $p < 0.01$ , Students T-test) decrease in the mitochondrial membrane potential of the UVA bystander cells compared to the control group. This suggests possible induction of apoptosis in the bystander cells within the same time frames that have previously detected increase in H2AX in the UVA bystander populations.

This work was then repeated in the in normal human dermal fibroblast cell lines, which had previously been demonstrated to show an increase in H2AX phosphorylation following exposure to signals from irradiated HaCaT cells. Using the trans-well set up cells were assessed for changes in mitochondrial membrane potential in fibroblast cells using confocal microscopy.

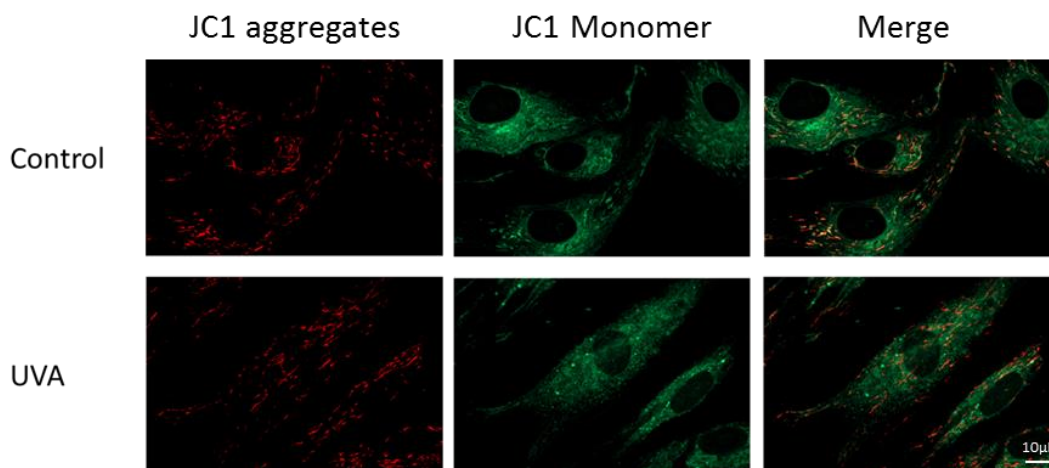


**Figure 4.18 There is no detectable difference in mitochondrial membrane potential of UVA bystander dermal fibroblast cells compared to the control**

*Normal human dermal fibroblast cells were grown on a trans-well insert (pore size 1.0µm), irradiated with 100kJ/m<sup>2</sup>, immediately after irradiation the irradiated or sham irradiated cells were co-cultured with dermal fibroblast bystander cells grown on glass coverslips on a six well plate. After 48 hours of co-culture JC1 was added to the bystander cells at a concentration of 1µg/ml and incubated for 20 minutes at 37 °C before analysis by confocal microscopy. A representative (n=3) image is shown.*

Figure 4.18 demonstrates that there is no difference in the mitochondrial membrane potential of UVA bystander dermal fibroblast cells compared to the control. This is different to what was observed with the HaCaT cell line. Figure 4.17 indicates that there is no increase in apoptosis induction in the UVA bystander cells, suggesting a difference in behaviour between the two cell lines. It is possible that in the case of fibroblasts that senescence is being induced rather than apoptosis, which is not associated with changes in the mitochondrial membrane potential.

#### **4.4 Discussion**

The bystander effect has been shown to induce a number of detrimental effects in cells challenged only by proximity to irradiated cells. Most recent work has focused on the DNA damage response in bystander cells, in particular the presence of double strand breaks by the detection of  $\gamma$ H2AX in bystander populations. Work carried out on ionising radiation has shown the presence of  $\gamma$ H2AX in bystander cells (Sokolov et al., 2005; Yang et al., 2005b; Sedelnikova et al., 2007a). The presence of double strand breaks in un-irradiated cells poses an increased risk to human health; Double strand breaks (DSBs) are considered to be one of the most dangerous forms of DNA damage; repair of DSBs is critical to avoid cell death, chromosomal aberrations, and mutations. In some cases presence of DSBs can directly initiate pathological events such as cancers (Mah et al., 2010).

In this work the ability of UVA to induce  $\gamma$ H2AX formation in bystander cells was investigated and attempts to identify the cell populations that contained  $\gamma$ H2AX were made. Further analysis attempted to identify the type of DNA damage that had caused the H2AX phosphorylation in the bystander cells and the effect of catalase and DPI on the formation of  $\gamma$ H2AX in bystander cells was also studied.

The data shown in this chapter indicated that UVA is able to induce the formation of  $\gamma$ H2AX in bystander cells. An increase in  $\gamma$ H2AX intensity is seen at both 24 and 48 hours compared to their time matched control. The levels of  $\gamma$ H2AX are higher in the 48 hour bystander cells compared to the 24 hour ( Figure 4.4 ), supporting earlier work that suggested that the release of signals for the UVA bystander effect is a delayed event; previous work in our laboratory demonstrated that a decrease in clonogenic survival occurred only when bystander cells were incubated with UVA irradiated feeder cells for 48 hours and not 24 hours (Whiteside et al., 2011) This is also in agreement with work carried out with ionising radiation, where  $\gamma$ H2AX was observed in bystander cells for up

to 5 days post irradiation (Sedelnikova et al., 2007a). The delay in up regulation of foci formation in bystander cells compared to directly irradiated cells is similar to results that have been seen previously with ionising radiation where the formation of  $\gamma$ H2AX foci was seen to have increased at 18 hours post co culture when in directly irradiated cells  $\gamma$ H2AX is seen to be up regulated 30 minutes after irradiation. In addition the levels of  $\gamma$ H2AX in bystander cells remain elevated at 48 hours (Sokolov et al., 2005).

Figure 4.4 showed that not all UVA bystander cells contained  $\gamma$ H2AX foci (figure 4.5), indicating that only a portion of the cells were susceptible to the bystander effect, supporting earlier work which also found only a subset of bystander cells to be positive for  $\gamma$ H2AX foci (Burdak-Rothkamm et al., 2007; Yang et al., 2005a). The same finding has also been recorded in 3D tissue models (Sedelnikova et al., 2007b). It has previously been demonstrated that not all cell types are equally susceptible to the bystander effect; rapidly dividing cell lines (Shao et al., 2008a) have been found to be more susceptible to bystander signals, suggesting a role for replication on a cells susceptibility to the bystander effect.

Counterstaining the nuclei with EdU demonstrated that only cells positive for EdU staining were positive for  $\gamma$ H2AX foci (figures 4.5 and 4.6); that is, only cells that are in S phase or later are positive for  $\gamma$ H2AX. This was shown in both HaCaT and Normal Human Dermal Fibroblast cell lines. This data suggested that the demonstrated upregulation of  $\gamma$ H2AX is as a result of stalled replication forks rather than direct double strand break formation. This finding supports earlier work carried out using X rays, which showed bystander cells deficient in ATR did not form  $\gamma$ H2AX foci whilst those incubated with inhibitor to ATM and DNA-PK did. The same group also showed that only S phase cells were positive for foci (Burdak-Rothkamm et al., 2007).

EdU analysis of the data revealed that there were an increased proportion of S-Phase cells in the UVA bystander populations for both the HaCaT (figure 4.7) and the dermal

fibroblast (figure 4.8) cell lines. A decrease in intensity of EdU staining was seen in the UVA bystander cells compared to the control, once again this was seen in both the cell lines studied (Figures 4.7 and 4.8). Additionally, it was demonstrated that Chk 1 was phosphorylated in UVA bystander cells (Figure 4.9), to our knowledge this is the first experimental report of p-Chk1 (ser345) up regulation in bystander populations. This further suggests that the pathway activated in the bystander cells is that in response to stalled replication forks and not double strand break formation (Feijoo et al., 2001).

Incubations with both catalase (figures 4.12 and 4.13) and DPI (figures 4.14 and 4.15) caused a decrease in  $\gamma$ H2AX in UVA bystander cells. This was seen in both HaCaT and Normal Dermal Fibroblasts confirming work that has been previously shown by our group suggesting that both hydrogen peroxide and superoxide play a role in the UVA bystander effect (Whiteside 2006). In work shown here DPI had a more pronounced effect on  $\gamma$ H2AX foci formation suggesting that superoxide may possibly play a larger role than hydrogen peroxide; however, our data does not tell us how much of the hydrogen peroxide is eliminated by the dose of catalase that was utilised. Therefore more direct work into the levels of hydrogen peroxide with and without catalase would need to be carried out before this suggested conclusion can be confirmed.

Although, this was in agreement with work carried out on ionising radiation that found the addition of DPI or SOD caused a more marked decrease in micronuclei formation than catalase (Little et al., 2002) indicating that superoxide could play a more pronounced role in bystander response than hydrogen peroxide. However neither Catalase nor DPI caused a decrease in the levels of  $\gamma$ H2AX in the UVA bystander cells to that of the control, suggesting that neither hydrogen peroxide nor superoxide are solely responsible for the initiation of the bystander effect. This is in agreement with much of the work carried out in the area which suggests that it is likely that a number of signalling molecules and reactive oxygen species are involved in the initiation of the bystander effect.

Altogether our data show that UVA is able to induce DNA damage in bystander cells as measured by the increased presence of  $\gamma$ H2AX in bystander populations, S phase cells seem more susceptible to the bystander signals, and although both catalase and DPI have caused a decrease in the  $\gamma$ H2AX detected neither of them fully abrogated it suggesting that a number of ROS are involved in the bystander signalling pathways.

The use of an ATR inhibitor at a concentration of 1 $\mu$ M for 48 hours caused an increase in detectable levels of  $\gamma$ H2AX in both the control and the UVA bystander populations (figure 4.10). The staining seen in the control cells treated with ATRi showed an increase in pan nuclear staining in S phase cells, this is consistent with work that knocked down the ATR-p-chk1 pathway and found an increase in apoptosis in S phase cells, as well as an increase in activation of an ATM/JNK dependent apoptotic pathways which stimulates high levels of pan nuclear  $\gamma$ H2AX (de Feraudy et al., 2010; Domon and Rauth, 1969).

When the cells were exposed to ATMi for a prolonged (48 hour) period an increase in distinct H2AX foci was seen, the staining pattern seen following ATMi treatment was strikingly different to that seen with prolonged treatment of the ATR inhibitor (Figure 4.10), the increase in foci in untreated cells is seen primarily in cells that also stained positive for EdU; this increase is only seen in S phase cells, suggesting the increase in  $\gamma$ H2AX is seen only in actively replicating cells. ATM plays a crucial role in the induction of cell cycle arrest following DNA damage; this illustrated increase in foci could be as a result of unrepaired endogenous damage as a result of insufficient cell cycle arrest due to the inhibition of ATM, this cell cycle arrest could lead to the activation of ATR, and consequent H2AX phosphorylation.

To overcome the issue with increase H2AX phosphorylation in the control cells following prolonged incubation with the ATM/ATR inhibitors, the incubation time was decreased to 24 hours; this incubation time did not cause an increase in  $\gamma$ H2AX in the control recipient cells (figure 4.11). However no decrease in  $\gamma$ H2AX in the UVA bystander cells following

incubation with either inhibitor was seen. This was in contrast with work carried out in ionising radiation which suggested a role for ATR in the phosphorylation of H2AX in bystander cells (Burdak-Rothkamm et al., 2007), in cells with mutated ATR rather than the use of an inhibitor. This work was also carried out on different cell lines to the ones used in this chapter.

Additionally, the bystander cells were studied for changes in mitochondrial membrane potential, which indicates the early stages of apoptosis. The same timeframes that had been studied for the DDR were utilised to assess changes in mitochondrial membrane potential in our bystander populations. Un-irradiated HaCaT cells were exposed to conditioned media collected from UVA-irradiated HaCaTs at 48 hours post for 24 hours before assessment by flow cytometry. Additionally, once again used the trans-well system as previously described to assess the mitochondrial membrane potential by confocal microscopy. Both of these experimental approaches showed a detectable decrease in mitochondrial membrane potential in the bystander population at 48 hours but not 24 hours, this was consistent both with work on the DNA damage response in this chapter and earlier work on the timeframes of the UVA bystander effect measured by clonogenic survival (Whiteside et al., 2011)

Both the confocal images and the flow cytometry (Figures 4.16 and 4.17) data show that there are two distinct populations for the bystander 48 hour group but not the other group(s) indicating that, in this group a sub-population of cells have altered mitochondrial membrane potential, an early indicator of apoptosis. This was similar to what was observed in the directly irradiated cells in chapter 3. The flow cytometry data demonstrated that in the bystander cells there is an average of 37% of cells in the population that demonstrated a decreased mitochondrial membrane potential, this a 4-fold increase compared to the control. This was a lower increase than what was seen in

the directly irradiated cells where a 6 fold increase was seen in cells with a decreased mitochondrial membrane potential.

Interestingly, unlike what was demonstrated in the work on the DDR a difference in response between our two cell lines was seen in these experiments. A significant decrease in mitochondrial membrane potential in the HaCaT cells was detected but no detectable change in mitochondrial membrane potential was seen in the dermal fibroblast cell line (Figure 4.18). This indicated apoptosis in the HaCaT cells but not the dermal fibroblast cell lines. There is some evidence to suggest that fibroblasts are more likely to become senescent than apoptotic in response to UV (Lewis et al., 2008).

The ability of UVA to induce a bystander effect could mean that the consequences of UVA exposure to both the deeper layers of the dermis and other tissues are due to bystander signals as well as direct irradiation and could extend the carcinogenic effect of UVA in particular in the induction of melanoma, for which UVA has been suggested to play a role (Pleasant et al., 2010; Noonan et al., 2012; Zhang, 2006). It is possible therefore that the UVA bystander effect could play a role in the initiation of melanoma. Melanocytes have been seen to have increased vulnerability to oxidative damage (Jimbow et al., 2001) and to be more susceptible to the UVA bystander signals than other dermal cell lines (Redmond et al., 2014). The UVA bystander effect has also been seen to induce melanogenesis in both melanoma and normal melanocyte cell lines (Nishiura et al., 2012).

Further work should focus on a deeper understanding of the mechanism involved in the bystander effect, potentially allowing for better chemotherapy approaches for cancer treatment. The ability of UVA to indirectly induce genotoxic damage, in addition to its well-established direct effects, could have implications for the carcinogenicity of UVA. Our data suggest that current methodologies could possibly be underestimating the genotoxic burden of UVA; many studies that have looked for the presence of genetic damage in skin or skin equivalents following UVA irradiation have focused on comparatively early time-

points post-irradiation. Our data suggests that UVA is able to initiate damage for extended time periods post irradiation. Moreover, the delay in induction of this effect and its dependence on ROS suggest a potential role for antioxidants in ameliorating the effects of UVA exposure.

**Chapter 5 The effect of  
UVA on MMP release in  
keratinocyte and  
fibroblast cell lines**

## **5.1 Introduction**

Exposure to UV is considered the most important factor in extrinsic skin ageing, and thought to account for 80% of the damage seen in extrinsically aged skin (Poljšak and Dahmane, 2012) Extrinsic skin ageing is also commonly referred to as photoaging. Drastic changes in the dermal layer of the skin are a characteristic of photoaging and matrix metalloproteinases (MMPs) have been implicated as playing a key role by increasing collagen breakdown. In this chapter the ability of UVA to increase the activation of MMPs in keratinocyte and fibroblast cell lines will be studied.

### **5.1.1 The structure of the dermis**

Human skin is made up of two distinct layers, the epidermis and the dermis. The general structure of the skin has been discussed previously in chapter 1. In the following section I will be focusing on describing the structure of the dermal layers of the skin to provide context when the clinical features of photoaging, which are primarily seen in the dermal layer are discussed later in this chapter.

The dermal layer of the skin is much thicker than the epidermis and is responsible for the strength and maintenance of the skin. The main component of the dermal layers is the extracellular matrix (ECM). There are two main classes of molecule which form the ECM, these are, fibrous structural proteins, such as collagen and proteoglycans, polysaccharides and water. The cells in the dermal layers are surrounded by the ECM. The main constituent of the ECM is collagen, which makes up 75% of the dry weight of skin and is seen to be strikingly disrupted in extrinsically aged skin.

### **5.1.2 ECM turnover**

Collagen is responsible for maintenance of the structure and elasticity of the skin and is highly regulated under normal conditions. Collagens are released from fibroblasts as precursor proteins (Pieraggi et al., 1985) and their maturation and degradation are closely controlled, undergoing almost constant remodelling and maintenance by transforming growth factor (TGF)- $\beta$  (Igotz and Massagué, 1986) and activator protein (AP)-1 (Fisher and Voorhees, 1998). The cytokine TGF- $\beta$  causes the maturation of collagen fibres from their pre protein through cleavage of the the protein portion of the fibre . TGF- $\beta$  also plays a role in the inhibition of MMP activity and increasing the activation of p38MAPK which in turn increases fibroblast proliferation (Zhong et al., 2011). Breakdown of collagen is mediated by activator protein one (AP1) which drives the synthesis of MMPs, a family of proteases which together are able to degrade all constituents of the extracellular matrix (Quan et al., 2009). Additionally the presence of damaged collagen has been seen to cause a decrease in synthesis of pre-collagen further exacerbating the effects of UV (Varani et al., 2002).

Second harmonic generation (SHG) microscopy has been utilised to quantify collagen breakdown. SHG is a non-linear optical process in which photons interacting with a non-linear material effectively combine to create a new photon with twice the energy and half the wavelength of the original photon (Campagnola and Loew, 2003). This technique has been used to compare ratios of elastin and collagen in photoaged and non photoaged skin (Koehler et al., 2006). To show the possible use of SHG in diagnostics, Zhou et al used SHG microscopy to quantify collagen change in normal and photoaged skin. This work demonstrated the potential SHG to quantify collagen in the dermis and therefore its use in the diagnosing of photoaging (Liao et al., 2010) . The use of this technique to characterise loss of collagen in the dermal layers of the skin as a biomarker in humans raises ethical issues; however use of animal models and 3D skin models could be used to assess the suitability of collagen breakdown as a biomarker for UVA exposure.

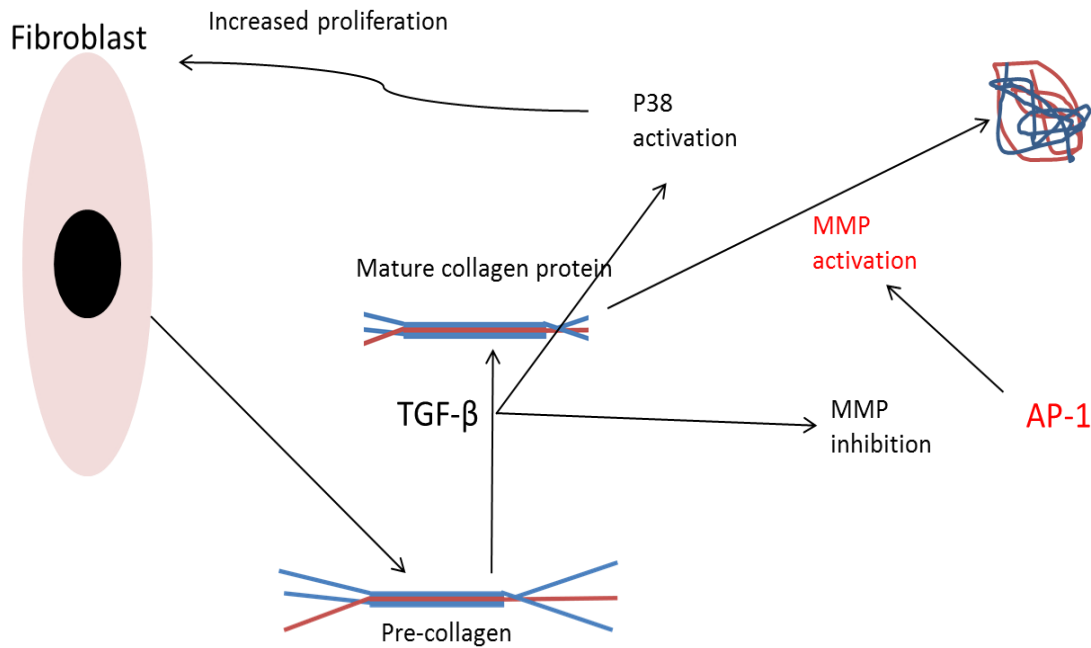


**Figure 5.1 Collagen turnover in the extracellular matrix**

*Schematic representation of collagen turnover in the extracellular matrix, procollagen is released from fibroblasts and subsequently cleaved to form the mature protein by TGFβ. Collagen is broken down by MMPs, activated by transcription factor AP1. All of which is tightly regulated in normal conditions to maintain skin homeostasis.*

### **5.1.3 Matrix Metalloproteinases**

Matrix metalloproteinases (MMPs) are a family of zinc and calcium dependent degradation enzymes which are implicated in a large number of diseases including carcinogenesis (Stetler-Stevenson et al., 1993) and photoaging (Berneburg et al., 2000). In addition, the MMP family also play a role in normal extracellular matrix (ECM) turnover and other developmental events such as embryogenesis (Malemud, 2006). The role of MMPs in carcinogenesis and photoaging makes them of great interest in respect to defining biomarkers for UVA damage. Dysregulated in both major disorders associated with UVA there is some scope for a biomarker within the MMP family. The MMP family is split into sub groups depending on both their substrates and structure. Major families

include collagenases and gelatinases (Visse and Nagase, 2003) . To date 28 different MMPs have been identified (Lohi et al., 2001) and their subtypes and substrates are described in table 5.1.

**Table 5.1 MMPs and their substrates**

MMP subtype	MMP name	ECM substrates	
<b>Collagenases</b>	MMP1	Collagens I, II, III, VII, VIII and X. Gelatin, proteoglycans, tenascin, entactin.	
	MMP8	Collagens I, II, III, V, VIII and X. Gelatin, aggrecan	
	MMP13	Collagens I, II, III, IV, IX and X. Gelatin, aggrecan, tenascin, fibronectin, osteonectin	
<b>Gelatinases</b>	MMP2	Collagens I, IV, V, VII, X, XI and XIV. Gelatin, elastin, fibronectin, laminin, aggrecan, versican, osteonectin and proteoglycans.	
	MMP9	Collagens IV, V, VII X and XIV, Gelatin, elastin, aggrecan, versican, osteonectin and proteoglycans.	
<b>Stromelysins</b>	MMP3	Collagens III, IV, V and IX. Gelatin, aggrecan, versican, proteoglycans, tenascin, fibronectin, laminin and osteonectin.	
	MMP10	Collagens III, IV and V. Gelatin, casein, aggrecan, elastin and proteoglycans.	
	MMP11	Casein, laminin, fibronectin, gelatin, collagen IV, transferrin	
	MMP14	Collagens I, II, III, casein, elastin, tenascin, vitronectin, proteoglycans, laminin, entactin and fibronectin.	
<b>Membrane type</b>	MMP15	Tenascin, fibronectin, laminin	
	MMP16	Collagen III, gelatin, casein and fibronectin.	
	MMP17, MMP24 and MMP25.	Not defined	
	<b>Others</b>	MMP7	Collagens IV and X, gelatin, aggrecan, proteoglycans, fibronectin, laminin, entactin, tenascin, integrin b, osteonectin, elastin, casein and transferrin.
		MMP12	Collagen IV, elastin, casein, gelatin, proteoglycans, fibronectin, laminin, vitronectin and enactin
	MMP20	amelogenin	
	MMP26	Collagen IV, fibronectin, fibrinogen and casein	
	MMP28	Casein	
	MMP 23 and MMP27	Not defined	

MMP levels are tightly regulated at each stage of their production; transcriptionally, processing and blocking the enzyme activity. The expression of MMP genes are activated by a variety of molecules, from pathways activated by wide ranging stimuli (Yan and Boyd, 2007). The transcription factor AP-1 is considered a key mediator and is able to induce the expression of a number of MMPs including MMP1, 3 and 9 (Fisher et al., 1997). AP-1 is composed of two subunits, c-fos and c-jun. C-fos is expressed constitutively whereas c-jun can be induced by exposure to UV (Fisher and Voorhees, 1998), ultimately resulting in increased MMP expression.

The resultant product is a latent pre-enzyme which then needs processing before it is in an active form (Harper et al., 1971). The pre-protein is released with an additional domain, containing a cysteine residue which ensures that the MMP remains latent (Woessner, 1998). The cysteine residue binds to  $Zn^{2+}$  on the catalytic domain of the enzyme causing it to be inactive. This is often referred to as the cysteine switch. Once this bond is broken the  $Zn^{2+}$  is free to co-ordinate to substrates. In addition the additional domain is cleaved after the breaking of the cysteine  $Zn^{2+}$  bond. Activation of the enzyme can be blocked by tissue inhibitors of matrix proteases (TIMP) (Nelson et al., 2000).

Four TIMPS have been identified in mammalian cells and between them they have the ability to inhibit most MMPs (Gomez et al., 1997) and therefore play a crucial role in maintaining MMP activity. Dysregulation of these enzymes is seen in a number of diseases including cancers (Lambert et al., 2004).

MMPs play a key yet complex role in carcinogenesis and are involved in a number of stages of cancer progression see review by (Egeblad and Werb, 2002). The mechanisms involved in each stage were recently reviewed by Gialeli et al (2011). As they highlight in recent decades it has emerged that the relationship between tumour cells and their microenvironment plays a pivotal role in cancer progression and the evidence suggesting

a role for matrix modelling proteases such as MMPs in this relationship is increasing (Gialeli et al., 2011).

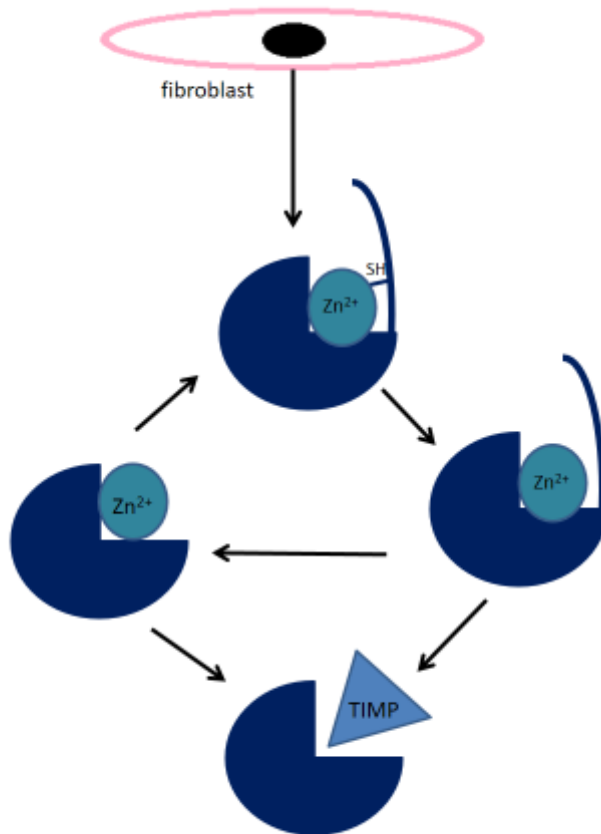


**Figure 5.2 MMP activation and Inactivation**

*A schematic representation of MMP activation and inactivation. MMPs are secreted by fibroblasts as inactive pre-proteins. Activation occurs if the cysteine switch is broken, cleavage of the pre protein portion can also occur at this point. The MMPs remain active until they are bound by a TIMP. This binding disables the ability of the MMP to degrade its substrate.*

Increased expression of a number of MMPs is seen in both NMSC and MM. In SCC MMPs expression is increased in both the tumour and the stromal cells whereas in BCC it is seen only in tumour cells (Hussein, 2005). Although the role that MMPs play in these processes can vary depending on the stage of cancer, for example some MMPs can have both pro and anti-apoptotic effects (López-Otín and Matrisian, 2007) and so the broader spectrum inhibitors could therefore aid the cancer progression. This lead to attempts at identifying individual MMPs as either anti- tumour or anti-targets (Gialeli et al., 2011). This pivotal role of MMPs in carcinogenesis made them good candidates for a therapeutic target. The production of pharmacological inhibitors of MMPs has been an area of interest for over 20 years, but as of yet the results of clinical trials have generally been poor. Although they have shown promise in cancers in which the tumour stroma interactions are key to the development of the tumour. The poor clinical trial outcomes are thought to be due to the complex effect that MMPs have; the expression of MMPs varies greatly throughout the progression of cancer and expression profile vary depending on the cancer type, therefore making MMPs a more challenging target for cancer treatment (Gialeli et al., 2011)

#### **5.1.4 Extrinsic skin ageing**

Skin ageing can be affected by both intrinsic and extrinsic factors (Bergfeld, 1997). Whilst little can be done to overcome the intrinsic factors associated with skin ageing the extrinsic factors can be controlled. Extrinsic factors which can cause accelerated ageing of the skin include smoking, exposure to environmental pollutants, general health and lifestyle choices and exposure to UV. It is the chronic exposure to UV that is believed to have the strongest effect on extrinsic skin ageing, which is commonly referred to as photoaging (Gilchrest, 1989).

However photoaging is not merely accelerated ageing of the skin, the features associated with photoaging differ from those of intrinsic ageing at both the histological and clinical level. Intrinsic ageing of the skin occurs inevitably as a natural consequence of

physiological changes over time at variable yet inalterable genetically determined rates examples of factors which can affect the rate of intrinsic ageing include ethnicity or hormonal changes (Farage et al., 2008).

At first glance, photoaged skin is distinct from intrinsically aged skin, photoaged skin is associated with coarse wrinkles, changes in pigmentation and telangiectasia but the most characteristic sign of photoaging is a loss of collagen fibres (Puizina-Ivić et al., 2008) This characteristic change is caused by two distinct mechanisms – inhibition of pro - collagen synthesis and the increase in collagen breakdown.

In addition an increase of elastin is seen in the dermal layers of photoaged skin. The accumulation of elastin appears to fill the areas of extra cellular matrix where the collagen would have been previously (El-Domyati et al., 2002). Elastin content of the skin tends to decrease with chronological age but elastin content of skin is seen to increase in proportion to the sun exposure received by the skin (Lewis et al., 2004).

### **5.1.5 UV and photoaging mechanisms**

UV is well established to be the most important environmental factor in photoaging (Gilchrest, 1989). Exposure to UV has been seen to cause dysregulation of collagen, acting on both pathways involved in collagen turnover; decreased collagen production and increased breakdown (Berneburg et al., 2000). However, much of this data examining the effects of UV irradiation does not define roles for the individual wavebands in photoaging. In order to further understand the role of UVA and UVB irradiation in photoaging attempts have been made to study the effects of each waveband individually.

Following UV irradiation one of the earliest events detected is activation of a number of cytokines and growth factor cell surface receptors; these include EGFR (Fisher and Voorhees, 1998; Sachsenmaier et al., 1994) and Il-1 (Rosette and Karin, 1996). These

events occur within minutes of exposure to UV, EGFR is activated within 10 minutes (Miller et al., 1994) and TNF- $\alpha$  and Il-1 within 15 minutes (Fisher et al., 2002). The activation of EGFR by UV appears to be tyrosine kinase mediated, UV is unable to activate EGFR in mutants lacking tyrosine kinase activity (Coffer et al., 1995). The activation of cytokine and growth factor receptors results in the recruitment of adaptor proteins which function to mediate downstream signalling, which results in the activation of Ras, Rac and Cdc42 members of the GTP-binding protein family. These proteins are well established to be key regulators of the MAP kinase family (Pawson and Scott, 1997) acting through select pathways to activate each of the MAP kinase pathways. Rac-1 activates MAP kinase pathways through interactions with NADPH oxidase resulting in increased ROS (Fisher and Voorhees, 1998). Rac-1 along with Cdc42 is able to bind to regulatory sequences of MEKK1, an upstream effector of the JNK pathway (Minden et al., 1994) whereas Ras activates Raf-1 kinase, an upstream regulator of ERK (Vojtek et al., 1993).

AP-1 was one of the earliest transcription factors discovered, it has a dimeric structure made up of proteins from the fos and jun families, cfos is constantly expressed throughout the epidermal and dermal layers of the skin, however c-jun is expressed minimally in normal dermis, but both the expression and protein levels of c-jun are rapidly increased following exposure to UV; mRNA expression is seen to be maximal within two hours of UV exposure, after which point it slowly declines before reaching the basal level 24 hours after exposure. C-Jun protein is maximally expressed 8 hours after exposure and remains at this maximal levels for at least 24 hours (Fisher and Voorhees, 1998), indicating a prolonged increase in protein level from a single exposure. Due to the differences in expression levels and response to stress stimuli it is clear that the activation of AP-1 is strongly reliant on the levels of C-JUN.

AP-1 plays a central role in photoaging, it both upregulates the expression of MMPs (Fisher et al., 1997) and inhibits the synthesis of collagen. AP-1 regulates the expression of numerous genes involved in the regulation of growth and differentiation; however it is

the ability of AP-1 to regulate the expression of the MMP family that is of particular interest in respect to photoaging. Most notably AP-1 is able to upregulate MMP1, MMP3 and MMP9 (Fisher et al., 1997; Fisher et al., 1996). Together, these three MMPs have the ability to completely breakdown collagen in skin (Fisher et al., 1997).

Exposure to a single dose of UV has been seen to decrease the levels of procollagens I and III at both the mRNA and protein level throughout the dermal layers of skin. The mRNA levels are seen to be decreased by 8 hours post exposure and remain decreased for 24 hours; the same pattern of reduction has been seen in the protein levels (Fisher et al., 2000). The duration of this decrease in procollagen expression was similar to the increase in C-JUN that has previously been detected following UV exposure (Fisher and Voorhees, 1998). Furthermore, over expression of wild type JUN in UV exposed cells caused a further decrease in procollagen synthesis. Upregulation of the C-JUN leads to an increase in AP-1, and previous work had detected a binding site in the promotor region of procollagen I which requires AP1 binding, (Jimenez et al., 1994) which no longer forms AP-1 in UV treated skin therefore demonstrating that AP-1 plays a negative regulatory role in the synthesis of procollagen

A role for cytokines has been implicated in photoaging. . For example comparison of chronologically aged and photoaged mice has shown an imbalance in pro and anti-inflammatory cytokines in photoaged skin compared to chronologically aged skin (Sakura et al., 2014). In normal skin cytokines and the ECM work together to regulate fundamental process such as differentiation and apoptosis. In addition, cytokines can influence the turnover and expression of ECM components and some membrane derived peptides can mediate the cytokine release. It is well established that cytokines play a role in elastosis and in collagen regulation, through regulation of MMPs (Mauviel, 1993). As previously mentioned increased elastin has been repeatedly detected in photoaged skin compared to chronologically aged skin (Kligman, 1969), through increased levels of TGF $\beta$  and IL-1 (Hsu-Wong et al., 1994). Additionally cytokines play a role in breakdown of the

ECM through the regulation of MMPs. The production of MMP from fibroblasts is induced by Il-1, IL6, PDGF, TNF, TGF $\beta$  and EGF.

#### **5.1.6 The role of Mitochondria**

One of the characteristic molecular hallmarks of photoaging is an increase in the number of large scale mtDNA deletions in photoaged skin (Berneburg et al., 1997; Birch-Machin et al., 1998) and in particular an increase in the common mitochondrial deletion which has been seen to be up to 10 times more common in photoaged skin compared to sun protected skin of the same individual (Berneburg et al., 1997). Interestingly, no correlation has been seen between accumulations of this common deletion with chronological ageing (Koch et al., 2001). Additionally, in vitro work has shown an increase in the common deletion is associated with an increase in expression of MMP1 in human fibroblasts, notably corresponding increase in TIMP1 is seen (Berneburg et al., 2000). A forty-fold increase in the common mutations has been seen in dermal but not epidermal layers of human skin exposed to a biologically relevant dose of UVA, this increase in the common deletion has been demonstrated to persist long after exposure. Further increases have also been seen even in the absence of further UV exposure (Berneburg et al., 2004).

The studies mentioned above lead to the hypothesis that the increase in common deletions in the dermal layers results in the structural and functional changes that are considered the hallmarks of photoaging. This area is challenging, it is difficult to distinguish whether changes seen in photoaging are as a result of the increase in mtDNA deletions or as a result of UV- activated signalling pathways, independent to the mtDNA damage. Mouse models develop increases in point mutations in mtDNA rather than the large scale deletions that are associated with UV exposure in humans (Trifunovic et al., 2004). One group used ethidium bromide to induce large scale mtDNA deletions in fibroblasts and detected changes of expression in ECM associated genes that are

reminiscent of the pattern that is seen in photoaging; for example an increase in *MMP1* expression was detected with no concurrent increase in *TIMP1*. In addition they also detected a decrease in *Coll1 $\alpha$ 1*, indicating a resultant decrease in synthesis of procollagen

1.

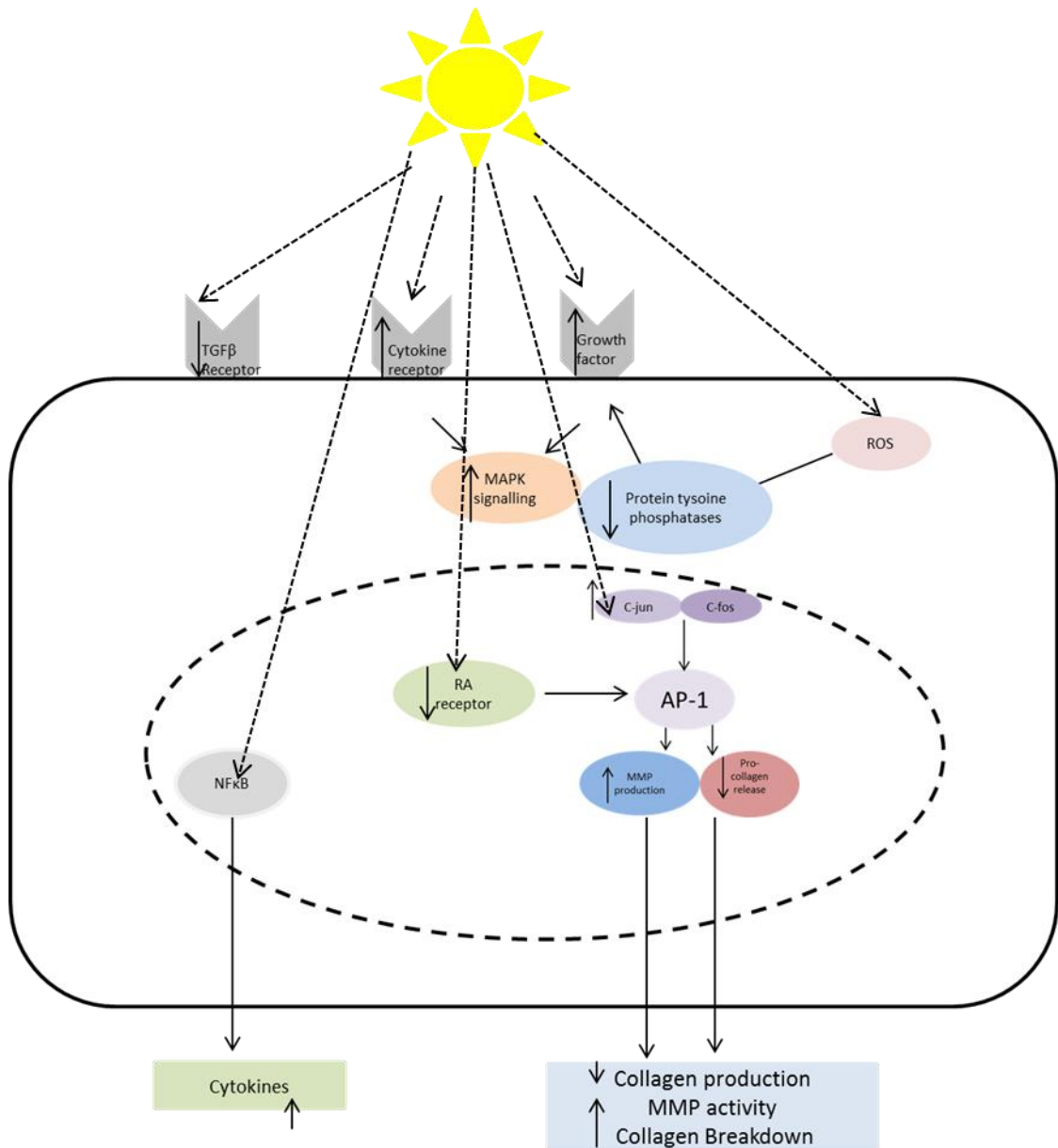


**Figure 5.3 Mechanism of photoaging**

*Schematic representation of the mechanisms of photoaging following UV exposure, collagen turnover is dysregulated following UV as a result of abnormal signalling pathways and increased cytokine activation.*

### **5.1.7 UV and matrix metalloproteases**

The main characteristics of photoaging are seen in the dermal layers of the skin, which is reached only by UVA wavelengths and not UVB, this led to the suggestion that it is UVA and not UVB that plays a prominent role in photoaging, 50% of UVA rays reach the dermal layers of the skin, whereas UVB is far less penetrative and only 14% of UVB reaches the lower levels of the epidermis. Although some in vitro work has revealed that both UVA and UVB are able to induce MMPs (Ramos et al., 2004), the main focus of our work is the effect of UVA on MMP activation, so the following section will focus on published work investigating the effect of UVA on photoaging.

Levels of MMPs are controlled for the most part at the transcriptional level and low levels are detected in normal healthy skin. Most of the MMPs have a conserved cis element in their promoter sequence, which means MMPs are often co-expressed in response to appropriate stimuli (Yan and Boyd, 2007). The major transcription factor that regulates MMP expression is AP1 and its upregulation is associated with photoaging.

An increase in AP1 has been detected in both fibroblast and keratinocyte cell lines following exposure to UVA (Djavaheri-Mergny et al., 1996). Additionally UVA was seen to induce both components of AP1, and induce increased AP1 expression in a keratinocyte cell line at an earlier time point than was observed with UVB (Chen et al., 1998). The increase in AP1 expression was later found to be as a result of increase p38 and JNK signalling in response to UVA (Silvers et al., 2003). Increased expression of AP1 has been seen to be an early event following UVA: within 15 minutes of exposure to UVA radiation the levels of AP1 are elevated and remain elevated for up to 24 hours after exposure (Helfrich et al., 2008). AP1 has been shown to be redox sensitive and UVA is able to alter the redox state of and activate the components of AP1 (Tyrrell, 2012). C-JUN has been found to be a common protein in 5 pathways activated by UVA initiated by receptors EGFR, Interleukin 1, tumour necrosis factor receptor, platelet derived growth factor and

platelet activator factor and this is differentially expressed in response to stressors, suggesting it could be a protein of great importance in increasing understanding of photoaging and combating it (Chauhan and Shakya, 2009).

The effect of UVA on the transcription and activity of MMPs has been conflicting. It was suggested that the effect of UVA on MMP activity was both cell line and MMP-dependent; in dermal fibroblast cells MMP1, 2 and 3 were seen to increase both at the transcriptional level and the level secreted into media following UVA. Increase in activation of MMP1 has also been observed in another study which also detected no change in TIMP1 activity (Song et al., 2004). However MMP 2 and 9 were seen to decrease in NHEK and HaCaT cell at 24 hours post exposure to UVA (Steinbrenner et al., 2003). MMP1 and MMP10 were found to increase in a SCC cell line following exposure to UVA (Ramos et al., 2004). Work on HaCaT cell lines has revealed increased expression of MMP1 and 10 at 5 hours post irradiation (Wertz et al., 2004) and increased activity of MMPs 2 and 9 at 12 hours post irradiation (Beak et al., 2004).

There remains some debate about which cell type in the skin is the major source of MMPs. A study on full thickness skin indicated that keratinocytes are the main source of MMPs following UVA irradiation (Quan et al., 2009), whereas a study utilising a 3D cell culture model containing both keratinocyte and fibroblast cell lines found that fibroblasts were the source of MMPs following exposure to UV but this was reliant on signalling from the epidermis (Fagot et al., 2004) suggesting cross talk between the cell lines. The same group had previously demonstrated that UVB was able to induce MMP1 in dermal fibroblasts both through direct radiation and indirectly through exposure to medium of irradiated keratinocytes (Fagot et al., 2002).

### **5.1.8 Aims**

The aim for the work discussed in this chapter was to look for a marker of UVA irradiation associated with photoaging. I chose to look for increase in MMP activity because this plays a role in increased collagen turnover, a characteristic of photoaging, and because of the previous reports in the literature that were discussed in the previous chapters.

Additionally previous work in our laboratory had reported that there is increased expression of both *MMP1* and *MMP3* in response to UVA irradiation.

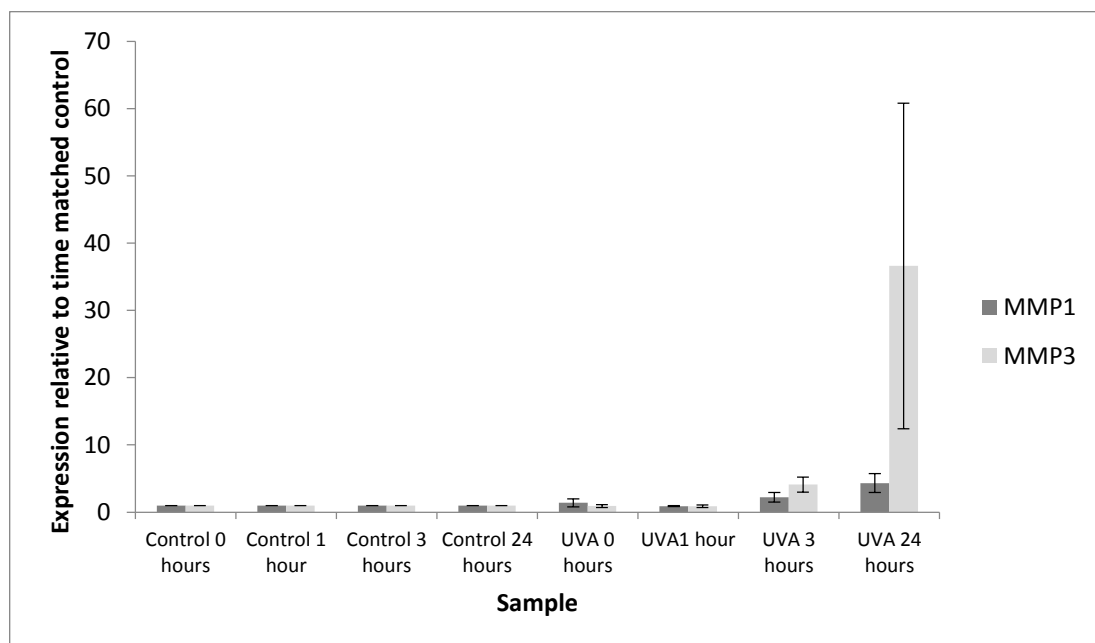


**Figure 5.4 MMP1 and MMP3 expression is increased following UVA radiation**

*HaCaT cells were both sham irradiated or irradiated with 100kJ/m<sup>2</sup> and RNA was extracted using Qiagen's RNeasy kit at 0, 1, 3 or 24 hours post exposure. The levels of MMP1 and MMP3 expression were measured using RTPCR techniques; the expression of beta actin was used as a control to calculate the relative gene expression of each MMP for each sample. Finally the fold changes of the UVA irradiated samples were normalised to the time matched control.*

Figure 5.4 demonstrates a 36 fold increase of the expression levels of MMP3 in UVA irradiated cells at 24 hours post exposure compared to the time matched control. This increase was highly significant ( $p < 0.0001$ , Students T-test). The levels of *MMP3* expression was also significantly increased at 3 hours post UVA irradiation ( $p < 0.01$ ). *MMP1* expression was also seen to increase 4 fold following UVA exposure, again this was highly significant ( $p < 0.001$ , Students T test). The expression of *MMP1*, like *MMP3* peaked at 24 hours post radiation but the increase seen was much less than what was observed for *MMP3*. In addition no increase in expression of *MMP1* was seen at 3 hours. This was consistent with what has previously been demonstrated in the literature (Jean et al., 2011). This data indicated that UVA induced an increase in the expression of multiple MMPs although this indicated upregulation of MMPs following UVA did not give us information in the activity of MMPs, which are secreted as inactive zymogens and need to be processed and the cysteine switch cleaved before they become active. Therefore assessing activation of MMPs would be a more direct way of detecting possible links to photoaging.

## **5.2 Experimental Design**

This chapter aimed to look at MMP activity in both fibroblast and keratinocyte cell lines in response to UVA irradiation because, as mentioned in section 5.1 there is some debate over whether it is keratinocytes or fibroblasts which release MMPs. The cells were grown in media with serum-substitute, as serum, has previously been seen to affect both the release and the detection of MMPs (Koob et al., 1980). Instead media containing the serum replacement KOSR was used.

Previous work in the laboratory has shown increased levels of mRNA for both *MMP1* and *MMP3* in HaCaT cells in response to a biologically relevant dose of UVA. However this data alone does not give us an insight into if the levels of MMP activity are increased in our model following UVA irradiation. MMPs are released as latent proteins and are

activated through cleavage of the cysteine switch therefore only assessing MMP activity would give an accurate assessment of the ability of UVA to induce photoaging through increased MMPs activation.

To assess MMP activity substrate zymography techniques were utilized. Zymography is an electrophoretic method to assess proteolytic activity. Samples are loaded onto a gel containing a protein substrate, in this case casein, which is degraded by proteases within the sample. When the gel is subsequently stained with Coomassie, areas which have been degraded appear white; the intensity of colour can be correlated to the protease activity and an estimate of the size of protease can be made, however the incorporation of the protein substrate in the gels will have some effect on the ability of the samples to diffuse.

The time points that were looked at were the same as those that had been used previously to assess MMP expression levels, however additionally the MMP activity levels at 48 hours post-irradiation were studied. Expression levels of MMP-1 and 3 had previously been shown to be increased at 24 hours, however because the secreted protein must be processed to become active later time points such as 48 hours were considered to allow time for the pre protein to be processed and become the active MMP as shown in figure 5.2.

## **5.3 Results**

### **5.3.1 Optimisation of casein zymography**

Initially a titration experiment was carried out to establish the quantity of protein that must be loaded into the zymogram gel to achieve quantifiable casein digestion. The amount of protein that has been loaded in published work varies from 10µg and 50µg per well. The samples used in this titration experiment were 24 hours post UVA irradiation and a time matched control. These time points were used because much of the published work looking at MMP activity following UV radiation has used later time points such as 24 hours. Therefore it was likely that these time points would contain a detectable level of MMPs to be able to assess MMP activity.

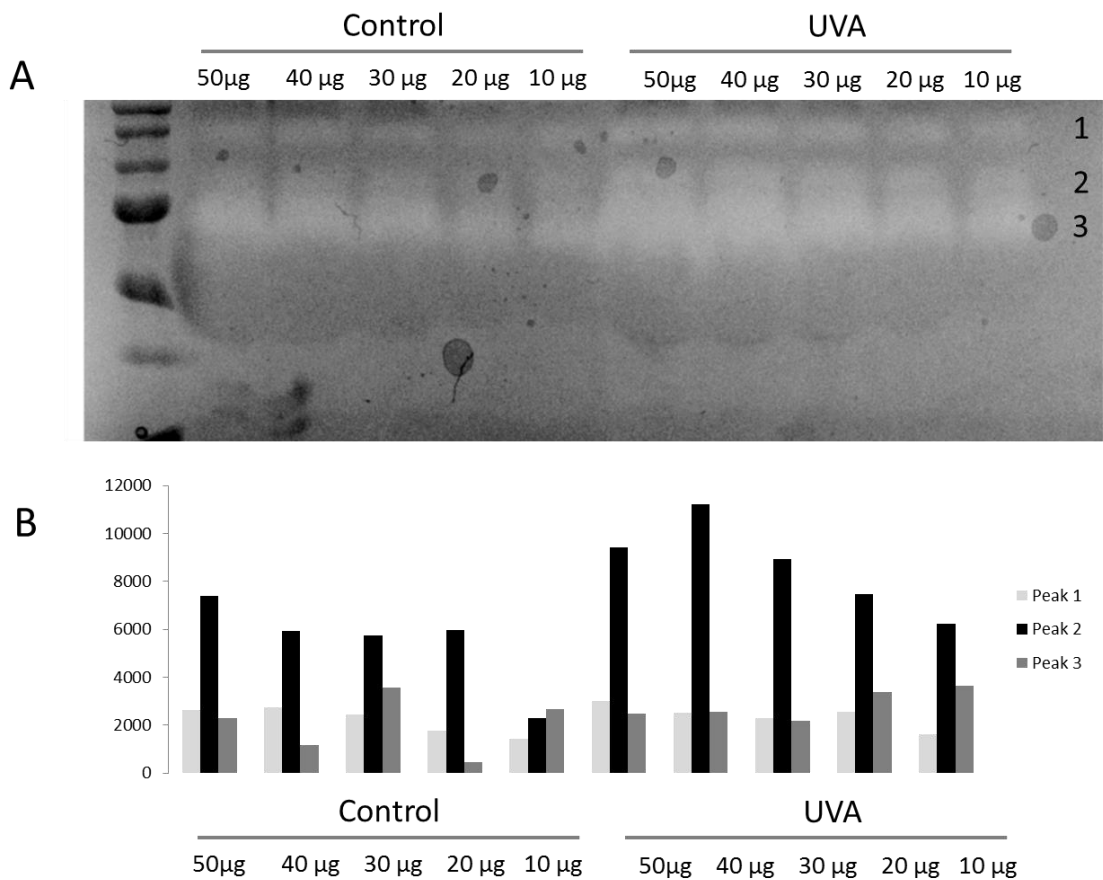


**Figure 5.5 loading of 20µg of protein is optimal for casein detection of conditioned media**

- A) Conditioned media was collected from HaCaT cells at 24 hours post UVA irradiation. Protein content was analysed by Bradford assay. Various amounts of protein (10µg-50µg) were loaded into each well of a 12.5%SDS PAGE gel. The gel was re-natured with 0.25% Triton, developed overnight in developing buffer stained with Coomassie and de-stained in methanol: acetic acid: water (40:10:50).
- B) Band density was measured using Image J and plotted on a bar chart to establish appropriate loading density for future experiments.

Figure 5.5 demonstrates that each of the samples showed some level of casein digestion. When the higher concentrations of media were loaded the bands seen in the gel were diffuse, which is undesirable, it can make it difficult to distinguish between separate bands of digestion. Therefore, a loading concentration of 20 $\mu$ g was chosen for all subsequent experiments. In addition the staining of the gel was quite faint so the quantity of casein contained in the gel was increased for subsequent experiments to make the bands easier to detect and improve accuracy of quantitation. Additionally, an increase in staining was noticed at the bottom of the gel compared to the top, so in subsequent experiments the gel was pre run prior to loading samples.

### **5.3.2 Measurement of activity of MMPs in response to UVA**

After optimising the zymography procedure, the initial experiment aimed to compare the quantity of casein digesting MMPs present in conditioned media from both control and UVA-irradiated HaCaT cells at both short and long term time points following UVA. Samples of media were collected at 0, 1, 3, 24 and 48 hours post UVA (100kJ/m<sup>2</sup>) and sham irradiation. The protein content of each sample was quantified and 20 $\mu$ g of sample was loaded onto a casein containing gel. In addition a sample of the media was loaded onto the gel to assess any casein degrading activity of proteins in the media which could affect our analysis.

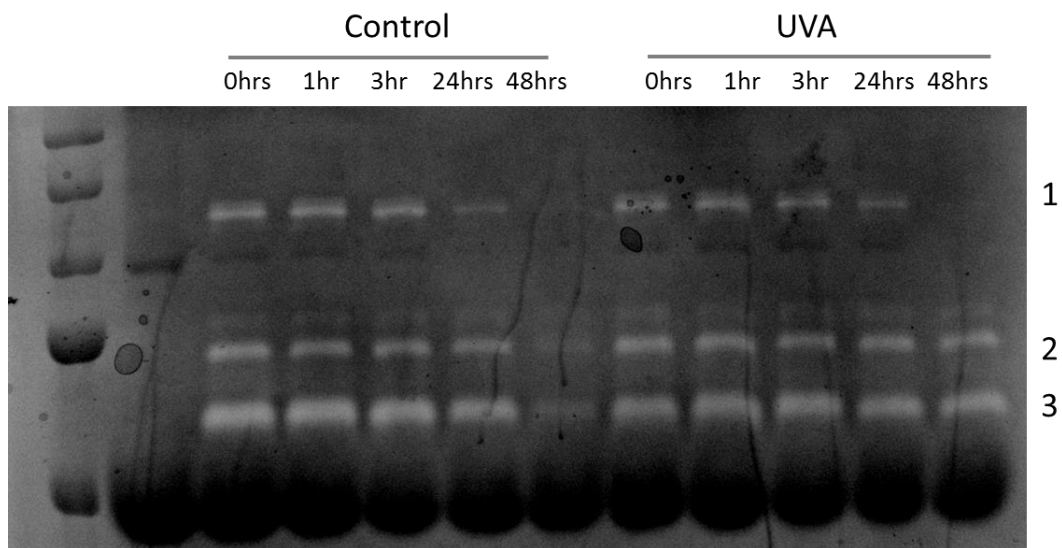


**Figure 5.6 Casein degradation constituents of sham irradiated but not UVA irradiated conditioned media decrease over time**

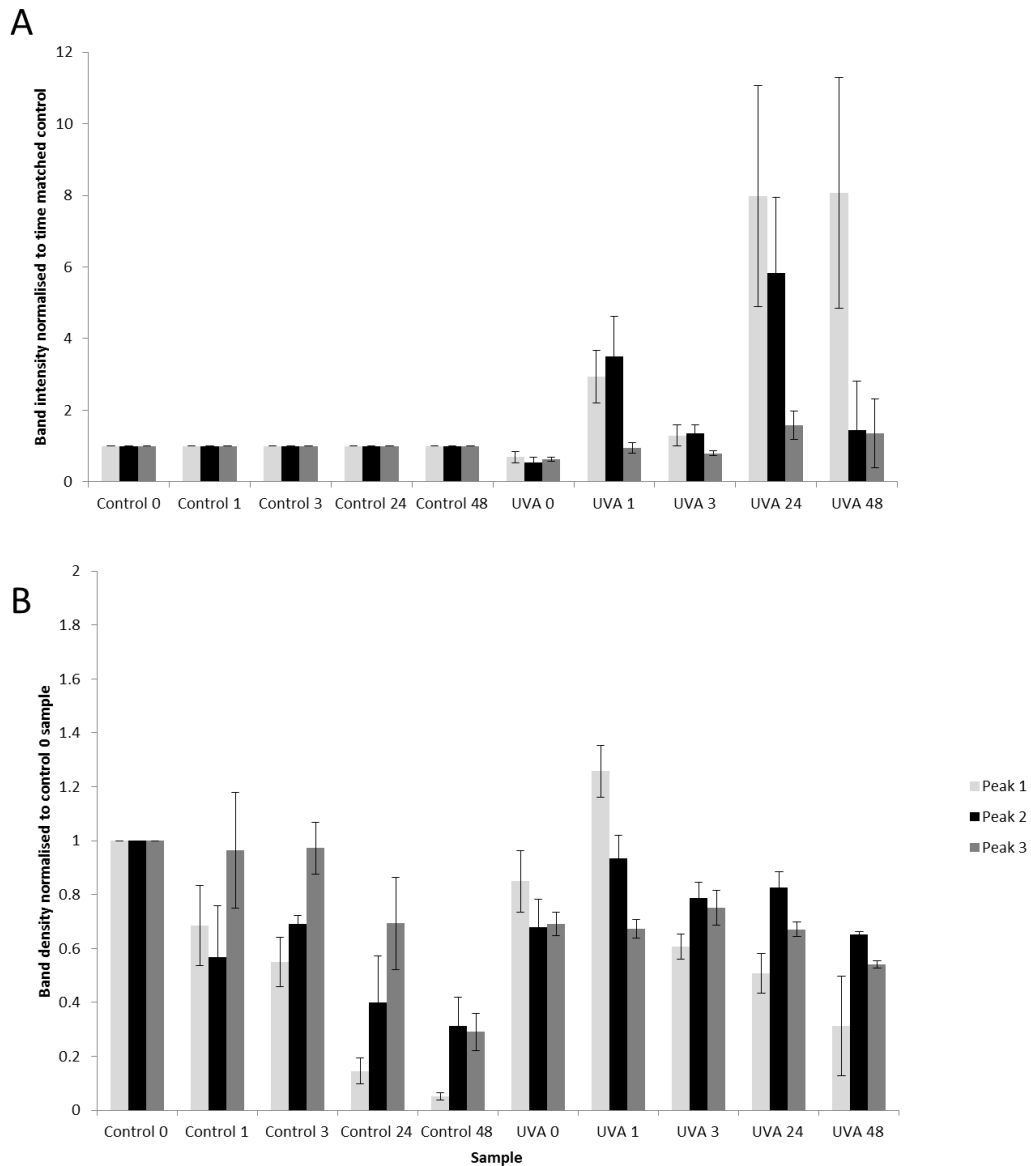
*A casein zymogram containing samples of conditioned media from both UVA irradiated and un-irradiated HaCaT cells. 300,000 HaCaT cells were seeded in phenol red free DMEM +KOSR, incubated overnight and sham irradiated or irradiated with 100kJ/m<sup>2</sup> UVA. The cells were then incubated for 48 hours and samples of the conditioned media were harvested at 0, 1, 3 24 and 48 hours post irradiation or sham irradiation. 20µg of each sample of conditioned media protein were loaded into each well of a 12.5%SDS PAGE gel. The gel was re-natured with 0.25% Triton, developed for 4 hours in developing buffer at 37 °C then stained with Coomassie and de-stained in methanol: acetic acid: water (40:10:50). A representative (n=3) image is shown.*

Figure 5.6 shows that, importantly, there was no caseinolytic activity in the sample of media that was loaded onto the zymogram gel; therefore any areas of digestion seen are as a result of cells releasing them into the media and not because of a constituent of the media itself. All of the samples of conditioned media showed the presence of casein digesting MMPs, 3 bands of varying sizes were seen for each sample. An immediate observation made was that the casein degradation decreased over time in the samples collected from the un-irradiated cells.

### **5.3.3 Effect of Confluence on MMP expression in HaCaT cells**

It was postulated that the decrease in casein degrading activity seen over time in the un-irradiated group was due to increasing confluence of the cells throughout this 48 hour time period. The same increase in confluence did not occur in the UVA irradiated cells due to increased cell death following UVA irradiation. This presented a possible issue when analysing the data, because there was a large difference in confluence between the UVA and the control samples, which could affect the MMP production of the cells as well as whether or not the cells had been exposed to irradiation.

Therefore, the analysis was carried out in two ways. Firstly, the band density was measured using Image J and the size of peaks measured for each band. This was carried out for 3 biological replicates and an average was calculated. The band density was then normalised to the time matched control and to the control 0 sample. A bar chart was plotted for each data set and is shown in figure 5.7.



**Figure 5.7 Analysis of casein degradation following UVA irradiation**

*Band density of 3 biologically independent casein zymograms was measured using Image J software, the peak sizes were calculated, and the average band density of each peak was calculated across the replicates. The band densities of each sample were normalised to A) The time matched control OR B) The control 0hr sample. The data was plotted on a bar chart showing the average band density and the error bars show standard deviation.*

Figure 5.7 demonstrates the analysis of the zymogram band densities, comparing the band density of the UVA samples to their time matched control and also comparing all samples to the un-irradiated sample at time 0. The two data sets look strikingly different. When the UVA irradiated samples were normalised to their time matched control (A) the graph shows an increase in casein degradation following UVA irradiation at the two later time points. Analysed in this way, the increase is significant compared to the time matched control and to the control 0 time point ( $p < 0.05$ , Students T-test). However the graphical representation does not match what is seen in the zymogram; by normalising the UVA samples to their time matched control the graph does not indicate the loss of casein degradation in the control samples at later time points that is apparent in the zymogram shown in figure 5.6, suggesting that this is not the best way to represent the data set.

Figure 5.7 B is a graphical representation of the mean band density of each sample normalised to the control 0hr time point. Here the decrease in casein degradation over time is apparent in the control samples, as seen previously in the zymogram shown in figure 5.6. Very little increase is seen in casein degradation following UVA irradiation at any of the time points that were looked at when comparing it to the casein degradation in the control 0hr time point. There is no significant change in level of casein degradation compared to the control 0hr time point ( $p = 0.406$ , Students T-test) However, a significant difference was seen in the casein digestion activity between the control 0 and control 48 time points ( $P < 0.05$ , Students T-test). This further suggested to that the differences seen between the casein degradation activity of the control and UVA samples at later time points was as a result of a difference in confluence of the two samples rather than as a result of UVA irradiation. The decrease in activity in UVA is also demonstrated here, however the cause for this is not increased confluence, but it is possible it could be as a result of cell death and therefore few cells releasing MMPs into the media.

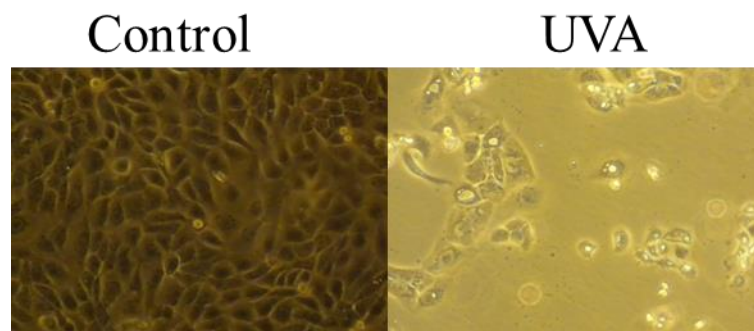


**Figure 5.8 there is a stark difference in confluence between sham and UVA irradiated cells 48 hours post irradiation.**

*A representative image of HaCaT cells to compare confluence of UVA irradiated and sham irradiated cells 48 hours after irradiation. Images were taken using a Nikon COOLPIX P6000 camera mounted on a Nikon eclipse TE200 light microscope.*

Figure 5.6 is a photograph to demonstrate the difference in the confluence of the control and the UVA irradiated cells at the 48 hour time point. Comparing the MMP activity of these two cell populations is undesirable because the difference in confluence is so large and cells at a high level of confluence do not behave in the same way as cells of lower confluence. There have been reports that increased confluence can have an effect on the release of MMPs; the secretion of MMPs has been seen to be decreased in a number of cell lines including tumour cell lines as the cell density has increased (Bachmeier et al., 2005).

Therefore in order to establish if the increased confluence was the cause of the decrease in casein digestion the cells were grown to 90% confluence before irradiation or sham irradiation. A sample was collected at 1 hour for the control and at 1 and 24 hours for the UVA irradiated group. These time points were chosen because previous work in the laboratory had indicated an increase in MMP expression in UVA irradiated cells at 24 hours post irradiation. The samples from the confluent populations were ran on a gel alongside a control sample from non-confluent cells, as a positive control to check that the experiment had worked successfully.

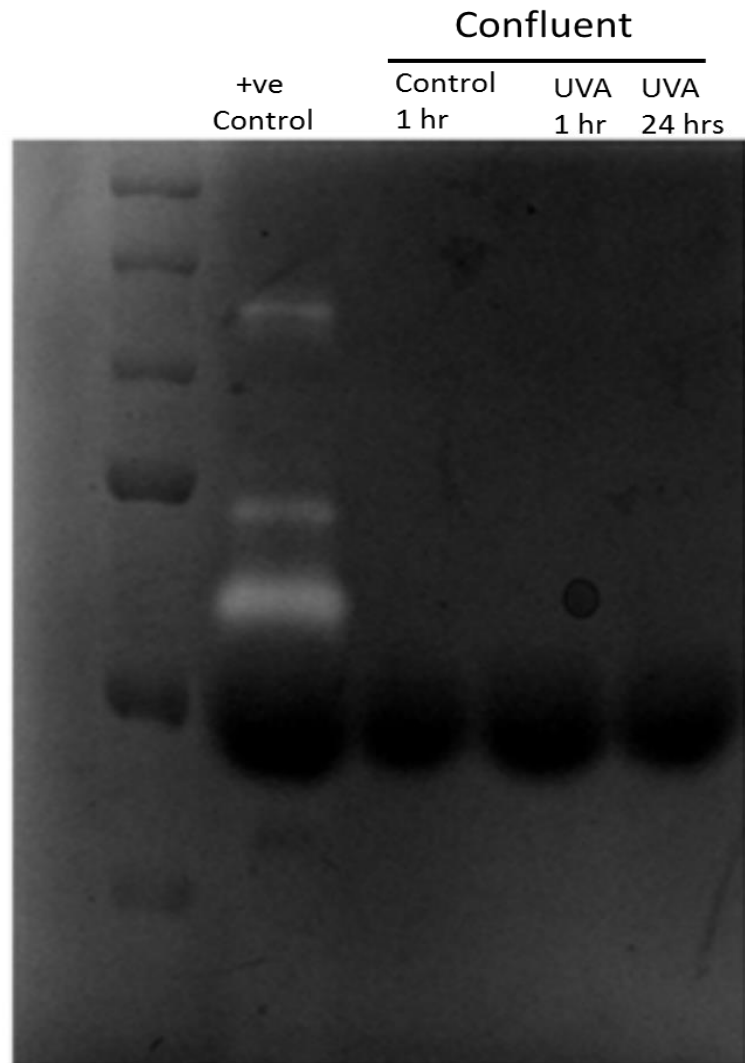


**Figure 5.9 No casein degradation is seen in conditioned media collected from sham or UVA irradiated confluent populations**

*HaCaT cells were grown to 90% confluence in 2ml phenol red free DMEM +20% KOSR. A sample of the conditioned media was taken once the cells had reached confluence; the cells were then irradiated with 100kj/m<sup>2</sup> UVA. A sample of the conditioned media was taken immediately after irradiation and 24 hours after irradiation. The samples were then loaded into a 10% SDS PAGE gel containing 2mg/ml casein and zymography analysis was carried out as previously described. A representative (n=3) image is shown.*

Figure 5.9 shows that there was no casein digestion for any of the samples from cells of high confluence whether they had been irradiated with UVA or not. This indicates that confluent cells do not release MMPs, or that MMPs are not activated in the media from confluent cells even after UVA exposure. Digestion was seen for the positive control sample which showed that the experiment had been successful. Therefore, this suggests that the previous result seen in figure 5.6 was likely due to a difference in confluence between the UVA irradiated and the sham irradiated groups and not as a result of UVA exposure.

#### **5.3.4 The effect of confluence on MMP expression in HaCaT cells**

The results described above led to the reanalysis of the previously generated q-PCR data. In the original analysis the expression of MMPs following UVA was normalized to the time matched control. Work shown so far in this chapter has indicated that confluence is likely to play a role in the differences seen in MMP activity between un-irradiated and UVA-irradiated samples. Therefore to avoid comparing samples which were of different confluences the data was reanalyzed. This time normalizing the MMP expression of the UVA-irradiated sample to the expression of MMPs at the control 0hrs time point, this is demonstrated in Figure 5.10

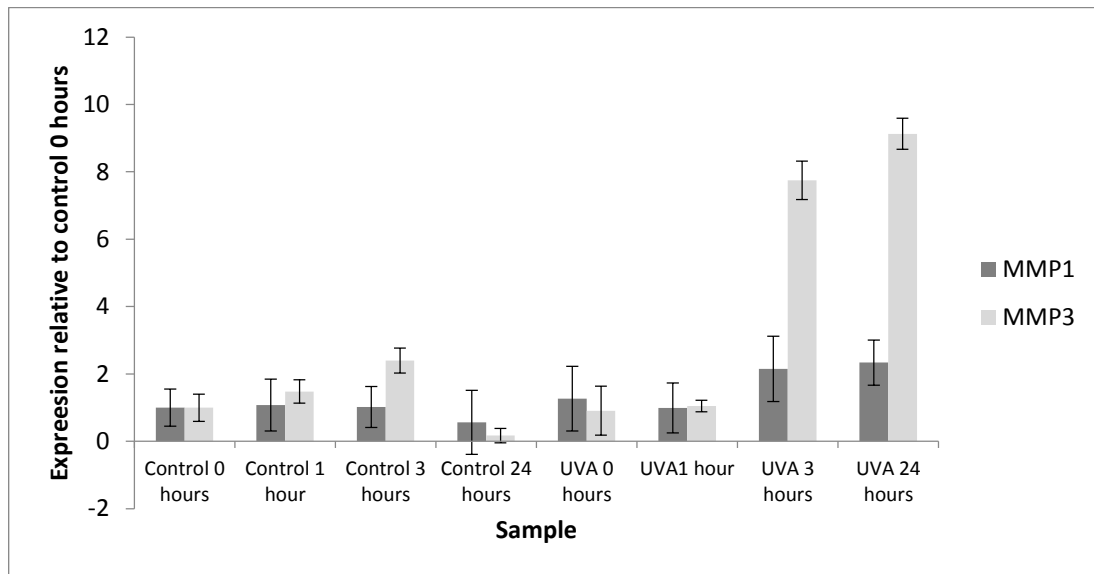


**Figure 5.10 MMP expression is affected by confluence**

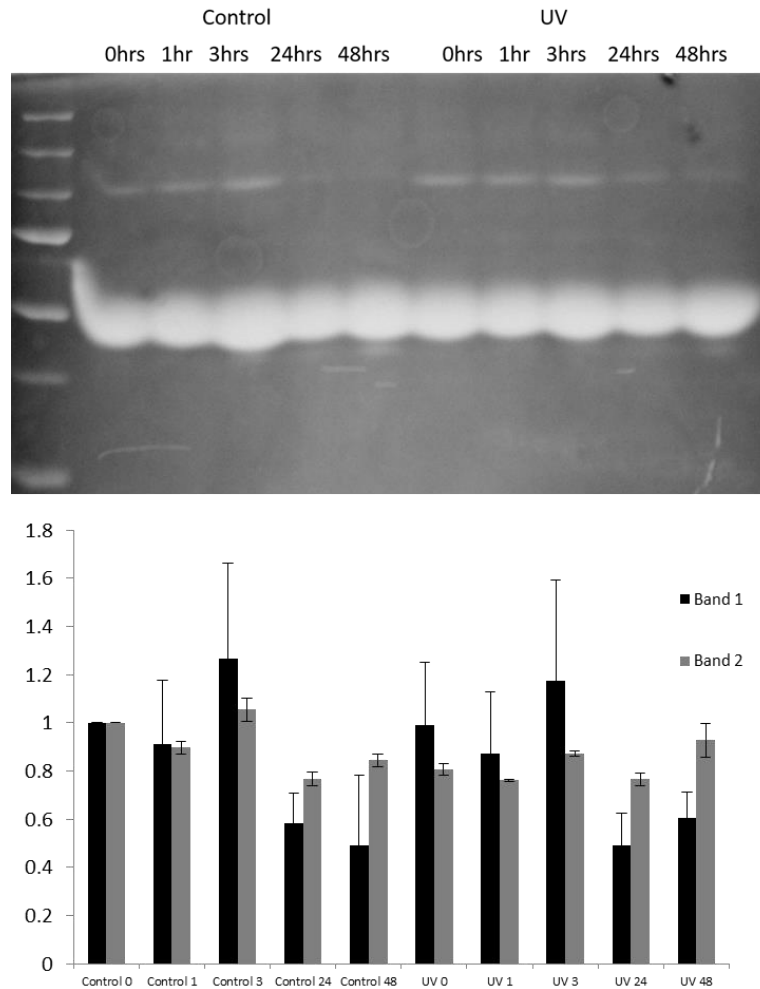
*HaCaT cells were both sham irradiated or irradiated with 100kJ/m<sup>2</sup> and RNA was extracted using Qiagen's RNeasy kit at 0, 1, 3 or 24 hours post exposure. The levels of MMP1 and MMP3 expression were measured using RTPCR techniques; the expression of beta actin was used as a control to calculate the relative gene expression of each MMP for each sample. Finally the fold changes of the UVA irradiated samples were normalised to the expression of the control 0 time point. Error bars show the standard deviation.*

Figure 5.10 demonstrates that the increased expression of MMPs following UVA that was demonstrated in figure 5.5 was, at least partially due to a difference in confluence between UVA and the control at 24 hours post irradiation. The fold increase of MMP1 was 4 in the previous analysis, however, reanalysed to the control 0 time point the fold increase at 24 hours was now 2.5, this was not a significant increase in expression when compared to the control 0 time point ( $p=0.156$ , Students T-test), additionally there was no significant difference between the expression of MMP1 at the control 0 and 24 hour time points ( $P=0.995$ , Students T-test).

The fold increase for MMP3 was previously 36, when reanalysed to the control 0 time point the fold increase was 9, this increase was still significant ( $p=0.049$ , Students T-test). Additionally, analysing the data in this way shows a decrease in both the expression of MMP-1 and MMP3 at 24 hours relative to the control 0hrs time point, this decrease in expression was significant ( $p=0.029$ , Students T-test). This again suggests that MMP levels decrease in our cell line as the confluence of the cells increases. Additionally, this data suggests that control of MMPs could be at the transcriptional level rather than occurring later at the processing stage.

### **5.3.5 The effect of UV irradiation on MMP activity in HaCaT cells**

In the experiments described above, the cells had only been exposed to UVA, a situation that individuals are only exposed to on rare occasions, such as through use of tanning beds, or through windows. This work additionally looked at the effect of a biologically relevant dose of solar simulated light on the release of casein degrading MMPs in the HaCaT cells. The same time-points were used that had used previously and following earlier analysis the band densities of each sample would be compared to the control 0hrs time point.



**Figure 5.11 A biologically relevant dose of SS has no effect on release of casein degrading MMPs**

- A) A casein zymogram containing samples of conditioned media from both UVA irradiated and un-irradiated HaCaT cells. 300,000 HaCaT cells were seeded in phenol red free DMEM +KOSR in 35mm dishes, incubated overnight and sham irradiated or irradiated with 100kJ/m<sup>2</sup> solar-simulating UV. The cells were then incubated for 48 hours and samples of the conditioned media were harvested at 0, 1, 3 24 and 48 hours post irradiation or sham irradiation. Protein content analysed with the Bradford assay. 20µg of each sample of conditioned media protein were loaded into each well of a 12.5%SDS PAGE gel. The gel was re-natured with 0.25% Triton, developed for 4 hours in developing buffer at 37 °C then stained with Coomassie and de-stained in methanol: acetic acid: water (40:10:50).
- B) A bar chart to represent average band density. Error bars show the standard deviation.

Figure 5.11 once more shows the decrease in casein degrading activity in the control cells once more, that I now know to be as a result of increasing confluence. Once again this is not seen for the UV irradiated group, due to a decrease in confluence compared to the un-irradiated samples. However, no difference is seen in the casein degrading activity taken from the UV irradiated sample at any time points when compared to the control 0hr time point, suggesting the exposure to solar simulated radiation, like UVA, does not have an effect on the activity of casein degrading MMPs in our model.

### **5.3.6 The effect of UVA on MMP activity in dermal fibroblasts**

The work shown so far in this chapter was carried out on HaCaTs, a keratinocyte cell line. We additionally looked at the effect of UVA on MMP activity levels in dermal fibroblasts, this was done for two reasons, firstly the hallmarks of photoaging are seen primarily in the dermal layers of the skin and it is fibroblast and not keratinocytes that make up much of the dermal layer. Additionally, there are some conflicting reports over whether keratinocytes or fibroblasts are the primary source of MMPs. The initial experiment looked at MMP activity in media collected at 1, 24 and 48 hours post UVA irradiation.

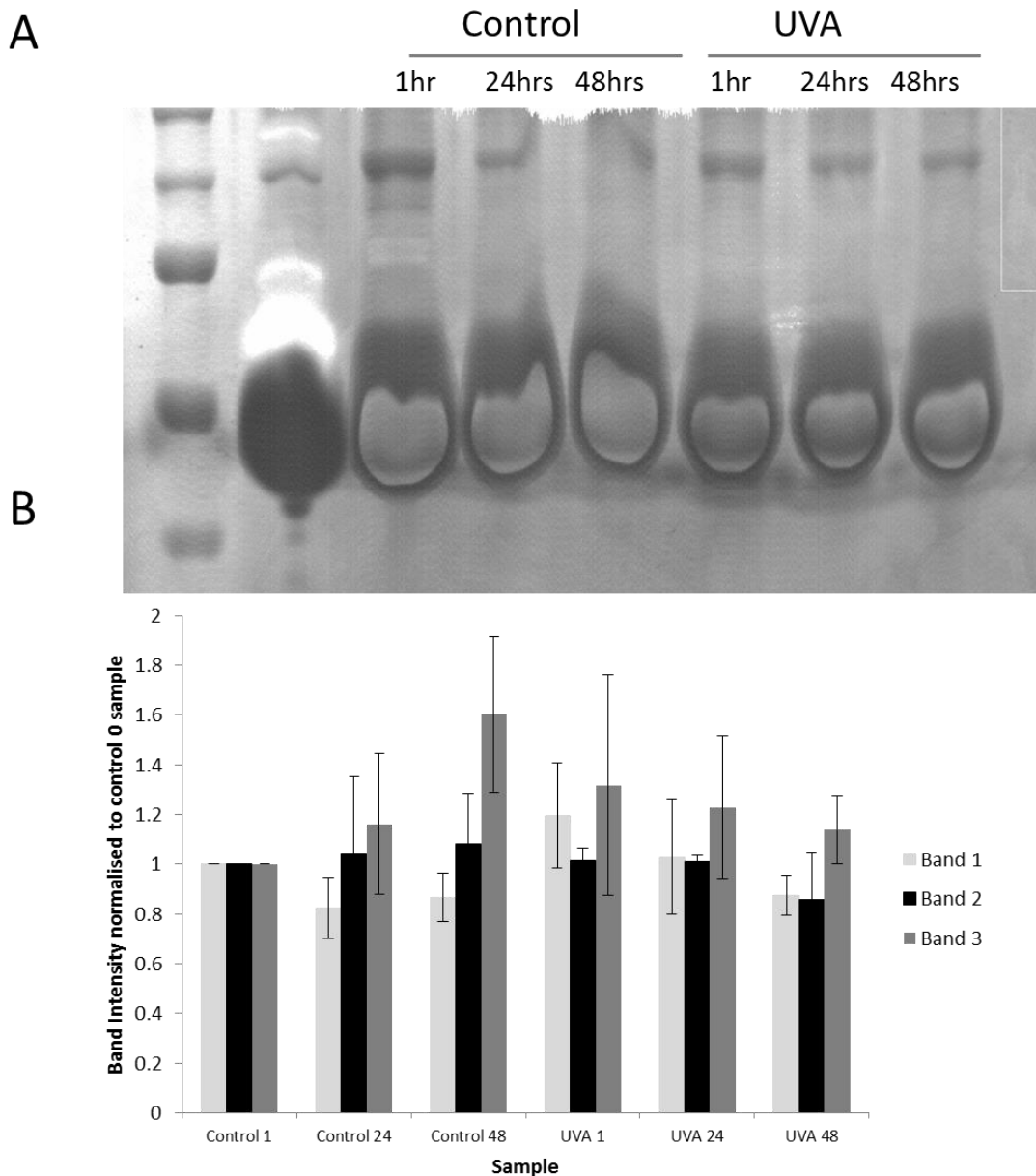


**Figure 5.12 a zymogram containing conditioned media from UVA irradiated and sham irradiated fibroblasts**

- A) Dermal fibroblasts were either sham irradiated or irradiated with 100kj/m<sup>2</sup> UVA. The cells were then incubated at 37° and 5%CO<sub>2</sub> for 48 hours and samples of conditioned media were collected at 1, 24 and 48 hours post irradiation. The samples were then loaded into a 10% SDS PAGE gel containing 2mg/ml casein and zymography analysis was carried out as before. A representative (n=3) image is shown.
- B) A bar chart to represent average band density. Error bars show the standard deviation.

Figure 5.12 shows that, unlike for the HaCaT cells the MMP activity of the un-irradiated cells does not decrease over time. Additionally, there was no increase in activity seen between the control 48 time point and the control 0 time point ( $P=0.936$ , Students T-test) or the UVA 48 hour sample compared to the control 1 hour ( $p=0.953$ , Students T-test). Once again images of the cells at the 48 hour time points were taken to establish the level of confluence.

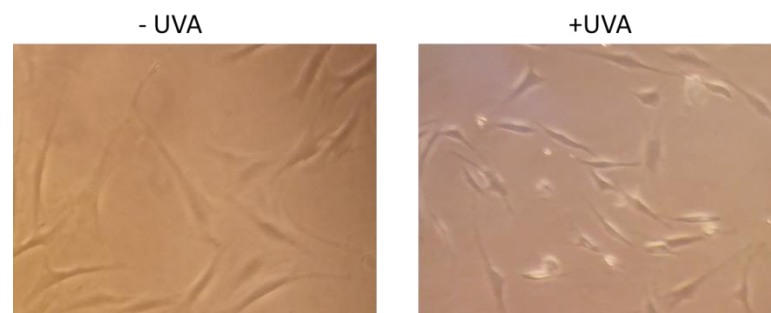


**Figure 5.13 The confluence of dermal fibroblasts 48 hours after sham and UVA irradiation.**

*A representative image of normal human dermal fibroblast cells to compare confluence of UVA irradiated and sham irradiated cells 48 hours after irradiation. Images were taken using the Nikon COOLPIX P6000 camera mounted on a Nikon eclipse TE200 light microscope.*

Figure 5.15 demonstrates the difference in confluence between the UVA and sham irradiated dermal fibroblasts at 48 hours post irradiation. There is, similar to what was demonstrated with the HaCaT cells a stark difference in confluence between the UVA treated and the control cells. However, unlike the HaCaTs the un- irradiated dermal fibroblasts had not reached confluence and were roughly 70% confluent at the 48 hour time point. The lower level of confluence could explain why the zymography still detected MMP activity in the fibroblast cells at 48 hours whereas at this time point in the HaCaTs no MMP activity was detected.

### **5.3.7 The effect of confluence on MMP activity in dermal fibroblasts**

The next experiments aimed to assess the MMP activity in confluent dermal fibroblast populations to see if the decrease in confluent populations was seen in numerous cell lines and not a cell specific effect of HaCaT cells. The dermal fibroblast cells were grown to confluence and irradiated, a sample of conditioned media was collected from the sham irradiated cells immediately after irradiation and from the UVA irradiated population both immediately after and 24 hours post irradiation. The samples were ran on a casein containing zymogram alongside a positive control sample.

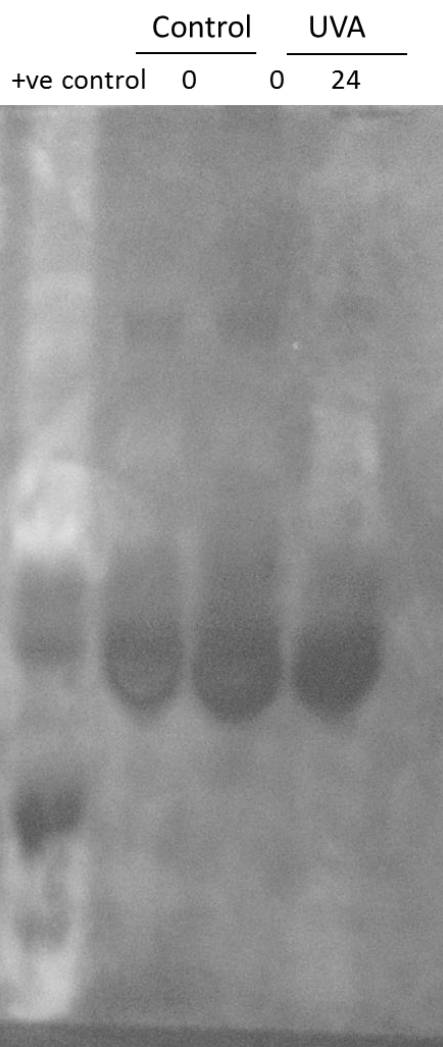


**Figure 5.14 No casein degradation is seen in conditioned media collected from sham or UVA irradiated confluent dermal fibroblast populations**

*Dermal fibroblast cells were grown to confluence before irradiation with 100kJ/m<sup>2</sup> UVA or sham irradiation, a sample of conditioned media from each was collected immediately and 24 hours later for the UVA irradiated sample. 10µg of each sample was loaded into a casein containing gel along with a positive control sample. The gel was re-natured with 0.25% Triton, developed for 4 hours in developing buffer at 37 °C then stained with Coomassie and de-stained in methanol: acetic acid: water (40:10:50). A representative (n=3) image is shown.*

Figure 5.14 demonstrates that there is no casein degradation activity in confluent fibroblast, whether or not they have been irradiated with UVA. This is the same result that was seen in the HaCaT cell line indicating that a decrease in MMP activity with increasing confluence is not a cell line specific finding. As mentioned previously there has been in vivo evidence to suggest MMP levels decrease with increased confluence.

## **5.4 Discussion**

The results shown in this chapter indicate that a biologically relevant dose of UVA had no significant effect on the release of casein digesting MMPs into the media in either HaCaT or dermal fibroblast cell lines. Published work on this area has been a little conflicting, both the expression of and the activity levels of MMPs have been studied and MMP levels have been seen to be both up- and down-regulated following UVA and UVB irradiation depending on the cell line, dose and system used (Jean et al., 2011; Wlaschek et al., 1994; Herrmann et al., 1993; Wang and Bi, 2006; Buechner et al., 2008; Steinbrenner et al., 2003; Brenneisen et al., 1998; Zaid et al., 2007).

I feel that rather than demonstrating any effect for UVA on the activity levels of MMPs the results shown in this chapter highlight the importance of appropriate controls. In the first instance, in HaCaT cells, when the activity of the UVA sample at 48 hours was compared to the time matched controls a significant ( $P < 0.05$ , Students T-test) increase in casein degradation activity was indicated (Figure 5.7A). However, analysing the results in this way was not a true representation of the data. The decrease in casein degradation over time in the control cells which is visible in the zymogram gel (Figure 5.6) is not apparent when the data are analysed in this way. When the data was subsequently analysed comparing the activity of each sample to that of the control 0hr samples (Figure 5.7B), the graphical interpretation was a better representation of what is seen in the zymogram gel, the decrease in casein degradation activity over time in the control cells was apparent, statistical analysis revealed the decrease in casein degradation activity seen between the control 0 and the control 48 hour time points was significant ( $P < 0.05$ , Students T-test). Additionally there was no increase in band intensity seen in the UVA irradiated groups indicating that UVA irradiation had no effect on the casein degrading MMPs in HaCaT cell lines.

Observationally, a striking difference in confluence was observed at 24 hours and 48 hours post UVA irradiation compared to the sham irradiated cells (Figure 5.8). Therefore

it was hypothesised that the difference in MMP activity between the time matched UVA and control samples could be as a result of a difference in confluence rather than as a result of UVA radiation. Furthermore, it was postulated that the decrease over time seen in the control cells was as a result of increasing confluence. The cells were grown to 90% confluence; this was the same level of confluence that has been used in a number of studies, therefore allowed the comparison of results generated in this chapter to data seen in the literature. When confluent cells were irradiated no casein digestion was seen for either the sham irradiated or the UVA irradiated cells (Figure 5.9). A positive control showed casein digestion which demonstrated that the assay had been successful, from this it was concluded that confluent cells do not release MMP, or that they release increased levels of TIMPs which inactivate any MMPs. The media was collected immediately after irradiation of the confluent cells and at 24 hours, later time points were not taken because the confluence of the UVA cells had decreased at this time point and once again there would have been a large difference in confluence of the UVA and control cells.

Levels of both MMP transcription and activity have also been seen to decrease in a number of breast cancer cell lines with varying invasiveness. MMPs 1, 2, 3 and 9 were seen to decrease in breast cancer cell lines with increasing confluence (Bachmeier et al., 2005) which was in agreement with earlier work that found higher levels of transcription factors involved in MMP regulation in endothelial cells when they were at lower confluence (Igarashi et al., 2001). Further in vivo studies found differences in the levels of MMP transcription and activity in areas of tumours with different cell densities (Bachmeier et al., 2005). The published work mentioned here along with the data shown in this chapter suggests that as confluence of these cells increase in culture their ability to release MMPs into the media decreases. It looks likely that this is not a cell line specific finding.

In addition, a slight decrease in the MMP degrading activity in the HaCaT cell line but not the fibroblast cell lines was seen, a possible explanation for this could be that keratinocytes and fibroblasts react differently to UV in vivo, keratinocytes are more likely to undergo apoptosis than enter a senescent state whereas the opposite is true for fibroblast cells (Gilchrest, 2013) UVA has been seen to induce both immediate (within 4 hours) and delayed apoptosis, occurring after 24 hours, whereas UVB has only been seen to induce delayed apoptosis (Godar et al., 1994).

A decrease in casein degradation activity was not seen over time in the fibroblast cell line, possibly because these cells become senescent rather than undergoing apoptosis. Data shown in chapter 4 indicated that HaCaTs but not fibroblasts show a decrease in mitochondrial membrane potential, a marker commonly used to indicate apoptosis in bystander populations exposed to signalling from UVA irradiated HaCaT cells. It is well established that MMPs are released as part of the senescence associated secretory phenotype (SASP). The SASP has been demonstrated in fibroblasts (Coppé et al., 2010). The induction of cellular senescence may be expected to cause an increase in the level of MMPs, which is not evident for our data; however some reports suggest that although cells may appear senescent the SASP can show a delay when compared to appearance of a senescent morphology.

#### **6.4.1 Conclusions**

To conclude, there was no significant change in levels of MMP activity seen following UVA irradiation in either HaCaTs or dermal fibroblast cells. Although a difference in MMP activity was, initially thought to be seen at the later time points, further experiments suggested that the increase in MMP activity in the UVA irradiated cells compared to the sham irradiated cells was because of a difference in confluence rather than as a result of UVA irradiation. In confluent cells no MMP activity was detected in either the UVA

irradiated cells or the sham irradiated cells. This was seen in both HaCaT and dermal fibroblasts suggesting that it may not be a cell line specific phenomenon.

I feel that although this data does not definitively show that UVA has no effect on MMP expression it indicates that investigating this using cells at high levels of confluence such as 90% is unsuitable, these high levels have been used commonly in published work, and the findings of this chapter could help to explain why published work has been conflicting in this area, in particular, difference have been seen between published work on the fast growing immortalised HaCaT cell line and the slower growing dermal fibroblast and it is possible that differences in confluence of control groups could account for this.

#### **5.4.2 Further Work**

Further work could focus on a variety of areas; there is some evidence to suggest that UVB irradiation of keratinocytes induces an increase in MMP release from fibroblasts through a paracrine mechanism as a result of factors secreted into the media. It would be of interest to measure the ability of UV irradiation to induce MMPs compared to UVA. This was not tested with the samples used in this chapter because the samples were not collected from the same experiment and I did not wish to compare the activity of samples collected from cells in different experiments, I felt this could bias the results due to biological variation of cells in culture and therefore the MMP activity of these samples are not directly comparable.

In addition, it would be interesting to look for increases in MMP activity at later time points in the dermal fibroblasts, there is evidence to suggest that a full SASP is only seen 5 days after the cell becomes senescent (Coppé et al., 2010), this could be a possible explanation for why data shown here did not detect an increase in MMP activity levels in this cell line despite published work suggesting this more strongly than has been suggested keratinocyte cell lines. Further work could look at later time points in the

dermal fibroblast cell lines as well as looking for markers of senescence such as the  $\beta$ -gal assay.

Zymography is also non-specific; it only identifies the class of MMPs present in a sample, although the size of bands of digestion can give some indication into which specific MMPs are present. There can be issues when trying to confirm the presence of individual MMPs with Western blot analysis because zymography is a much more sensitive technique and can detect MMPs at nanomolar levels which is not the case with western blotting. However there are a number of commercially available fluorescence assays that are specific to individual MMPs which could be utilized.

Furthermore, it is well established that MMPs play a role in both acute and chronic wound healing, but there is suggestion that MMPs are dysregulated in chronic wound healing, so perhaps the decrease in MMP is not unexpected. To further confirm the findings, the levels of MMPs could be assessed after scratch tests, to further show if the level of MMP is affected by cell confluence as has been suggested by our data so far. Alternatively, cells could be seeded at different confluences, and allowed to adhere before samples of media are collected. Additionally this would discount the possibility that MMPs could decrease with increased passage number of cells in culture.

# **Chapter 6 – General Discussion**

The incidence of skin cancer, both non-melanoma skin cancer (NMSC) and malignant melanoma is rising year on year. Currently, between 2 and 3 million NMSCs and 132,000 melanoma skin cancers occur globally each year (WHO, WWW) and there is evidence that the number is an under estimate of the true figure. The presence of more than one melanoma or NMSC in an individual is often registered as a single case. Exposure to UV is well established to be the biggest risk factor in the development of both NMSC and melanoma. Both UVA and UVB wavebands have been classified as class one carcinogens, meaning that they are able initiate each stage of cancer progression (IARC, WWW). Additionally, tanning beds, which emit primarily UVA wavelengths have now been classed as a carcinogen and individuals who regularly use tanning beds increase their lifetime risk of melanoma by 75% (Bonniol et al., 2012).

Melanoma, although less frequent than NMSC, is associated with a poorer prognosis, and is known to metastasise early (Kohler et al., 2011). NMSC is associated with exposure to UVB irradiation and mutations in p53 (Brash et al., 1996; Nataraj et al., 1995), amongst others but melanoma remains poorly understood (Sage et al., 2012). Evidence from epidemiological studies (Moan et al., 1999; Bonniol et al., 2012) and animal models have suggested that UVA plays a key role in melanoma induction (Noonan et al., 2012) and so a greater understanding of the mechanisms of damage UVA causes to cells could aid in improving our understanding of melanoma.

The initial aim of this PhD work was to identify biomarkers of UVA damage to help improve UVA protection offered by sun creams. Current methods of assessing the UVA protection afforded by sun creams is the 5-star system, which is based on assessment of UVA protection offered compared to UVB protection. This number is therefore a ratio, and can be difficult for the user to understand, for example a sun cream with a 5 star UVA rating and an SPF of 20 would offer less UVA protection than a sun cream with a 3 star UVA rating but a SPF of 50. Therefore, it is desirable to design a new way of assessing UVA

protection that is clearer to understand. So, identifying markers of UVA damage would allow a more biologically relevant method of assessing the UVA protection offered by individual sun creams.

### **6.1 The ability of UVA to form double strand breaks**

In chapter 3 the ability of both UVA and UVB to induce the phosphorylation of H2AX was studied. An increase in H2AX phosphorylation is seen in response to the presence of either double strand breaks (Burma et al., 2001) or stalled replication forks (Ward and Chen, 2001), and depending on which of these have occurred there are different mediators involved in the phosphorylation of H2AX. The presence of  $\gamma$ H2AX is a marker commonly used for double strand breaks, the ability of UVA to induce DSBs independently of replication remains controversial. Recent work on this has been conflicting with one group finding no indication of the presence of DSBs in UVA irradiated cells even at very high doses, perhaps even higher than could be considered biologically relevant (Rizzo et al., 2011). Another group subsequently showed the ability of UVA to induce DSBs at a biologically relevant dose in G1 arrested keratinocytes and fibroblasts (Greinert et al., 2012a). The work shown in this chapter looked at both wavebands because it was preferable that the desired biomarker was not induced in an identical way by UVA and UVB.

The data in chapter 3 indicated that UVA and UVB were both able to induce  $\gamma$ H2AX in our model, although the timeframes and kinetics behind phosphorylation of H2AX were different for each waveband. In figures 3.3 and 3.4 peaks in H2AX phosphorylation at 1-hour post UVA irradiation were seen. This was demonstrated in both HaCaT and NHEK cells, indicating it is likely to be a finding conserved between cell lines. This was in agreement with published work by Greinert et al (2012), who saw up-regulation of  $\gamma$ H2AX in both fibroblast and keratinocytes cell lines. Although the data generated here did indicate increased levels  $\gamma$ H2AX than utilizing much lower doses of UVA than in their

work. This is likely due to difference in the experimental design, in particular they used G1 arrested cells and in this work asynchronous cells were used. There is some suggestion that cells arrested in G1 are protected against DNA damage and in particular against oxidative damage (Rancourt et al., 2002). The differences seen between my work on asynchronous cell populations and the above mentioned published work suggest that G1 cells may not be good model for studying UVA, because they are protected against oxidative DNA damage, which is thought to be the main mechanism by which UVA causes cellular effects. Although I cannot definitively say that the increase in H2AX phosphorylation that was detected following UVA is as a result of double strand break formation our data strongly suggests that this is what is occurring. The data shown in chapter 3 indicated that H2AX phosphorylation in response to UVA is cell cycle independent (figure 3.10) and ATM (figure 3.13) and MRN (figure 3.20) dependent. Additionally, an increase in 53BP1 foci (figure 5.21) was seen in the UVA-irradiated cells compared to the time-matched control all of which indicate the presence of double strand breaks and not stalled replication forks (Burma et al., 2001; Ward and Chen, 2001; Schultz et al., 2000).

In chapter 3, through immunofluorescence dose response (figures 3.7 and 3.8) and clonogenic survival experiments (Figures 3.1 and 3.2) it was indicated that UVA is able to initiate the formation of  $\gamma$ H2AX foci at a lower relative cytotoxic dose than UVB, and that, at a higher doses phosphorylated H2AX remains in the cells at 48 hours' post exposure suggesting that repair mechanisms are unable to fully repair the damage. This indicates that protection against UVA is of huge importance, due to its ability to induce a high number of what appear to be double strand breaks. The lowest dose of UVA that was utilised was able to induce detectable H2AX phosphorylation resulted in just a 20% decrease in cell survival. So these are not doses which are causing high levels of cell death. Additionally, repair of double strand breaks is well established to be intrinsically more challenging than the repair of other lesions. In particular, NHEJ is prone to errors in repair

(Featherstone and Jackson, 1999) which can lead to induction of mutations and chromosomal rearrangements, both of which are hallmarks of cancer. Further work in this area should focus on the ability of UVA to initiate double strand break formation in other models which better represent human skin, such as 3D cell culture, and in the mouse HGF model, which is strongly regarded as a good model for human skin, in particular for melanoma induction (Noonan et al., 2000). This data would better indicate if the findings in this thesis are likely to hold true to human skin *in vivo*.

Furthermore, the work by Greinert et al established that the double strand breaks they detected in G1 arrested cells were as a result of clustered oxidative damage. This would be interesting further work for our model, work shown in chapter 3 utilized both a lower dose of UVA and looked at asynchronous cells rather than G1 arrested cells. Clustered damage is considered a unique marker of ionising radiation. Clustered damage is seen very infrequently in un-irradiated cells with exogenous damages (Sutherland et al., 2003; Bennett et al., 2004) and it is well established that the repair of clustered damage is much more difficult than for single lesions (David-Cordonnier et al., 2002) leading to a higher rate of mutation.

There are currently little data to suggest that UVA is able to initiate the formation of clustered DNA damage, so further work in this area would be of great interest. If UVA is shown to form clustered damage at biologically relevant doses, this could have considerable consequences and due to the difficulty to repair clustered damage could lead to a high level of mutations. Melanoma is now known to have a high mutational load compared to other cancers (Greenman et al., 2007). Increased work in this area could establish if there is any role for UVA and the induction of clustered damage in this high mutation load. Another area of particular interest could be the suggestion that clustered damage that includes 8-oxoG has been shown to be particularly difficult to repair. The presence of 8-OxoG in clustered damage retards the ability of the ligase complex that is responsible for completing repair of the damage, thus inhibiting the repair rate (Lomax et

al., 2004). This results in increased mutagenicity of 8-oxoG in clustered lesions (Pearson et al., 2004). 8-oxoG is long associated with UVA irradiation and so this could potentially lead to highly mutagenic lesions.

Furthermore, the work shown in this chapter has indicated both different time frames and mechanisms of apoptosis induction following UVA and UVB. Immediate apoptosis was demonstrated to be induced following UVA and this was independent of the DDR, whereas delayed apoptosis was seen in the UVB irradiated populations and this was dependent on activation of the DNA damage response. Apoptosis, following UV normally manifests as erythema (sunburn), the data in this chapter would indicate that in response to UVB, this is as a result of DNA damage, but the data indicated that UVA-induced apoptosis was independent of DNA damage,

## **6.2 The ability of UVA to induce H2AX phosphorylation in bystander cells**

UVA has been seen to induce the bystander effect in both keratinocyte and fibroblast cell lines as measured by clonogenic survival experiments (Whiteside and McMillan, 2009). Using the co-culture system, a delay in the release of signals that are able to induce the bystander effect has been seen (Whiteside et al., 2011). To date, much work into bystander signaling has been carried out, a wide variety of biological endpoints have been studied (Prise et al., 1998; Sawant et al., 2002; Zhou et al., 2002) and current interest has focused on the presence of H2AX and double strand breaks in bystander populations (Sokolov et al., 2005; Dickey et al., 2009). The presence of  $\gamma$ H2AX has been detected in ionising radiation bystander populations. This is seen to occur as a much later event than in cells directly exposed to directly irradiated cells.

The presence of  $\gamma$ H2AX in UVA bystander cells has not been extensively studied and so I aimed to look for the presence of H2AX phosphorylation in our UVA bystander model. The data indicated a significant increase in H2AX phosphorylation in the bystander population

after 48 hours of exposure to directly irradiated cells, suggesting a delay in release of signals, which is consistent with earlier work from our laboratory (Whiteside et al., 2011). Additionally, it was shown that H2AX phosphorylation was only present in S-phase cells, suggesting that H2AX phosphorylation in UVA bystander cells is a cell cycle dependent event, this is consistent with what has been seen in bystander populations exposed to signals from cells exposed to ionising radiation (Burdak-Rothkamm et al., 2007).

Previous work by our group have suggested that bystander signaling continues for at least 72 hours after the initial exposure to UVA, resulting in a decreased clonogenic survival experiments survival of bystander populations (Whiteside et al., 2011). Therefore, this indicates that UVA is able to cause genetic damage both directly and indirectly for long time periods after initial exposure, indicating that in order to fully understand the effects of UVA its effects must be studied at later time points than are currently utilized in much of the published work.

The ability of UVA to release bystander signals and cause damage to cells which have not been directly targeted raises concern for current UV therapies used to treat conditions such as psoriasis. Currently both UVA and UVB are used to treat psoriasis, although UVA alone is not effective and so UVA is used in combination with the photosensitiser psoralen. The evidence surrounding the ability of UVB to induce bystander effects has been controversial, with one group detecting no bystander effects following UVB irradiation, (Whiteside and McMillan, 2009) whereas others have seen a bystander effect following UVB (Widel et al., 2014a). It is difficult to draw conclusions on the effect of UVB psoriasis treatments to induce melanoma in patients at a later date; there are both a lack of studies in this area and the studies that have been carried out conflict (Weischer et al., 2004; Osmanovic et al., 2014). Conversely there is much published work looking at the risks of PUVA treatment, which has been associated with increased risks of both NMSC and melanoma, in particular SCC (Stern and Study, 2012; Maiorino et al., 2016). Increasing our understanding of the mechanisms behind the UVA bystander effect could help to

prevent skin cancer in PUVA patients. An area of particular interest could be to assess the immune response in response to UVA and UVB in cell lines which show a bystander response to UVA irradiation only. This could help to identify key signaling molecules underpinning the UVA bystander effect.

### **6.3 DNA damage response in directly irradiated and UVA bystander cells**

In chapters 3 and 4 I have shown that UVA is able to induce  $\gamma$ H2AX in both directly UVA-irradiated and bystander cells, however the mechanisms behind these are distinct. This is much like what has been seen with work on ionising radiation (Nagasawa and Little, 1999; Zhou et al., 2001). The data indicates that in directly UVA irradiated cells double strand breaks are being formed whereas in the bystander populations the data suggests that stalled replication forks are present. This difference in mechanism for damage, and indeed damage that is occurring in directly exposed and bystander cells is important and further understanding into this area could help increase understanding of melanoma. There has been substantial evidence to suggest that the genes frequently seen to be mutated in melanoma on sun exposed and non-exposed areas vary. Furthermore the mutations seen in the non-sun exposed areas are not the traditional UV signature mutations arising from CPDs. (Curtin et al., 2005; Whiteman et al., 2003; Davies et al., 2002; Maldonado et al., 2003). High proportions of point mutations have been seen in these melanomas. Previous work has indicated that point mutations are commonly seen in ionising radiation bystander populations (Nagasawa and Little, 1999). The presence of point mutations in UVA bystander cells has not been studied but it would be of great interest to look further into this area.

#### **6.4 The effect of UVA on MMP activity**

Matrix metalloproteases are dysregulated in both cancer (Stetler-Stevenson et al., 1993) and photoaging (Berneburg et al., 2000). The ability of UV to affect both the expression of and activity levels of MMPs is of great interest, in particular in term of photoaging, a characteristic of which is a decrease in collagen in the dermal layers of the skin. This is a characteristic that is not present in chronologically aged skin and so can be directly attributed to factors which induce photoaging. It has long been accepted that UV is the external factor which most influences photoaging. In particular, UVA has been highlighted as playing a key role in photoaging. This is because the characteristics of photoaging are present in the dermal layers of the skin and it is only UVA and not UVB which is able to penetrate to the dermal layers (Bruls et al., 1984). Additionally, increased levels ROS have been implicated in photoaging and it is well established that UVA rather than UVB results in increased ROS production (Keyse and Tyrrell, 1990; Pattison and Davies, 2006).

Published work on the ability of UVA to increase either the expression of or activity levels of MMPs have been conflicting. The expression and activity levels of MMPs have been seen to be both upregulated (Wertz et al., 2004) and down-regulated (Steinbrenner et al., 2003) in response to UVA irradiation, so it is difficult to draw conclusions on the ability of UVA to induce MMP activity. Earlier data from our laboratory suggested that the expression of both MMP-1 and MMP3 were up-regulated in response to UVA irradiation, I chose to build on this by looking for the levels of casein degrading MMPs following a biologically relevant dose of UVA in both keratinocyte and fibroblast cell lines.

The results indicated very little effect of UVA on the activity levels of casein degrading MMPs in either keratinocytes or fibroblast cell lines. Instead the data indicated that increased confluence of the cells in culture caused a decrease in the activity of casein degrading MMPs in the conditioned medium. The data show a decrease in MMP activity in cells at high levels of confluence regardless of exposure to UVA. The results presented in

this thesis did not indicate the mechanism behind the decreased activity. MMPs are released as inactive zymogens, are activated following the breaking of a cysteine switch and can be un-activated by the appropriate TIMP. So from the data generated in this work by zymography does not indicate whether the decrease in MMP activity is as a result of increase in TIMPS or a decrease in MMP expression.

The RT-PCR data generated previously was reanalyzed comparing the MMP expression to that of the control 0hr time point, this analysis revealed a decrease in the expression of MMPs in the control 24-hour point compared to the control 0-time point and therefore revealed a greatly diminished UVA-dependent increase of both MMP1 and MMP3. Additionally, this analysis indicated a decrease in MMP expression with increased influence of cells in culture, consistent with data published in the area (Bachmeier et al., 2005). Taken together the work presented in chapter 5 suggests that work aiming to look for upregulation of MMPs following ultraviolet irradiation should not be carried out at high levels of confluence because confluent, or near confluent cells show dramatically decreased levels of MMP activity.

### **Final Conclusions**

The broad aim of this PhD thesis was to identify biomarkers of UVA exposure, the work shown in chapter 5 did not indicate any significant increase in MMP activity in response to UVA irradiation and published work in this area has been conflicting. Therefore MMP activity levels following UVA lack the robustness to be useful as a biomarker when assessing UVA protection afforded by sun creams. This work has revealed activation of the DDR in both directly UVA irradiated and bystander cells; the timeframes and mechanism of the DDR appear to be different in each case and the data indicates that the damage occurring in the directly irradiated cells differs from the bystander cells. The evidence shown in chapter 3 indicates that DSBs are formed in cells directly exposed to UVA, based on this; I would suggest 53BP1 foci formation as a biomarker for UVA in

directly exposed cells. 53BP1 foci form rapidly in response to DSBs but not to stalled forks or other types of DNA lesion (Schultz et al., 2000). Conversely the data shown in chapter 4 indicated that stalled forks occur in UVA-bystander populations and therefore up-regulation of  $\gamma$ H2AX would be a suitable biomarker in UVA bystander populations.

## References

- Agar, N., Halliday, G., Barnetson, R., Ananthaswamy, H., Wheeler, M. & Jones, A. 2004. The Basal Layer in Human Squamous Tumors Harbors More UVA Than UVB Fingerprint Mutations: A Role for UVA in Human Skin Carcinogenesis. *Proceedings of the National Academy of Sciences of the United States of America*, 101(14), 4954-4959.
- Agarwal, S. & Sohal, R. S. 1994. DNA Oxidative Damage and Life Expectancy in Houseflies. *Proc Natl Acad Sci U S A*, 91(25), 12332-5.
- Allanson, M. & Reeve, V. E. 2004. Immunoprotective UVA (320–400 Nm) Irradiation Upregulates Heme Oxygenase-1 in the Dermis and Epidermis of Hairless Mouse Skin. *Journal of investigative dermatology*, 122(4), 1030-1036.
- Allen, R. & Tresini, M. 2000. Oxidative Stress and Gene Regulation. *Free Radical Biology and Medicine*, 28(3), 463-499.
- An, K. P., Athar, M., Tang, X., Katiyar, S. K., Russo, J., Beech, J., Aszterbaum, M., Kopelovich, L., Epstein, E. H., Mukhtar, H. & Bickers, D. R. 2002. Cyclooxygenase-2 Expression in Murine and Human Nonmelanoma Skin Cancers: Implications for Therapeutic Approaches. *Photochem Photobiol*, 76(1), 73-80.
- Aragane, Y., Kulms, D., Metze, D., Wilkes, G., Pöppelmann, B., Luger, T. A. & Schwarz, T. 1998. Ultraviolet Light Induces Apoptosis Via Direct Activation of Cd95 (Fas/Apo-1) Independently of Its Ligand Cd95l. *J Cell Biol*, 140(1), 171-82.
- Aydin, I. T., Melamed, R. D., Adams, S. J., Castillo-Martin, M., Demir, A., Bryk, D., Brunner, G., Cordon-Cardo, C., Osman, I., Rabadan, R. & Celebi, J. T. 2014. Fbxw7 Mutations in Melanoma and a New Therapeutic Paradigm. *J Natl Cancer Inst*, 106(6), dju107.
- Azzam, E. I., De Toledo, S. M., Gooding, T. & Little, J. B. 1998. Intercellular Communication Is Involved in the Bystander Regulation of Gene Expression in Human Cells Exposed to Very Low Fluences of Alpha Particles. *Radiat Res*, 150(5), 497-504.
- Azzam, E. I., De Toledo, S. M. & Little, J. B. 2001. Direct Evidence for the Participation of Gap Junction-Mediated Intercellular Communication in the Transmission of Damage Signals from Alpha -Particle Irradiated to Nonirradiated Cells. *Proc Natl Acad Sci U S A*, 98(2), 473-8.
- Azzam, E. I., De Toledo, S. M., Spitz, D. R. & Little, J. B. 2002. Oxidative Metabolism Modulates Signal Transduction and Micronucleus Formation in Bystander Cells from Alpha-Particle-Irradiated Normal Human Fibroblast Cultures. *Cancer Res*, 62(19), 5436-42.

- Bachelor, M. A. & Bowden, G. T. 2004a. Ultraviolet A-Induced Modulation of Bcl-Xl by P38 Mapk in Human Keratinocytes: Post-Transcriptional Regulation through the 3'-Untranslated Region. *J Biol Chem*, 279(41), 42658-68.
- Bachelor, M. A. & Bowden, G. T. 2004b. Uva-Mediated Activation of Signaling Pathways Involved in Skin Tumor Promotion and Progression. *Semin Cancer Biol*, 14(2), 131-8.
- Bachelor, M. A., Silvers, A. L. & Bowden, G. T. 2002. The Role of P38 in UVA-Induced Cyclooxygenase-2 Expression in the Human Keratinocyte Cell Line, Hacat. *Oncogene*, 21(46), 7092-9.
- Bachmeier, B. E., Albini, A., Vené, R., Benelli, R., Noonan, D., Weigert, C., Weiler, C., Lichtinghagen, R., Jochum, M. & Nerlich, A. G. 2005. Cell Density-Dependent Regulation of Matrix Metalloproteinase and Timp Expression in Differently Tumorigenic Breast Cancer Cell Lines. *Exp Cell Res*, 305(1), 83-98.
- Baier, J., Maisch, T., Maier, M., Engel, E., Landthaler, M. & Bäuml, W. 2006. Singlet Oxygen Generation by UVA Light Exposure of Endogenous Photosensitizers. *Biophys J*, 91(4), 1452-9.
- Bakkenist, C. J. & Kastan, M. B. 2003. DNA Damage Activates ATM through Intermolecular Autophosphorylation and Dimer Dissociation. *Nature*, 421(6922), 499-506.
- Banerjee, G., Gupta, N., Kapoor, A. & Raman, G. 2005. UV Induced Bystander Signaling Leading to Apoptosis. *Cancer Lett*, 223(2), 275-84.
- Barbu, A., Welsh, N. & Saldeen, J. 2002. Cytokine-Induced Apoptosis and Necrosis Are Preceded by Disruption of the Mitochondrial Membrane Potential ( $\Delta\psi(M)$ ) in Pancreatic Rinm5f Cells: Prevention by Bcl-2. *Mol Cell Endocrinol*, 190(1-2), 75-82.
- Bartek, J. & Lukas, J. 2003. Chk1 and Chk2 Kinases in Checkpoint Control and Cancer. *Cancer Cell*, 3(5), 421-9.
- Bartek, J. & Lukas, J. 2007. DNA Damage Checkpoints: From Initiation to Recovery or Adaptation. *Curr Opin Cell Biol*, 19(2), 238-45.
- Basu-Modak, S., Lüscher, P. & Tyrrell, R. M. 1996. Lipid Metabolite Involvement in the Activation of the Human Heme Oxygenase-1 Gene. *Free Radical Biology and Medicine*, 20(7), 887-897.
- Basu-Modak, S. & Tyrrell, R. M. 1993. Singlet Oxygen: A Primary Effector in the Ultraviolet a/near-Visible Light Induction of the Human Heme Oxygenase Gene. *Cancer research*, 53(19), 4505-4510.
- Batty, D. P. & Wood, R. D. 2000. Damage Recognition in Nucleotide Excision Repair of DNA. *Gene*, 241(2), 193-204.

- Beak, S. M., Paek, S. H., Jahng, Y., Lee, Y. S. & Kim, J. A. 2004. Inhibition of UVA Irradiation-Modulated Signaling Pathways by Rutaecarpine, a Quinazolinocarbolone Alkaloid, in Human Keratinocytes. *Eur J Pharmacol*, 498(1-3), 19-25.
- Bedard, K. & Krause, K. H. 2007. The Nox Family of Ros-Generating NADPH Oxidases: Physiology and Pathophysiology. *Physiological reviews*, 87(1), 245-313.
- Bekker-Jensen, S., Lukas, C., Melander, F., Bartek, J. & Lukas, J. 2005. Dynamic Assembly and Sustained Retention of 53BP1 at the Sites of DNA Damage Are Controlled by MDC1/NFDB1. *J Cell Biol*, 170(2), 201-11.
- Bellei, B., Mastrofrancesco, A., Briganti, S., Aspite, N., Ale-Agha, N., Sies, H. & Picardo, M. 2008. Ultraviolet a Induced Modulation of Gap Junctional Intercellular Communication by P38 Mapk Activation in Human Keratinocytes. *Exp Dermatol*, 17(2), 115-24.
- Belyakov, O. V., Malcolmson, A. M., Folkard, M., Prise, K. M. & Michael, B. D. 2001. Direct Evidence for a Bystander Effect of Ionizing Radiation in Primary Human Fibroblasts. *Br J Cancer*, 84(5), 674-9.
- Bender, K., Blattner, C., Knebel, A., Iordanov, M., Herrlich, P. & Rahmsdorf, H. J. 1997. UV-Induced Signal Transduction. *J Photochem Photobiol B*, 37(1-2), 1-17.
- Bennett, D. C. 2008. Ultraviolet Wavebands and Melanoma Initiation. *Pigment Cell Melanoma Res*, 21(5), 520-4.
- Bennett, P. V., Cintron, N. S., Gros, L., Laval, J. & Sutherland, B. M. 2004. Are Endogenous Clustered DNA Damages Induced in Human Cells? *Free Radic Biol Med*, 37(4), 488-99.
- Berg, R. J., Van Kranen, H. J., Rebel, H. G., De Vries, A., Van Vloten, W. A., Van Kreijl, C. F., Van Der Leun, J. C. & De Gruijl, F. R. 1996. Early P53 Alterations in Mouse Skin Carcinogenesis by UVB Radiation: Immunohistochemical Detection of Mutant P53 Protein in Clusters of Preneoplastic Epidermal Cells. *Proc Natl Acad Sci U S A*, 93(1), 274-8.
- Berger, M. F., Hodis, E., Heffernan, T. P., Deribe, Y. L., Lawrence, M. S., Protopopov, A., Ivanova, E., Watson, I. R., Nickerson, E., Ghosh, P., Zhang, H., Zeid, R., Ren, X., Cibulskis, K., Sivachenko, A. Y., Wagle, N., Sucker, A., Sougnez, C., Onofrio, R., Ambrogio, L., Auclair, D., Fennell, T., Carter, S. L., Drier, Y., Stojanov, P., Singer, M. A., Voet, D., Jing, R., Saksena, G., Barretina, J., Ramos, A. H., Pugh, T. J., Stransky, N., Parkin, M., Winckler, W., Mahan, S., Ardlie, K., Baldwin, J., Wargo, J., Schadendorf, D., Meyerson, M., Gabriel, S. B., Golub, T. R., Wagner, S. N., Lander, E. S., Getz, G., Chin, L. & Garraway, L. A. 2012. Melanoma Genome Sequencing Reveals Frequent Prex2 Mutations. *Nature*, 485(7399), 502-6.

- Bergfeld, W. F. 1997. The Aging Skin. *Int J Fertil Womens Med*, 42(2), 57-66.
- Berneburg, M., Gattermann, N., Stege, H., Grewe, M., Vogelsang, K., Ruzicka, T. & Krutmann, J. 1997. Chronically Ultraviolet-Exposed Human Skin Shows a Higher Mutation Frequency of Mitochondrial DNA as Compared to Unexposed Skin and the Hematopoietic System. *Photochem Photobiol*, 66(2), 271-5.
- Berneburg, M., Grether-Beck, S., Kürten, V., Ruzicka, T., Briviba, K., Sies, H. & Krutmann, J. 1999. Singlet Oxygen Mediates the Uva-Induced Generation of the Photoaging-Associated Mitochondrial Common Deletion. *J Biol Chem*, 274(22), 15345-9.
- Berneburg, M., Plettenberg, H. & Krutmann, J. 2000. Photoaging of Human Skin. *Photodermatol Photoimmunol Photomed*, 16(6), 239-44.
- Berneburg, M., Plettenberg, H., Medve-König, K., Pfahlberg, A., Gers-Barlag, H., Gefeller, O. & Krutmann, J. 2004. Induction of the Photoaging-Associated Mitochondrial Common Deletion in Vivo in Normal Human Skin. *J Invest Dermatol*, 122(5), 1277-83.
- Bernstein, L. R. & Colburn, N. H. 1989. Ap1/Jun Function Is Differentially Induced in Promotion-Sensitive and Resistant Jb6 Cells. *Science*, 244(4904), 566-9.
- Birch-Machin, M. A., Tindall, M., Turner, R., Haldane, F. & Rees, J. L. 1998. Mitochondrial DNA Deletions in Human Skin Reflect Photo- Rather Than Chronologic Aging. *J Invest Dermatol*, 110(2), 149-52.
- Boniol, M., Autier, P., Boyle, P. & Gandini, S. 2012. Cutaneous Melanoma Attributable to Sunbed Use: Systematic Review and Meta-Analysis. *BMJ*, 345, e4757.
- Brash, D. E. 2016. UV-Induced Melanin Chemiexcitation: A New Mode of Melanoma Pathogenesis. *Toxicol Pathol*.
- Brash, D. E., Rudolph, J. A., Simon, J. A., Lin, A., Mckenna, G. J., Baden, H. P., Halperin, A. J. & Pontén, J. 1991. A Role for Sunlight in Skin Cancer: UV-Induced P53 Mutations in Squamous Cell Carcinoma. *Proc Natl Acad Sci U S A*, 88(22), 10124-8.
- Brash, D. E., Ziegler, A., Jonason, A. S., Simon, J. A., Kunala, S. & Leffell, D. J. 1996. Sunlight and Sunburn in Human Skin Cancer: P53, Apoptosis, and Tumor Promotion. *J Invest Dermatol Symp Proc*, 1(2), 136-42.
- Brenneisen, P., Wenk, J., Klotz, L. O., Wlaschek, M., Briviba, K., Krieg, T., Sies, H. & Scharffetter-Kochanek, K. 1998. Central Role of Ferrous/Ferric Iron in the Ultraviolet B Irradiation-Mediated Signaling Pathway Leading to Increased Interstitial Collagenase (Matrix-Degrading Metalloprotease (MMP)-1) and Stromelysin-1 (MMP-3) mRNA Levels in Cultured Human Dermal Fibroblasts. *J Biol Chem*, 273(9), 5279-87.

- Breuckmann, F., Von Kobyletzki, G., Avermaete, A., Radenhausen, M., Höxtermann, S., Pieck, C., Schöneborn, P., Gambichler, T., Freitag, M., Hoffmann, K. & Altmeyer, P. 2003. Mechanisms of Apoptosis: UVA1-Induced Immediate and UVB-Induced Delayed Apoptosis in Human T Cells in Vitro. *J Eur Acad Dermatol Venereol*, 17(4), 418-29.
- Bruls, W. A., Slaper, H., Van Der Leun, J. C. & Berrens, L. 1984. Transmission of Human Epidermis and Stratum Corneum as a Function of Thickness in the Ultraviolet and Visible Wavelengths. *Photochem Photobiol*, 40(4), 485-94.
- Bruzzone, R. & Meda, P. 1988. The Gap Junction: A Channel for Multiple Functions? *Eur J Clin Invest*, 18(5), 444-53.
- Buechner, N., Schroeder, P., Jakob, S., Kunze, K., Maresch, T., Calles, C., Krutmann, J. & Haendeler, J. 2008. Changes of MMP-1 and Collagen Type Ialpha1 by UVA, UVB and Irradiation Are Differentially Regulated by Trx-1. *Exp Gerontol*, 43(7), 633-7.
- Bunting, S. F., Callén, E., Wong, N., Chen, H. T., Polato, F., Gunn, A., Bothmer, A., Feldhahn, N., Fernandez-Capetillo, O., Cao, L., Xu, X., Deng, C. X., Finkel, T., Nussenzweig, M., Stark, J. M. & Nussenzweig, A. 2010. 53BP1 Inhibits Homologous Recombination in BRCA1-Deficient Cells by Blocking Resection of DNA Breaks. *Cell*, 141(2), 243-54.
- Burdak-Rothkamm, S., Short, S. C., Folkard, M., Rothkamm, K. & Prise, K. M. 2007. Atr-Dependent Radiation-Induced Gamma H2AX Foci in Bystander Primary Human Astrocytes and Glioma Cells. *Oncogene*, 26(7), 993-1002.
- Burma, S., Chen, B. P., Murphy, M., Kurimasa, A. & Chen, D. J. 2001. ATM Phosphorylates Histone H2AX in Response to DNA Double-Strand Breaks. *J Biol Chem*, 276(45), 42462-7.
- Byrne, S. N., Spinks, N. & Halliday, G. M. 2002. Ultraviolet A Irradiation of C57bl/6 Mice Suppresses Systemic Contact Hypersensitivity or Enhances Secondary Immunity Depending on Dose. *J Invest Dermatol*, 119(4), 858-64.
- Byrne, S. N., Spinks, N. & Halliday, G. M. 2006. The Induction of Immunity to a Protein Antigen Using an Adjuvant Is Significantly Compromised by Ultraviolet A Radiation. *J Photochem Photobiol B*, 84(2), 128-34.
- Cadet, J., Anselmino, C., Douki, T. & Voituriez, L. 1992. Photochemistry of Nucleic Acids in Cells. *J Photochem Photobiol B*, 15(4), 277-98.
- Cadet, J., Douki, T., Ravanat, J. L. & Di Mascio, P. 2009. Sensitized Formation of Oxidatively Generated Damage to Cellular DNA by UVA Radiation. *Photochem Photobiol Sci*, 8(7), 903-11.

- Campagnola, P. & Loew, L. 2003. Second-Harmonic Imaging Microscopy for Visualizing Biomolecular Arrays in Cells, Tissues and Organisms. *Nature Biotechnology*, 21(11), 1356-1360.
- Carson, C. T., Schwartz, R. A., Stracker, T. H., Lilley, C. E., Lee, D. V. & Weitzman, M. D. 2003. The Mre11 Complex Is Required for Atm Activation and the G2/M Checkpoint. *EMBO J*, 22(24), 6610-20.
- Chauhan, P. & Shakya, M. 2009. Modeling Signaling Pathways Leading to Wrinkle Formation: Identification of the Skin Aging Target. *Indian Journal of Dermatology Venereology & Leprology*, 75(5), 463-468.
- Chedekel, M. R., Smith, S. K., Post, P. W., Pokora, A. & Vessell, D. L. 1978. Photodestruction of Pheomelanin: Role of Oxygen. *Proc Natl Acad Sci U S A*, 75(11), 5395-9.
- Chen, I. P., Henning, S., Faust, A., Boukamp, P., Volkmer, B. & Greinert, R. 2012. UVA-Induced Epigenetic Regulation of P16(Ink4a) in Human Epidermal Keratinocytes and Skin Tumor Derived Cells. *Photochem Photobiol Sci*, 11(1), 180-90.
- Chen, S., Zhao, Y., Han, W., Zhao, G., Zhu, L., Wang, J., Bao, L., Jiang, E., Xu, A., Hei, T. K., Yu, Z. & Wu, L. 2008. Mitochondria-Dependent Signalling Pathway Are Involved in the Early Process of Radiation-Induced Bystander Effects. *Br J Cancer*, 98(11), 1839-44.
- Chen, S., Zhao, Y., Zhao, G., Han, W., Bao, L., Yu, K. N. & Wu, L. 2009. Up-Regulation of ROS by Mitochondria-Dependent Bystander Signaling Contributes to Genotoxicity of Bystander Effects. *Mutat Res*, 666(1-2), 68-73.
- Chen, W., Borchers, A. H., Dong, Z., Powell, M. B. & Bowden, G. T. 1998. Uvb Irradiation-Induced Activator Protein-1 Activation Correlates with Increased C-Fos Gene Expression in a Human Keratinocyte Cell Line. *J Biol Chem*, 273(48), 32176-81.
- Cheng, K. C., Cahill, D. S., Kasai, H., Nishimura, S. & Loeb, L. A. 1992. 8-Hydroxyguanine, an Abundant Form of Oxidative DNA Damage, Causes G----T and a----C Substitutions. *J Biol Chem*, 267(1), 166-72.
- Cleaver, J. E. 1968. Defective Repair Replication of DNA in Xeroderma Pigmentosum. *Nature*, 218(5142), 652-6.
- Coffer, P. J., Burgering, B. M., Peppelenbosch, M. P., Bos, J. L. & Kruijer, W. 1995. UV Activation of Receptor Tyrosine Kinase Activity. *Oncogene*, 11(3), 561-9.
- Collins, A. R., Dusinská, M., Gedik, C. M. & Stětina, R. 1996. Oxidative Damage to DNA: Do We Have a Reliable Biomarker? *Environ Health Perspect*, 104 Suppl 3, 465-9.
- Coppé, J. P., Desprez, P. Y., Krtolica, A. & Campisi, J. 2010. The Senescence-Associated Secretory Phenotype: The Dark Side of Tumor Suppression. *Annu Rev Pathol*, 5, 99-118.

- Cotter, M., Thomas, J., Cassidy, P., Robinette, K., Jenkins, N., Florell, S., Leachman, S., Samlowski, W. & Grossman, D. 2007. N-Acetylcysteine Protects Melanocytes against Oxidative Stress/Damage and Delays Onset of Ultraviolet Induced Melanoma in Mice. *Clinical Cancer Research*, 13(19), 5952-5958.
- Courdavault, S., Baudouin, C., Charveron, M., Favier, A., Cadet, J. & Douki, T. 2004. Larger Yield of Cyclobutane Dimers Than 8-Oxo-7,8-Dihydroguanine in the DNA of UVA-Irradiated Human Skin Cells. *Mutat Res*, 556(1-2), 135-42.
- Curtin, J. A., Fridlyand, J., Kageshita, T., Patel, H. N., Busam, K. J., Kutzner, H., Cho, K. H., Aiba, S., Bröcker, E. B., Leboit, P. E., Pinkel, D. & Bastian, B. C. 2005. Distinct Sets of Genetic Alterations in Melanoma. *N Engl J Med*, 353(20), 2135-47.
- Dahle, J., Angell-Petersen, E., Steen, H. B. & Moan, J. 2001. Bystander Effects in Cell Death Induced by Photodynamic Treatment UVA Radiation and Inhibitors of ATP Synthesis. *Photochem Photobiol*, 73(4), 378-87.
- Dahle, J. & Kvam, E. 2003. Induction of Delayed Mutations and Chromosomal Instability in Fibroblasts after UVA-, UVB-, and X-Radiation. *Cancer research*, 63(7), 1464-1469.
- Dahle, J., Kvam, E. & Stokke, T. 2005. Bystander Effects in Uv-Induced Genomic Instability: Antioxidants Inhibit Delayed Mutagenesis Induced by Ultraviolet A and B Radiation. *J Carcinog*, 4, 11.
- David-Cordonnier, M. H., Cunniffe, S. M., Hickson, I. D. & O'neill, P. 2002. Efficiency of Incision of an AP Site within Clustered DNA Damage by the Major Human AP Endonuclease. *Biochemistry*, 41(2), 634-42.
- Davies, H., Bignell, G. R., Cox, C., Stephens, P., Edkins, S., Clegg, S., Teague, J., Woffendin, H., Garnett, M. J., Bottomley, W., Davis, N., Dicks, E., Ewing, R., Floyd, Y., Gray, K., Hall, S., Hawes, R., Hughes, J., Kosmidou, V., Menzies, A., Mould, C., Parker, A., Stevens, C., Watt, S., Hooper, S., Wilson, R., Jayatilake, H., Gusterson, B. A., Cooper, C., Shipley, J., Hargrave, D., Pritchard-Jones, K., Maitland, N., Chenevix-Trench, G., Riggins, G. J., Bigner, D. D., Palmieri, G., Cossu, A., Flanagan, A., Nicholson, A., Ho, J. W., Leung, S. Y., Yuen, S. T., Weber, B. L., Seigler, H. F., Darrow, T. L., Paterson, H., Marais, R., Marshall, C. J., Wooster, R., Stratton, M. R. & Futreal, P. A. 2002. Mutations of the BRAF Gene in Human Cancer. *Nature*, 417(6892), 949-54.
- De Fabo, E. C., Noonan, F. P., Fears, T. & Merlino, G. 2004. Ultraviolet B but Not Ultraviolet A Radiation Initiates Melanoma. *Cancer Res*, 64(18), 6372-6.
- De Feraudy, S., Revet, I., Bezrookove, V., Feeney, L. & Cleaver, J. E. 2010. A Minority of Foci or Pan-Nuclear Apoptotic Staining of GammaH2AX in the S Phase after UV Damage Contain DNA Double-Strand Breaks. *Proc Natl Acad Sci U S A*, 107(15), 6870-5.

- De Gruijl, F. R. 2002. Photocarcinogenesis: UVA Vs. UVB Radiation. *Skin Pharmacol Appl Skin Physiol*, 15(5), 316-20.
- De Laat, A., Kroon, E. D. & De Gruijl, F. R. 1997. Cell Cycle Effects and Concomitant P53 Expression in Hairless Murine Skin after Longwave UVA (365 Nm) Irradiation: A Comparison with UVB Irradiation. *Photochem Photobiol*, 65(4), 730-5.
- Desagher, S. & Martinou, J. C. 2000. Mitochondria as the Central Control Point of Apoptosis. *Trends Cell Biol*, 10(9), 369-77.
- Dickey, J. S., Baird, B. J., Redon, C. E., Avdoshina, V., Palchik, G., Wu, J., Kondratyev, A., Bonner, W. M. & Martin, O. A. 2012. Susceptibility to Bystander DNA Damage Is Influenced by Replication and Transcriptional Activity. *Nucleic Acids Res*, 40(20), 10274-86.
- Dickey, J. S., Baird, B. J., Redon, C. E., Sokolov, M. V., Sedelnikova, O. A. & Bonner, W. M. 2009. Intercellular Communication of Cellular Stress Monitored by Gamma-H2AX Induction. *Carcinogenesis*, 30(10), 1686-95.
- Diffey, B. L. 2002. Sources and Measurement of Ultraviolet Radiation. *Methods*, 28(1), 4-13.
- Ding, L., Kim, M., Kanchi, K. L., Dees, N. D., Lu, C., Griffith, M., Fenstermacher, D., Sung, H., Miller, C. A., Goetz, B., Wendl, M. C., Griffith, O., Cornelius, L. A., Linette, G. P., Mcmichael, J. F., Sondak, V. K., Fields, R. C., Ley, T. J., Mulé, J. J., Wilson, R. K. & Weber, J. S. 2014. Clonal Architectures and Driver Mutations in Metastatic Melanomas. *PLoS One*, 9(11), e111153.
- Djavaheri-Mergny, M., Mergny, J. L., Bertrand, F., Santus, R., Mazière, C., Dubertret, L. & Mazière, J. C. 1996. Ultraviolet-A Induces Activation of AP-1 in Cultured Human Keratinocytes. *FEBS Lett*, 384(1), 92-6.
- Dolmans DE, Fukumura D, Jain RK. Photodynamic therapy for cancer. *Nature Reviews Cancer* 2003; 3(5):380–387  
Dolmans DE, Fukumura D, Jain RK. Photodynamic therapy for cancer. *Nature Reviews Cancer* 2003; 3(5):380–387
- Domann, F. E., Levy, J. P., Finch, J. S. & Bowden, G. T. 1994. Constitutive AP-1 DNA Binding and Transactivating Ability of Malignant but Not Benign Mouse Epidermal Cells. *Mol Carcinog*, 9(2), 61-6.
- Domon, M. & Rauth, A. M. 1969. Effects of Caffeine on Ultraviolet-Irradiated Mouse L Cells. *Radiat Res*, 39(1), 207-21.

- Douki, T., Reynaud-Angelin, A., Cadet, J. & Sage, E. 2003. Bipyrimidine Photoproducts Rather Than Oxidative Lesions Are the Main Type of DNA Damage Involved in the Genotoxic Effect of Solar Uva Radiation. *Biochemistry*, 42(30), 9221-6.
- Drobetsky, E. A., Turcotte, J. & Châteauneuf, A. 1995. A Role for Ultraviolet A in Solar Mutagenesis. *Proc Natl Acad Sci U S A*, 92(6), 2350-4.
- Dunkern, T. R., Fritz, G. & Kaina, B. 2001. Ultraviolet Light-Induced DNA Damage Triggers Apoptosis in Nucleotide Excision Repair-Deficient Cells Via Bcl-2 Decline and Caspase-3/-8 Activation. *Oncogene*, 20(42), 6026-38.
- Durinck, S., Ho, C., Wang, N. J., Liao, W., Jakkula, L. R., Collisson, E. A., Pons, J., Chan, S. W., Lam, E. T., Chu, C., Park, K., Hong, S. W., Hur, J. S., Huh, N., Neuhaus, I. M., Yu, S. S., Grekin, R. C., Mauro, T. M., Cleaver, J. E., Kwok, P. Y., Leboit, P. E., Getz, G., Cibulskis, K., Aster, J. C., Huang, H., Purdom, E., Li, J., Bolund, L., Arron, S. T., Gray, J. W., Spellman, P. T. & Cho, R. J. 2011. Temporal Dissection of Tumorigenesis in Primary Cancers. *Cancer Discov*, 1(2), 137-43.
- Earnshaw, W. C., Martins, L. M. & Kaufmann, S. H. 1999. Mammalian Caspases: Structure, Activation, Substrates, and Functions During Apoptosis. *Annu Rev Biochem*, 68, 383-424.
- Egeblad, M. & Werb, Z. 2002. New Functions for the Matrix Metalloproteinases in Cancer Progression. *Nat Rev Cancer*, 2(3), 161-74.
- El-Domyati, M., Attia, S., Saleh, F., Brown, D., Birk, D., Gasparro, F., Ahmad, H. & Uitto, J. 2002. Intrinsic Aging Vs. Photoaging: A Comparative Histopathological, Immunohistochemical, and Ultrastructural Study of Skin. *Experimental dermatology*, 11(5), 398-405.
- Enninga, I. C., Groenendijk, R. T., Filon, A. R., Van Zeeland, A. A. & Simons, J. W. 1986. The Wavelength Dependence of U.V.-Induced Pyrimidine Dimer Formation, Cell Killing and Mutation Induction in Human Diploid Skin Fibroblasts. *Carcinogenesis*, 7(11), 1829-36.
- Facoetti, A., Ballarini, F., Cherubini, R., Gerardi, S., Nano, R., Ottolenghi, A., Prise, K. M., Trott, K. R. & Zilio, C. 2006. Gamma Ray-Induced Bystander Effect in Tumour Glioblastoma Cells: A Specific Study on Cell Survival, Cytokine Release and Cytokine Receptors. *Radiat Prot Dosimetry*, 122(1-4), 271-4.
- Fagot, D., Asselineau, D. & Bernerd, F. 2002. Direct Role of Human Dermal Fibroblasts and Indirect Participation of Epidermal Keratinocytes in MMP-1 Production after UV-B Irradiation. *Arch Dermatol Res*, 293(11), 576-83.
- Fagot, D., Asselineau, D. & Bernerd, F. 2004. Matrix Metalloproteinase-1 Production Observed after Solar-Simulated Radiation Exposure Is Assumed by Dermal

- Fibroblasts but Involves a Paracrine Activation through Epidermal Keratinocytes. *Photochem Photobiol*, 79(6), 499-505.
- Farage, M.A., Miller, K.W., Elsner, P. and Maibach, H.I., 2008. Intrinsic and extrinsic factors in skin ageing: a review. *International Journal of Cosmetic Science*, 30(2), pp.87-95.
- Featherstone, C. & Jackson, S. P. 1999. DNA Double-Strand Break Repair. *Curr Biol*, 9(20), R759-61.
- Feijoo, C., Hall-Jackson, C., Wu, R., Jenkins, D., Leitch, J., Gilbert, D. M. & Smythe, C. 2001. Activation of Mammalian Chk1 During DNA Replication Arrest: A Role for Chk1 in the Intra-S Phase Checkpoint Monitoring Replication Origin Firing. *J Cell Biol*, 154(5), 913-23.
- Fernandez-Capetillo, O., Chen, H. T., Celeste, A., Ward, I., Romanienko, P. J., Morales, J. C., Naka, K., Xia, Z., Camerini-Otero, R. D., Motoyama, N., Carpenter, P. B., Bonner, W. M., Chen, J. & Nussenzweig, A. 2002. DNA Damage-Induced G2-M Checkpoint Activation by Histone H2AX and 53BP1. *Nat Cell Biol*, 4(12), 993-7.
- Fisher, G. J., Datta, S., Wang, Z., Li, X. Y., Quan, T., Chung, J. H., Kang, S. & Voorhees, J. J. 2000. C-Jun-Dependent Inhibition of Cutaneous Procollagen Transcription Following Ultraviolet Irradiation Is Reversed by All-Trans Retinoic Acid. *J Clin Invest*, 106(5), 663-70.
- Fisher, G. J., Datta, S. C., Talwar, H. S., Wang, Z. Q., Varani, J., Kang, S. & Voorhees, J. J. 1996. Molecular Basis of Sun-Induced Premature Skin Ageing and Retinoid Antagonism. *Nature*, 379(6563), 335-9.
- Fisher, G. J., Kang, S., Varani, J., Bata-Csorgo, Z., Wan, Y., Datta, S. & Voorhees, J. J. 2002. Mechanisms of Photoaging and Chronological Skin Aging. *Arch Dermatol*, 138(11), 1462-70.
- Fisher, G. J. & Voorhees, J. J. 1998. Molecular Mechanisms of Photoaging and Its Prevention by Retinoic Acid: Ultraviolet Irradiation Induces Map Kinase Signal Transduction Cascades That Induce AP-1-Regulated Matrix Metalloproteinases That Degrade Human Skin in Vivo. *J Investig Dermatol Symp Proc*, 3(1), 61-8.
- Fisher, G. J., Wang, Z. Q., Datta, S. C., Varani, J., Kang, S. & Voorhees, J. J. 1997. Pathophysiology of Premature Skin Aging Induced by Ultraviolet Light. *N Engl J Med*, 337(20), 1419-28.
- Frederick, J., Snell, H. & Haywood, E. 1989. Solar Ultraviolet Radiation at the Earth's Surface. *Photochemistry and Photobiology*, 50(4), 443-450.
- Freeman, S. E., Hacham, H., Gange, R. W., Maytum, D. J., Sutherland, J. C. & Sutherland, B. M. 1989. Wavelength Dependence of Pyrimidine Dimer Formation in DNA of Human Skin Irradiated in Situ with Ultraviolet Light. *Proc Natl Acad Sci U S A*, 86(14), 5605-9.

- Freeman, S. E. & Ryan, S. L. 1990. Wavelength Dependence for Uv-Induced Pyrimidine Dimer Formation in DNA of Human Peripheral Blood Lymphocytes. *Mutat Res*, 235(3), 181-6.
- Gailani, M. R., Stähle-Bäckdahl, M., Leffell, D. J., Glynn, M., Zaphiropoulos, P. G., Pressman, C., Undén, A. B., Dean, M., Brash, D. E., Bale, A. E. & Toftgård, R. 1996. The Role of the Human Homologue of Drosophila Patched in Sporadic Basal Cell Carcinomas. *Nat Genet*, 14(1), 78-81.
- Garbe, C. & Blum, A. 2001. Epidemiology of Cutaneous Melanoma in Germany and Worldwide. *Skin Pharmacol Appl Skin Physiol*, 14(5), 280-90.
- Gartner, J. J., Parker, S. C., Prickett, T. D., Dutton-Regester, K., Stitzel, M. L., Lin, J. C., Davis, S., Simhadri, V. L., Jha, S., Katagiri, N., Gotea, V., Teer, J. K., Wei, X., Morken, M. A., Bhanot, U. K., Chen, G., Elnitski, L. L., Davies, M. A., Gershenwald, J. E., Carter, H., Karchin, R., Robinson, W., Robinson, S., Rosenberg, S. A., Collins, F. S., Parmigiani, G., Komar, A. A., Kimchi-Sarfaty, C., Hayward, N. K., Margulies, E. H., Samuels, Y. & Program, N. C. S. 2013. Whole-Genome Sequencing Identifies a Recurrent Functional Synonymous Mutation in Melanoma. *Proc Natl Acad Sci U S A*, 110(33), 13481-6.
- Ghandhi, S. A., Yaghoubian, B. & Amundson, S. A. 2008. Global Gene Expression Analyses of Bystander and Alpha Particle Irradiated Normal Human Lung Fibroblasts: Synchronous and Differential Responses. *BMC Med Genomics*, 1, 63.
- Gialeli, C., Theocharis, A. D. & Karamanos, N. K. 2011. Roles of Matrix Metalloproteinases in Cancer Progression and Their Pharmacological Targeting. *Febs Journal*, 278(1), 16-27.
- Gilchrest, B. A. 1989. Skin Aging and Photoaging: An Overview. *J Am Acad Dermatol*, 21(3 Pt 2), 610-3.
- Gilchrest, B. A. 2013. Photoaging. *J Invest Dermatol*, 133(E1), E2-6.
- Gillet, L. C. & Schärer, O. D. 2006. Molecular Mechanisms of Mammalian Global Genome Nucleotide Excision Repair. *Chem Rev*, 106(2), 253-76.
- Godar, D. E. & Lucas, A. D. 1995. Spectral Dependence of UV-Induced Immediate and Delayed Apoptosis: The Role of Membrane and DNA Damage. *Photochem Photobiol*, 62(1), 108-13.
- Godar, D. E., Miller, S. A. & Thomas, D. P. 1994. Immediate and Delayed Apoptotic Cell Death Mechanisms: UVA Versus UVB and UVC Radiation. *Cell Death Differ*, 1(1), 59-66.

- Gomez, D., Alonso, D., Yoshiji, H. & Thorgeirsson, U. 1997. Tissue Inhibitors of Metalloproteinases: Structure, Regulation and Biological Functions. *European journal of cell biology*, 74(2), 111.
- Green, D. R. 2000. Apoptotic Pathways: Paper Wraps Stone Blunts Scissors. *Cell*, 102(1), 1-4.
- Greenman, C., Stephens, P., Smith, R., Dalgliesh, G. L., Hunter, C., Bignell, G., Davies, H., Teague, J., Butler, A., Stevens, C., Edkins, S., O'meara, S., Vastrik, I., Schmidt, E. E., Avis, T., Barthorpe, S., Bhamra, G., Buck, G., Choudhury, B., Clements, J., Cole, J., Dicks, E., Forbes, S., Gray, K., Halliday, K., Harrison, R., Hills, K., Hinton, J., Jenkinson, A., Jones, D., Menzies, A., Mironenko, T., Perry, J., Raine, K., Richardson, D., Shepherd, R., Small, A., Tofts, C., Varian, J., Webb, T., West, S., Widaa, S., Yates, A., Cahill, D. P., Louis, D. N., Goldstraw, P., Nicholson, A. G., Brasseur, F., Looijenga, L., Weber, B. L., Chiew, Y. E., Defazio, A., Greaves, M. F., Green, A. R., Campbell, P., Birney, E., Easton, D. F., Chenevix-Trench, G., Tan, M. H., Khoo, S. K., Teh, B. T., Yuen, S. T., Leung, S. Y., Wooster, R., Futreal, P. A. & Stratton, M. R. 2007. Patterns of Somatic Mutation in Human Cancer Genomes. *Nature*, 446(7132), 153-8.
- Greinert, R., Volkmer, B., Henning, S., Breitbart, E. W., Greulich, K. O., Cardoso, M. C. & Rapp, A. 2012a. UVA-Induced DNA Double-Strand Breaks Result from the Repair of Clustered Oxidative DNA Damages. *Nucleic Acids Res*, 40(20), 10263-73.
- Greinert, R., Volkmer, B., Henning, S., Breitbart, E. W., Greulich, K. O., Cardoso, M. C. & Rapp, A. 2012b. UVA-Induced DNA Double-Strand Breaks Result from the Repair of Clustered Oxidative DNA Damages. *Nucleic Acids Research*, 40(20), 10263-10273.
- Grether-Beck, S., Bonizzi, G., Schmitt-Brenden, H., Felsner, I., Timmer, A., Sies, H., Johnson, J. P., Piette, J. & Krutmann, J. 2000. Non-Enzymatic Triggering of the Ceramide Signalling Cascade by Solar UVA Radiation. *EMBO J*, 19(21), 5793-800.
- Grether-Beck, S., Olaizola-Horn, S., Schmitt, H., Grewe, M., Jahnke, A., Johnson, J. P., Briviba, K., Sies, H. & Krutmann, J. 1996. Activation of Transcription Factor AP-2 Mediates Uva Radiation- and Singlet Oxygen-Induced Expression of the Human Intercellular Adhesion Molecule 1 Gene. *Proc Natl Acad Sci U S A*, 93(25), 14586-91.
- Griewank, K. G., Murali, R., Schilling, B., Schimming, T., Möller, I., Moll, I., Schwaborn, M., Sucker, A., Zimmer, L., Schadendorf, D. & Hillen, U. 2013. Tert Promoter Mutations Are Frequent in Cutaneous Basal Cell Carcinoma and Squamous Cell Carcinoma. *PLoS One*, 8(11), e80354.

- Griffiths, C. E., Russman, A. N., Majmudar, G., Singer, R. S., Hamilton, T. A. & Voorhees, J. J. 1993. Restoration of Collagen Formation in Photodamaged Human Skin by Tretinoin (Retinoic Acid). *N Engl J Med*, 329(8), 530-5.
- Gruber, F., Mayer, H., Lengauer, B., Mlitz, V., Sanders, J. M., Kadl, A., Bilban, M., De Martin, R., Wagner, O. & Kensler, T. W. 2010. Nf-E2-Related Factor 2 Regulates the Stress Response to UVA-1-Oxidized Phospholipids in Skin Cells. *The FASEB Journal*, 24(1), 39-48.
- Günes, C. & Rudolph, K. L. 2013. The Role of Telomeres in Stem Cells and Cancer. *Cell*, 152(3), 390-3.
- Hahn, H., Wicking, C., Zaphiropoulous, P. G., Gailani, M. R., Shanley, S., Chidambaram, A., Vorechovsky, I., Holmberg, E., Uden, A. B., Gillies, S., Negus, K., Smyth, I., Pressman, C., Leffell, D. J., Gerrard, B., Goldstein, A. M., Dean, M., Toftgard, R., Chenevix-Trench, G., Wainwright, B. & Bale, A. E. 1996. Mutations of the Human Homolog of Drosophila Patched in the Nevoid Basal Cell Carcinoma Syndrome. *Cell*, 85(6), 841-51.
- Harper, E., Bloch, K. J. & Gross, J. 1971. The Zymogen of Tadpole Collagenase. *Biochemistry*, 10(16), 3035-41.
- Haywood, R. M., Lee, M. & Linge, C. 2006. Synthetic Melanin Is a Model for Soluble Natural Eumelanin in UVA-Photosensitised Superoxide Production. *J Photochem Photobiol B*, 82(3), 224-35.
- He, Y. Y., Huang, J. L., Block, M. L., Hong, J. S. & Chignell, C. F. 2005. Role of Phagocyte Oxidase in UVA-Induced Oxidative Stress and Apoptosis in Keratinocytes. *J Invest Dermatol*, 125(3), 560-6.
- He, Y. Y., Huang, J. L. & Chignell, C. F. 2004. Delayed and Sustained Activation of Extracellular Signal-Regulated Kinase in Human Keratinocytes by UVA: Implications in Carcinogenesis. *J Biol Chem*, 279(51), 53867-74.
- Hei, T. K., Zhou, H., Ivanov, V. N., Hong, M., Lieberman, H. B., Brenner, D. J., Amundson, S. A. & Geard, C. R. 2008. Mechanism of Radiation-Induced Bystander Effects: A Unifying Model. *J Pharm Pharmacol*, 60(8), 943-50.
- Helfrich, Y. R., Sachs, D. L. & Voorhees, J. J. 2008. Overview of Skin Aging and Photoaging. *Dermatol Nurs*, 20(3), 177-83; quiz 184.
- Herrmann, G., Wlaschek, M., Lange, T. S., Prenzel, K., Goerz, G. & Scharffetter-Kochanek, K. 1993. Uva Irradiation Stimulates the Synthesis of Various Matrix-Metalloproteinases (MMPs) in Cultured Human Fibroblasts. *Exp Dermatol*, 2(2), 92-7.

- Hodis, E., Watson, I. R., Kryukov, G. V., Arold, S. T., Imielinski, M., Theurillat, J. P., Nickerson, E., Auclair, D., Li, L., Place, C., Dicara, D., Ramos, A. H., Lawrence, M. S., Cibulskis, K., Sivachenko, A., Voet, D., Saksena, G., Stransky, N., Onofrio, R. C., Winckler, W., Ardlie, K., Wagle, N., Wargo, J., Chong, K., Morton, D. L., Stenke-Hale, K., Chen, G., Noble, M., Meyerson, M., Ladbury, J. E., Davies, M. A., Gershenwald, J. E., Wagner, S. N., Hoon, D. S., Schadendorf, D., Lander, E. S., Gabriel, S. B., Getz, G., Garraway, L. A. & Chin, L. 2012. A Landscape of Driver Mutations in Melanoma. *Cell*, 150(2), 251-63.
- Hoeijmakers, J. H. 2001. Dna Repair Mechanisms. *Maturitas*, 38(1), 17-22; discussion 22-3.
- Horn, S., Figl, A., Rachakonda, P. S., Fischer, C., Sucker, A., Gast, A., Kadel, S., Moll, I., Nagore, E., Hemminki, K., Schadendorf, D. & Kumar, R. 2013. TERT Promoter Mutations in Familial and Sporadic Melanoma. *Science*, 339(6122), 959-61.
- Hsu-Wong, S., Katchman, S. D., Ledo, I., Wu, M., Khillan, J., Bashir, M. M., Rosenbloom, J. & Uitto, J. 1994. Tissue-Specific and Developmentally Regulated Expression of Human Elastin Promoter Activity in Transgenic Mice. *J Biol Chem*, 269(27), 18072-5.
- Hu, B., Wu, L., Han, W., Zhang, L., Chen, S., Xu, A., Hei, T. K. & Yu, Z. 2006. The Time and Spatial Effects of Bystander Response in Mammalian Cells Induced by Low Dose Radiation. *Carcinogenesis*, 27(2), 245-51.
- Huang, F. W., Hodis, E., Xu, M. J., Kryukov, G. V., Chin, L. & Garraway, L. A. 2013. Highly Recurrent TERT Promoter Mutations in Human Melanoma. *Science*, 339(6122), 957-9.
- Huang, T. T. & D'andrea, A. D. 2006. Regulation of DNA Repair by Ubiquitylation. *Nat Rev Mol Cell Biol*, 7(5), 323-34.
- Huang, X. X., Scolyer, R. A., Abubakar, A. & Halliday, G. M. 2012. Human 8-Oxoguanine-DNA Glycosylase-1 Is Downregulated in Human Basal Cell Carcinoma. *Mol Genet Metab*, 106(1), 127-30.
- Huen, M. S., Huang, J., Leung, J. W., Sy, S. M., Leung, K. M., Ching, Y. P., Tsao, S. W. & Chen, J. 2010. Regulation of Chromatin Architecture by the PWWP Domain-Containing DNA Damage-Responsive Factor Expand1/Mum1. *Mol Cell*, 37(6), 854-64.
- Hull, M. A. 2005. Cyclooxygenase-2: How Good Is It as a Target for Cancer Chemoprevention? *Eur J Cancer*, 41(13), 1854-63.
- Hussein, M. R. 2005. Ultraviolet Radiation and Skin Cancer: Molecular Mechanisms. *Journal of cutaneous pathology*, 32(3), 191-205.
- Ibuki, Y., Allanson, M., Dixon, K. M. & Reeve, V. E. 2007. Radiation Sources Providing Increased UVA/UVB Ratios Attenuate the Apoptotic Effects of the UVB Waveband

- UVA-Dose-Dependently in Hairless Mouse Skin. *J Invest Dermatol*, 127(9), 2236-44.
- Ichijima, Y., Sakasai, R., Okita, N., Asahina, K., Mizutani, S. & Teraoka, H. 2005. Phosphorylation of Histone H2AX at M Phase in Human Cells without DNA Damage Response. *Biochem Biophys Res Commun*, 336(3), 807-12.
- Igarashi, T., Abe, M., Oikawa, M., Nukiwa, T. & Sato, Y. 2001. Retinoic Acids Repress the Expression of Ets-1 in Endothelial Cells. *Tohoku J Exp Med*, 194(1), 35-43.
- Ignatz, R. A. & Massagué, J. 1986. Transforming Growth Factor-Beta Stimulates the Expression of Fibronectin and Collagen and Their Incorporation into the Extracellular Matrix. *J Biol Chem*, 261(9), 4337-45.
- Jang, E. R., Choi, J. D., Park, M. A., Jeong, G., Cho, H. & Lee, J. S. 2010. ATM Modulates Transcription in Response to Histone Deacetylase Inhibition as Part of Its DNA Damage Response. *Exp Mol Med*, 42(3), 195-204.
- Jayaraman, S. S., Rayhan, D. J., Hazany, S. & Kolodney, M. S. 2014. Mutational Landscape of Basal Cell Carcinomas by Whole-Exome Sequencing. *J Invest Dermatol*, 134(1), 213-20.
- Jean, C., Bogdanowicz, P., Haure, M. J., Castex-Rizzi, N., Fournié, J. J. & Laurent, G. 2011. Uva-Activated Synthesis of Metalloproteinases 1, 3 and 9 Is Prevented by a Broad-Spectrum Sunscreen. *Photodermatol Photoimmunol Photomed*, 27(6), 318-24.
- Jiang, S., Liu, X. M., Dai, X., Zhou, Q., Lei, T. C., Beermann, F., Wakamatsu, K. & Xu, S. Z. 2010. Regulation of Dhica-Mediated Antioxidation by Dopachrome Tautomerase: Implication for Skin Photoprotection against UVA Radiation. *Free Radic Biol Med*, 48(9), 1144-51.
- Jiang, Y., Rabbi, M., Kim, M., Ke, C., Lee, W., Clark, R., Mieczkowski, P. & Marszalek, P. 2009. UVA Generates Pyrimidine Dimers in DNA Directly. *Biophysical Journal*, 96(3), 1151-1158.
- Jimbow, K., Chen, H., Park, J. S. & Thomas, P. D. 2001. Increased Sensitivity of Melanocytes to Oxidative Stress and Abnormal Expression of Tyrosinase-Related Protein in Vitiligo. *Br J Dermatol*, 144(1), 55-65.
- Jimenez, S. A., Varga, J., Olsen, A., Li, L., Diaz, A., Herhal, J. & Koch, J. 1994. Functional Analysis of Human Alpha 1(I) Procollagen Gene Promoter. Differential Activity in Collagen-Producing and -Nonproducing Cells and Response to Transforming Growth Factor Beta 1. *J Biol Chem*, 269(17), 12684-91.
- Johnson, G. L. & Lapadat, R. 2002. Mitogen-Activated Protein Kinase Pathways Mediated by ERK, JNK, and P38 Protein Kinases. *Science*, 298(5600), 1911-2.

- Kagoura, M., Toyoda, M., Matsui, C. & Morohashi, M. 2001. Immunohistochemical Expression of Cyclooxygenase-2 in Skin Cancers. *J Cutan Pathol*, 28(6), 298-302.
- Kanavy, H. E. & Gerstenblith, M. R. 2011. Ultraviolet Radiation and Melanoma. *Semin Cutan Med Surg*, 30(4), 222-8.
- Kappes, U. P., Luo, D., Potter, M., Schulmeister, K. & Runger, T. M. 2006. Short- and Long-Wave UV Light (UVB and UVA) Induce Similar Mutations in Human Skin Cells. *J Invest Dermatol*, 126(3), 667-75.
- Kelfkens, G., De Gruijl, F. R. & Van Der Leun, J. C. 1990. Ozone Depletion and Increase in Annual Carcinogenic Ultraviolet Dose. *Photochem Photobiol*, 52(4), 819-23.
- Keyse, S. M. & Tyrrell, R. M. 1989. Heme Oxygenase Is the Major 32-Kda Stress Protein Induced in Human Skin Fibroblasts by UVA Radiation, Hydrogen Peroxide, and Sodium Arsenite. *Proc Natl Acad Sci U S A*, 86(1), 99-103.
- Keyse, S. M. & Tyrrell, R. M. 1990. Induction of the Heme Oxygenase Gene in Human Skin Fibroblasts by Hydrogen Peroxide and UVA (365 Nm) Radiation: Evidence for the Involvement of the Hydroxyl Radical. *Carcinogenesis*, 11(5), 787-91.
- Kick, G., Messer, G., Plewig, G., Kind, P. & Goetz, A. E. 1996. Strong and Prolonged Induction of C-JUN and C-Fos Proto-Oncogenes by Photodynamic Therapy. *Br J Cancer*, 74(1), 30-6.
- Kielbassa, C., Roza, L. & Epe, B. 1997. Wavelength Dependence of Oxidative DNA Damage Induced by UV and Visible Light. *Carcinogenesis*, 18(4), 811-6.
- Killela, P. J., Reitman, Z. J., Jiao, Y., Bettegowda, C., Agrawal, N., Diaz, L. A., Friedman, A. H., Friedman, H., Gallia, G. L., Giovanella, B. C., Grollman, A. P., He, T. C., He, Y., Hruban, R. H., Jallo, G. I., Mandahl, N., Meeker, A. K., Mertens, F., Netto, G. J., Rasheed, B. A., Riggins, G. J., Rosenquist, T. A., Schiffman, M., Shih, I. M., Theodorescu, D., Torbenson, M. S., Velculescu, V. E., Wang, T. L., Wentzensen, N., Wood, L. D., Zhang, M., Mclendon, R. E., Bigner, D. D., Kinzler, K. W., Vogelstein, B., Papadopoulos, N. & Yan, H. 2013. TERT Promoter Mutations Occur Frequently in Gliomas and a Subset of Tumors Derived from Cells with Low Rates of Self-Renewal. *Proc Natl Acad Sci U S A*, 110(15), 6021-6.
- Kim, J. K., Patel, D. & Choi, B. S. 1995. Contrasting Structural Impacts Induced by Cis-Syn Cyclobutane Dimer and (6-4) Adduct in DNA Duplex Decamers: Implication in Mutagenesis and Repair Activity. *Photochem Photobiol*, 62(1), 44-50.
- Kimlin, M. G., Parisi, A. V., Sabburg, J. & Downs, N. J. 2002. Understanding the UVA Environment at a Sub-Tropical Site and Its Consequent Impact on Human UVA Exposure. *Photochem Photobiol Sci*, 1(7), 478-82.

- Kligman, A. M. 1969. Early Destructive Effect of Sunlight on Human Skin. *JAMA*, 210(13), 2377-80.
- Klotz, L. O., Briviba, K. & Sies, H. 1997. Singlet Oxygen Mediates the Activation of JNK by UVA Radiation in Human Skin Fibroblasts. *FEBS Lett*, 408(3), 289-91.
- Klotz, L. O., Holbrook, N. J. & Sies, H. 2001. UVA and Singlet Oxygen as Inducers of Cutaneous Signaling Events. *Curr Probl Dermatol*, 29, 95-113.
- Kobayashi, N., Nakagawa, A., Muramatsu, T., Yamashina, Y., Shirai, T., Hashimoto, M. W., Ishigaki, Y., Ohnishi, T. & Mori, T. 1998. Supranuclear Melanin Caps Reduce Ultraviolet Induced DNA Photoproducts in Human Epidermis. *J Invest Dermatol*, 110(5), 806-10.
- Koch, H., Wittern, K. P. & Bergemann, J. 2001. In Human Keratinocytes the Common Deletion Reflects Donor Variabilities Rather Than Chronologic Aging and Can Be Induced by Ultraviolet A Irradiation. *J Invest Dermatol*, 117(4), 892-7.
- Koehler, M., Konig, K., Elsner, P., Buckle, R. & Kaatz, M. 2006. In Vivo Assessment of Human Skin Aging by Multiphoton Laser Scanning Tomography. *Optics Letters*, 31(19), 2879-2881.
- Kohler, B. A., Ward, E., Mccarthy, B. J., Schymura, M. J., Ries, L. A., Ehemann, C., Jemal, A., Anderson, R. N., Ajani, U. A. & Edwards, B. K. 2011. Annual Report to the Nation on the Status of Cancer, 1975-2007, Featuring Tumors of the Brain and Other Nervous System. *J Natl Cancer Inst*, 103(9), 714-36.
- Koob, T. J., Jeffrey, J. J., Eisen, A. Z. & Bauer, E. A. 1980. Hormonal Interactions in Mammalian Collagenase Regulation. Comparative Studies in Human Skin and Rat Uterus. *Biochim Biophys Acta*, 629(1), 13-23.
- Krauthammer, M., Kong, Y., Bacchicocchi, A., Evans, P., Pornputtpong, N., Wu, C., Mccusker, J. P., Ma, S., Cheng, E., Straub, R., Serin, M., Bosenberg, M., Ariyan, S., Narayan, D., Sznol, M., Kluger, H. M., Mane, S., Schlessinger, J., Lifton, R. P. & Halaban, R. 2015. Exome Sequencing Identifies Recurrent Mutations in Nf1 and Rasopathy Genes in Sun-Exposed Melanomas. *Nat Genet*, 47(9), 996-1002.
- Krauthammer, M., Kong, Y., Ha, B. H., Evans, P., Bacchicocchi, A., Mccusker, J. P., Cheng, E., Davis, M. J., Goh, G., Choi, M., Ariyan, S., Narayan, D., Dutton-Regester, K., Capatana, A., Holman, E. C., Bosenberg, M., Sznol, M., Kluger, H. M., Brash, D. E., Stern, D. F., Materin, M. A., Lo, R. S., Mane, S., Ma, S., Kidd, K. K., Hayward, N. K., Lifton, R. P., Schlessinger, J., Boggan, T. J. & Halaban, R. 2012. Exome Sequencing Identifies Recurrent Somatic Rac1 Mutations in Melanoma. *Nat Genet*, 44(9), 1006-14.
- Kulms, D. & Schwarz, T. 2002. Independent Contribution of Three Different Pathways to Ultraviolet-B-Induced Apoptosis. *Biochem Pharmacol*, 64(5-6), 837-41.

- Kuluncsics, Z., Perdiz, D., Brulay, E., Muel, B. & Sage, E. 1999. Wavelength Dependence of Ultraviolet-Induced DNA Damage Distribution: Involvement of Direct or Indirect Mechanisms and Possible Artefacts. *J Photochem Photobiol B*, 49(1), 71-80.
- Kumar, N. M. & Gilula, N. B. 1992. Molecular Biology and Genetics of Gap Junction Channels. *Semin Cell Biol*, 3(1), 3-16.
- Kurihara, H., Torigoe, S., Omura, M., Saito, K., Kurihara, M. & Matsubara, S. 1998. DNA Fragmentation Induced by a Cytoplasmic Extract from Irradiated Cells. *Radiation research*, 150(3), 269-274.
- Kusewitt, D. F., Applegate, L. A. & Ley, R. D. 1991. Ultraviolet Radiation-Induced Skin Tumors in a South American Opossum (*Monodelphis Domestica*). *Vet Pathol*, 28(1), 55-65.
- Kvam, E. & Tyrrell, R. M. 1997. Induction of Oxidative DNA Base Damage in Human Skin Cells by UV and near Visible Radiation. *Carcinogenesis*, 18(12), 2379-84.
- Lambert, E., Dassé, E., Haye, B. & Petitfrère, E. 2004. TIMPs as Multifacial Proteins. *Crit Rev Oncol Hematol*, 49(3), 187-98.
- Lambeth, J. D. 2004. Nox Enzymes and the Biology of Reactive Oxygen. *Nature Reviews Immunology*, 4(3), 181-189.
- Lambeth, J. D. 2007. Nox Enzymes, Ros, and Chronic Disease: An Example of Antagonistic Pleiotropy. *Free Radical Biology and Medicine*, 43(3), 332-347.
- Landa, I., Ganly, I., Chan, T. A., Mitsutake, N., Matsuse, M., Ibrahimasic, T., Ghossein, R. A. & Fagin, J. A. 2013. Frequent Somatic Tert Promoter Mutations in Thyroid Cancer: Higher Prevalence in Advanced Forms of the Disease. *J Clin Endocrinol Metab*, 98(9), E1562-6.
- Larsen, E., Kwon, K., Coin, F., Egly, J. M. & Klungland, A. 2004. Transcription Activities at 8-Oxog Lesions in DNA. *DNA Repair (Amst)*, 3(11), 1457-68.
- Lautier, D., Luscher, P. & Tyrrell, R. M. 1992. Endogenous Glutathione Levels Modulate Both Constitutive and UVA Radiation/Hydrogen Peroxide Inducible Expression of the Human Heme Oxygenase Gene. *Carcinogenesis*, 13(2), 227-32.
- Lee, C. H., Wu, S. B., Hong, C. H., Yu, H. S. & Wei, Y. H. 2013. Molecular Mechanisms of UV-Induced Apoptosis and Its Effects on Skin Residential Cells: The Implication in UV-Based Phototherapy. *Int J Mol Sci*, 14(3), 6414-35.
- Lee, J. H. & Paull, T. T. 2005. ATM Activation by DNA Double-Strand Breaks through the Mre11-Rad50-Nbs1 Complex. *Science*, 308(5721), 551-4.
- Lee, J. S. 2007. Activation of ATM-Dependent DNA Damage Signal Pathway by a Histone Deacetylase Inhibitor, Trichostatin A. *Cancer Res Treat*, 39(3), 125-30.

- Lehman, T. A., Modali, R., Boukamp, P., Stanek, J., Bennett, W. P., Welsh, J. A., Metcalf, R. A., Stampfer, M. R., Fusenig, N. & Rogan, E. M. 1993. P53 Mutations in Human Immortalized Epithelial Cell Lines. *Carcinogenesis*, 14(5), 833-9.
- Lewis, K. G., Bercovitch, L., Dill, S. W. & Robinson-Bostom, L. 2004. Acquired Disorders of Elastic Tissue: Part I. Increased Elastic Tissue and Solar Elastotic Syndromes. *Journal of the American Academy of Dermatology*, 51(1), 1-21.
- Lewis, D.A., Yi, Q., Travers, J.B. and Spandau, D.F., 2008. UVB-induced senescence in human keratinocytes requires a functional insulin-like growth factor-1 receptor and p53. *Molecular biology of the cell*, 19(4), pp.1346-1353.
- Ley, R. D. 1997. Ultraviolet Radiation A-Induced Precursors of Cutaneous Melanoma in *Monodelphis Domestica*. *Cancer Res*, 57(17), 3682-4.
- Li, K., Li, Y., Shelton, J. M., Richardson, J. A., Spencer, E., Chen, Z. J., Wang, X. & Williams, R. S. 2000. Cytochrome C Deficiency Causes Embryonic Lethality and Attenuates Stress-Induced Apoptosis. *Cell*, 101(4), 389-99.
- Liao, C. S., Zhuo, Z. Y., Yu, J. Y., Chao, P. H. G. & Chu, S. W. In Situ Observation of Collagen Thermal Denaturation by Second Harmonic Generation Microscopy. BiOS, 2010. International Society for Optics and Photonics, 756928-756928-6.
- Limoli, C. L. & Ward, J. F. 1994. DNA Damage in Bromodeoxyuridine Substituted Sv40 Dna and Minichromosomes Following UVA Irradiation in the Presence of Hoechst Dye 33258. *Int J Radiat Biol*, 66(6), 717-28.
- Lin, A. & Dibling, B. 2002. The True Face of JNK Activation in Apoptosis. *Aging Cell*, 1(2), 112-6.
- Little, J. B., Azzam, E. I., De Toledo, S. M. & Nagasawa, H. 2002. Bystander Effects: Intercellular Transmission of Radiation Damage Signals. *Radiat Prot Dosimetry*, 99(1-4), 159-62.
- Little, J. B., Gorgojo, L. & Vetrovs, H. 1990. Delayed Appearance of Lethal and Specific Gene Mutations in Irradiated Mammalian Cells. *International Journal of Radiation Oncology\* Biology\* Physics*, 19(6), 1425-1429.
- Little, J. B., Nagasawa, H., Pfenning, T. & Vetrovs, H. 1997. Radiation-Induced Genomic Instability: Delayed Mutagenic and Cytogenetic Effects of X Rays and Alpha Particles. *Radiation research*, 148(4), 299-307.
- Lohi, J., Wilson, C. L., Roby, J. D. & Parks, W. C. 2001. Epilysin, a Novel Human Matrix Metalloproteinase (MMP-28) Expressed in Testis and Keratinocytes and in Response to Injury. *J Biol Chem*, 276(13), 10134-44.
- Lomas, A., Leonardi-Bee, J. & Bath-Hextall, F. 2012. A Systematic Review of Worldwide Incidence of Nonmelanoma Skin Cancer. *Br J Dermatol*, 166(5), 1069-80.

- Lomax, M. E., Cunniffe, S. & O'Neill, P. 2004. 8-Oxog Retards the Activity of the Ligase Iii/Xrcc1 Complex During the Repair of a Single-Strand Break, When Present within a Clustered DNA Damage Site. *DNA Repair (Amst)*, 3(3), 289-99.
- López-Camarillo, C., Ocampo, E. A., Casamichana, M. L., Pérez-Plasencia, C., Alvarez-Sánchez, E. & Marchat, L. A. 2012. Protein Kinases and Transcription Factors Activation in Response to UV-Radiation of Skin: Implications for Carcinogenesis. *Int J Mol Sci*, 13(1), 142-72.
- López-Otín, C. & Matrisian, L. M. 2007. Emerging Roles of Proteases in Tumour Suppression. *Nature reviews cancer*, 7(10), 800-808.
- Mah, L. J., El-Osta, A. & Karagiannis, T. C. 2010. GammaH2AX: A Sensitive Molecular Marker of DNA Damage and Repair. *Leukemia*, 24(4), 679-86.
- Mahns, A., Wolber, R., Stäb, F., Klotz, L. O. & Sies, H. 2004. Contribution of UVB and UVA to UV-Dependent Stimulation of Cyclooxygenase-2 Expression in Artificial Epidermis. *Photochem Photobiol Sci*, 3(3), 257-62.
- Maiorino, A., De Simone, C., Perino, F., Caldarola, G. & Peris, K. 2016. Melanoma and Non-Melanoma Skin Cancer in Psoriatic Patients Treated with High-Dose Phototherapy. *J Dermatolog Treat*, 1-5.
- Maldonado, J. L., Fridlyand, J., Patel, H., Jain, A. N., Busam, K., Kageshita, T., Ono, T., Albertson, D. G., Pinkel, D. & Bastian, B. C. 2003. Determinants of BRAF Mutations in Primary Melanomas. *J Natl Cancer Inst*, 95(24), 1878-90.
- Malemud, C. J. 2006. Matrix Metalloproteinases (MMPs) in Health and Disease: An Overview. *Front Biosci*, 11(1), 1696-1701.
- Mar, V. J., Wong, S. Q., Li, J., Scolyer, R. A., Mclean, C., Papenfuss, A. T., Tothill, R. W., Kakavand, H., Mann, G. J., Thompson, J. F., Behren, A., Cebon, J. S., Wolfe, R., Kelly, J. W., Dobrovic, A. & McArthur, G. A. 2013. Braf/Nras Wild-Type Melanomas Have a High Mutation Load Correlating with Histologic and Molecular Signatures of UV Damage. *Clin Cancer Res*, 19(17), 4589-98.
- Marples, B., Wouters, B. & Joiner, M. 2003. An Association between the Radiation-Induced Arrest of G2-Phase Cells and Low-Dose Hyper-Radiosensitivity: A Plausible Underlying Mechanism? *Radiation research*, 160(1), 38-45.
- Matsumoto, H., Hayashi, S., Hatashita, M., Ohnishi, K., Shioura, H., Ohtsubo, T., Kitai, R., Ohnishi, T. & Kano, E. 2001. Induction of Radioresistance by a Nitric Oxide-Mediated Bystander Effect. *Radiat Res*, 155(3), 387-96.
- Matsuoka, S., Huang, M. & Elledge, S. J. 1998. Linkage of ATM to Cell Cycle Regulation by the Chk2 Protein Kinase. *Science*, 282(5395), 1893-7.

- Matthews, Y. J., Halliday, G. M., Phan, T. A. & Damian, D. L. 2010. Wavelength Dependency for UVA-Induced Suppression of Recall Immunity in Humans. *Journal of dermatological science*, 59(3), 192-197.
- Mauviel, A. 1993. Cytokine Regulation of Metalloproteinase Gene Expression. *J Cell Biochem*, 53(4), 288-95.
- Mcmanus, K. J. & Hendzel, M. J. 2005. ATM-Dependent DNA Damage-Independent Mitotic Phosphorylation of H2AX in Normally Growing Mammalian Cells. *Mol Biol Cell*, 16(10), 5013-25.
- Mellon, I., Spivak, G. & Hanawalt, P. C. 1987. Selective Removal of Transcription-Blocking DNA Damage from the Transcribed Strand of the Mammalian DHFR Gene. *Cell*, 51(2), 241-9.
- Merwald, H., Klosner, G., Kokesch, C., Der-Petrossian, M., Hönigsmann, H. & Trautinger, F. 2005. UVA-Induced Oxidative Damage and Cytotoxicity Depend on the Mode of Exposure. *Journal of Photochemistry and Photobiology B: Biology*, 79(3), 197-207.
- Miller, C. C., Hale, P. & Pentland, A. P. 1994. Ultraviolet B Injury Increases Prostaglandin Synthesis through a Tyrosine Kinase-Dependent Pathway. Evidence for UVB-Induced Epidermal Growth Factor Receptor Activation. *J Biol Chem*, 269(5), 3529-33.
- Minden, A., Lin, A., McMahon, M., Lange-Carter, C., Dérijard, B., Davis, R. J., Johnson, G. L. & Karin, M. 1994. Differential Activation of ERJ and JNK Mitogen-Activated Protein Kinases by Raf-1 and MEKK. *Science*, 266(5191), 1719-23.
- Mitchell, D. L., Fernandez, A. A., Nairn, R. S., Garcia, R., Paniker, L., Trono, D., Thames, H. D. & Gimenez-Conti, I. 2010. Ultraviolet A Does Not Induce Melanomas in a Xiphophorus Hybrid Fish Model. *Proc Natl Acad Sci U S A*, 107(20), 9329-34.
- Moan, J., Dahlback, A. & Setlow, R. B. 1999. Epidemiological Support for an Hypothesis for Melanoma Induction Indicating a Role for UVA Radiation. *Photochem Photobiol*, 70(2), 243-7.
- Moreno, G. 1986. Photosensitization of Mammalian Cells by Psoralens and Porphyrins. *Biochimie*, 68(6), 869-873.
- Mothersill, C., Rea, D., Wright, E. G., Lorimore, S. A., Murphy, D., Seymour, C. B. & O'malley, K. 2001. Individual Variation in the Production of a 'Bystander Signal' Following Irradiation of Primary Cultures of Normal Human Urothelium. *Carcinogenesis*, 22(9), 1465-71.
- Mothersill, C. & Seymour, C. 1998. Cell-Cell Contact During Gamma Irradiation Is Not Required to Induce a Bystander Effect in Normal Human Keratinocytes: Evidence

- for Release During Irradiation of a Signal Controlling Survival into the Medium. *Radiation research*, 149(3), 256-262.
- Mouret, S., Baudouin, C., Charveron, M., Favier, A., Cadet, J. & Douki, T. 2006. Cyclobutane Pyrimidine Dimers Are Predominant DNA Lesions in Whole Human Skin Exposed to UVA Radiation. *Proc Natl Acad Sci U S A*, 103(37), 13765-70.
- Mouret, S., Leccia, M. T., Bourrain, J. L., Douki, T. & Beani, J. C. 2011. Individual Photosensitivity of Human Skin and UVA-Induced Pyrimidine Dimers in DNA. *J Invest Dermatol*, 131(7), 1539-46.
- Mouret, S., Philippe, C., Gracia-Chantegrel, J., Banyasz, A., Karpati, S., Markovitsi, D. & Douki, T. 2010. UVA-Induced Cyclobutane Pyrimidine Dimers in DNA: A Direct Photochemical Mechanism? *Organic & Biomolecular Chemistry*, 8(7), 1706-1711.
- Murphy, J. E., Nugent, S., Seymour, C. & Mothersill, C. 2005. Mitochondrial Dna Point Mutations and a Novel Deletion Induced by Direct Low-LET Radiation and by Medium from Irradiated Cells. *Mutat Res*, 585(1-2), 127-36.
- Murray, H. C., Maltby, V. E., Smith, D. W. & Bowden, N. A. 2015. Nucleotide Excision Repair Deficiency in Melanoma in Response to UVA. *Exp Hematol Oncol*, 5, 6.
- Nagasawa, H. & Little, J. B. 1992. Induction of Sister Chromatid Exchanges by Extremely Low Doses of A-Particles. *Cancer research*, 52(22), 6394-6396.
- Nagasawa, H. & Little, J. B. 1999. Unexpected Sensitivity to the Induction of Mutations by Very Low Doses of Alpha-Particle Radiation: Evidence for a Bystander Effect. *Radiation research*, 152(5), 552-557.
- Nance, M. A. & Berry, S. A. 1992. Cockayne Syndrome: Review of 140 Cases. *Am J Med Genet*, 42(1), 68-84.
- Narayanan, P., Goodwin, E. H. & Lehnert, B. 1997. A Particles Initiate Biological Production of Superoxide Anions and Hydrogen Peroxide in Human Cells. *Cancer research*, 57(18), 3963-3971.
- Nataraj, A. J., Trent, J. C. & Ananthaswamy, H. N. 1995. P53 Gene Mutations and Photocarcinogenesis. *Photochem Photobiol*, 62(2), 218-30.
- Nelson, A. R., Fingleton, B., Rothenberg, M. L. & Matrisian, L. M. 2000. Matrix Metalloproteinases: Biologic Activity and Clinical Implications. *Journal of Clinical Oncology*, 18(5), 1135-1135.
- Network, C. G. A. 2015. Genomic Classification of Cutaneous Melanoma. *Cell*, 161(7), 1681-96.
- Nikolaev, S. I., Rimoldi, D., Iseli, C., Valsesia, A., Robyr, D., Gehrig, C., Harshman, K., Guipponi, M., Bukach, O., Zoete, V., Michielin, O., Muehlethaler, K., Speiser, D., Beckmann, J. S., Xenarios, I., Halazonetis, T. D., Jongeneel, C. V., Stevenson, B. J. &

- Antonarakis, S. E. 2012. Exome Sequencing Identifies Recurrent Somatic MAP2K1 and MAP2K2 Mutations in Melanoma. *Nat Genet*, 44(2), 133-9.
- Nishiura, H., Kumagai, J., Kashino, G., Okada, T., Tano, K. & Watanabe, M. 2012. The Bystander Effect Is a Novel Mechanism of UVA-Induced Melanogenesis. *Photochem Photobiol*, 88(2), 389-97.
- Noonan, F. P., Otsuka, T., Bang, S., Anver, M. R. & Merlino, G. 2000. Accelerated Ultraviolet Radiation-Induced Carcinogenesis in Hepatocyte Growth Factor/Scatter Factor Transgenic Mice. *Cancer Res*, 60(14), 3738-43.
- Noonan, F. P., Zaidi, M. R., Wolnicka-Glubisz, A., Anver, M. R., Bahn, J., Wielgus, A., Cadet, J., Douki, T., Mouret, S., Tucker, M. A., Popratiloff, A., Merlino, G. & De Fabo, E. C. 2012. Melanoma Induction by Ultraviolet A but Not Ultraviolet B Radiation Requires Melanin Pigment. *Nat Commun*, 3, 884.
- Osmancevic, A., Gillstedt, M., Wennberg, A. M. & Larkö, O. 2014. The Risk of Skin Cancer in Psoriasis Patients Treated with UVB Therapy. *Acta Derm Venereol*, 94(4), 425-30.
- Otterbein, L. E. & Choi, A. M. 2000. Heme Oxygenase: Colors of Defense against Cellular Stress. *Am J Physiol Lung Cell Mol Physiol*, 279(6), L1029-37.
- Pan, M. H., Chiou, Y. S., Chen, W. J., Wang, J. M., Badmaev, V. & Ho, C. T. 2009. Pterostilbene Inhibited Tumor Invasion Via Suppressing Multiple Signal Transduction Pathways in Human Hepatocellular Carcinoma Cells. *Carcinogenesis*, 30(7), 1234-42.
- Pattison, D. I. & Davies, M. J. 2006. Actions of Ultraviolet Light on Cellular Structures. *EXS*, (96), 131-57.
- Pawson, T. & Scott, J. D. 1997. Signaling through Scaffold, Anchoring, and Adaptor Proteins. *Science*, 278(5346), 2075-80.
- Pearson, C. G., Shikazono, N., Thacker, J. & O'Neill, P. 2004. Enhanced Mutagenic Potential of 8-Oxo-7,8-Dihydroguanine When Present within a Clustered DNA Damage Site. *Nucleic Acids Res*, 32(1), 263-70.
- Perdiz, D., Grof, P., Mezzina, M., Nikaido, O., Moustacchi, E. & Sage, E. 2000. Distribution and Repair of Bipyrimidine Photoproducts in Solar UV-Irradiated Mammalian Cells. Possible Role of Dewar Photoproducts in Solar Mutagenesis. *J Biol Chem*, 275(35), 26732-42.
- Perelman, A., Wachtel, C., Cohen, M., Haupt, S., Shapiro, H. & Tzur, A. 2012. Jc-1: Alternative Excitation Wavelengths Facilitate Mitochondrial Membrane Potential Cytometry. *Cell Death Dis*, 3, e430.
- Petrini, J. H. & Stracker, T. H. 2003. The Cellular Response to DNA Double-Strand Breaks: Defining the Sensors and Mediators. *Trends Cell Biol*, 13(9), 458-62.

- Phillipson, R. P., Tobi, S. E., Morris, J. A. & Mcmillan, T. J. 2002. UVA Induces Persistent Genomic Instability in Human Keratinocytes through an Oxidative Stress Mechanism. *Free Radical Biology and Medicine*, 32(5), 474-480.
- Pieraggi, M. T., Bouissou, H., Angelier, C., Uhart, D., Magnol, J. P. & Kokolo, J. 1985. [the Fibroblast]. *Ann Pathol*, 5(2), 65-76.
- Pleasance, E. D., Cheetham, R. K., Stephens, P. J., McBride, D. J., Humphray, S. J., Greenman, C. D., Varela, I., Lin, M. L., Ordóñez, G. R., Bignell, G. R., Ye, K., Alipaz, J., Bauer, M. J., Beare, D., Butler, A., Carter, R. J., Chen, L., Cox, A. J., Edkins, S., Kokko-Gonzales, P. I., Gormley, N. A., Grocock, R. J., Haudenschild, C. D., Hims, M. M., James, T., Jia, M., Kingsbury, Z., Leroy, C., Marshall, J., Menzies, A., Mudie, L. J., Ning, Z., Royce, T., Schulz-Trieglaff, O. B., Spiridou, A., Stebbings, L. A., Szajkowski, L., Teague, J., Williamson, D., Chin, L., Ross, M. T., Campbell, P. J., Bentley, D. R., Futreal, P. A. & Stratton, M. R. 2010. A Comprehensive Catalogue of Somatic Mutations from a Human Cancer Genome. *Nature*, 463(7278), 191-6.
- Poljšak, B. & Dahmane, R. 2012. Free Radicals and Extrinsic Skin Aging. *Dermatology Research and Practice*, 2012.
- Premi, S., Wallisch, S., Mano, C. M., Weiner, A. B., Bacchiocchi, A., Wakamatsu, K., Bechara, E. J., Halaban, R., Douki, T. & Brash, D. E. 2015. Photochemistry. Chemiexcitation of Melanin Derivatives Induces Dna Photoproducts Long after UV Exposure. *Science*, 347(6224), 842-7.
- Prise, K. M., Belyakov, O. V., Folkard, M. & Michael, B. D. 1998. Studies of Bystander Effects in Human Fibroblasts Using a Charged Particle Microbeam. *Int J Radiat Biol*, 74(6), 793-8.
- Prota, G. 2000. Melanins, Melanogenesis and Melanocytes: Looking at Their Functional Significance from the Chemist's Viewpoint. *Pigment Cell Res*, 13(4), 283-93.
- Provost, N., Moreau, M., Leturque, A. & Nizard, C. 2003. Ultraviolet A Radiation Transiently Disrupts Gap Junctional Communication in Human Keratinocytes. *Am J Physiol Cell Physiol*, 284(1), C51-9.
- Puizina-Ivić, N., Zorc, H., Vanjaka-Rogošić, L., Mirić, L. & Peršin, A. 2008. Fractionated Illumination Improves the Outcome in the Treatment of Precancerous Lesions with Photodynamic Therapy. *Collegium antropologicum*, 32(2), 67-73.
- Pukkala, E., Aspholm, R., Auvinen, A., Eliasch, H., Gundestrup, M., Haldorsen, T., Hammar, N., Hrafnkelsson, J., Kyyrönen, P., Lannersjö, A., Rafnsson, V., Storm, H. & Tveten, U. 2003. Cancer Incidence among 10,211 Airline Pilots: A Nordic Study. *Aviat Space Environ Med*, 74(7), 699-706.

- Quan, T., Qin, Z., Xia, W., Shao, Y., Voorhees, J. J. & Fisher, G. J. 2009. Matrix-Degrading Metalloproteinases in Photoaging. *J Invest Dermatol Symp Proc*, 14(1), 20-4.
- Rafnsson, V., Hrafnkelsson, J. & Tulinius, H. 2000. Incidence of Cancer among Commercial Airline Pilots. *Occup Environ Med*, 57(3), 175-9.
- Rajagopalan, H., Bardelli, A., Lengauer, C., Kinzler, K. W., Vogelstein, B. & Velculescu, V. E. 2002. Tumorigenesis: Raf/Ras Oncogenes and Mismatch-Repair Status. *Nature*, 418(6901), 934.
- Ramos, M. C., Steinbrenner, H., Stuhlmann, D., Sies, H. & Brenneisen, P. 2004. Induction of MMP-10 and MMP-1 in a Squamous Cell Carcinoma Cell Line by Ultraviolet Radiation. *Biol Chem*, 385(1), 75-86.
- Rancourt, R. C., Hayes, D. D., Chess, P. R., Keng, P. C. & O'reilly, M. A. 2002. Growth Arrest in G1 Protects against Oxygen-Induced DNA Damage and Cell Death. *J Cell Physiol*, 193(1), 26-36.
- Redmond, R. W., Rajadurai, A., Udayakumar, D., Sviderskaya, E. V. & Tsao, H. 2014. Melanocytes Are Selectively Vulnerable to UVA-Mediated Bystander Oxidative Signaling. *J Invest Dermatol*, 134(4), 1083-90.
- Reeve, V. E. & Tyrrell, R. M. 1999. Heme Oxygenase Induction Mediates the Photoimmunoprotective Activity of UVA Radiation in the Mouse. *Proceedings of the National Academy of Sciences*, 96(16), 9317-9321.
- Ridley, A. J., Whiteside, J. R., Mcmillan, T. J. & Allinson, S. L. 2009. Cellular and Sub-Cellular Responses to UVA in Relation to Carcinogenesis. *Int J Radiat Biol*, 85(3), 177-95.
- Rizzo, J. L., Dunn, J., Rees, A. & Runger, T. M. 2011. No Formation of DNA Double-Strand Breaks and No Activation of Recombination Repair with UVA. *J Invest Dermatol*, 131(5), 1139-48.
- Rochette, P. J., Therrien, J. P., Drouin, R., Perdiz, D., Bastien, N., Drobetsky, E. A. & Sage, E. 2003. UVA-Induced Cyclobutane Pyrimidine Dimers Form Predominantly at Thymine-Thymine Dipyrimidines and Correlate with the Mutation Spectrum in Rodent Cells. *Nucleic Acids Res*, 31(11), 2786-94.
- Rogakou, E. P., Pilch, D. R., Orr, A. H., Ivanova, V. S. & Bonner, W. M. 1998. DNA Double-Stranded Breaks Induce Histone H2AX Phosphorylation on Serine 139. *J Biol Chem*, 273(10), 5858-68.
- Rosette, C. & Karin, M. 1996. Ultraviolet Light and Osmotic Stress: Activation of the JNK Cascade through Multiple Growth Factor and Cytokine Receptors. *Science*, 274(5290), 1194-7.
- Routaboul, C., Denis, A. & Vinche, A. 1999. Immediate Pigment Darkening: Description, Kinetic and Biological Function. *Eur J Dermatol*, 9(2), 95-9.

- Rundhaug, J. E. & Fischer, S. M. 2008. Cyclo-Oxygenase-2 Plays a Critical Role in UV-Induced Skin Carcinogenesis. *Photochem Photobiol*, 84(2), 322-9.
- Rupnik, A., Grenon, M. & Lowndes, N. 2008. The MRN Complex. *Curr Biol*, 18(11), R455-7.
- Rünger, T. M., Farahvash, B., Hatvani, Z. & Rees, A. 2012. Comparison of DNA Damage Responses Following Equimutagenic Doses of UVA and UVB: A Less Effective Cell Cycle Arrest with UVA May Render UVA-Induced Pyrimidine Dimers More Mutagenic Than UVB-Induced Ones. *Photochem Photobiol Sci*, 11(1), 207-15.
- Rünger, T. M. & Kappes, U. P. 2008. Mechanisms of Mutation Formation with Long-Wave Ultraviolet Light (UVA). *Photodermatology, photoimmunology & photomedicine*, 24(1), 2-10.
- Sachsenmaier, C., Radler-Pohl, A., Zinck, R., Nordheim, A., Herrlich, P. & Rahmsdorf, H. J. 1994. Involvement of Growth Factor Receptors in the Mammalian UVC Response. *Cell*, 78(6), 963-72.
- Sage, E., Girard, P. & Francesconi, S. 2012. Unravelling UVA-Induced Mutagenesis. *Photochemical & Photobiological Sciences*, 11(1), 74-80.
- Sanlorenzo, M., Vujic, I., Posch, C., Cleaver, J. E., Quaglino, P. & Ortiz-Urda, S. 2015. The Risk of Melanoma in Pilots and Cabin Crew: UV Measurements in Flying Airplanes. *JAMA Dermatol*, 151(4), 450-2.
- Sawant, S. G., Zheng, W., Hopkins, K. M., Randers-Pehrson, G., Lieberman, H. B. & Hall, E. J. 2002. The Radiation-Induced Bystander Effect for Clonogenic Survival. *Radiat Res*, 157(4), 361-4.
- Schultz, L. B., Chehab, N. H., Malikzay, A. & Halazonetis, T. D. 2000. P53 Binding Protein 1 (53bp1) Is an Early Participant in the Cellular Response to DNA Double-Strand Breaks. *J Cell Biol*, 151(7), 1381-90.
- Schwabe, R. F., Bradham, C. A., Uehara, T., Hatano, E., Bennett, B. L., Schoonhoven, R. & Brenner, D. A. 2003. C-Jun-N-Terminal Kinase Drives Cyclin D1 Expression and Proliferation During Liver Regeneration. *Hepatology*, 37(4), 824-32.
- Sedelnikova, O. A., Nakamura, A., Kovalchuk, O., Koturbash, I., Mitchell, S. A., Marino, S. A., Brenner, D. J. & Bonner, W. M. 2007a. DNA Double-Strand Breaks Form in Bystander Cells after Microbeam Irradiation of Three-Dimensional Human Tissue Models. *Cancer Res*, 67(9), 4295-302.
- Seger, R. & Krebs, E. G. 1995. The MAPK Signaling Cascade. *FASEB J*, 9(9), 726-35.
- Selvanayagam, C. S., Davis, C. M., Cornforth, M. N. & Ullrich, R. L. 1995. Latent Expression of P53 Mutations and Radiation-Induced Mammary Cancer. *Cancer Res*, 55(15), 3310-7.

- Sen, C. K. & Packer, L. 1996. Antioxidant and Redox Regulation of Gene Transcription. *The FASEB journal*, 10(7), 709-720.
- Setlow, R. B., Woodhead, A. D. & Grist, E. 1989. Animal Model for Ultraviolet Radiation-Induced Melanoma: Platyfish-Swordtail Hybrid. *Proc Natl Acad Sci U S A*, 86(22), 8922-6.
- Shain, A. H., Garrido, M., Botton, T., Talevich, E., Yeh, I., Sanborn, J. Z., Chung, J., Wang, N. J., Kakavand, H., Mann, G. J., Thompson, J. F., Wiesner, T., Roy, R., Olshen, A. B., Gagnon, A., Gray, J. W., Huh, N., Hur, J. S., Busam, K. J., Scolyer, R. A., Cho, R. J., Murali, R. & Bastian, B. C. 2015. Exome Sequencing of Desmoplastic Melanoma Identifies Recurrent Nfkbie Promoter Mutations and Diverse Activating Mutations in the MAPK Pathway. *Nat Genet*, 47(10), 1194-9.
- Shao, C., Folkard, M. & Prise, K. 2008a. Role of TGF-B1 and Nitric Oxide in the Bystander Response of Irradiated Glioma Cells. *Oncogene*, 27(4), 434-440.
- Shao, C., Stewart, V., Folkard, M., Michael, B. D. & Prise, K. M. 2003. Nitric Oxide-Mediated Signaling in the Bystander Response of Individually Targeted Glioma Cells. *Cancer Res*, 63(23), 8437-42.
- Shorrocks, J., Paul, N. D. & Mcmillan, T. J. 2008. The Dose Rate of UVA Treatment Influences the Cellular Response of Hacat Keratinocytes. *J Invest Dermatol*, 128(3), 685-93.
- Silverman, J., Takai, H., Buonomo, S. B., Eisenhaber, F. & De Lange, T. 2004. Human Rif1, Ortholog of a Yeast Telomeric Protein, Is Regulated by ATM and 53BP1 and Functions in the S-Phase Checkpoint. *Genes Dev*, 18(17), 2108-19.
- Silvers, A. L., Bachelor, M. A. & Bowden, G. T. 2003. The Role of JNK and P38 Mapk Activities in UVA-Induced Signaling Pathways Leading to AP-1 Activation and C-Fos Expression. *Neoplasia*, 5(4), 319-29.
- Sluss, H. K., Barrett, T., Dérijard, B. & Davis, R. J. 1994. Signal Transduction by Tumor Necrosis Factor Mediated by JNK Protein Kinases. *Mol Cell Biol*, 14(12), 8376-84.
- Sokolov, M. V., Dickey, J. S., Bonner, W. M. & Sedelnikova, O. A. 2007. Gamma-H2AX in Bystander Cells: Not Just a Radiation-Triggered Event, a Cellular Response to Stress Mediated by Intercellular Communication. *Cell Cycle*, 6(18), 2210-2.
- Sokolov, M. V., Smilenov, L. B., Hall, E. J., Panyutin, I. G., Bonner, W. M. & Sedelnikova, O. A. 2005. Ionizing Radiation Induces DNA Double-Strand Breaks in Bystander Primary Human Fibroblasts. *Oncogene*, 24(49), 7257-65.
- Sola, Y. & Lorente, J. 2015. Contribution of UVA Irradiance to the Erythema and Photoaging Effects in Solar and Sunbed Exposures. *J Photochem Photobiol B*, 143, 5-11.

- Song, X. Z., Xia, J. P. & Bi, Z. G. 2004. Effects of (-)-Epigallocatechin-3-Gallate on Expression of Matrix Metalloproteinase-1 and Tissue Inhibitor of Metalloproteinase-1 in Fibroblasts Irradiated with Ultraviolet A. *Chin Med J (Engl)*, 117(12), 1838-41.
- Stark, M. S., Woods, S. L., Gartside, M. G., Bonazzi, V. F., Dutton-Regester, K., Aoude, L. G., Chow, D., Sereduk, C., Niemi, N. M., Tang, N., Ellis, J. J., Reid, J., Zismann, V., Tyagi, S., Muzny, D., Newsham, I., Wu, Y., Palmer, J. M., Pollak, T., Youngkin, D., Brooks, B. R., Lanagan, C., Schmidt, C. W., Kobe, B., Mackeigan, J. P., Yin, H., Brown, K. M., Gibbs, R., Trent, J. & Hayward, N. K. 2012. Frequent Somatic Mutations in MAP3K5 and MAP3K9 in Metastatic Melanoma Identified by Exome Sequencing. *Nat Genet*, 44(2), 165-9.
- Steinbrenner, H., Ramos, M. C., Stuhlmann, D., Sies, H. & Brenneisen, P. 2003. UVA-Mediated Downregulation of MMP-2 and MMP-9 in Human Epidermal Keratinocytes. *Biochem Biophys Res Commun*, 308(3), 486-91.
- Stern, R. S. & Study, P. F.-U. 2012. The Risk of Squamous Cell and Basal Cell Cancer Associated with Psoralen and Ultraviolet A Therapy: A 30-Year Prospective Study. *J Am Acad Dermatol*, 66(4), 553-62.
- Stetler-Stevenson, W. G., Liotta, L. A. & Kleiner, D. E. 1993. Extracellular Matrix 6: Role of Matrix Metalloproteinases in Tumor Invasion and Metastasis. *FASEB J*, 7(15), 1434-41.
- Stiff, T., O'driscoll, M., Rief, N., Iwabuchi, K., Löbrich, M. & Jeggo, P. A. 2004. ATM and DNA-PK Function Redundantly to Phosphorylate H2AX after Exposure to Ionizing Radiation. *Cancer Res*, 64(7), 2390-6.
- Stone, D. M., Hynes, M., Armanini, M., Swanson, T. A., Gu, Q., Johnson, R. L., Scott, M. P., Pennica, D., Goddard, A., Phillips, H., Noll, M., Hooper, J. E., De Sauvage, F. & Rosenthal, A. 1996. The Tumour-Suppressor Gene Patched Encodes a Candidate Receptor for Sonic Hedgehog. *Nature*, 384(6605), 129-34.
- Stracker, T. H. & Petrini, J. H. 2011. The Mre11 Complex: Starting from the Ends. *Nat Rev Mol Cell Biol*, 12(2), 90-103.
- Straight, R. C. & Spikes, J. D. 1985. Preliminary Studies with Implanted Polyvinyl Alcohol Sponges as a Model for Studying the Role of Neointerstitial and Neovascular Compartments of Tumors in the Localization, Retention and Photodynamic Effects of Photosensitizers. *Adv Exp Med Biol*, 193, 77-89.
- Stucki, M., Clapperton, J. A., Mohammad, D., Yaffe, M. B., Smerdon, S. J. & Jackson, S. P. 2005. MDC1 Directly Binds Phosphorylated Histone H2AX to Regulate Cellular Responses to DNA Double-Strand Breaks. *Cell*, 123(7), 1213-26.

- Stucki, M. & Jackson, S. P. 2006. GammaH2AX and MDC1: Anchoring the DNA-Damage-Response Machinery to Broken Chromosomes. *DNA Repair (Amst)*, 5(5), 534-43.
- Sutherland, B. M., Bennett, P. V., Cintron, N. S., Guida, P. & Laval, J. 2003. Low Levels of Endogenous Oxidative Damage Cluster Levels in Unirradiated Viral and Human DNAs. *Free Radic Biol Med*, 35(5), 495-503.
- Sutherland, J. C. & Griffin, K. P. 1981. Absorption Spectrum of DNA for Wavelengths Greater Than 300 Nm. *Radiat Res*, 86(3), 399-409.
- Syed, D. N., Afaq, F. & Mukhtar, H. 2012. Differential Activation of Signaling Pathways by UVA and UVB Radiation in Normal Human Epidermal Keratinocytes. *Photochem Photobiol*, 88(5), 1184-90.
- Syed, D. N., Malik, A., Hadi, N., Sarfaraz, S., Afaq, F. & Mukhtar, H. 2006. Photochemopreventive Effect of Pomegranate Fruit Extract on UVA-Mediated Activation of Cellular Pathways in Normal Human Epidermal Keratinocytes. *Photochem Photobiol*, 82(2), 398-405.
- Takayama, H., La Rochelle, W. J., Anver, M., Bockman, D. E. & Merlino, G. 1996. Scatter Factor/Hepatocyte Growth Factor as a Regulator of Skeletal Muscle and Neural Crest Development. *Proc Natl Acad Sci U S A*, 93(12), 5866-71.
- Thoma, F. 1999. Light and Dark in Chromatin Repair: Repair of UV-Induced DNA Lesions by Photolyase and Nucleotide Excision Repair. *EMBO J*, 18(23), 6585-98.
- Thomas, N. E., Berwick, M. & Cordeiro-Stone, M. 2006. Could BRAF Mutations in Melanocytic Lesions Arise from DNA Damage Induced by Ultraviolet Radiation? *J Invest Dermatol*, 126(8), 1693-6.
- Tong, Z., Singh, G. & Rainbow, A. J. 2002. Sustained Activation of the Extracellular Signal-Regulated Kinase Pathway Protects Cells from Photofrin-Mediated Photodynamic Therapy. *Cancer Res*, 62(19), 5528-35.
- Toyooka, T., Ishihama, M. & Ibuki, Y. 2011. Phosphorylation of Histone H2AX Is a Powerful Tool for Detecting Chemical Photogenotoxicity. *J Invest Dermatol*, 131(6), 1313-21.
- Trenz, K., Smith, E., Smith, S. & Costanzo, V. 2006. ATM and ATR Promote Mre11 Dependent Restart of Collapsed Replication Forks and Prevent Accumulation of DNA Breaks. *EMBO J*, 25(8), 1764-74.
- Trifunovic, A., Wredenberg, A., Falkenberg, M., Spelbrink, J. N., Rovio, A. T., Bruder, C. E., Bohlooly-Y, M., Gidlöf, S., Oldfors, A., Wibom, R., Törnell, J., Jacobs, H. T. & Larsson, N. G. 2004. Premature Ageing in Mice Expressing Defective Mitochondrial Dna Polymerase. *Nature*, 429(6990), 417-23.
- Tu, Y., Ji, C., Yang, B., Yang, Z., Gu, H., Lu, C. C., Wang, R., Su, Z. L., Chen, B., Sun, W. L., Xia, J. P., Bi, Z. G. & He, L. 2013. DNA-Dependent Protein Kinase Catalytic Subunit (DNA-

- PKcs)-Sin1 Association Mediates Ultraviolet B (UVB)-Induced Akt Ser-473 Phosphorylation and Skin Cell Survival. *Mol Cancer*, 12(1), 172.
- Tyrrell, R. M. 2012. Modulation of Gene Expression by the Oxidative Stress Generated in Human Skin Cells by UVA Radiation and the Restoration of Redox Homeostasis. *Photochem Photobiol Sci*, 11(1), 135-47.
- Uden, A. B., Holmberg, E., Lundh-Rozell, B., Stähle-Bäckdahl, M., Zaphiropoulos, P. G., Toftgård, R. & Vorechovsky, I. 1996. Mutations in the Human Homologue of Drosophila Patched (Ptch) in Basal Cell Carcinomas and the Gorlin Syndrome: Different in Vivo Mechanisms of Ptch Inactivation. *Cancer Res*, 56(20), 4562-5.
- Uziel, T., Lerenthal, Y., Moyal, L., Andegeko, Y., Mittelman, L. & Shiloh, Y. 2003. Requirement of the MRN Complex for ATM Activation by DNA Damage. *EMBO J*, 22(20), 5612-21.
- Van 'T Veer, L. J., Burgering, B. M., Versteeg, R., Boot, A. J., Ruiter, D. J., Osanto, S., Schrier, P. I. & Bos, J. L. 1989. N-Ras Mutations in Human Cutaneous Melanoma from Sun-Exposed Body Sites. *Mol Cell Biol*, 9(7), 3114-6.
- Van Kranen, H. J., De Laat, A., Van De Ven, J., Wester, P. W., De Vries, A., Berg, R. J., Van Kreijl, C. F. & De Gruijl, F. R. 1997. Low Incidence of P53 Mutations in UVA (365-Nm)-Induced Skin Tumors in Hairless Mice. *Cancer Res*, 57(7), 1238-40.
- Varani, J., Perone, P., Fligel, S. E., Fisher, G. J. & Voorhees, J. J. 2002. Inhibition of Type I Procollagen Production in Photodamage: Correlation between Presence of High Molecular Weight Collagen Fragments and Reduced Procollagen Synthesis. *J Invest Dermatol*, 119(1), 122-9.
- Vayssiere, J. L., Petit, P. X., Risler, Y. & Mignotte, B. 1994. Commitment to Apoptosis Is Associated with Changes in Mitochondrial Biogenesis and Activity in Cell Lines Conditionally Immortalized with Simian Virus 40. *Proc Natl Acad Sci U S A*, 91(24), 11752-6.
- Vile, G. F. & Tyrrell, R. M. 1995. Uva Radiation-Induced Oxidative Damage to Lipids and Proteins in Vitro and in Human Skin Fibroblasts Is Dependent on Iron and Singlet Oxygen. *Free Radic Biol Med*, 18(4), 721-30.
- Visse, R. & Nagase, H. 2003. Matrix Metalloproteinases and Tissue Inhibitors of Metalloproteinases Structure, Function, and Biochemistry. *Circulation research*, 92(8), 827-839.
- Vojtek, A. B., Hollenberg, S. M. & Cooper, J. A. 1993. Mammalian Ras Interacts Directly with the Serine/Threonine Kinase Raf. *Cell*, 74(1), 205-14.
- Von Thaler, A., Kamenisch, Y. & Berneburg, M. 2010. The Role of Ultraviolet Radiation in Melanomagenesis. *Experimental Dermatology*, 19(2), 81-88.

- Wagner, E. F. & Nebreda, A. R. 2009. Signal Integration by JNK and P38 MAPK Pathways in Cancer Development. *Nat Rev Cancer*, 9(8), 537-49.
- Wang, X. Y. & Bi, Z. G. 2006. UVB-Irradiated Human Keratinocytes and Interleukin-1alpha Indirectly Increase MAP Kinase/AP-1 Activation and MMP-1 Production in UVA-Irradiated Dermal Fibroblasts. *Chin Med J (Engl)*, 119(10), 827-31.
- Ward, I. M. & Chen, J. 2001. Histone H2AX Is Phosphorylated in an ATR-Dependent Manner in Response to Replicational Stress. *J Biol Chem*, 276(51), 47759-62.
- Wei, X., Walia, V., Lin, J. C., Teer, J. K., Prickett, T. D., Gartner, J., Davis, S., Stemke-Hale, K., Davies, M. A., Gershenwald, J. E., Robinson, W., Robinson, S., Rosenberg, S. A., Samuels, Y. & Program, N. C. S. 2011. Exome Sequencing Identifies GRIN2a as Frequently Mutated in Melanoma. *Nat Genet*, 43(5), 442-6.
- Weischer, M., Blum, A., Eberhard, F., Röcken, M. & Berneburg, M. 2004. No Evidence for Increased Skin Cancer Risk in Psoriasis Patients Treated with Broadband or Narrowband UVB Phototherapy: A First Retrospective Study. *Acta Derm Venereol*, 84(5), 370-4.
- Wells, R. L. & Han, A. 1984. Action Spectra for Killing and Mutation of Chinese Hamster Cells Exposed to Mid- and near-Ultraviolet Monochromatic Light. *Mutat Res*, 129(2), 251-8.
- Wertz, K., Seifert, N., Hunziker, P. B., Riss, G., Wyss, A., Lankin, C. & Goralczyk, R. 2004. Beta-Carotene Inhibits UVA-Induced Matrix Metalloprotease 1 and 10 Expression in Keratinocytes by a Singlet Oxygen-Dependent Mechanism. *Free Radic Biol Med*, 37(5), 654-70.
- Westphal, C. H., Rowan, S., Schmaltz, C., Elson, A., Fisher, D. E. & Leder, P. 1997. ATM and P53 Cooperate in Apoptosis and Suppression of Tumorigenesis, but Not in Resistance to Acute Radiation Toxicity. *Nat Genet*, 16(4), 397-401.
- Whiteman, D. C., Watt, P., Purdie, D. M., Hughes, M. C., Hayward, N. K. & Green, A. C. 2003. Melanocytic Nevi, Solar Keratoses, and Divergent Pathways to Cutaneous Melanoma. *J Natl Cancer Inst*, 95(11), 806-12.
- Whiteside, J. R., Allinson, S. L. & Mcmillan, T. J. 2011. Timeframes of UVA-Induced Bystander Effects in Human Keratinocytes. *Photochem Photobiol*, 87(2), 435-40.
- Whiteside, J. R. & Mcmillan, T. J. 2009. A Bystander Effect Is Induced in Human Cells Treated with UVA Radiation but Not UVB Radiation. *Radiat Res*, 171(2), 204-11.
- Whitmarsh, A. J. & Davis, R. J. 1996. Transcription Factor AP-1 Regulation by Mitogen-Activated Protein Kinase Signal Transduction Pathways. *J Mol Med (Berl)*, 74(10), 589-607.

- Widel, M., Krzywon, A., Gajda, K., Skonieczna, M. & Rzeszowska-Wolny, J. 2014a. Induction of Bystander Effects by UVA, UVB, and UVC Radiation in Human Fibroblasts and the Implication of Reactive Oxygen Species. *Free Radic Biol Med*, 68, 278-87.
- Winter-Vann, A. M. & Johnson, G. L. 2007. Integrated Activation of MAP3Ks Balances Cell Fate in Response to Stress. *J Cell Biochem*, 102(4), 848-58.
- Wlaschek, M., Heinen, G., Poswig, A., Schwarz, A., Krieg, T. & Scharffetter-Kochanek, K. 1994. UVA-Induced Autocrine Stimulation of Fibroblast-Derived Collagenase/MMP-1 by Interrelated Loops of Interleukin-1 and Interleukin-6. *Photochem Photobiol*, 59(5), 550-6.
- Woessner, J. 1998. The Matrix Metalloproteinase Family. *Matrix metalloproteinases*, 1-14.
- Wong, S. Q., Behren, A., Mar, V. J., Woods, K., Li, J., Martin, C., Sheppard, K. E., Wolfe, R., Kelly, J., Cebon, J., Dobrovic, A. & McArthur, G. A. 2015. Whole Exome Sequencing Identifies a Recurrent Rqcd1 P131I Mutation in Cutaneous Melanoma. *Oncotarget*, 6(2), 1115-27.
- Wu, D., Zhao, J. & Zhang, J. 2011. Ultraviolet A Exposure Induces Reversible Disruption of Gap Junction Intercellular Communication in Lens Epithelial Cells. *Int J Mol Med*, 28(2), 239-45.
- Wu, L.-J., Randers-Pehrson, G., Xu, A., Waldren, C. A., Geard, C. R., Yu, Z. & Hei, T. K. 1999. Targeted Cytoplasmic Irradiation with Alpha Particles Induces Mutations in Mammalian Cells. *Proceedings of the National Academy of Sciences*, 96(9), 4959-4964.
- Wäster, P. K. & Ollinger, K. M. 2009. Redox-Dependent Translocation of P53 to Mitochondria or Nucleus in Human Melanocytes after UVA- and UVB-Induced Apoptosis. *J Invest Dermatol*, 129(7), 1769-81.
- Yan, C. & Boyd, D. D. 2007. Regulation of Matrix Metalloproteinase Gene Expression. *J Cell Physiol*, 211(1), 19-26.
- Yang, H., Asaad, N. & Held, K. D. 2005a. Medium-Mediated Intercellular Communication Is Involved in Bystander Responses of X-Ray-Irradiated Normal Human Fibroblasts. 24(12), 2096-2103.
- Young, A. R., Chadwick, C. A., Harrison, G. I., Nikaido, O., Ramsden, J. & Potten, C. S. 1998. The Similarity of Action Spectra for Thymine Dimers in Human Epidermis and Erythema Suggests That DNA Is the Chromophore for Erythema. *J Invest Dermatol*, 111(6), 982-8.
- Zaid, M. A., Afaq, F., Syed, D. N., Dreher, M. & Mukhtar, H. 2007. Inhibition of UVB-Mediated Oxidative Stress and Markers of Photoaging in Immortalized Hacat Keratinocytes by Pomegranate Polyphenol Extract Pomx. *Photochem Photobiol*, 83(4), 882-8.

- Zamzami, N., Marchetti, P., Castedo, M., Zanin, C., Vayssière, J. L., Petit, P. X. & Kroemer, G. 1995. Reduction in Mitochondrial Potential Constitutes an Early Irreversible Step of Programmed Lymphocyte Death in Vivo. *J Exp Med*, 181(5), 1661-72.
- Zhang, H. 2006. P53 Plays a Central Role in UVA and UVB Induced Cell Damage and Apoptosis in Melanoma Cells. *Cancer Lett*, 244(2), 229-38.
- Zhang, J. & Bowden, G. T. 2012. Activation of P38 MAP Kinase and JNK Pathways by UVA Irradiation. *Photochem Photobiol Sci*, 11(1), 54-61.
- Zhang, T., Dutton-Regester, K., Brown, K. M. & Hayward, N. K. 2016. The Genomic Landscape of Cutaneous Melanoma. *Pigment Cell Melanoma Res*, 29(3), 266-83.
- Zhang, X., Jeffs, G., Ren, X., O'donovan, P., Montaner, B., Perrett, C. M., Karran, P. & Xu, Y. Z. 2007. Novel DNA Lesions Generated by the Interaction between Therapeutic Thiopurines and UVA Light. *DNA Repair (Amst)*, 6(3), 344-54.
- Zhang, Y., Ma, W. Y., Kaji, A., Bode, A. M. & Dong, Z. 2002. Requirement of ATM in UVA-Induced Signaling and Apoptosis. *J Biol Chem*, 277(5), 3124-31.
- Zhong, J., Hu, N., Xiong, X., Lei, Q. & Li, L. 2011. A Novel Promising Therapy for Skin Aging: Dermal Multipotent Stem Cells against Photoaged Skin by Activation of Tgf-B/Smad and P38 MAPK Signaling Pathway. *Medical Hypotheses*, 76(3), 343-346.
- Zhou, B. B. & Elledge, S. J. 2000. The DNA Damage Response: Putting Checkpoints in Perspective. *Nature*, 408(6811), 433-9.
- Zhou, H., Ivanov, V. N., Gillespie, J., Geard, C. R., Amundson, S. A., Brenner, D. J., Yu, Z., Lieberman, H. B. & Hei, T. K. 2005a. Mechanism of Radiation-Induced Bystander Effect: Role of the Cyclooxygenase-2 Signaling Pathway. *Proceedings of the National Academy of Sciences of the United States of America*, 102(41), 14641-14646.
- Zhou, H., Ivanov, V. N., Lien, Y.-C., Davidson, M. & Hei, T. K. 2008a. Mitochondrial Function and Nuclear Factor-Kb-Mediated Signaling in Radiation-Induced Bystander Effects. *Cancer research*, 68(7), 2233-2240.
- Zhou, H., Randers-Pehrson, G., Suzuki, M., Waldren, C. A. & Hei, T. K. 2002. Genotoxic Damage in Non-Irradiated Cells: Contribution from the Bystander Effect. *Radiat Prot Dosimetry*, 99(1-4), 227-32.
- Zhou, H., Suzuki, M., Randers-Pehrson, G., Vannais, D., Chen, G., Trosko, J. E., Waldren, C. A. & Hei, T. K. 2001. Radiation Risk to Low Fluences of A Particles May Be Greater Than We Thought. *Proceedings of the National Academy of Sciences*, 98(25), 14410-14415.
- Zhuang, S. & Schnellmann, R. G. 2006. A Death-Promoting Role for Extracellular Signal-Regulated Kinase. *J Pharmacol Exp Ther*, 319(3), 991-7.

- Ziegler, A., Jonason, A. S., Leffell, D. J., Simon, J. A., Sharma, H. W., Kimmelman, J., Remington, L., Jacks, T. & Brash, D. E. 1994. Sunburn and P53 in the Onset of Skin Cancer. *Nature*, 372(6508), 773-6.
- Zou, L. & Elledge, S. J. 2003. Sensing DNA Damage through ATRIP Recognition of Rpa-Ssdna Complexes. *Science*, 300(5625), 1542-8.

# Appendix

# Platinum Trimethyl Bipyridyl Thiolates – New, Tunable, Red- to Near IR Emitting Luminophores for Bioimaging Applications

Accepted 00th January 20xx

Harriet L. Steel,<sup>a</sup> Sarah L. Allinson,<sup>a</sup> Jane Andre,<sup>a</sup> Michael P. Coogan,<sup>b,\*</sup> and James A. Platts<sup>c</sup>

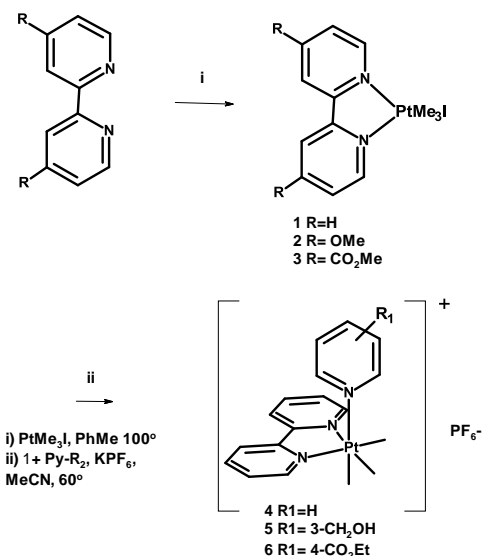
DOI: 10.1039/x0xx00000x

www.rsc.org/

**Synthetic, spectroscopic, computational and biological imaging studies of platinum trimethyl bipyridyl thiolate complexes of the general formula  $[\text{PtMe}_3(\text{bpy})\text{SR}]$  reveal these to be easily accessed, tunable bioimaging agents which feature an unusual  $\sigma\text{-}\pi^*$  Inter-Ligand Charge Transfer (ILCT) transition, and in some cases emit into the Near infra-red (NIR).**

Platinum (IV) trimethyl iodide exists as a cubic tetramer which reacts with a large range of ligands to give stable octahedral complexes of the general formula  $\text{fac-}[\text{Pt}(\text{Me})_3(\text{L})_2\text{I}]$  which have been extensively studied.<sup>1</sup> In the case of chelating bis-heterocyclic ligands such as bipyridine, the derived complexes, e.g.  $\text{fac-}[\text{Pt}(\text{Me})_3(\text{N}^{\wedge}\text{N})\text{I}]$  **1**, are luminescent, showing room temperature phosphorescence from excited states assigned as  $^3\text{IL } \pi\text{-}\pi^*$ .<sup>1</sup> The photochemistry of these units has been widely explored, with photo-reduction to the square-planar Pt(II) species typically observed,<sup>2</sup> but there are few applications of Pt(IV)Me<sub>3</sub> complexes in luminescence, while there is much data on cyclometallated Pt(II) complexes as lumophores.<sup>3-5</sup>

The analogous  $\text{fac-}[\text{Re}(\text{CO})_3(\text{N}^{\wedge}\text{N})\text{L}]$  complexes are widely applied lumophores<sup>6</sup> in which systematic variations in the (N<sup>^</sup>N) unit tune the absorption and emission characteristics, while variations in L (usually substituted pyridines) control solubility and other physical characteristics.<sup>7</sup> It is generally the case that substituted complexes, in which L is a nitrogen heterocycle, have attractive photophysical properties and stability while the precursor halido-complexes are unstable and tend to be toxic in biological work due to halide lability.<sup>8</sup> Therefore, an investigation was undertaken of the synthesis and photophysical characteristics of a series of  $\text{fac-}[\text{Pt}(\text{Me})_3]$  complexes of chelating and monodentate ligands. Reaction of  $\text{PtI}(\text{Me})_3$  with substituted bipyridines gave analogues of **1** with



**Scheme 1** Synthesis of complexes 1-6

electron donating (OMe, complex **2**) and withdrawing (CO<sub>2</sub>Me, complex **3**) groups in the 4,4' positions (Scheme 1).

These complexes showed the respective blue- and red- shifted absorptions and emissions which would be predicted from the electronic structures (Table 1). Complexes of the general formula  $\text{fac-}[\text{Pt}(\text{Me})_3(\text{bpy})\text{L}]$ , where L is a substituted pyridine, were easily synthesised by the reaction of **1** with the appropriate pyridine in the presence of  $\text{KPF}_6$  to give complexes **4-6** (Scheme 1). However, the yellow colour of **1** had been lost, and while these complexes were luminescent (see Table 1) u.v. excitation was required. Reaction of **1** with triphenyl phosphine or aniline gave complexes **7** and **8**, but these complexes too required u.v. excitation. As it seemed that substituting the iodide led to loss of the low energy band responsible for visible absorption and excitation, a re-examination of the nature of this band was required. It is not clear why substitution of iodide for N- and P- donor ligands leads to complete loss of this transition, which has previously been assigned as a formally disallowed  $^3\text{IL } \pi\text{-}\pi^*$  transition.<sup>1</sup>

**Table 1.** Photophysical data of complexes 1-10.

	$\lambda_{\text{max}}$ abs <sup>a</sup>	$\lambda_{\text{max}}$ abs <sup>b</sup>	$\lambda_{\text{max}}$ ex	$\lambda_{\text{max}}$ em	Quantum Yield $\Phi^c$
<b>1</b>	297, 308	344	380	530	See ref.1
<b>2</b>	280, 289, 299	356	330	520	$1.3 \times 10^{-2}$
<b>3</b>	314, 323	372	420	600	$2.6 \times 10^{-4}$
<b>4</b>	300, 311	-	330	470	<sup>d</sup>
<b>5</b>	300, 310	-	333	470	<sup>d</sup>

6	290, 300, 310	-	330	470	<sup>d</sup>
7	304, 313	-	325	470	<sup>d</sup>
8	290, 298, 310	-	345	540	<sup>d</sup>
9	301, 308, 358	440	450	660	$4.1 \cdot 10^{-4}$
10	310, 350	500	490	560	$3.7 \cdot 10^{-4}$

a) Strongest bands >275 nm; b) Lowest energy band / shoulder; c) Measurements performed irradiating into ILCT band for each complex in aerated acetonitrile solutions, using [Ru(bpy)<sub>3</sub>](PF<sub>6</sub>)<sub>2</sub> as a standard ( $\Phi_{em} = 0.018$ )<sup>17</sup> d) ILCT band absent.

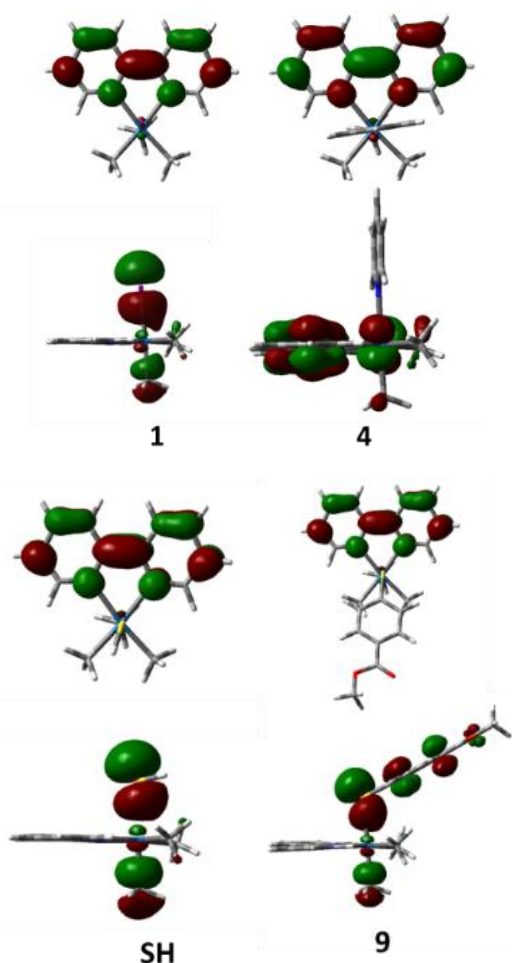
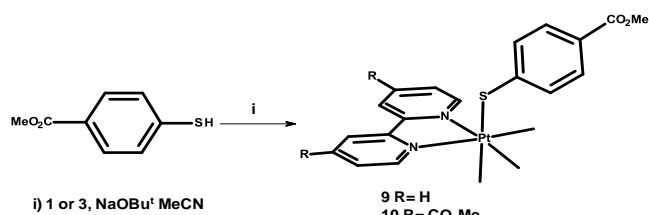


**Figure 1:** Occupied (bottom) and unoccupied (top) orbitals of **1**, **4**, Pt(Me)<sub>3</sub>(bpy)SH and **9** involved in low energy absorption bands.



**Scheme 2.** Synthesis of complexes **9** and **10**. i) MeCN, NaO-t-Bu.

We therefore carried out time-dependent density functional theory (TD-DFT)<sup>9-16</sup> calculations on **1** and **4** to compare the absorption

bands in these species in detail (see ESI for details). This predicts absorption bands for **1** at 358 and 294 nm, in reasonable agreement with the experimental values of 344, 308 and 297 nm. In contrast, **4** is predicted to absorb at 294 and 284 nm (experimental values 311 and 300 nm). The band at 358 nm in **1** corresponds to excitation from an orbital made up largely of a Pt-I  $\sigma$ -bond, along with a lesser amount of *trans*- Pt-Me, to the  $\pi^*$  MO on bpy, as illustrated in Figure 1. Hence this low energy band is best described as Inter-Ligand Charge Transfer rather than either <sup>3</sup>IL  $\pi$ - $\pi^*$  or MLCT. ILCT between halogen and bipyridine antibonding orbitals is also seen admixed with MLCT in the analogous Re complexes,<sup>6</sup> which occasionally may cause problems in biological studies due to halide lability leading to interaction of the heavy metal centre with biomolecules (e.g. DNA).<sup>18</sup> These results therefore call into question the literature assignment, but do explain the change in absorption patterns between **1** and **4**, since the latter does not contain a low energy orbital of the correct symmetry to reproduce such absorption. They also suggest a strategy for combining the desirable properties of visible absorption and kinetic stability in [Pt(Me)<sub>3</sub>N<sup>N</sup>L]<sup>+</sup> complexes, *i.e.* to find L that combines a strong Pt-L bond with suitable electronic structure for interaction with bpy  $\pi^*$ . Thiols satisfy both requirements, so further TD-DFT calculations were performed for [Pt(Me)<sub>3</sub>(bpy)(SH)], from which we predict an absorption band at 393 nm corresponding to S lone pair/Pt-S  $\sigma$ -bond to bpy  $\pi^*$  orbitals (Figure 1).

Having obtained computational support for the hypothesis that thio-substituted complexes should show low energy absorption, methyl-4-mercaptobenzoate was selected as a model ligand which would (through variations of the ester) allow the incorporation of a variety of substituents at the sulphur ligand, giving the tuneable lipophilicity *etc.* which has proven important in the development of metallo-imaging agents. Treatment of **1** with a small excess of methyl-4-mercaptobenzoate in acetonitrile in the presence of sodium t-butoxide gave the thiobenzoate-substituted complex **9** (Scheme 2: full data in ESI), and reaction with **3** gave the ester-substituted analogue **10**. Electronic spectroscopy confirmed that **9** exhibits low energy absorption, observed as a shoulder centred at 440 nm, along with higher energy bands around 300 / 350 nm (TD-DFT predicts absorption at 440 nm due to S LP  $\rightarrow$   $\pi^*$ /S-Pt  $\rightarrow$   $\pi^*$ , Figure 1). Luminescence spectroscopy indicated that the maximum excitation band was centred at ca. 450 nm, correlating with the likely true maximum of the band observed as a shoulder at 440 nm in the uv-vis spectrum. Exciting at 450 nm gave rise to intense emission as a broad band centred around 660 nm (Figure 2).

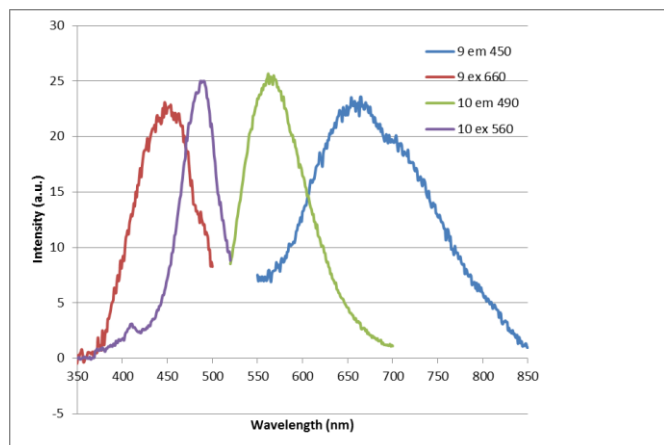


**Figure 2** Excitation and emission spectra for 9 and 10.

Complex **9** is air- and water stable, resistant to ligand substitution of the coordinated thiolate under physiological conditions, and with visible excitation, a Stokes shift of over 200 nm and red emission is an ideal candidate for fluorescence imaging experiments.

Complex **8** bearing electron withdrawing ester substituents was likewise converted to the methyl 4-mercaptobenzoate complex **10** and showed a low energy absorption band centred at ca. 500 nm (DFT prediction 532 nm), and an excitation maximum at 490 nm, (Figure 2) confirming that the photophysics of these complexes is susceptible to significant variations accessible by ligand variations. However, unexpectedly the emission maximum of **10** was blue-shifted in comparison to that of **9** indicating that simple assumptions regarding substituent effects can be misleading, especially in the case of emission from triplet states where the Stokes shift is a function of energy losses through relaxation into triplet geometries, the magnitude of which cannot be estimated intuitively from electron donating/withdrawing arguments.

As a preliminary assessment of the potential for applications of complexes such as **9**, a study of cellular uptake was undertaken by flow cytometry and fluorescence microscopy. This used the well characterised HeLa human cervical carcinoma cell line, and was performed at 0-4 °C to inhibit endocytosis. Flow cytometry detecting between 655-735 nm (Fig. 3, PerCP-Cy5.5) appeared to

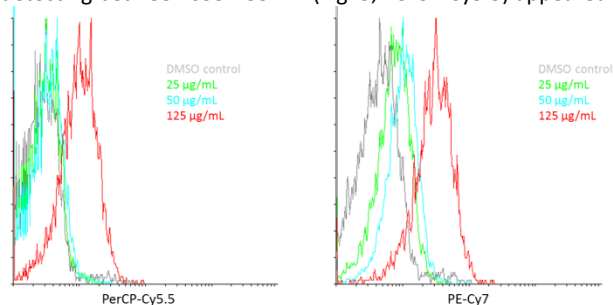


**Figure 3** : Flow cytometric analysis of **9** uptake by HeLa cells; x-axis = fluorescence intensity, y-axis = counts. Flow cytometry histograms of gated cells treated with the indicated concentrations of **9** for 10 minutes are shown. The PerCP-Cy5.5 channel detects fluorescence between 655 and 735 nm and the PE-Cy7 channel detects fluorescence between 750 and 810 nm.

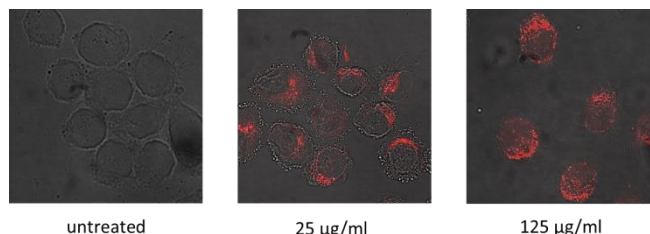


**Figure 4**: Microscopy images of HeLa S3 cells treated with **9** at the indicated concentrations. Images show overlay of brightfield and confocal fluorescence (excitation 458 nm 30 mW Ar laser 50% power output 16% transmission; emission longpass 560 nm filter) fields.

indicate little increase in fluorescence over background at < 125 µg/mL, then a dramatic increase in uptake due to interference from autofluorescence at lower concentrations. However, taking advantage of the emission band of **9** which extends well into the NIR, detection between 750 and 810 nm (Fig. 3, PerCP-Cy7) clearly showed good uptake of **9** with a dose-dependent response with the number of cells showing enhanced intensity of emission increasing as a function of concentration.

Confocal microscopy of HeLa S3 cells confirmed the dose-dependent cellular uptake observed in the flow cytometry correlated with uptake in intact cells (Fig. 4). The luminescence from **9** formed a punctate pattern of discrete staining of compartments in the perinuclear region of the cytoplasm at 25 µg / mL, and at 125 µg / mL more generalised staining of the cytoplasmic region was observed. **9** was not designed with any of the features associated with a preference for localisation in a particular organelle, but is a prototype of this new class of lumophores, so it was pleasing that it appeared not to be retained in the plasma membrane but is capable of permeating the cytoplasm, which bodes well for the design of targeted imaging agents. While some deformations of the membrane surfaces were observed in confocal microscopy even at 25 µg, flow cytometry forward scatter and side scatter profiles indicate cells remained largely intact, even at 125 µg/mL (see ESI). The combination of NIR detection and the ability to penetrate the cell membrane without causing cell lysis is an indication that these complexes have promise as lumophores in cell imaging. While Pt(II) complexes have previously been applied in cellular imaging,<sup>19-21</sup> and have a well-established role in therapy,<sup>22</sup> we believe this to be the first application of Pt(IV) species in fluorescence microscopy.<sup>23</sup> The possibility of theranostic approaches with a Pt(IV) imaging agent of low cytotoxicity, which could be tailored through imaging studies to target organisms and organelles of interest, and reduced, or photoactivated, to a highly cytotoxic Pt(II) species is particularly interesting.

In summary, complexes of the general structure [PtMe<sub>3</sub>(N<sup>^</sup>N)SR], where (N<sup>^</sup>N) represents a bisimine ligand such as 2,2'-bipyridine, are visible absorbing, red or NIR emitting lumophores which are easily synthesised in a few steps from commercially available materials. DFT data indicate that absorption and excitation stems from promotion of an electron localised in the S-Pt bond into the π\* orbital on bipyridine. Absorption and emission profiles are therefore tuneable through simple ligand substitutions. Preliminary experiments show that biological applications as fluorescent agents are possible with these complexes. The NIR emission

can be used to differentiate agent-based emission from autofluorescence even at low levels of uptake and emission intensity.

## Notes and references

‡ We thank the BBSRC and Boots UK Ltd for funding (HLS), the EPSRC mass spectrometry service, Swansea for mass spectra, Drs Fraser White, Daniel Baker and Marcus Winter (Agilent Technologies, Yarnton, UK) for assistance with the X-ray structures of **2-4**, the EPSRC UK National Crystallography Service at the University of Southampton for the collection of the crystallographic data for **9** and **10**<sup>24</sup> and Prof Peter Heard (Sunway University) for drawing our attention to the analogy between the [PtMe<sub>3</sub>] and [Re(CO)<sub>3</sub>] cations.

- 1 H. Kunkely and A. Vogler, *Coord. Chem. Rev.*, 1991, **111**, 15.
- 2 D. C. L. Perkins, R. J. Puddephatt and C. F. H. Tipper, *J. Organomet. Chem.*, 1979, **166**, 261.
- 3 E. Baggaley, J. A. Weinstein and J. A. G. Williams, *Coord. Chem. Rev.*, 2012, **256**, 1762.
- 4 S.-W. Lai and C.-M. Che, *Top. Curr. Chem.*, 2004, **241**, 27.
- 5 I. Eryazici, C. N. Moorefield and G. R. Newkome, *Chem. Rev.*, 2008, **108**, 1834.
- 6 A. Coleman, C. Brennan, J.G. Vos and M. T. Pryce, *Coord. Chem. Rev.*, 2008, **252**, 2585; M. Bartholomä, J. Valliant, K. P. Maresca, J. Babich and J. Zubieta, *Chem. Commun.*, 2009, 493; S. Clede and C. Policar, *Chem. Eur. J* 2015, **21**, 942
- 7 L. A. Worl, R. Duesing, P. Chen, L. D. Ciana and T. J. Meyer, *Dalton Trans.*, 1991, 849.
- 8 R. G. Balasingham, M. P. Coogan and F. L. Thorp-Greenwood, *Dalton Trans.*, 2011, **41**, 11663.
- 9 Gaussian 09, Revision C.01, M. J. Frisch *et al* , Gaussian, Inc., Wallingford CT, 2010.
- 10 A. D. Becke, *J. Chem. Phys.*, 1993, **98**, 5648.
- 11 C. Lee, W. Yang, R. G. Parr, *Phys. Rev. B*, 1988, **37**, 785.
- 12 D. Andrae, U. Haeussermann, M. Dolg, H. Stoll, and H. Preuss, *Theor. Chem. Acc.*, 1990, **77**, 123-41.
- 13 W. J. Hehre, R. Ditchfield and J. A. Pople, *J. Chem. Phys.*, 1972, **56**, 2257.
- 14 M. M. Francl, W. J. Pietro, W. J. Hehre, J. S. Binkley, M. S. Gordon, D. J. Defrees and J. A. Pople, *J. Chem. Phys.*, 1982, **77**, 3654.
- 15 T. Clark, J. Chandrasekhar, G. W. Spitznagel and P. V. Schleyer, *J. Comput. Chem.*, 1983, **4**, 294.
- 16 J. Tomasi, B. Mennucci, and R. Cammi, *Chem. Rev.*, 2005, **105**, 2999-3093, and references cited therein.
- 17 K. Suzuki, A. Kobayashi, S. Kaneko, K. Takehira, T. Yoshihara, H. Ishida, Y. Shiina, S. Oishic and Seiji Tobita, *Phys. Chem. Chem. Phys.*, 2009, **11**, 9850
- 18 A. J. Amoroso, M. P. Coogan, J. E. Dunne, V. Fernández-Moreira, J. B. Hess, A. J. Hayes, D. Lloyd, C. Millet, S. J. A. Pope and C. Williams, *Chem. Commun.*, 2007, 3066.
- 19 C. Yik-Sham Chung, S. Po-Yam Li, M.-W. Louie, K. K.-W. Lo and V. Wing-Wah Yam, *Chem. Sci.*, 2013, **4**, 2453.
- 20 S. W. Botchway, M. Charnley, J. W. Haycock, A. W. Parker, D. L. Rochester, J. A. Weinstein and J. A. G. Williams, *Proc. Natl. Acad. Sci. U. S. A.*, 2008, **105**, 16071.
- 21 R. R. de Haas, R. P. M. van Gijlswijk, E. B. van der Tol, J. Veuskens, H. E. van Gijssel, R. B. Tijdens, J. Bonnet, N. P. Verwoerd and H. J. Tanke, *J. Histochem. Cytochem.*, 1999, **47**, 183.
- 22 L. Kelland, *Nature Reviews Cancer* 2007, **7**, 573.
- 23 M. P. Coogan and V. Fernández-Moreira, *Chem. Commun.*, 2014, **50**, 384.
- 24 S. J. Coles and P.A., Gale, *Chem. Sci.*, 2012, **3**, 683.